PROPENE PARTIAL OXIDATION WITH MOLECULAR OXYGEN OVER ALKALI MODIFIED CuO_x/SiO_2 CATALYSTS

Janvit Teržan

Doctoral Dissertation
Jožef Stefan International Postgraduate School
Ljubljana, Slovenia

Supervisor: Asst. Prof. Matjaž Spreitzer, Jožef Stefan Institute, Ljubljana, Slovenia
Co-Supervisor: Dr. Petar Djinović, National Institute of Chemistry, Ljubljana, Slovenia

Evaluation Board:
Prof. Iztok Arčon, Chair, University of Nova Gorica, Nova Gorica, Slovenia
Asst. Prof. Boštjan Genorio, Member, University of Ljubljana, Faculty of Chemistry and Chemical Technology, Ljubljana, Slovenia
Prof. Stefania Specchia, Member, Politecnico di Torino, Torino, Italy

MEDNARODNA PODIPLOMSKA ŠOLA JOŽEFA STEFANA
JOŽEF STEFAN INTERNATIONAL POSTGRADUATE SCHOOL

Janvit Teržan

PROPENE PARTIAL OXIDATION WITH MOLECULAR OXYGEN OVER ALKALI MODIFIED CuO_x/SiO_2 CATALYSTS

Doctoral Dissertation

DELNA OKSIDACIJA PROPENA Z MOLEKULARNIM KISIKOM NA KATALIZATORJIH CuO_x/SiO_2, MODIFICIRANIH Z ALKALIJSKIMI KOVINAMI

Doktorska disertacija

Supervisor: Asst. Prof. Matjaž Spreitzer

Co-Supervisor: Dr. Petar Djinović

Ljubljana, Slovenia, July 2020

To my brother Andraž,
to my dear Anja,
and to my family.

Acknowledgments

I would like to express my deep gratitude to my mentor Prof. Dr. Petar Djinović for all his guidance, his patience, and his time. He gave me complete freedom in my work, but was always there when I required assistance. Petar has helped me become the researcher I am today by challenging me to critically asses all aspects of my work. With his reassurance and words of encouragement he also helped me become a better person. I would also like to thank my co-supervisor Asst. Prof. Matjaž Spreitzer for his help with some of my research, and his help in scholastic issues.

I sincerely thank Dr. Janez Zavašnik (Center for Electron Microscopy and Microanalysis, Jožef Stefan Institute, Slovenia) for his prompt and expert electron microscopy analyses. I also wish to acknowledge all the knowledge and work contributed by Prof. Dr. Iztok Arčon (Laboratory of Quantum Optics, University of Nova Gorica, Slovenia). His work with X-ray absorption spectroscopy gave me invaluable insight into my work. I would also like to extend my gratitude to Dr. Matej Huš (Department of Catalysis and Chemical Reaction Engineering, National Institute of Chemistry, Slovenia) for his theoretical work. I would like to acknowledge the fruitful and constructive talks offered by all the people mentioned in this paragraph.

Special thanks go to the Jožef Stefan International Postgraduate School (IPS), and to the Slovenian Research Agency for the provided funding. The access to synchrotron radiation facilities of ELETTRA is acknowledged, and the support by the project CALIPSOplus under EU Framework Programme for Research and Innovation HORIZON 2020 for the XAS experiment at Elettra.

My deepest gratitude also goes to all my co-workers who in one way or another helped me complete all my work. For all the constructive debates, help with analyses and interpretations, I would like to thank all the people who worked with me in the D05 department. It was my absolute pleasure to work alongside such wonderful people.

I would like to thank my family. They have carefully guided me all my life, with support and love, to all my achievements, my mother Polona, father Robert and my best friend and brother Andraž. And Anja, who with her love and patience helped me to achieve my best self.

Abstract

Propylene oxide (PO) is a very versatile industrial raw material. It is used in the production of many consumer goods. With the improving living standards and an increase in global population, the global demand for PO is steadily increasing. Currently implemented production methods with organic peroxides or chlorohydrin have several drawbacks such as pollution, high costs of production, and low demand for side products of the reaction. For decades researchers have studied the direct propylene epoxidation reaction using molecular oxygen as the oxidant. So far, the tested catalysts have fallen short of the industrially applicable conditions (activity, stability, and selectivity).

In my work, I focused on copper-based catalysts, where amorphous silica was used as the support. I subsequently modified these catalysts with different alkali (Na, K, and Cs) and alkaline earth metals (Ca). The goal was to gain new understanding on the requirements and reaction pathway for molecular oxygen and propylene activation in the direct propylene oxidation reaction using molecular oxygen. Furthermore, we wanted to understand the underlying factors that determine catalyst selectivity and stability. To examine the viability of the materials in propylene epoxidation, the catalysts were tested in a fixed-bed quartz reactor at atmospheric pressure. Additional *in-situ* and *ex-situ* techniques were employed to acquire more information about the mechanism of the reaction. Active phase properties were studied with *ex-* and *in-situ* UV/vis, Diffuse Reflectance Infrared Fourier transform (DRIFT) spectroscopy, Temperature Programmed Desorption of CO_2 (CO_2-TPD), and pyridine saturation were employed to probe the acidic/basic properties of the surface. The materials were imaged with the help of scanning and transmission electron microscopy. Local structure and oxidation state of copper during reaction was observed with *in-situ* XAS. All the experimental data was complemented by theoretical techniques.

We successfully synthesized highly dispersed modified and unmodified CuO_x nanoparticles that were, on average, smaller than 1 nm. With unmodified catalysts we observed significant deactivation as a result of sintering. This was greatly reduced by alkali and earth alkaline modification, and in the case of Cs modification completely eliminated. We found that with our materials, Lewis acid sites have negligible impact on PO selectivity. Catalytic tests showed that only the modification with alkali metals increases PO selectivity. This modification generates additional basic sites of moderate strength on the catalyst surface. We propose these sites are oxygen species with a more electrophilic character, which are selective for propylene epoxidation. Different reduction dynamics were observed depending on the modifying adatom. This indicates altered kinetics of oxygen abstraction and replenishment. A similar amount of Cu^+ was seen for the unmodified, Na^+, and Ca^{2+} modified catalysts, which have very different selectivities. This shows that Cu^+ amount is not the only factor determining PO selectivity. We found that, in general, alkali metal modification (Na) reduces the average Cu-O bond length, and earth alkaline metals (Ca) have the opposite effect.

We propose that the Cu-O bond length reduction shows a reduction in the nucleophilic character of surface-bound oxygen species. Consequently, allylic hydrogen stripping (AHS)

is prevented and oxametallacycle (OMC) formation is promoted. From this we constructed a tentative reaction mechanism. This was additionally confirmed by theoretical techniques, which disclosed a drastic increase in the activation barrier (AB) of AHS. Additionally, a slight increase in the AB for OMC formation was noted, however it was energetically favorable compared to AHS. A decrease in the AB for ring closure and PO desorption was observed with alkali modification.

Povzetek

Propilen oksid (PO) je vsestransko uporabna industrijska surovina. Najpogosteje je uporabljen v proizvodnji številnih potrošnih materialov. Zanimanje zanj se zaradi dviga življenjskega standarda in večjega števila prebivalcev ves čas povečuje. Trenutne proizvodne metode imajo številne pomanjkljivosti, kot so onesnaževanje, visoki stroški proizvodnje in majhno povpraševanje po stranskih produktih. Raziskovalci zato že desetletja intenzivno preučujejo neposredno epoksidacijo propena z uporabo molekularnega kisika kot oksidanta. Do sedaj preizkušeni katalizatorji ne dosegajo standardov za industrijsko uporabo (aktivnost, stabilnost in selektivnost).

Pri delu sem se osredotočil na katalizatorje na osnovi bakra, pri katerih sem kot nosilec uporabil amorfni silicijev dioksid. V nadaljevanju sem jih modificiral z različnimi alkalijskimi (Na, K, Cs) in zemljoalkalijskimi kovinami (Ca). Cilj je bil sinteza morfološko definiranih, selektivnih in stabilnih katalizatorjev, ki bodo primerni za reakcijo neposredne oksidacije propilena z uporabo molekularnega kisika. Želel sem pojasniti in razumeti dejavnike, ki vplivajo na selektivnost za PO in stabilnost katalizatorja. Materiale, ki so uporabni za direktno epoksidacijo propena z molekularnim kisikom, sem testiral pri atmosferskem tlaku v cevnem kvarčnem reaktorju s strnjenim slojem katalizatorja.

Za boljše razumevanje mehanizma reakcije sem uporabil različne *in-situ in ex-situ* tehnike. Morfološke lastnosti aktivne faze sem preučeval z *ex-* in *in-situ* UV/VIS spektroskopijo. Za preverjanje kislinsko/bazičnih lastnosti površine sem uporabil infrardečo (DRIFT) spektroskopijo, temperaturno programirano desorpcijo (H_2O, CO_2) (TPD) in kemisorpcijo s piridinom. Morfologijo materialov sem preučil z vrstičnim in presevnim elektronskim mikroskopom. Z uporabo *in-situ* XAS tehnike sem analiziral lokalno strukturo bakrovih atomov tekom reakcije epoksidacije. Vsi eksperimentalni podatki so bili podkrepljeni s teoretičnimi DFT izračuni.

Uspešno sem sintetiziral modificirane in nemodificirane dispergirane CuO_x nanodelce, ki so bili povprečno manjši od 1 nm. Pri nemodificiranih katalizatorjih sem opazil znatno deaktivacijo, ki je posledica sintranja. Slednja se je z modifikacijo katalizatorjev močno zmanjšala ali, v primeru modifikacije s Cs, celo popolnoma ustavila.

Z DRIFT in s katalitskimi testi sem dokazal, da šibka Lewisova kisla mesta, prisotna na površini katalizatorjev, zanemarljivo vplivajo na selektivnost za PO. Pri modifikaciji z alkalijskimi kovinami se selektivnost za PO poveča, saj pride do nastanka novih zmernih bazičnih mest na katalizatorju. Sklepam, da so ta mesta kisikove specije, katerih elektrofilna narava spodbuja nastanek »oxametallacycle« (OMC) intermediata ter posledično PO. Različna hitrost redukcije katalizatorjev, ki sem jo izmeril s pomočjo XAS, nakazuje na spremenjeno kinetiko aktivacije kisika.

Pri različnih katalizatorjih (nemodificiran, modificiran z Na in Ca) sem tekom reakcije opazil zelo različne selektivnosti in nastanek podobnih količin Cu^+. To dokazuje, da slednja ni edini faktor, ki določa selektivnost za PO. Sočasno sem opazil korelacijo med količino Cu^+ in deaktivacijo katalizatorja. Pri modifikaciji z alkalijskimi kovinami (Na) se povprečna dolžina vezi Cu-O zmanjša. Zmanjšanje dolžine vezi pripisujemo zmanjšanju nukleofilnosti površinsko vezanih kisikovih specij. Posledica tega je favoriziran nastanek

OMC in ne abstrakcija alilnega vodika (AAV). Pri zemljoalkalijskih kovinah (Ca) je opazen nasprotni učinek.

Iz vseh eksperimentalnih podatkov sem sestavil okvirni mehanizem reakcije, ki sem ga podkrepil s teoretičnimi DFT izračuni. Slednji so pri katalizatorjih, ki so bili modificirani z alkalijskimi kovinami, pokazali drastično povečanje aktivacijske bariere (AB) za AAV. Hkrati se je rahlo povečala AB za nastanek OMC, vendar je bila še vedno nižja od AB za AAV. Prav tako sem pri modifikaciji z alkalijsko kovino opazil rahlo znižanje AB za zapiranje epoksidnega obroča in desorpcijo PO.

Contents

List of Figures **xv**

List of Tables **xvii**

Abbreviations **xix**

1 Introduction **1**
1.1 Propylene oxide ... 3
1.2 Liquid phase catalysis ... 4
1.3 Gas phase catalysis ... 7
1.3.1 Silver containing catalysts ... 7
1.3.2 Copper containing catalysts ... 15
1.3.3 Various catalysts ... 21
1.4 Mechanism of propylene epoxidation ... 27

2 Alkali and earth alkali modified CuO_x/SiO_2 catalysts for propylene partial oxidation: What determines the selectivity? **31**
2.1 Alkali and earth alkali modified CuO_x/SiO_2 catalysts for propylene partial oxidation: What determines the selectivity? ... 33
2.2 Supplementary Information 1 ... 47

3 Effect of Na, Cs and Ca on propylene epoxidation selectivity over CuO_x/SiO_2 catalysts studied by catalytic tests, *in-situ* XAS and DFT **57**
3.1 Effect of Na, Cs and Ca on propylene epoxidation selectivity over CuO_x/SiO_2 catalysts studied by catalytic tests, *in-situ* XAS and DFT ... 58
3.2 Supplementary Information 2 ... 67

4 Conclusions and future outlook **103**

References **107**

Bibliography **113**

Biography **115**

List of Figures

Figure 1: Reaction schematic of total and partial oxidation of propylene. 1
Figure 2: Main industrial propylene oxide production processes and their schematic representation. 3
Figure 3: Schematic representation of the chlorohydrin process. 4
Figure 4: Schematic representation of the PO/TBA process. 4
Figure 5: Schematic representation of the PO/SM (R=H) and CHP ($R=CH_3$) processes. 4
Figure 6: Schematic representation of a continuous slurry reactor used by Liu et al. Reproduced with permission from Ref. [11]. Copyright 2015 American Chemical Society. 5
Figure 7: Different silanols as Brønsted acid sites as predicted by Signorile et al. Reproduced with permission from Ref. [13]. Copyright 2018 American Chemical Society. 6
Figure 8: Schematic representation of the porous membrane reactor used by Bere et al. [30] 10
Figure 9: Ag_{19} and Ag_{20} clusters investigated by Cheng et al. Reproduced with permission from Ref. [35]. Copyright 2013 American Chemical Society. 12
Figure 10: Schematic representation of Ni-Ag core-shell catalysts used by Yu et al. Reproduced with permission from Ref. [38]. Copyright 2018 Elsevier B.V. 13
Figure 11: Reaction mechanism for the formations of primary products over the CuO_x/SiO_2 catalysts proposed by He et al. Reproduced with permission from Ref. [54]. Copyright 2012 Elsevier Inc. 17
Figure 12: Catalytic performance of the 2 wt % Cu and 5 wt % Ru on commercial SiO_2 catalyst modified by different alkaline metal salts (GHSV = 20,000 h^{-1}, gas composition: C_3H_6 : O_2 = 1:2, T = 300 °C). Reproduced with permission from Ref. [56]. Copyright Springer Science+Business Media New York 2014. 18
Figure 13: Analysis of energetic span model with surface O^{2-}, O^-, and O_2^- species on $Cu_2O(111)$. Reproduced with permission from Ref. [58]. Copyright 2018 American Chemical Society. 19
Figure 14: Reaction pathways for the oxidation of C_3H_6 over the 1 wt % FeO_x/SBA-15 with and without modification by KCl (K/Fe = 5) proposed by Wang et al. Reproduced with permission from Ref. [65]. Copyright 2005 American Chemical Society. 23
Figure 15: Synergistic effect between MoO_3 and Bi_2SiO_5 in propylene epoxidation proposed by Pang et al. Reproduced with permission from Ref. [71]. Copyright 2014 WILEY-VCH Verlag GmbH & Co. KGaA, Weinheim. 25
Figure 16: Percent PO selectivities (A) and propylene conversions (B) as a function of Sb–Cu–Na concentrations on the SiO_2 support at 250 °C. All catalysts had a total metal loading of 18 wt % and were calcined at 500 °C. Reproduced with permission from Ref. [74]. Copyright 2015 The Korean Society of Industrial and Engineering Chemistry. Published by Elsevier B.V. 26

Figure 17: Structure of two oxametallacycle intermediates as proposed by Medlin et al. (OMMP1 left and OMMP 2 right). 28
Figure 18: Reaction scheme of propylene oxidation by atomic and molecular oxygen proposed by Dai et al. Reproduced with permission from Ref. [83]. Copyright the Owner Societies 2017. 29

List of Tables

Table 1: Effect of a chlorine promoter on the efficiency of silver catalyst. [22] 8
Table 2: Propylene epoxidation over silver catalysts modified with different promoters. [24] 8
Table 3: Propylene epoxidation over silver catalysts modified with different promoters. [28] 9
Table 4: Reaction conditions used by Wang et al. [52]: catalyst weight, 0.20 g; partial pressures of C_3H_6 and O_2, 2.5 and 98.8 kPa, respectively; total flow rate, 60 mL min^{-1}. 16
Table 5: Results of propylene photooxidation reported by Yoshida et al. [62]. 21
Table 6: Results of photo-oxidation of propylene over Rb^+ modified silica supported catalysts (Rb–VS) samples reported by Amano and Tanaka [69]. (V_2O_5 loading 0.5 wt %.) 23

Abbreviations

AB	... Activation barrier
Alumina	... Aluminum oxide (Al_2O_3)
AHS	... Allylic hydrogen stripping
CHPO	... Chlorohydrin process
CHP	... Cumene hydroperoxide
DFT	... Density functional theory
DRIFT	... Diffuse reflectance infrared Fourier transform
EXAFS	... Extended X-ray absorption fine structure
FTIR	... Fourier-transform infrared spectroscopy
GHSV	... Gas hourly space velocity ($\frac{\text{Volumetric gas flow}}{\text{Catalyst Volume}}$)
HPPO	... Hydrogen peroxide to propylene oxide process
HREELS	... High resolution electron energy loss spectroscopy
ICP-AES	... Inductively coupled plasma atomic emission spectroscopy
LMCT	... Ligand to metal charge transfer
OMC	... Oxametallacycle
PO	... Propylene oxide; Propene oxide; 2-Methyloxirane
PO/SM	... Ethylbenzene hydroperoxide process
PO/TBA	... *tert*-butyl hydroperoxide process
TOS	... Time on stream
TPR	... Temperature programmed reduction
TPD	... Temperature programmed desorption
UV/vis DR	... Diffuse reflectance UV/vis spectroscopy
wt %	... Weight percent
XANES	... X-ray absorption near edge structure
XAS	... X-ray absorption spectroscopy
XPS	... X-ray photoelectron spectroscopy
XRD	... X-ray diffraction

Chapter 1

Introduction

Propene (C_3H_6), commonly referred to as propylene (as it will also be referred to in this work), is the main resource for propylene oxide production. It is produced during oil refining as a result of cracking larger hydrocarbons. In the presence of oxygen and a catalyst, it can be oxidized to several oxygenates (Figure 1). Total oxidation is undesired as cheaper fuels with a higher energy density exist. For propylene partial oxidation to acrolein, isopropanol, acetone, and others, the chemistry is known and they are prepared with high efficiency. Among all the possible oxidation reactions of propylene, the transformation to propylene oxide (epoxidation) is the main topic of this doctoral dissertation.

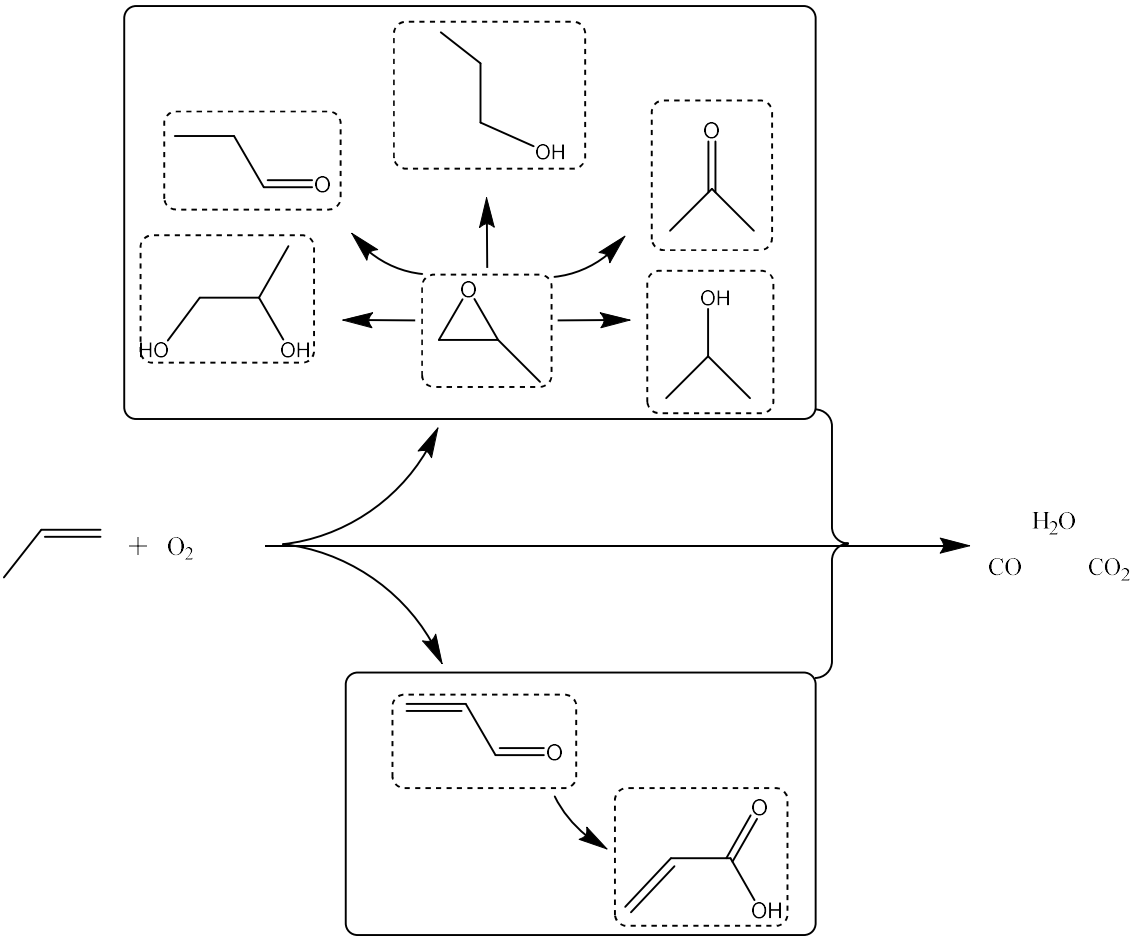

Figure 1: Reaction schematic of total and partial oxidation of propylene.

1.1 Propylene Oxide

Propylene oxide (PO) is an organic compound, a colorless volatile liquid with a high commercial value ($10.5 billion market value in 2017, Olefin Derivatives: Global Markets to 2022, July 2018, BCC). It is a raw material in the manufacture of various products such as polyols, which are used for the production of polyurethane foams used in the housing and the automobile industry. This accounts for the majority, about 60 %[1], of the propylene oxide use. The rest is hydrolyzed to propylene glycol (about 20 % [1]), is used as a solvent, or finds its way into some niche uses (fixating agent in microscopy, fumigant, etc. [1]). Propylene glycol is further used as a feedstock for unsaturated polyester resins production [1], [2], in the food industry, and as antifreeze, among others. Since it is such a versatile raw material, PO was the fourth largest segment in the global market with a significant share of the market (over 13 %, about $10 billion) [BCC research]. Growth of the population accompanied with an increase in living standards is the driving force behind the rising demand for propylene oxide (products such as furniture and automobile seating, insulation foam, and food packaging). The latter reached almost 10 Mt in 2017 and projections show that by 2025, the annual PO demand will exceed 20 Mt [3].

There are several techniques for PO production; however all of them have environmental or economic issues (Figure 2).

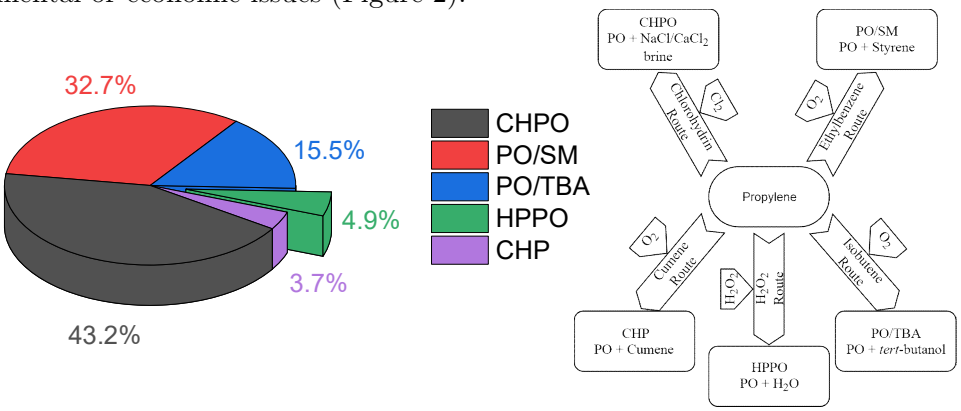

Figure 2: Main industrial propylene oxide production processes and their schematic representation.

The first production method developed and used was the chlorohydrin processes (

Figure 3). In 2008, the majority of PO was produced via the chlorohydrin process (over 43 %), but even though it is still profitable, no new chlorohydrin plants are opening. The problem lies in the side product of the reaction, the NaCl or $CaCl_2$ brine (approximately 2.2 tons per 1.0 ton of PO [4]), which has limited use, and the disposal is not easy.

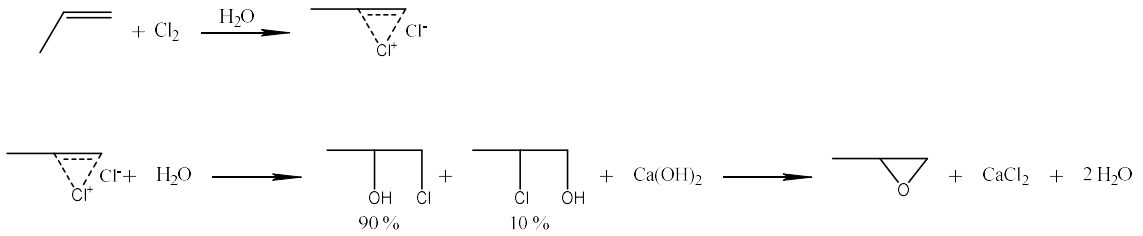

Figure 3: Schematic representation of the chlorohydrin process.

To avoid using chlorine, epoxidation of propylene using organic hydroperoxides has been implemented. The organic intermediates are ethylbenzene (PO/SM), isobutene (PO/TBA) (Figure 4), or cumene (CHP), which produce 32.7, 15.5, and 3.7 % of PO, respectively [Nexant report 2009]. In these cases, the reaction is always a two-step process.

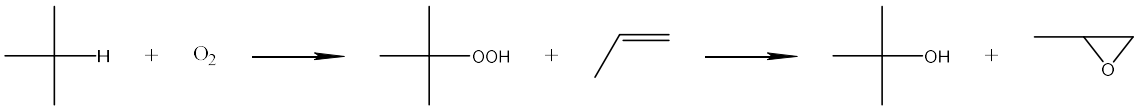

Figure 4: Schematic representation of the PO/TBA process.

First, the intermediate molecule is peroxidized, and the product is then used to produce PO. The drawback when using isobutene or ethylbenzene (Figure 5) is that while the co-products can be sold, they are produced in large quantities. Additionally, the market is much smaller than that for PO. Cumene has the advantage that dimethylphenylmethanol, the co-product in the process can be recycled to cumene by dehydration and hydrogenation (Figure 5). In 2008, Evonik (former Degussa) commercialized a process (HPPO) where hydrogen peroxide is used to directly epoxidize propylene (4.9 % PO produced in 2008), with water being the only side product. However, the high price of the commercially available hydrogen peroxide is comparable to that of PO, which is a major economic downside of this process [5], [6].

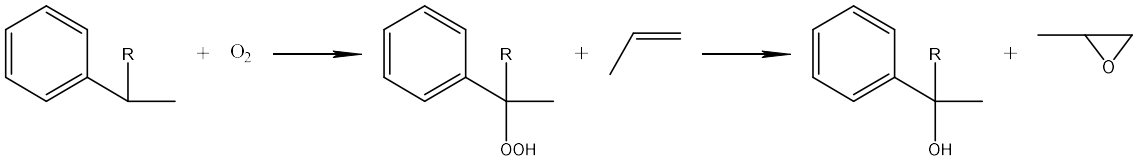

Figure 5: Schematic representation of the PO/SM (R=H) and CHP ($R=CH_3$) processes.

The several drawbacks of all the described processes have driven research into direct propylene epoxidation using molecular oxygen or an oxygen/hydrogen gas mixture. The main focus was gas phase reactions, although some liquid phase research has been done.

1.2 Liquid Phase Catalysis

To avoid the use of peroxide, chlorine and organic peroxides, direct oxidation using molecular oxygen or oxygen-containing gases has been extensively researched. Several soluble and insoluble catalysts were tested in the liquid phase, such as silver chelates using benzene as the solvent [7]. The reaction was carried out in stainless steel autoclave at a total pressure of 45 atm. A conceptual process for the epoxidation of propylene using

molten nitrate salts and a co-catalyst was patented by the OLIN Corp [8]. Similar experiments were also performed by Nijhuis et al. [9] where they studied the mechanism by which the molten salts aid in the epoxidation. They used several salts and eutectic mixtures, combined with blank experiments to elucidate the effect of salts. The results with molten salts were very similar to those of the blank reactor; however the reaction rate was noticeably higher. They attributed this to radical formation which allowed for shorter reaction times or lower pressures.

Lately, work has been more focused on water/methanol mixtures using H_2O_2 or a H_2/O_2 gas mixture. Jiang et al. [10] were studying the mechanism of epoxidation using a gas mixture of CO, O_2. The reaction was run in a methanol/water mixture, with ^{18}O labeled molecular oxygen. The catalysts they used were a mixture of Au-loaded titania (TiO_2) and titanium silicalite (TS-1). They provided definitive evidence that the bridging oxygen in PO comes from O_2 and not H_2O. The work they did offered a novel epoxidation method that is environmentally much friendlier than the traditional methods used.

Liu et al. [11] tested several TS-1, from nanosized to microsized and even extrudates with H_2O_2 being the oxidizing agent. The epoxidation was run in a continuous slurry reactor for 247 h, with methanol as the solvent (Figure 6). They achieved very good results, with the PO selectivity as high as 98.7 % with a yield of 96.4 %. Even though the catalysts slowly deactivated during the reaction, substantial catalytic activity can be regained after washing in H_2O_2.

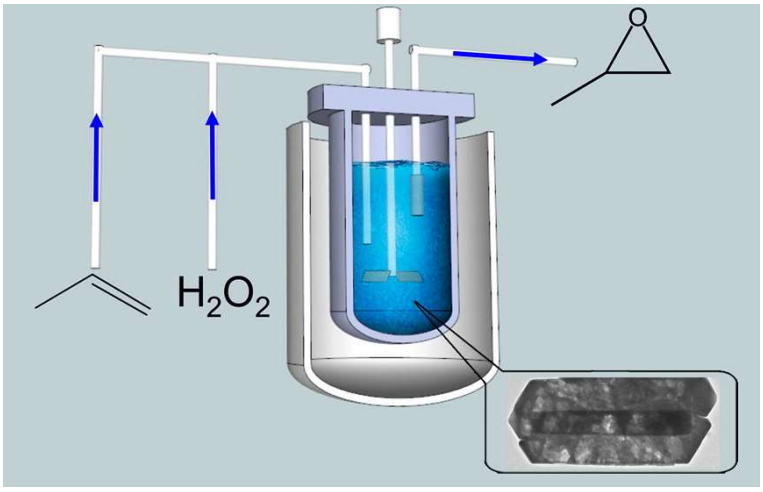

Figure 6: Schematic representation of a continuous slurry reactor used by Liu et al. Reproduced with permission from Ref. [11]. Copyright 2015 American Chemical Society.

Kertalli et al. [12] used methanol as the solvent with a H_2/O_2 gas mixture and Pd catalysts. They tested pure Pd, Pd-Pt, and Pd-Au loaded TS-1 catalysts for their PO selectivity and H_2O_2 productivity. They found that combining Pd with Pt with an excess of oxygen has a positive impact on PO yield due to reduced propylene hydrogenation. Although the addition of Pt increased PO productivity, it also increased the decomposition rate of H_2O_2. On the other hand, combining Pd with Au increased H_2O_2 productivity, but due to propylene hydrogenation, the overall PO yield was smaller than with the Pd-Pt catalyst.

Signorile et al. [13] tested three TS-1 catalysts containing different amounts and titanium species. They found that the samples had a varied amount of weak Brønsted sites (silanols and titanols, Figure 7), and only a weak correlation could be made between the abundance of these sites and byproduct formation. There was also no correlation between H_2O_2 conversion and non-framework, i.e. not tetrahedral Ti species. Moreover, these sites

could not be associated with PO degradation considering the by-products formed (methyl esters and propylene glycol). The only quantitative correlation was found between tetrahedral isolated Ti sites and catalytic activity.

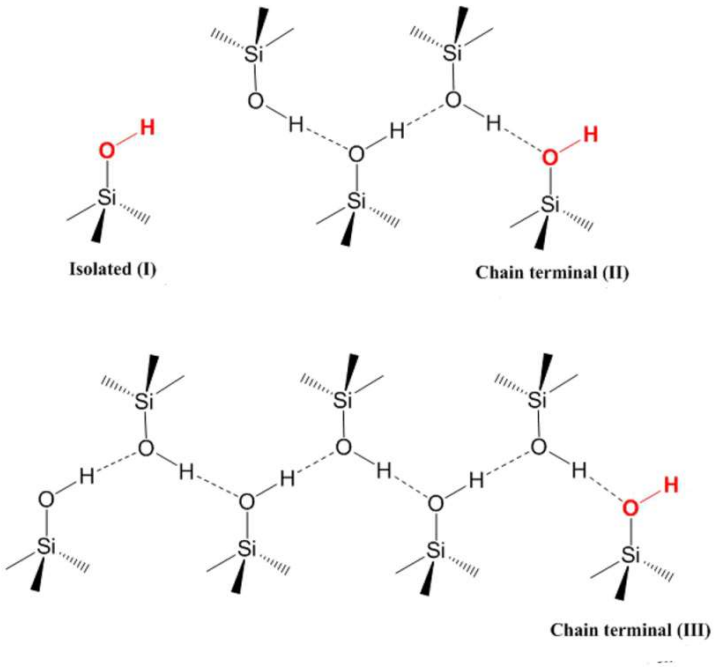

Figure 7: Different silanols as Brønsted acid sites as predicted by Signorile et al. Reproduced with permission from Ref. [13]. Copyright 2018 American Chemical Society.

Despite the fact that very good conversions (over 50 % [12]) and selectivities (up to 98.7 % [11]) can be achieved in the liquid phase, there are still several drawbacks. Hydrogen peroxide has a high price, using a H_2/O_2 mixture has associated risks: hydrogenation of propylene, broad range of explosion limits, etc.

1.3 Gas Phase Catalysis

Producing propylene oxide with the techniques mentioned so far has several drawbacks. Many, if not most, of these problems can be avoided by direct epoxidation of propylene using molecular oxygen in the gas phase. Several materials were studied for their ability to oxidize propylene, either thermo- or photocatalytically [5]. In 1998, Hayashi et al. [14] reported that gold nanoparticles exhibit a very good PO selectivity (over 90 %) using a mixture of H_2/O_2. The H_2/O_2 mixture is required for *in-situ* formation of peroxo species, which are the selective oxidants enabling the epoxidation pathway. Since then, several studies have been done using this gas mixture [5], [15]–[18]. In this work, however, we will focus on direct epoxidation without the use of hydrogen and in turn attempt to modify the active site in order to favor the selective oxidizing species directly from molecular oxygen. The various types of catalysts will be discussed in the following sections.

1.3.1 Silver containing catalysts

Since silver was already used commercially to produce ethylene oxide, it was also a starting point for research in propylene oxidation. It was discovered early on that silver preferentially oxidizes the allylic hydrogen, resulting in acrolein as the main reaction product [19]. However, direct acrolein production pathways are of little interest since this chemistry can be selectively performed over multicomponent systems containing Mo-Bi-Fe oxides.

Several studies were performed to elucidate the mechanistic principle that leads to lower PO selectivities when silver is used. Portela et al. [20] proposed that propylene adsorbs on diatomic oxygen and either desorbs as epoxide or stays bound in an open-chain form. The catalyst they used was unsupported Cr-doped Ag powder. Since total combustion and epoxidation proceed through the same intermediate, the selectivity is independent of the temperature. It is however dependent on the partial pressure of oxygen in the reaction mixture. Through intramolecular hydrogen transfer, hydroperoxides can form which leads to total propylene combustion.

Using TPD, MS and IR spectroscopy, Henriques et al. [21] showed that the selectivity towards epoxides (ethylene/propylene) can be increased by reducing the amount of surface-bound oxygen. When comparing two unsupported silver-based catalysts, they showed that the higher selectivity comes not from increased epoxide production, but from decreased CO_2 production. The decomposition of the epoxides proceeds through formate and acetate intermediates.

To improve the selectivity of the Ag-based catalysts, Lu and Zuo [22] tried modifying the catalyst with NaCl, $BaCl_2$, LiCl, or NH_4Cl. The highest improvement in PO yield was achieved by NaCl and $BaCl_2$ modification. With the NaCl-modified catalyst, the best results achieved were at approximately 3.8 wt % with selectivity of 33.4 % at a conversion of 18.6 %, at 350 °C (Table 1). These results were achieved at a relative air concentration of 90 % (10 % propylene). Further increases in air concentration lead to a significantly lower PO selectivity (10 % at 350 °C).

Table 1: Effect of a chlorine promoter on the efficiency of a silver catalyst [22].

Catalyst[1]		Temperature [°C]				
		250	280	310	350	390
Ag-NaCl	propylene conversion [%]	2.2	4.2	7.8	18.6	29.9
	propylene oxide selectivity [%]	51.6	34.5	25	33.4	11.9
Ag-$BaCl_2$	propylene conversion [%]	2.2	3.4	5.3	24.6	30.6
	propylene oxide selectivity [%]	0	15.5	19	26.1	14.7
Ag-LiCl	propylene conversion [%]	0	2.3	5.1	8.2	14.1
	propylene oxide selectivity [%]	0	0	12.1	27.5	18
Ag-NH_4Cl	propylene conversion [%]	0.8	1.2	2.1	3.2	4.6
	propylene oxide selectivity [%]	35.8	17.1	0	0	0

[1] The loading of Cl^- in the catalyst is kept constant and the loading of NaCl in Ag-NaCl is 3.8 wt %.

Zemichael et al. [23] were investigating the effect silver metal particle size has on propylene oxide selectivity. The reaction was run with molecular oxygen at atmospheric pressure, and the maximum PO selectivity was achieved at 483 K. They found that increasing the potassium promotor content (1.7 % of K) in their $Ag/CaCO_3$ catalyst initially slightly decreases the silver particle size (from 70 nm to 20-40 nm). Further increasing the K loading produces a combination of smaller and larger particles. The selectivity for PO passes a maximum at K loading of 1.7 %. This indicates that for optimal PO selectivity, the promoted silver particles should be in the range of 20–40 nm.

The electronic properties of silver have a significant impact on the selectivity in propylene epoxidation. For that reason Lu et al. [24] prepared an unsupported modified silver catalyst. For comparison purposes they also prepared Ag_2O, AgCl, and pure Ag modified with several sodium and potassium salts. The reaction was run at atmospheric pressure and at 350 °C, except for the NaF-modified catalyst. They found that pure silver is the most active (32.5 % conversion), but only the NaCl-modified catalyst produced perceptible amounts of PO (29.1 % PO selectivity) (Table 2). Modifying the catalyst with NaF significantly increased the activity (40 % conversion at 250 °C) but lowered the selectivity (3.3 % PO selectivity). Using different potassium salts had a small impact on activity, but gave no increase in PO selectivity (0.9 % PO selectivity).

Table 2: Propylene epoxidation over silver catalysts modified with different promoters [24].

Catalyst[1]	Propylene conversion [%]	Selectivity [%]	
		Epoxide	Acetone
NaF/Ag[2]	40	3.3	–
NaCl/Ag	11.2	29.1	2.1
NaBr/Ag	2.4	12.1	–
KF/Ag	10.7	0.9	–
KCl/Ag	6.2	–	–
KBr/Ag	3.5	–2.9	–

[1]Promoter loading: 5wt %.

[2]Reaction temperature: 250 °C. All other experiments were performed at 350 °C.

Luo et al. [25] modified unsupported silver catalysts with metal chlorides to alter the nucleophilic properties of the oxygen species. The catalytic tests were run at atmospheric pressure and 350 °C, with air as the oxidant. From the several chlorides they tested (Cu, Fe, Mn, Au) only the CuCl modified catalyst showed any PO selectivity (30.6 %). Modifying the catalyst even with smaller amounts (less than 10 %) of copper chloride led to a significant drop in activity compared to pure Ag catalysts (33.2 % $\Longrightarrow$ 1.85 %). However, for optimal PO selectivity, the molar ratio of Ag/CuCl should be 1/0.5 or above. During the synthesis procedure also some AgCl and CuO were formed which could aid in propylene epoxidation.

Modification of the active sites (Ag) by MoO_3 was investigated by Jin et al. [26]. The catalytic reaction was run at 400 and 450 °C. They used a stainless steel reactor with 15.6 % C_3H_6, 12.2 % O_2 and balance N_2, at a slightly elevated pressure (140 kPa). The optimal MoO_3 wt % was found to be between 40 – 50 % (approximately 60 % PO selectivity). The optimal catalyst was further modified with several salts (NaCl, $Ce(NO_3)_3$, $BaCl_2$ or $CsNO_3$), where NaCl and $Ce(NO_3)_3$ were the best at increasing the PO selectivity. Overall, the best results were achieved with 50 wt % of MoO_3 and 2 % of NaCl. Increasing the calcination temperature by 50 °C can increase the PO selectivity by as much as 47 % (catalyst modified with $BaCl_2$), but lowers the conversion.

Wang et al. [27] studied epoxidation in air with co-feeding of hydrogen gas. Using a Ag/TS-1 catalyst and a H_2/O_2 gas mixture, they wanted to generate H_2O_2 *in-situ*, which would greatly improve the PO yield. The reaction was run in a fixed-bed, quartz glass reactor at 150 °C. An impressive selectivity of 92.51 % was achieved; however, the conversion was only 1.37 %. The optimum nominal silver loading was 2 % with a silica to titania ratio of 64 for the TS-1 support. When they tried to increase the conversion, either by increasing the temperature, decreasing the gas hourly space velocity (GHSV), increasing the H_2 concentration in the feed gas, the selectivity dropped off precipitously. The conclusion was that a higher Ag^0 content does not help increase the PO selectivity.

Lu et al. [28] synthesized modified silver catalysts, with alkali and precious metal promoters, supported on $CaCO_3$. Besides the latter, they tested several other supports such as MgO, CeO_2, γ-Al_2O_3, diamond, and SiC, however $CaCO_3$ loaded with 56 wt % Ag, showed the highest PO selectivity. In general, high surface area supports gave a lower selectivity than those with a lower specific surface area. This indicates that larger silver particles favor PO formation. The catalyst was further modified with 1 wt % of various salts and tested in the catalytic reaction at 260 °C (Table 3). From all the promotors tested, only NaCl showed any noticeable increase in PO selectivity. KCl also showed a small increase in selectivity, but was significantly outperformed by NaCl.

Table 3: Propylene epoxidation over silver catalysts modified with different promoters [28].

Catalyst	Propylene conversion [%]	Selectivity [%]	
		PO	Acrolein
Ag(14)–MoO_3(1)/$CaCO_3$	46.3	4.8	0
Ag(56)–Cu(0.04)/$CaCO_3$	41.8	2.5	0
Ag(56)–$Ce(NO_3)_3$(1)/$CaCO_3$	20.8	3.6	0
Ag(56)–$Ba(NO_3)_2$(1)/$CaCO_3$	17.5	4.2	0

Ag(56)–Ir(0.12)/$CaCO_3$	5.1	2.8	0.3
Ag(56)–K_2CO_3(1)/$CaCO_3$	4.4	3.6	0
Ag(14)–K_2CO_3(1)/$CaCO_3$	3.9	3.9	0
Ag(56)–Ir(0.12)/$CaCO_3$[1]	2.9	0	27.9
Ag(14)–$RhCl_3$(1)/$CaCO_3$	1	0	22.7
Ag(56)–NaCl(1)/$CaCO_3$	1.4	39.2	0
Ag(56)–NaCl(1)/$CaCO_3$(5)–α-Al_2O_3	3.3	30.4	0
Ag(56)–NaCl(1)/α-Al_2O_3	4.4	30.1	0
Ag(56)–KCl(1)/$CaCO_3$	1.4	15.3	0
Ag(56)–NaCl(1)/CeO_2	3.2	13.4	0
Ag(14)–NaCl(1)/$CaCO_3$	1.6	7.5	0
Ag(56)–NaCl(1)/SiC	1.7	5.2	0

[1]Prior to reaction, the catalyst was reduced in 20 mol % H_2 in He at 350 °C for 2 h.

DFT studies on Cu(111) and Ag(111) surfaces performed by Torres et al. [29] have shown that the reaction of propylene with adsorbed oxygen can either lead to dehydration and total combustion, or to an intermediary, the oxametallacycle (OMC). They found that propylene adsorption orientation is an important factor in PO selectivity. By using rate constants which were derived from transition-state theory, they estimated PO selectivity. On Ag(111), at 227 °C, around 99 % of propylene molecules that adsorb to the surface will undergo allylic hydrogen stripping (AHS). On Cu(111), the situation is very different, and the predicted PO selectivity is over 50 %. This significant difference was attributed to the contrast in the basic character of the adsorbed oxygen species between Ag and Cu. The lower basicity on the copper surface favors oxametallacycle formation.

Bere et al. [30] tested separate feeding of reactant gasses using an α-alumina membrane reactor. Propylene, N_2, and H_2O were fed through the inner, alumina tube, while O_2 and additional N_2 were fed into the outer stainless steel tube. Water was added since its steam can decrease the desorption energy of PO. The catalyst used was a Ag-Sr bimetal, impregnated into the pores of the alumina membrane, and the reaction was run at 240 °C (Figure 8). At lower catalyst loadings, the yield of PO was 3.7 %, however with increased metal content, the yield dropped due to combustion. A similar observation was noted, as by other researchers, that increasing the temperature does increase propylene conversion, but lowers PO selectivity. Separate gas sampling showed that most PO is found in the flow from the inner tube, however about 25 % can also be found in the outer tube. In the optimized system, propylene conversion was 6.5 %, with a PO selectivity of 57.4 %.

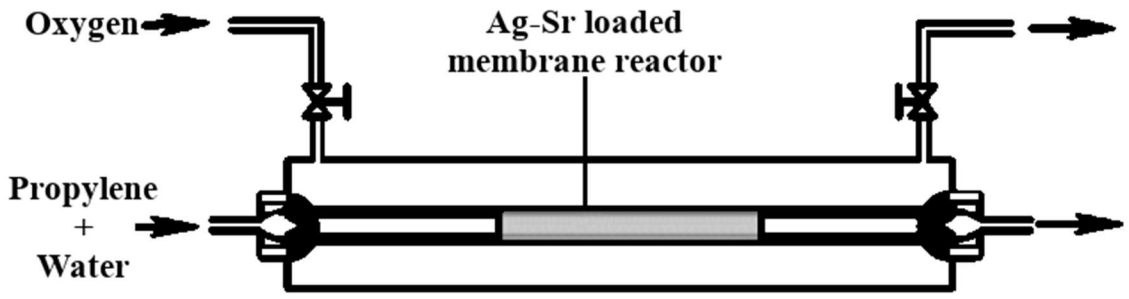

Figure 8: Schematic representation of the porous membrane reactor used by Bere et al. [30].

Yao et al. [31] studied the promotional effect of Y_2O_3 on Ag supported on α-Al_2O_3 catalysts, and the effect of support surface area. The catalytic reaction was run at 200 – 300 °C in a stainless steel fixed-bed reactor. Over the unmodified catalyst, no oxygenates were detected, only CO_2 and H_2O. When adding 0.1 % of K_2O to the catalyst, PO selectivity increased to 4.3 %, which was drastically increased (46.8 %) when Y_2O_3 was added. The temperature effect was similar to what was already observed in the literature, optimum selectivity was achieved at 245 °C (46.8 %) and dropped off drastically at 285 °C (6.7 %). The surface area of the support also played a key role in selectivity. If the specific surface area was 0.6 m^2/g, the selectivity for PO was only 19.1 %, whereas at 3.2 m^2/g, it increased to 45.5 %. They concluded that Y_2O_3 does not only change the basic properties of the active oxygen species, but also acts as a sintering barrier, preventing the agglomeration of Ag.

To see the size effect of silver nanoparticles on propylene oxide selectivity, Lei et al. [32] synthesized trimeric silver species and ~3.5 nm clusters on amorphous alumina films. On the silver trimers, up to 60 °C, acrolein was the primary product, with some PO. At 60 °C total combustion began with lowered acrolein selectivity. This indicates total combustion shares the same pathway as acrolein production, or that acrolein reacts further to CO_2 and H_2O. Catalysis over nanoparticles differs noticeably, since PO is the major product up to 130 °C. The normalized activity per surface Ag atom remains very close to that of timers (~1 s^{-1}). To illuminate the reason for the shift in selectivity, the authors performed DFT analysis. They found that the oxygen at the interface of silver and alumina is highly reactive. Reducing particle size increases the amount of this reactive oxygen which leads to allylic hydrogen abstraction and total combustion.

In order to prevent Ag sintering and reduce the reactivity of surface oxygen, Zheng et al. [33] modified Ag catalysts with Cu. They used $BaCO_3$ as the support, and loaded it with 3 % of Ag, the ratio of Ag : Cu was 95 : 5. The selectivity towards PO increased 5-fold with Cu modification and lowered when other metals were used (Fe, Co, Ni, Mn, Mo, V, and Zn). If the Cu content was 5 times lower, the selectivity for PO dropped by more than 50 %, and if the content was increased 4 times, the selectivity dropped by more than 70 %. Stability test showed that after 6 h of time on stream (TOS), the catalyst retained only ~40 % of initial activity, however PO selectivity remained stable. Using ICP-AES and XPS, the authors found that Cu enrichment of the surface is present in the catalysts. The surface ratio of Ag : Cu was 3.8 : 1.4, whereas bulk composition was 95 : 5.

Pulido et al. [34] investigated direct propylene oxidation with molecular oxygen with single-crystal Ag(100) and Ag(111) catalysts. They found that the most stable location for oxygen atoms on a clean Ag(100) is in hollow sites, where it is coordinated to four Ag atoms. On a clean Ag(111) surface, the most stable site is on threefold coordinated *fcc* hollow sites. This results in much smaller Ag-O interaction energies on the latter surface than on Ag(100). Looking at the activation barriers (AB) for OMC formation showed an energy requirement of 75 kJ/mol on the Ag(111) surface. The same AB is 20 kJ/mol lower on the Ag(100) surface. Theoretical results indicate that total oxidation is the preferred pathway regardless of the surface crystal plane. Nevertheless, propylene oxide and other oxygenates are produced with a higher selectivity on the Ag(100) surface. This was also supported by catalytic tests, where the allylic route was favored on the Ag(111) catalyst, and formation of PO and other oxygenates was observed over the Ag(100) surface.

While Cheng et al. [35] investigated nanocrystalline diamond-supported silver aggregates, they found no measurable activity for propylene epoxidation. This indicates that the metal-oxide interface sites are necessary for any measurable activity. Looking at unsupported Ag_{19} and Ag_{20} clusters and alumina-supported Ag_{19} showed that barriers for oxygen dissociation are small compared to that on crystalline surfaces (Figure 9). Additionally, the dissociation is favored at the interfacial sites. These two facts are likely

the reason nanoparticles are more active than crystalline silver. After dissociation, the oxygen on the Ag particle is more likely to epoxidize propylene, while the one on the support is likely to produce acrolein or combustion. Oxygen atoms at the metal-oxide interface are also more selective in epoxidation than the atoms on top of the Ag nanoparticle. The results presented by the authors are in good correlation with those reported previously by Lei et al. [32].

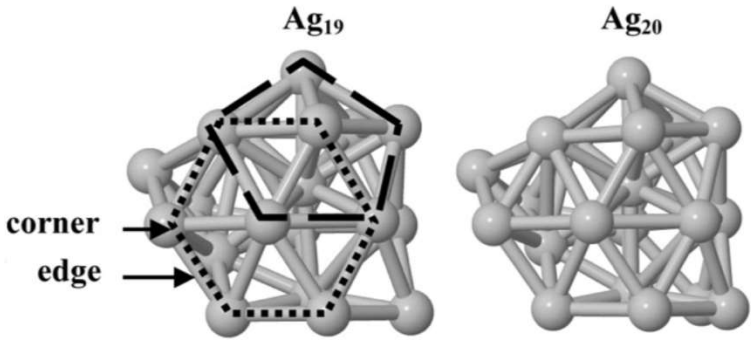

Figure 9: Ag_{19} and Ag_{20} clusters investigated by Cheng et al. Reproduced with permission from Ref. [35]. Copyright 2013 American Chemical Society.

Ghosh et al. [36] synthesized highly dispersed silver nanoparticles (2-5 nm) on WO_3 nanorods. The catalysts were highly active (15.5 % propylene conversion) and selective (83 % PO selectivity) in the propylene epoxidation reaction using molecular oxygen. They tested other supports such as Cr_2O_3 and MoO_3, and also Cu on tungsten oxide; however Ag/WO_3 outperformed all the others. The catalyst was very poor in propylene selective oxidation at atmospheric pressure and temperatures below 150 °C. Increasing both parameters significantly improved the yield of PO, where other oxygenates and CO_2 were detected only as side products. Increasing the temperature from 200 to 400 °C increased the propylene conversion from 9 % to 27 %, accompanied by a drop in selectivity from 91 % to 54 %. At a pressure of 1 MPa, the conversion was ∼7 % and the selectivity 39 %. At 3-4 MPa, the conversion (∼25 %) increased but, again, at the expense of selectivity (55 % PO selectivity). Optimal conditions were achieved at a temperature of 250 °C and a pressure of 2 MPa.

Lee et al. [37] modified Ag catalysts with an increasing Mo content. It was confirmed by XRD that some separate molybdenum phase was formed during synthesis, but the actual metal composition was very similar to the nominal. XPS analysis of the samples showed an increase in binding energy of the Ag 3d orbital. This stunts electron flow from the silver atom to the adsorbed oxygen, reducing its nucleophilic character. The reduced negative charge prevents total oxidation of adsorbed propylene or other preformed oxygenates. During the catalytic tests, PO selectivity correlated very well with the shift in binding energy. The selectivity also showed a high dependence on the Mo loading, which also correlated well with the results of XPS. At the optimal composition propylene conversion was ∼12.5 %, and PO selectivity was approximately 60 %. Catalysts remained mostly stable 6 h of TOS, and the optimal composition was reusable for another cycle of catalysis.

A series of core-shell, Ni-Ag/SBA-15 catalysts were synthesized by Yu et al. [38]. With this composition the authors expected an isomorphic effect, a contraction of the silver lattice parameter due to the presence of Ni. Nickel has the same *fcc* crystal structure but with a smaller lattice parameter. However, the opposite effect was observed by EXAFS, the Ag-Ag interatomic distance increased. Fitting of the Ag K-edge gave a coordination of 8 which is expected with small particles with a lot of surface un-coordinated sites. This

was attributed to a tremendously high ratio of surface to bulk silver atoms, since surface atoms are loosely packed. Fitting of the Ni K-edge gave a coordination of 10-11, when taking into account the Ni-Ag pairs. These results indicate that Ni is in a quasi-bulk-like position where the surface Ni atoms are in close contact with Ag atoms. With an optimal composition of $Ni_1Ag_{0.4}$/SBA-15 the core-shell catalysts exhibited excellent stability even after 10 h of TOS. The selectivity of the latter was over 70 %, however propylene conversion was under 1 %.

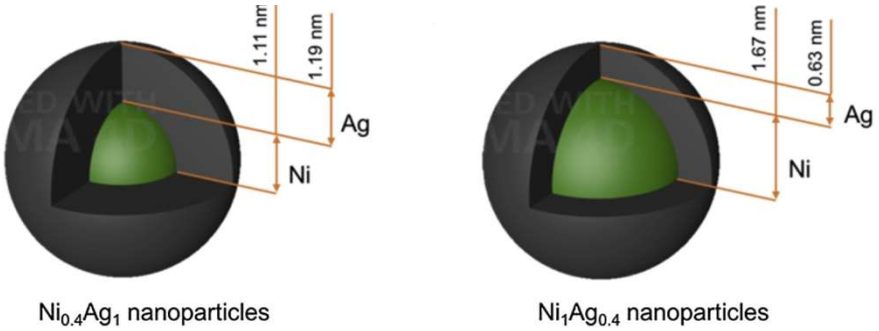

Figure 10: Schematic representation of Ni-Ag core-shell catalysts used by Yu et al. Reproduced with permission from Ref. [38]. Copyright 2018 Elsevier B.V.

Lanthanide oxides were examined as possible supports for Ag nanocubes and nanospheres. Yu et al. [39] tested La, Gd, Eu, Yb, and Lu oxides supports, and compared them to a commercial Al_2O_3. From the tested materials, silver supported on Yb_2O_3 and Lu_2O_3 produced no PO, while the other three supports all outperformed the commercial Al_2O_3. At the reaction temperature 270 °C, La_2O_3-supported silver nanocubes showed the highest propylene oxide yield with 51 % PO selectivity. The PO production rate was ~6-fold higher than the alumina-supported catalyst and ~100-fold higher than over La_2O_3-supported nanospheres. To elucidate the properties that enable such a high PO production rate, some DFT calculations were performed. The polar surface of La_2O_3 decomposes molecular oxygen, which then migrates to the Ag(100) plane of the nanocube. This forms electrophilic atomic adsorbed oxygen which reacts with propylene to form the oxametallacycle intermediate. A lower combustion and AHS rates are likely due to longer interatomic distances of the Ag(100) surface which stunts the reaction of adsorbed oxygen with the allylic hydrogen.

In summary, Portela et al. [20] found that partial pressure of oxygen contributes strongly to selectivity for PO, observed also by Henriques et al. [21], and Lu and Zuo [22]. In general, increasing oxygen content in the reaction mixture increases the conversion at the expense of selectivity for PO. This is most likely due to further combustion of the latter. Epoxidation is also very sensitive to temperature. Increasing it in all cases also increases propylene conversion, but is always accompanied by a decrease in PO selectivity. Lei et al. [32] found that highly dispersed silver particles prefer allylic hydrogen stripping, since the interfacial oxygen is more reactive and preferentially produces acrolein. A similar observation was noted by Cheng et al. [35] on Ag nanoparticles. Zemichael et al. [23] reported that the optimal silver particle size for epoxidation is between 20 and 40 nm. Modification of the Ag nanoparticles with other metals has shown to increase PO selectivity. Lu et al. [24] showed that the cation and anion part of the alkali salt used for catalyst modification affect the selectivity. Several other researchers noted a similar effect. Luo et al. [25] reported that catalyst modification by CuCl increased PO selectivity, while some other chlorides (Fe, Mn, Au) do not. Jin et al. [26] indicated that even modification by metal oxides such as MoO_3 can increase PO selectivity. Yao et al. [40] noted a similar

effect due to catalyst modification with Y_2O_3, while also reporting a reduction in catalysts sintering. Bere et al. [30] used an engineering approach to increase PO selectivity by using a membrane reactor to separate the reactants. They noted an increase in PO selectivity which indicates that further combustion of oxygenates is an issue. Ghosh et al. [36] found that selectivity over Ag/WO_3 increased with increased pressure, with the optimum at 2 MPa. Most of the research on propylene epoxidation agrees that the OMC is a necessary intermediate for PO formation. Pulido et al. [34] found that the exposed crystal plane of Ag affects the active oxygen species and the activation barrier for OMC formation. Work done by Lee [37] showed that Mo modification of the catalysts reduces the negative charge on oxygen and promotes OMC formation over AHS. Yu et al. [38] discovered that core shell Ni-Ag nanoparticles also show increased PO selectivity, due to altered electronic properties of the surface silver atoms. In their work, Yu et al. [39] proved that some lanthanide oxide supports decompose oxygen and produce electrophilic oxygen species. These favor OMC formation and increase PO selectivity.

1.3.2 Copper-containing catalysts

Copper, among other transition metal catalysts, has been extensively tested in propylene oxidation with molecular oxygen. The studies were focused more on acrolein and CO_2 pathways [41]–[46], and propylene oxide was rarely mentioned as a co-product [47]–[50]. The prevailing theory was that PO is formed by homogeneous reactions in the post-catalytic space [47], [48].

Daniel and Keulks [48] tested several bimetallic (Cu-Mo, Fe-Mo, and Mn-Mo) oxide catalysts and found PO as a co-product in all cases. The allyl radical reacts with the surface-bound oxygen, to produce allyl peroxide radicals or hydroperoxides. Although, a reaction of a free radical species with gas phase oxygen is also possible. The authors suggested that propylene oxide most likely forms from homogeneous reactions on the surface of the catalyst. The peroxide/hydroperoxide or a hydroxyl radical species, formed as a degradation product, reacts with propylene. All of the mentioned catalysts also produce acrolein, which is formed after allylic hydrogen abstraction. It was observed that packing the post-catalytic space with quartz wool increased acrolein yield. This suggests homogeneous reactions of oxygenates (formed over the catalyst) with oxygen to produce CO, CO_2, and water.

Abstraction of the allylic hydrogen that leads to acrolein production could not be studied under low pressure conditions, since the adsorption enthalpy for propylene is very low. To avoid this issue styrene was used to study alkene epoxidation [51]. Vaughan et al. [52] prepared simplistic Cu/SiO_2 catalysts and tested them in propylene epoxidation. Two different synthesis techniques were used to produce smaller and larger copper particles. Adding hydrogen gas to the reaction had no effect on selectivity or conversion for any of the catalysts. With differential tests, where propylene and acrolein were fed into the reactor, the authors wanted to determine why PO production drops off with increasing temperature. They found that in the absence of oxygen, copper can isomerize PO to propanal. The latter can undergo oxidative dehydrogenation to acrolein. In the tested catalysts, a NaCl promotor actually had a detrimental effect on PO selectivity. The authors concluded that the active phase is a highly dispersed form of metallic copper that achieves high selectivity (53 %) at low conversions (0.25 %).

Wang et al. [53] tested several transition metals, dispersed over SBA-15, modified with different alkali and alkaline earth salts. The catalysts (Ti, V, Cr, Mn, Fe, Co, Ni, Cu, Zn, Mo, W, Ag, and Au) were prepared by incipient wetness impregnation with a metal loading of 1 wt %. Among all the catalysts, copper exhibited the highest conversion of propylene with low selectivity for PO. Modification with group 1 metals decreased the activity in all catalysts, regardless of the metal, while group 2 metals had minimal effect on the activity. The best ratio between activity and selectivity was achieved when potassium was used as the modifying adatom. Several K^+ salts were further used to modify the CuO_x/SBA-15 catalyst such as KAc, KOH, KCl, K_2CO_3, and others. The highest PO selectivity achieved was 59 % at 0.4 % conversion, at 225 °C (Table 4). However, the selectivity dropped drastically (14 % PO selectivity, 13 % C_3H_6 conversion) when the reaction temperature was increased to 350 °C.

Table 4: Reaction conditions used by Wang et al. [53]: catalyst weight, 0.20 g; partial pressures of C_3H_6 and O_2, 2.5 and 98.8 kPa, respectively; total flow rate, 60 mL min^{-1}.

Catalyst[1]	T (K)	C_3H_6 conv. (%)	Selectivity (%)				
			PO	Acrolein	Others[2]	CO	CO_2
CuO_x/SBA-15	498	0.8	6.9	41	16	11	25
	523	2.7	4.1	25	6	14	51
	548	6.6	1.8	21	2.9	18	56
	573	14	0.6	17	1.3	20	62
	623	33	0.1	12	0.8	26	61
K^+-CuO_x/SBA-15	498	0.4	59	8.7	3.5	4.2	24
	523	1	46	6.4	1.9	5.5	40
	548	2.1	35	4.9	1.1	9.1	49
	573	4.7	26	4	0.7	10	60
	598	7.2	20	3.4	0.5	13	63
	623	13	14	2.9	0.3	16	67

[1]Copper content, 1.0 wt. %; K/Cu = 0.70.

[2]Other products include allyl alcohol, acetone and acetaldehyde.

Unsupported copper particles modified with vanadium showed a similar catalytic performance with a PO selectivity of 35 % at 0.78 % conversion. Yang et al. [54] found that the modification also increases copper dispersion from 0.48 % to 4.7 %. The selectivity for PO does not correlate with the increased dispersion but follows a bell curve, where the optimal V/Cu ratio is between 0.11-0.20. This indicates that the increase in Cu surface area could not account for higher PO yield. Additionally, the authors observed a gradual oxidation of the metallic copper to Cu^+. This indicates that for propylene epoxidation using molecular oxygen, copper should be oxidized to Cu_2O. Finally, with C_3H_6- TPR and H_2-TPR a reduction in the reactivity of the surface oxygen species was noted. Nucleophilic oxygen quickly reacts with the allylic hydrogen to produce acrolein. Vanadium modification changes these species from nucleophilic to electrophilic, which gives rise to higher PO selectivity.

He et al. [55] synthesized CuO_x/SiO_2 catalysts and modified them Cs^+. The primary products over the unmodified catalysts were PO, acrolein and CO_x, allyl alcohol is a product of PO isomerization. Increased contact time decreased the selectivity for PO and acrolein and increased the selectivity for CO_x, indicating that both propylene oxygenates can easily combust. With the Cs modification, the selectivity for PO was increased by 3-fold, to 65 %. Longer residence times also resulted in higher selectivity towards CO_x, but a lower selectivity towards allyl alcohol. This indicates that Cs^+ modification also inhibits the isomerization of PO. It also lowers the overall acidity of the synthesized catalysts, and alters the redox properties of the copper phase. The authors postulated that the decrease in acidity is what inhibits further isomerization of PO to other oxygenates. The lower reducibility also hinted at a decreased reactivity of the lattice oxygen, which prevents allylic hydrogen abstraction (Figure 11). Nevertheless, both propylene oxide and acrolein were formed simultaneously, even on the modified catalyst.

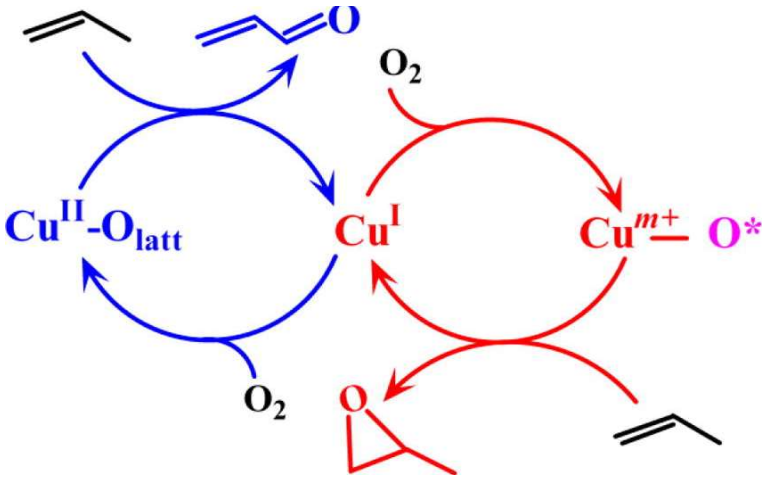

Figure 11: Reaction mechanism for the formations of primary products over the CuO_x/SiO_2 catalysts proposed by He et al. Reproduced with permission from Ref. [55]. Copyright 2012 Elsevier Inc.

Marimuthu et al. [56] studied copper oxidation state switching by localized surface plasmon resonance. The catalysts used were supported Cu nanoparticles on a silica matrix. They found that in purely thermal conditions, the selectivity for propylene oxide remained below 20 %. Under photothermal conditions, with low light intensity (<550 mW/cm^2) there was minimal change in the selectivity. However, once 550 mW/cm^2 were reached, the selectivity increased ~2.5-fold. Under the epoxidation conditions, the copper nanoparticles immediately oxidized, and formed a Cu_2O shell. With the help of XRD and UV-vis extinction analyses, the sudden rise in PO selectivity was attributed to a reduction of the Cu_2O shell on the nanoparticles. The reduction is mediated by radiative energy injection from the metallic core to the oxide shell. The energy facilitates an enhanced rate of electron transfer from the valence to the conductive band of the Cu_2O semiconductor. This weakens the Cu-O chemical bonds and eases the removal of the surface oxygen species. Increasing light intensity to the threshold (550 mW), and above, is accompanied by an increase in CO_2 selectivity as a result of total combustion of propylene oxygenates.

On the other hand, Kalyoncu et al. [57] tested a $CuO\text{-}RuO_2$ binary oxide catalyst with and without NaCl promotion, and found that a combination of Cu^+ and $Ru^{+\delta}$ is the selective phase. They tested several silica supports along with several Cu : Ru : Na combinations. The best performance is achieved by the 2 wt % Cu and 5 wt % Ru on commercial SiO_2 modified by 1.75 wt % NaCl. The catalyst achieved a PO selectivity of 35.6 % at 9.4 % propylene conversion. Interestingly, they only observed 8.1 % selectivity for PO, when potassium acetate was used as the modifying salt (Figure 12). The salt modification increases the PO selectivity while simultaneously decreasing the conversion of propylene. The authors proposed that the binary system retards the total reduction of the metal oxides. Modification with NaCl does cover some active sites, but alters the properties of the surface-bound oxygen species, evident from CO adsorption Fourier-transform infrared spectroscopy (FTIR) studies.

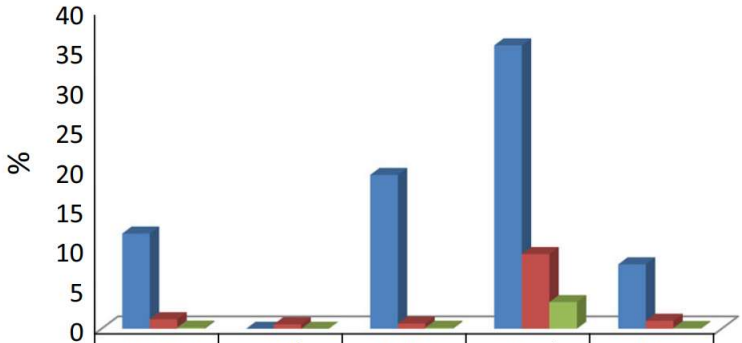

	NaNO3	LiCl	KNO3	NaCl	KAc
PO selectivity	11.97	0	19.30	35.60	8.10
Propylene Conversion	1.19	0.56	0.66	9.40	1.00
PO Yield	0.14	0	0.13	3.35	0.08

Figure 12: Catalytic performance of the 2 wt % Cu and 5 wt % Ru on commercial SiO_2 catalyst modified by different alkaline metal salts (GHSV = 20,000 h^{-1}, gas composition: C_3H_6 : O_2 = 1:2, T = 300 °C). Reproduced with permission from Ref. [57]. Copyright Springer Science+Business Media New York 2014.

A similar observation regarding copper (I) oxide has been observed by Yang et al. [58]. The authors prepared a $TiCuO_x$ on a Cu(111) surface to stabilize copper in the Cu^+ oxidation state. With high resolution electron energy loss spectroscopy (HREELS) supported by DFT analysis, they confirmed the presence of the propylene oxametallacycle on the surface of $TiCuO_x$. The peaks assigned to OMC binding were not observed on either the Cu(111) or Cu_2O. From the TPD analysis, where propylene and O_2 were co-exposed to the catalyst, the calculated PO selectivity was 69 %. The Cu^+ in the $TiCuO_x$ phase was not reduced during CO adsorption studies, which indicates a lessened reactivity (nucleophilicity/basicity) of the surface oxygen species. The combined analyses (TPD, XPS, and HREELS) performed showed that PO chemisorbs to the surface of the synthesized catalyst. More importantly, it desorbs as propylene oxide, the epoxide ring closes and no isomerization takes place. This is not the case when the surface is either Cu(111) or Cu_2O.

Song and Wang [59] used DFT analysis to study the different oxygen species (O^{2-}, O^-, and O_2^-) found on the $Cu_2O(111)$ catalyst (Figure 13). The most active species is the surface-bound O^-. For this species, the activation barriers (AB) for the transition states that lead to OMC formation are significantly higher than those for AHS, which leads to acrolein formation. The most selective species is the surface-bound O_2^-. It is less active than the O^- species, but more than the lattice O^{2-}. The AB for the transition states that lead to OMC formation are similar to those for AHS, which indicates PO is a likely product. With lattice O^{2-}, the AB for the ring closing step that leads from OMC to adsorbed propylene oxide are too high to give any noticeable PO selectivity. With a proton probe analysis the authors found that the binding strength of the H-atom is −0.80, −1.60, and −0.37 eV for the O_2^-, O^-, and O^{2-} species, respectively. From these results it is evident that the basicity of O^- is pointedly higher than for the other two species.

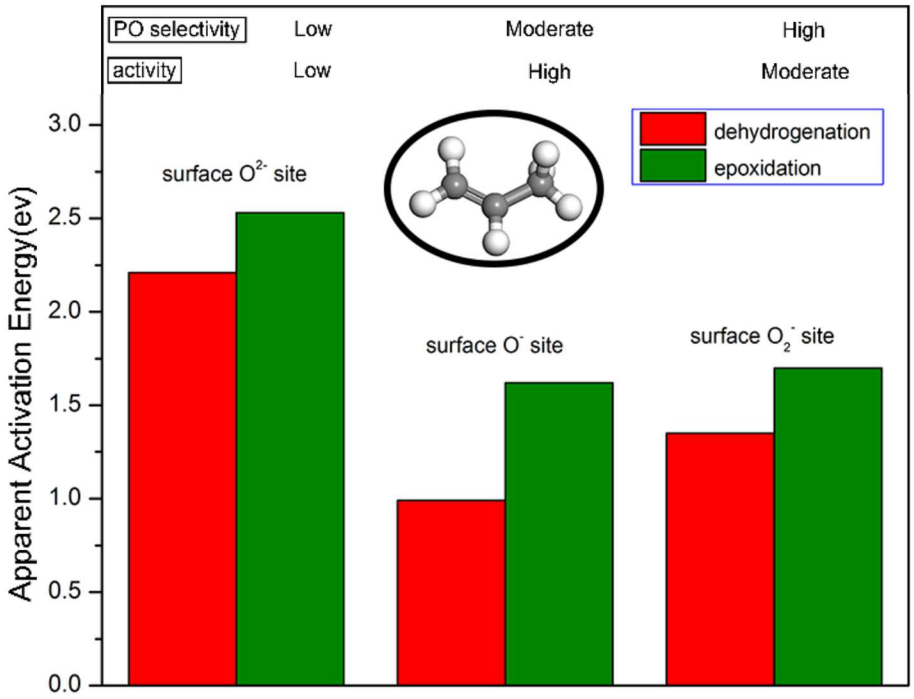

Figure 13: Analysis of energetic span model with surface O^{2-}, O^{-}, and O_2^{-} species on $Cu_2O(111)$. Reproduced with permission from Ref. [59]. Copyright 2018 American Chemical Society.

Diekmann et al. [60] studied the effect of copper oxide particle size on propylene oxide selectivity. They prepared catalysts with an increasing copper loading from 1.1 % up to 19.4 % using SBA-15 as the support. Increasing the loading also increased the particle size, but no crystalline copper was detected in the catalysts. The copper atoms were in octahedral (CuO_6) coordination with some tetragonal distortion. All the tested catalysts produced acrolein as well as PO. The selectivity for acrolein was much higher than that for PO. The selectivity for the latter exhibited a nearly linear correlation with the amount of bridging oxygen atoms (Cu^{2+}-O^{2-}-Cu^{2+}). These species, identified and relatively quantified by UV-Vis-DR, increased with increasing copper loading. Larger copper oxide particles give higher PO selectivity whereas acrolein selectivity was independent of copper loading. Increasing the size of copper particles increased the availability of bridging (electrophilic) oxygen species selective for propylene epoxidation.

To conclude, Vaughan et al. [52] found that copper oxide can isomerize PO to other oxygenates, thus lowering the apparent selectivity. They additionally postulated that dispersed copper, and not the larger copper oxide crystallites, is the active site for propylene epoxidation. Wang et al. [53] found that the low PO selectivity of pure copper oxide on a silica support can be increased by modification with potassium. Yang et al. [54] modified the metallic Cu catalysts with V and witnessed a gradual oxidation to Cu^{+}. They assume this is the selective oxidation state for PO. They additionally saw a reduction in the nucleophilicity of the surface oxygen species as a result of the modification. A similar observation was noted by He et al. [55] with Cs^{+} modified catalysts. Lower reducibility of the catalysts indicated a lower reactivity, and consequentially a higher PO selectivity for the modified catalysts. The authors also saw a decrease in surface acidity, which they assumed lowers the amount of PO that isomerizes to other oxygenates. They also found that increased contact time increases the selectivity for CO_x as a result of total oxidation of oxygenates. Yang et al. [58] prepared $TiCuO_x$ species to prevent the oxidation or reduction of Cu^{+} sites. As in other publications, they noted a decrease in surface oxygen

basicity/nucleophilicity, which leads to higher PO yields. A similar thing was reported by Kalyoncu [57] et al. with their NaCl-modified CuO-RuO_2 catalysts. The bimetallic nature prevented total reduction, while NaCl modification alters the electronic properties of the active sites. Marimuthu et al. [56], on the other hand, found that metallic copper gave a higher PO selectivity. They used the localized surface plasmon resonance effect to keep copper reduced. However, the mechanism of plasmon-mediated epoxidation reaction could be very different compared to regular photocatalytic one, explaining the relevance of metallic Cu for PO selectivity. Using DFT, Song et al. [59] calculated activation barriers for OMC formation and ring closure for different reactive oxygen species. They found that O_2^- is the most selective species for PO formation. The O^- species is the most reactive and favors AHS, and O^{2-} has a high activation barrier for ring closure. Diekmann et al. [60] found that increasing copper loading increases the amount of bridging Cu-O-Cu species. These have an electrophilic oxygen which is selective for PO formation.

1.3.3 Various catalysts

Besides copper- and silver-based materials, several other catalysts have been tested for the direct propylene oxidation reaction. Combinatorial studies performed on several metals [61] showed that there are several potential candidates for propylene epoxidation.

Yoshida et al. [62] tested the photocatalytic capability of pure silica and MgO-loaded silica, in the selective propylene oxidation reaction. They found that even pure silica shows some selective photooxidation to acetaldehyde and propylene oxide. The silica used was prepared by evacuation at high temperatures (800 °C), which produced coordinatively unsaturated silica sites. The addition of magnesium promoted the yield of all oxygenates. Regardless of the loading technique (chemisorption of incipient wetness impregnation), the catalysts with a lowest MgO loading (1 %) exhibited the highest PO selectivity. The sites that promote PO selectivity are highly dispersed, tetrahedrally coordinated Mg sites. MgO crystallites or islands mostly promote the oxidation to acetaldehyde.

A similar observation was noted by Yoshida et al. [63] with highly dispersed titania on silica. TiO_2 is a well-known photocatalyst, very active under UV-light illumination. The reaction was carried out in batch mode, in a closed quartz vessel. Bulk TiO_2 showed very good conversion of propylene (14.1 %) even after 1 h of irradiation, but the main product was CO_x (96.2 %, Table 5). The sol-gel and the impregnation methods used to prepare the catalyst produced highly dispersed tetrahedral titania species. The catalyst prepared by sol-gel showed excellent PO selectivity (57.5 %) and conversion of propylene (9.2 %) after 2 h of irradiation. After 8 h of irradiation the catalyst prepared by impregnation gave a PO yield of 9.2 %, and no further oxidation of PO was observed.

Table 5: Results of propylene photooxidation reported by Yoshida et al. [63].

Sample	Irradiation time [h]	Propylene conversion [%]	PO yield [%]	Selectivity[2] [%]							
				PO	PA	AC	AL	AA	ALC	HC	CO_x
SiO_2	2	0.7	0.2	27.1	1.4	26.7	8.9	16.8	6	8.8	4.3
TiO_2	1	14.1	0	0	0	1.3	0	0.8	0	1.7	96.2
T/S(0.1)[1]	2	9.1	3.7	40.8	3.3	11.3	4.2	24.5	3.6	2.3	10
T-S(0.34)[1]	2	9.2	5.3	57.5	2.7	5.8	1.2	21.1	0	5.1	6.6

[1] Number in parenthesis shows the molar % of titanium.

[2] (PO-Propylene oxide, PA-Propanal, AC-Acetone, AL-Acrolein, AA-Acetaldehyde, ALC-Alcohol, HC-Hydrocarbons, COx-CO and CO_2).

Murata et al. [64] used similar reaction conditions (a batch reactor with a 200 W Xe lamp) to see the epoxidation capability of chromium on silica. They produced highly dispersed chromate species on amorphous silica, with the impregnation method. Diffuse reflectance UV/vis results showed no absorption bands in the region above 580 nm (catalyst with 0.1 wt % Cr), which would indicate *d-d* transitions in bulk Cr_xO_y. The best performing catalyst achieved a propylene conversion of 16.7 % with a PO selectivity of 44 %, after 2h of irradiation. Using a cutoff filter had negligible effect on PO selectivity, but reduced the activity by approximately half. This shows that visible light is sufficient to epoxidize propylene to propylene oxide. Higher loading of chromium (1.5 wt %) did not increase the conversion, but did completely alter the selectivity (3.7 % PO selectivity, 61.5 % CO_x selectivity). When plotting the PO yield versus the relative photon absorption (altered by

cutoff filters), a linear correlation is observed. Excluding UV light did not affect the selectivity or the quantum yield of C_3H_6 epoxidation.

Softer oxidants than molecular oxygen were also examined. Duma and Hönicke [65] performed direct propylene epoxidation using nitrous oxide (N_2O). Several types of silica support were used, and the synthesized iron oxide nanoparticles measured less than 2 nm in diameter. All the samples were neutralized with Na acetate to reduce the acidity of the catalysts. The activity dependence on sodium loading followed a bell shape, with an optimum Na acetate concentration of 0.1 M (~70 % PO selectivity). The best support was found to have exclusively mesopores, approximately 5 nm in diameter. The selectivity for PO increased (~37 % PO selectivity) with increasing N_2O concentration up to 15 %, after that the selectivity decreased due to further oxidation of PO. As with other catalysts, with increasing temperature, the reaction rate increased, but the selectivity for PO decreased. Regeneration tests showed that some carbonaceous species bind to the catalyst and cause deactivation. Cleaning the catalysts in an oxidative atmosphere resulted in a relatively stable PO yield across 50 cycles of catalyst reuse. With TOS, the selectivity for PO steadily increased, which indicates that most active oxidation sites deactivate first. The reaction initiated by a non-dissociative adsorption of N_2O followed by a reaction with adsorbed propylene.

The exact nature of the modifying basic metal was investigated by Wang et al. [66], who investigated the effect of alkali salts on the selectivity of iron-catalyzed propylene oxidation. They also used N_2O as the oxidant and a highly dispersed iron on silica catalyst. For the FeO_x/SBA-15 catalyst used, KCl modification presented the highest PO yield. The modification increased the selectivity for PO (72 % PO selectivity) and increased the activity (4.5 % C_3H_6 conversion) of the catalyst. The authors found that the reactivity of the lattice oxygen is decreased, which suppresses AHS. Additionally, the dispersion of the iron species is enhanced, where the coordination of iron atoms is changed into a surface tetrahedral configuration. Finally, the surface acidity introduced by iron species is eliminated, which enables higher PO yields. The authors investigated further by co-modifying the catalysts with boron, and removing the halogen [67]. Boron addition further increased the selectivity (79 % PO selectivity for K^+ modification) and the activity (4.8 % C_3H_6 conversion for K^+ modification) of the catalysts, regardless of the modifying alkali adatom (K^+, R^+, or Cs^+). The drop in selectivity was less sensitive to an increase in temperature, where at 13 % propylene conversion, the PO selectivity remained at 55 %. Moens et al. [68] also used an iron catalyst modified with different alkali and alkaline earth metals. A similar conclusion was reached that both the anion and the cation are important in the modifying salt. The optimal catalyst composition in their case was 0.15 wt % Fe on silica loaded with 1.8 wt % of Rb_2SO_4. After 80 min of reaction, this catalyst achieved a propylene conversion of 16.8 % and a PO selectivity of 59 %. The selective sites were highly dispersed iron species in a distorted tetrahedral coordination. When the iron content was increased, it led to the formation of larger Fe_xO_y species which favor deep oxidation of propylene. If PO was fed into the reactor, pure silica isomerized it completely to other oxygenates (acrolein, propanal, and acetaldehyde). This was significantly reduced by Rb_2SO_4 addition (only 28.9 % PO conversion), likely due to the neutralization of acid sites.

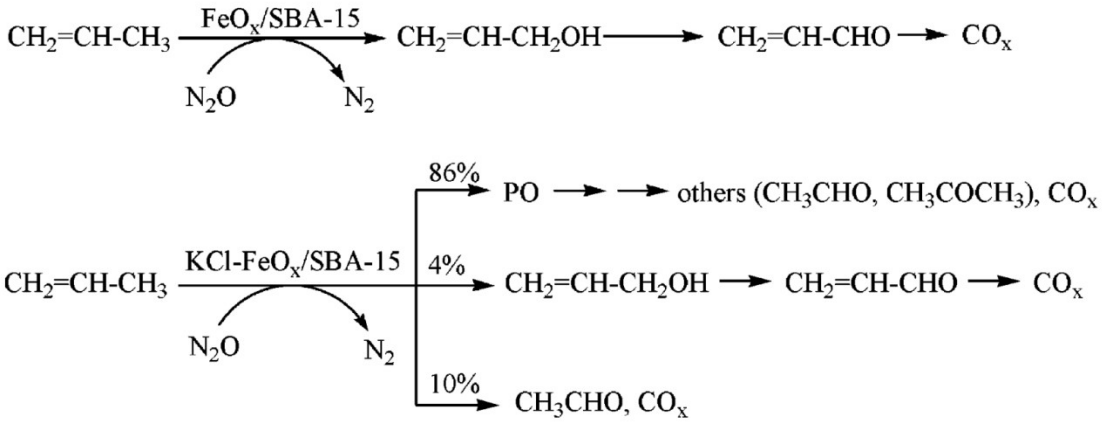

Figure 14: Reaction pathways for the oxidation of C_3H_6 over the 1 wt % FeO_x/SBA-15 with and without modification by KCl (K/Fe = 5) proposed by Wang et al. Reproduced with permission from Ref. [66]. Copyright 2005 American Chemical Society.

Lu et al. [69] used copper-vanadium bimetallic catalysts. The catalysts were subsequently modified with NaCl to boost PO selectivity. Higher valence states of copper were found to be non-selective, so H_2 was co-fed into the reactor. They worked in a flow reactor with air as the oxidant. Keeping Cu in a low valence leads to ~70 % PO selectivity and a stable catalyst for 9 h. Amano and Tanaka [70] used a pure vanadium oxide catalyst with a silica support. The catalysts were modified with several alkali metals (Li^+, Na^+, K^+, and Rb^+), but rubidium showed the highest increase in selectivity. The optimal Rb/V ratio was found to be 1.5 at 0.5 wt % vanadium loading. With this composition, the authors reported a C_3H_6 conversion of 1.39 % and a PO selectivity of 28.1 %, after 600 min of TOS (Table 6). A flow reactor was used and 10 % oxygen as the oxidant. UV/vis DR spectra of the unmodified material showed a band at approximately 400 nm assigned to ligand to metal charge transfer (LMCT) in VO_5/VO_6 species. When the Rb/V ratio was 1.0 or above, this band disappeared and PO yield increased. This indicates that the one-to-one rubidium-vanadium species are selective for PO.

Table 6: Results of photo-oxidation of propylene over Rb^+-modified silica-supported catalysts (Rb–VS) samples reported by Amano and Tanaka [70]. (V_2O_5 loading 0.5 wt %.).

Sample	Rb/V	TOS [min]	C3H6 conversion [%]	Selectivity [%]			
				PO	C_3[1]	Ethanal	CO2
VS	0	180	0.38	14	19	52	15
Rb–VS	0.5	60	0.59	28	7.7	31	33
	1	60	1.4	31	6.2	16	47
	1.5	60	1.56	31	6.8	15	47
		600	1.39	28	8.1	15	49
	3	60	1.5	19	4.6	10	66
	6	60	1.02	8.9	4.8	6.2	80
SiO2	–	180	0.01	72	0	Trace	28

[1] Oxygenated C_3 products; acrolein, acetone, and propanal.

Song et al. [71] examined molybdenum-based catalysts in a fixed bed reactor with a mixture of propylene and propane. Air was used as the oxidant, and a test was performed where NO was co-fed into the reactor. The PO produced originates from propylene, and propane only acts as an inert gas. The selectivity and the conversion were highly dependent on the reaction temperature. Increasing the temperature from 300 to 305 °C increased the conversion from 7 % to 22.9 % and lowered the PO selectivity from 28.2 % to 10.5 %. Adding NO to the reactant gasses and increasing the pressure to 4.5 atm had a significant effect on PO yield. At 300 °C, the conversion of C_3H_6 increased to 18.2 % and the selectivity lowered slightly to 24.0 %. The authors used a two-level reactor with a separately heated post-catalytic bed space. With this, they found that activity of the oxidation reaction is minimally dependent on the temperature of the catalytic bed, but very sensitive to the temperature of the post-catalytic bed space. This could indicate a formation of radicals and a possible gas-phase radical chain reaction. Pang et al. [72] modified MoO_3 catalysts with a Bi_2SiO_5 separate phase. In a flow reactor using O_2 as the oxidant, the authors achieved a conversion 21.99 % and a PO selectivity of 55.14 %. The optimal Mo/Bi ratio was found to be 5. Running the catalytic reaction for 10 h showed an increase in selectivity from ~50 % to ~56 %, which remained stable for 170 h. Catalyst activity decreased with TOS from ~23 % to ~16.5 % after 180 h. The decrease in activity was attributed to a slow agglomeration of the MoO_3 phase, and consequentially a decrease in the number of active sites. A possible synergistic effect was proposed, where the Mo phase activates propylene by stripping the allylic hydrogen. The Bismuth-containing phase activates oxygen which in turn reacts with the generated allylic radical to produce a superoxide allylic radical. The latter enters a chain reaction that ends in PO formation. To improve the stability of these catalysts, Xu et al. [73] pretreated the $Bi_xSi_{1-x}O_2$ with acid before loading it with Mo. In the catalytic reaction, they used similar conditions as Pang et al. [72]. The acid pretreatment affected the activity of the catalyst and had a negligible influence on the selectivity of the catalyst. Long term testing of the catalyst showed that in 220 h of TOS propylene conversion drops to 17.1 % from 20.2 %, at constant PO selectivity (~56 %). After regeneration in air, the catalyst regained most of its activity and had a C_3H_6 conversion of 19.2 % in the second cycle after 5 h of TOS. The catalysts were then further modified with Ti by Lei et al. [74]. This further increased the activity of the catalysts and their selectivity for PO. Under certain conditions (Ti/Mo = 0.3, Mo/Bi = 3, 0.1 g catalyst and 2 g quartz sand, $C_3H_6/O_2/N_2$ = 2/4/19 mL min^{-1}, T = 400 °C, reaction pressure 0.15 MPa), a conversion of 20.5 % with a PO selectivity of 64.7 % could be reached. It was found that Ti addition promotes the dispersion of the Mo phase. Additionally, the stronger acidity of the catalyst is suppressed and moderate acid sites are generated. By comparing the NH_3 desorption curves of the modified and unmodified samples, it is evident that a Ti/Mo ratio 0.3 gives the optimal acidity conditions. A lower reduction extent, seen in H_2-TPR measurements, of the modified samples indicates a reduced reactivity of lattice oxygen. This nucleophilic oxygen oxidizes the allylic hydrogen. Titanium sites were also proposed to be the active sites for allylic radical generation. This increases the generation of superoxide allylic radicals which react to PO, thus increasing the activity and the selectivity of the catalyst.

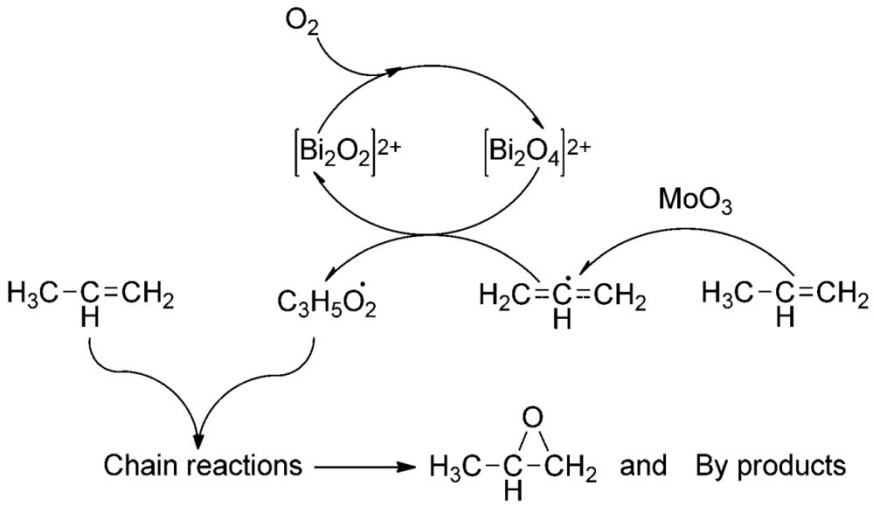

Figure 15: Synergistic effect between MoO_3 and Bi_2SiO_5 in propylene epoxidation proposed by Pang et al. Reproduced with permission from Ref. [72]. Copyright 2014 WILEY-VCH Verlag GmbH & Co. KGaA, Weinheim.

Seubsai et al. [75] synthesized trimetallic Sb_2O_3–CuO–NaCl/SiO_2 catalysts for selective propylene oxidation. The best performing combination had a Sb:Cu:Na ratio of 2:3:1 by weight, and achieved a PO selectivity of 43 % at 0.66 % propylene conversion (Figure 16). The co-existence of Sb_2O_3 and CuO crystalline phases is essential for PO production, and NaCl acts as a promotor reducing further oxidation or isomerization of the products. Sodium chloride presumably occupies the most active sites on the catalyst surface and consequently reduces propylene conversion. Testing the catalyst for 10 h did show some deactivation, from 0.95 % C_3H_6 conversion at the start, to 0.65 % at 10 h. The catalyst could be regenerated, however, by a dilute HCl treatment followed by calcination. The dilute HCl supposedly dissolves the sintered Sb_2O_3 and CuO crystallites, which are then re-dispersed during the calcination step. To improve the stability and selectivity, Seubsai et al. [76] combined CuO with RuO_2 and modified it with NaCl, TeO_2, Cs_2O, and TiO_2. The best performance was achieved at a Ru/Cu ratio of 3 and modified with NaCl, however the catalyst deactivated rapidly. The deactivation was a result of the loss of Cl^- due to steam formed during the reaction. The best stability/activity/selectivity was measured when TeO_2 was used as the promotor. NH_3-TPD analysis revealed a reduction in strong acid sites when the promotor was added, which is the likely reason for increased PO selectivity. Optimizing the reaction conditions led to a PO selectivity of 47 % at ~0.35 % C_3H_6 conversion, and the catalyst remained stable for 12 h of operation.

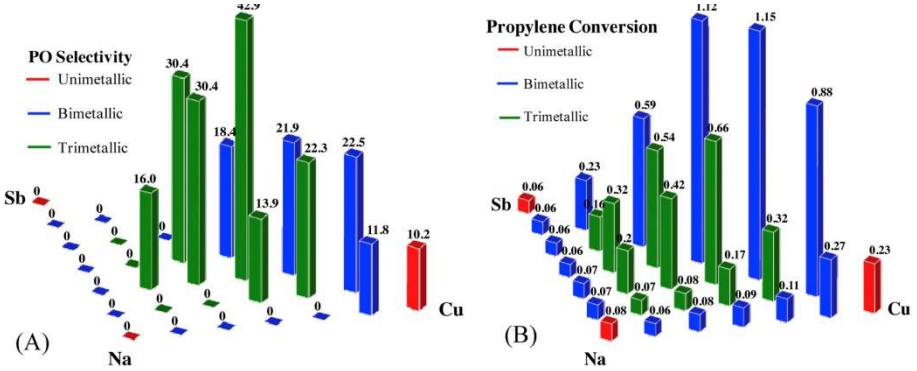

Figure 16: Percent PO selectivities (A) and propylene conversions (B) as a function of Sb–Cu–Na concentrations on the SiO_2 support at 250 °C. All catalysts had a total metal loading of 18 wt % and were calcined at 500 °C. Reproduced with permission from Ref. [75]. Copyright 2015 The Korean Society of Industrial and Engineering Chemistry. Published by Elsevier B.V.

Lee et al. [77] used a $CeZrO_2$-supported tungsten oxide catalyst. Increasing the Ce molar content from 0.05 to 0.5 increased the activity of the catalyst significantly (up to 24.7 %), but lowered the PO selectivity from 31.6 % to 0 %. The catalyst with a pure ZrO_2 support exhibited no propylene oxidation capacity, while a CeO_2 support converted 27.5 % propylene. The selectivity for PO in the latter case was only 11.7 %, which indicates either PO or propylene react with ceria lattice oxygen to form CO_x. The authors inferred that the acid sites on the catalyst promote PO formation, whereas basic sites promote AHS. In their case, they found a very good correlation between acid/base ratio and selectivity towards PO. Overall their best performing catalyst was 7 wt % of tungsten oxide on a mixed $CeZrO_2$ support, where the molar ration of Ce : Zr was 0.05 : 095. This catalyst converted 3.8 % of propylene with a PO selectivity of 46.8 %.

1.4 Mechanism of Propylene Epoxidation

In the epoxidation reaction, the oxygen addition into the double bond is an electrophilic addition process, while allylic hydrogen stripping (AHS) is a nucleophilic process (Figure 17). This means that the electronic properties of the oxidizing agent are very important. There are several theories as to what determines the selectivity in the direct propylene epoxidation reaction using molecular oxygen. From the different acid/base properties of the catalyst, the geometry of the active site, and so on. However, the consensus among the scientific community is that the necessary intermediate is the oxametallacycle (OMC) [78]–[85]. In the following section, the formation of this crucial intermediate is discussed.

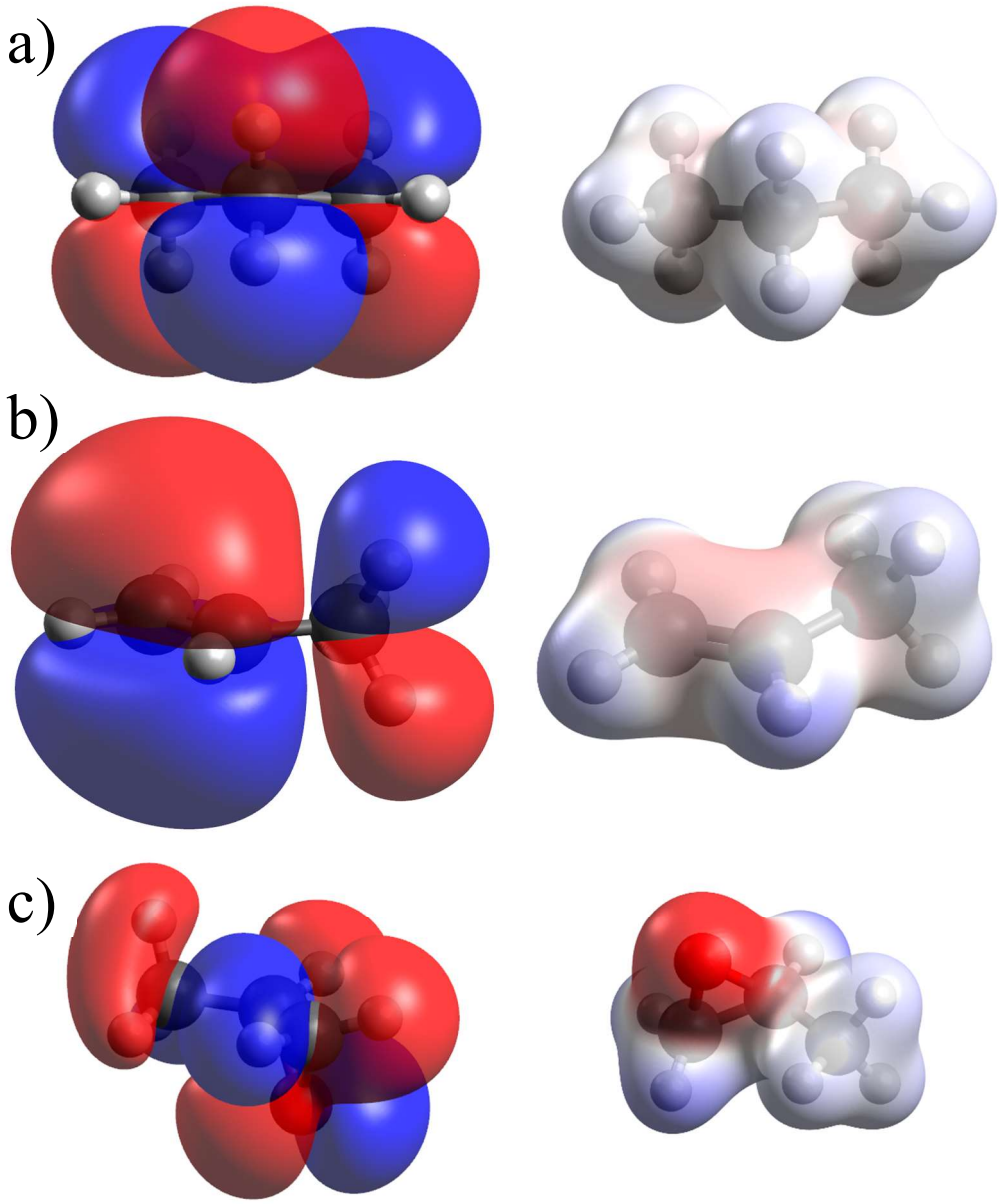

Figure 17: In the figure the HOMO orbitals (left) and the electron density (right) of propane a), propylene b) and propylene oxide c) are shown. The allylic hydrogens are the ones bound to the methyl group. In the electron density images, the areas colored red indicate areas of higher electron density, whereas areas colored blue indicate the opposite.

The calculation method was M06-2x/aug-cc-pVTZ; the isosurfaces shown are electronic: density 0.01 e/bohr^3; HOMO: 0.02; the charges shown are AIM charges.

During propylene oxidation, allylic hydrogen stripping is a persistent problem. Xu and Friend [78] studied oxidation of propylene to acetone over a rhodium catalyst. They found that on Rh the allylic C-H bond is not activated. With high oxygen surface coverage (over 0.45 monolayers), selective oxidation is preferred, while combustion is favored over low oxygen covered surfaces. They proposed an OMC intermediate must be formed on the surface, on one or two Rh atoms. When the intermediate is formed, an intermolecular hydrogen transfer must occur. The elimination of β-hydrogen and hydrogenation of the α-carbon is promoted due to the stabilization effect of the electronegative oxygen. This was confirmed by isotopic labeling of the allylic hydrogen atoms and the hydrogen atoms bound to α-carbon. Formation of the OMC on a Rh surface was also studied by Brown and Barteau [79]. They found that upon epoxide adsorption, the temperature-programmed desorption curves are similar to those of alcohols and not aldehydes. The desorption products included also CO and H_2 indicating decomposition of adsorbed PO. There were no C_1 or C_2 hydrocarbons detected among the desorbed products.

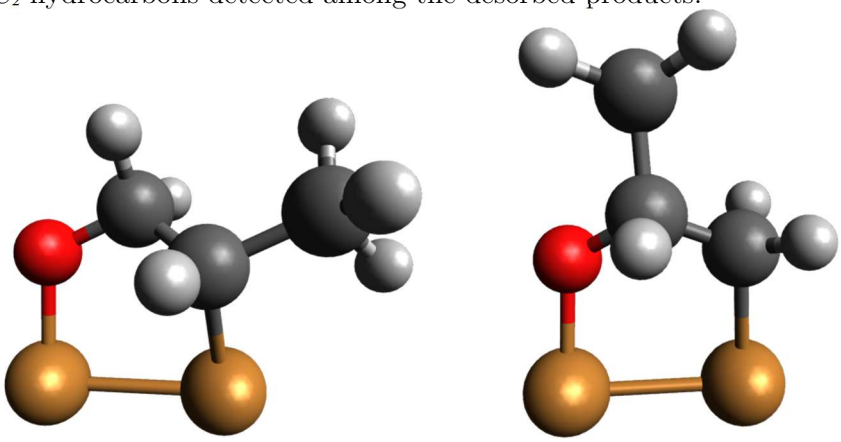

Figure 18: Structure of two oxametallacycle intermediates as proposed by Medlin et al. (OMMP1 left and OMMP 2 right). Red-Oxygen, black-Carbon, white-Hydrogen, and gold-Copper.

Medlin et al. [80] combined a theoretical and an experimental approach. They calculated the stability of different OMC intermediates on late-transition metals. The binding energy of the adsorbed intermediate generally decreases from left to right and from top to bottom. Two possible OMC isomers were proposed by the authors, the OMMP1 and the OMMP2 (Figure 18). The calculations showed that the OMMP2 isomer is more stable for all metals included in the study. This correlated well with experimental tests performed by several authors. On reduced Pd, Pt, Cu, and Ni, hydrogenolysis of propylene oxide predominantly led to the formation of ketones and secondary alcohols. These reduction products are preferred when OMMP2 is the intermediate formed. When the metals (Ni and Cu) are oxidized, the product spectrum mostly includes aldehydes and primary alcohols. This indicates the formation of the OMMP1 isomer. The authors propose that the oxygen shifts the electron density, resulting in a more electrophilic catalyst. This type of material favors cleavage of the C-O bond on the more substituted carbon.

Lately, several studies were focused on oxygen and its capacity to form the OMC intermediate. Dai et al. [84] focused on atomic versus molecular oxygen in the direct propylene epoxidation reaction over group IB metal catalysts. Looking at AHS they found

that atomic oxygen has lower activation barriers compared to molecular oxygen. This leads to lower PO selectivity if atomic oxygen is the oxidizing species. The activation barriers for OMC formation are noticeably lower when molecular oxygen is the oxidizing agent (Figure 19). Firstly, an OMC is formed with two oxygens, which eases the O-O bond cleavage and formation of a standard OMC. Deeper analyses revealed that a lower propylene activation barrier (in the molecular oxygen mechanism) leads to a better selectivity for OMC formation. Additionally, a good correlation was observed between hydrogen affinity for the oxidizing agent and the reaction barrier for AHS.

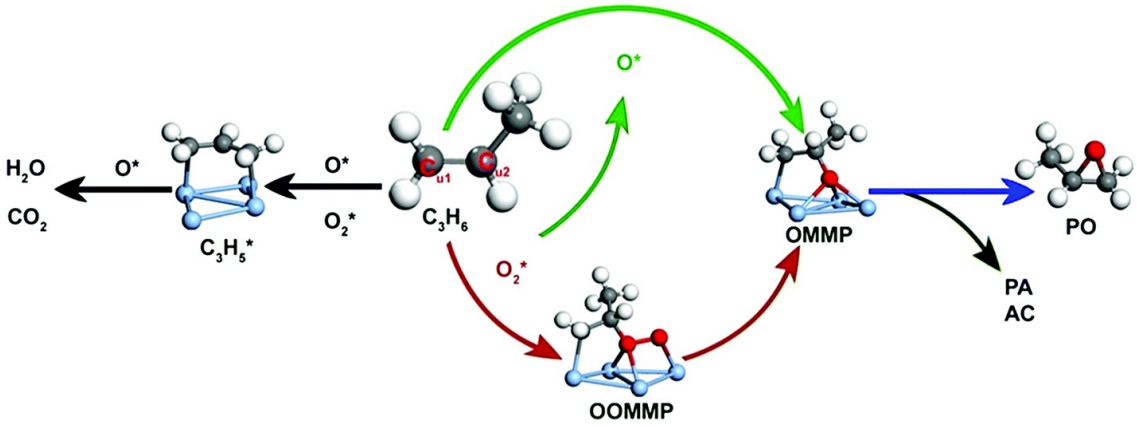

Figure 19: Reaction scheme of propylene oxidation by atomic and molecular oxygen proposed by Dai et al. Reproduced with permission from Ref. [84]. Copyright the Owner Societies 2017.

Zhao and Wang [85] analyzed the effect of promotors on molecular oxygen and the OMC formation over metallic Ag. They found that alkali addition mostly increases the activation barriers of all reaction steps, including OMC formation (primary chemistry) and epoxide ring closure (secondary chemistry). Chlorine addition, however, increases the activation barrier for AHS while simultaneously decreasing it for the primary and secondary chemistry. They found that alkali addition increases the electron density on oxygen and stabilizes its binding. This is most likely the underlying reason for little change in the predicted selectivity for OMC formation. Chlorine, on the other hand, reduces the electron density on oxygen, which in turn reduces the probability for AHS. Sodium addition to the catalyst has a strong stabilization effect on OMC that leads to increased selectivity for secondary chemistry. This is negated by the fact that Na addition has little effect on primary chemistry.

In summary, the OMC intermediate can form on several transition metals or their oxides. On metallic Rh, it forms and leads to PO formation when the oxygen coverage is high [78]. However, CO and H_2 was detected in PO-TPD, which indicates some decomposition also occurs [79]. Medlin et al. [80] found that on some late transition metals the OMC is very stable. According to the Sabatier principle, the binding strength cannot be too strong, since it would prevent ring closure and PO desorption. The authors also noted that if Ni and Cu are oxidized, a more electrophilic catalyst is formed. According to findings by other researchers, a more electrophilic oxygen favors OMC formation and not AHS. Dai et al. [84] confirmed this by calculating the activation barriers (AB) for AHS and OMC formation on atomic versus molecular oxygen. The more electrophilic species, molecular oxygen has a lower AB for OMC formation, while atomic oxygen favors AHS. Zhao and Wang [85] investigated the effect NaCl modification of metallic Ag catalysts has on activation barriers. They found that each ion has a different effect on AB for OMC

formation and ring closure. Therefore, there is no simple dopant to increase the AB for AHS while simultaneously decreasing the AB for OMC formation and ring closure.

Chapter 2

Alkali and Earth Alkali Modified CuO_x/SiO_2 Catalysts for Propylene Partial Oxidation: What Determines the Selectivity?

This chapter provides an overview of CuO_x/SiO_2 catalysts efficiency in direct propylene oxidation using molecular oxygen. The efficiency of different modifying alkali and alkaline earth metal adatoms is investigated. The morphological properties of materials are investigated with several *in-* and *ex-situ* techniques.

I investigated the surface area of the support, how it is affected by copper loading, and if it changes after alkali and alkaline earth metal modification. The mesoporous ordering of the support is confirmed by XRD at low angles and TEM imaging. The active copper phase is examined by UV/Vis diffuse reflectance under reducing, oxidizing and relevant reaction conditions. The acidic properties of the catalyst are studied by pyridine adsorption and DRIFT spectroscopy. Basic properties were probed by CO_2-TPD combined with DRIFT spectroscopy. With *in-situ* XANES we looked at the oxidation state of the catalysts during reaction conditions and their morphological properties. All of the results were correlated with catalyst activity and selectivity obtained from catalytic runs.

The synthesis technique used produced highly dispersed copper nanoclusters (less than 1 nm in diameter), with the actual loading very close to the nominal. Some sintering and subsequent deactivation is favorable under reducing (reaction) conditions. This is also seen from *in-situ* UV/Vis. Modification with any adatom increased stability, but only alkali metal modification increased PO selectivity. The latter modification generated additional basic sites of intermediate strength. Alkaline earth metal modification slightly increases acrolein selectivity. Different reduction dynamics observed indicate the modification alters the kinetics of oxygen abstraction and replenishment. A similar amount of Cu^+ during reaction conditions indicates its amount is not the only or a major determining factor governing PO selectivity. From the results, a tentative reaction mechanism was constructed.

Regarding my contribution: I performed all the syntheses and the catalytic tests. I also performed the N_2 sorption, UV/Vis diffuse reflectance, DRIFT spectroscopy, CO_2-TPD, and pyridine adsorption experiments. I additionally assisted with the acquisition of experimental X-ray absorption spectroscopy data and helped with interpretation of the results. Finally, I wrote the paper with the co-authors.

2.1 Alkali and Earth Alkali Modified CuO_x/SiO_2 Catalysts for Propylene Partial Oxidation: What Determines the Selectivity?

Applied Catalysis B: Environmental 237 (2018) 214–227

Contents lists available at ScienceDirect

Applied Catalysis B: Environmental

journal homepage: www.elsevier.com/locate/apcatb

Alkali and earth alkali modified CuO_x/SiO_2 catalysts for propylene partial oxidation: What determines the selectivity?

Janvit Teržan[a,b], Petar Djinović[a,*], Janez Zavašnik[c,d], Iztok Arčon[b,e], Gregor Žerjav[a], Matjaž Spreitzer[b,f], Albin Pintar[a]

[a] Department for Environmental Sciences and Engineering, National Institute of Chemistry, Hajdrihova 19, SI-1001 Ljubljana, Slovenia
[b] Jožef Stefan International Postgraduate School, Jamova cesta 39, SI-1000 Ljubljana, Slovenia
[c] Centre for Electron Microscopy and Microanalysis, Jožef Stefan Institute, Jamova cesta 39, 1000 Ljubljana, Slovenia
[d] Max-Planck-Institut für Eisenforschung GmbH, Max-Planck-Straße 1, 40237 Düsseldorf, Germany
[e] University of Nova Gorica Vipavska cesta 13, Nova Gorica, 5000, Slovenia
[f] Advanced Materials Department, Jožef Stefan Institute, Jamova cesta 39, 1000 Ljubljana, Slovenia

ARTICLE INFO

Keywords:
Propylene
Acrolein
Selective oxidation
Epoxidation
Alkali doping
Nucleophilic oxygen

ABSTRACT

In this work, CuO_x/SiO_2 catalysts were investigated in the propylene partial oxidation reaction. Ordered mesoporous silica (KIT-6) was used to deposit 1–10 wt. % copper and subsequently modified with Na, K and Ca. The synthesized materials were characterized by N_2 physisorption, XRD, TEM-EDS, CO_2-TPD, *operando* UV/Vis DRS, *operando* XANES and pyridine DRIFT spectroscopy. Regardless of the CuO_x loading, catalyst deactivation was observed during propylene oxidation reaction in non-modified catalysts, which was related to sintering of oligomeric $[Cu\text{-}O\text{-}Cu]_n$ species. Sintering of CuO_x is strongly promoted under a reducing propylene atmosphere and related to the presence of Cu^{+1}. The resulting bulk CuO_x promotes acrolein selectivity. We produced modified catalysts with finely dispersed alkali metal cations, associated with the subnanometer CuO_x phase, resulting in a greatly stabilized morphology and catalytic activity. *Operando* XANES analysis revealed that a substantial fraction of Cu^{2+} is transformed to Cu^{+} during the propylene oxidation reaction (52–68%, depending on the modifying atom). Also, the dynamics of reaching the quasi steady oxidation state differ strongly. The kinetics of oxygen abstraction and replenishment are substantially different, indicative of modified chemistry of the nucleophilic oxygen species, present in 5CuNa catalyst in contrast to others (5Cu and 5CuCa). We propose that Cu^{+} is not crucial for PO formation. Instead the electropositive Na^{+} and K^{+} decrease the nucleophilic strength of oxygen in CuO_x, by attracting its electrons. Consequently, the catalytic action of oxygen changes from oxidative attack on the allylic hydrogen to oxygen insertion into the C=C bond of propylene. This results in a noticeable selectivity shift from acrolein to propylene oxide. The effect of calcium on decreasing the nucleophilic character of O species in CuO_x is negated by charge compensation by strongly adsorbed hydroxyl groups and Ca modification for PO selectivity is inefficient. Additionally we found, that further oxidation of propylene oxide is, most likely, the main factor determining high selectivity for CO_x products. The alkali modification which increases the PO selectivity does not function via elimination of LAS, but exclusively through attenuation of nucleophilic character of oxygen species.

1. Introduction

Propylene can be catalytically converted into several useful C_3 oxygenates, such as propylene oxide (PO), propanal and acrolein [1]. Propylene oxide is a highly desired chemical as it is used in the production of propylene glycol ethers, propylene glycol and polyether polyols [2]. Most PO is produced by the mature and industrially established chlorohydrin process (CHPO), PO/styrene and PO/tert-butyl processes through a peroxidized intermediate and lately the hydrogen peroxide to propylene oxide (HPPO) process over single-site TS-1 or Ti-MWW catalysts using H_2O_2 as an oxidant. HPPO process uses H_2O_2 as the oxidant and produces PO with a selectivity of 99% [3]. There are several drawbacks for each of these processes, such as high cost of the reactants (H_2O_2), large quantity and a low price of the co-products (styrene monomer or tert-butyl alcohol) and environmental pollution (chlorinated lime as side product) [2,4].

The above mentioned drawbacks have driven research into direct gas-phase epoxidation of propylene using molecular oxygen. The

* Corresponding author.
E-mail address: petar.djinovic@ki.si (P. Djinović).

https://doi.org/10.1016/j.apcatb.2018.05.092
Received 4 April 2018; Received in revised form 28 May 2018; Accepted 30 May 2018
Available online 31 May 2018
0926-3373/

reaction suffers from conversion vs. selectivity issue: at low conversions (~1%), high PO selectivities can be achieved (~77%), whereas at higher conversions (above 15%), low PO selectivities (below 40%) are obtained [4]. By using a gas mixture of H_2 and O_2 as the oxidant over Au/TS-1 or Ti doped amorphous silica catalyst, PO selectivity above 90% can be achieved, but the conversions are very low (below 1%) [5]. With titanium-containing catalysts, deactivation is a persistent problem and is related to irreversible binding of reaction intermediates to the active sites, forming stable bidentate species [6,7].

Considerable amount of research has been performed on silver based catalyst, as silver is a very efficient ethylene epoxidation catalyst [4]. The issue with silver is that it is a very strong oxidant of the allylic hydrogen (which is not present in ethylene), resulting in PO selectivity during propylene epoxidation being substantially shifted towards total combustion [8,9]. For example, Lu et al. [9] performed propylene epoxidation over Ag catalysts immobilized on several supports (MgO, $CaCO_3$, CeO_2, …) and observed that CO_2 and H_2O were the main reaction products with the highest PO selectivity of 5.4%.

Regardless of the oxidant and metal used for propylene epoxidation, several studies have shown that an oxametallacycle (OMMC) is the necessary intermediate [10–12]. DFT calculations of the OMMC stability on several transition metals (Me) have shown that the metal plays a significant role. It was also predicted that for achieving high PO selectivity, the relative stability of the OMMC (desorption enthalpy) should be similar to the relative heat of PO adsorption on the same surfaces [10]. In a study of ethylene epoxidation, Kokalj et al. [11] also showed that specific bond strengths (Me-C vs. Me-O) and consequently order of their cleavage during OMMC desorption has a critical impact on selectivity. Their calculations showed that in case when Me-O bond cleaves first, acetaldehyde is produced, whereas initial cleavage of the Me-C bond results in ethylene oxide as the preferred product.

Copper catalysts also received a fair share of attention in regards to propylene epoxidation and oxametallacycle formation [1,8,13–16]. Torres et al. [1] studied the ability of Ag and Cu to oxidize the allylic hydrogen and form an oxametallacycle. Their studies were aimed at a metal catalyst (modelled as a perfect slab), and showed that copper, in contrast to silver, favours oxymetallacycle formation and not allylic hydrogen striping. They also calculated that the surface bound oxygen species on copper are less basic (less nucleophilic) than the ones bound on silver, indicating their lower tendency to react with allylic hydrogen. DFT studies performed by Yang et al. [12] have shown that copper in +1 oxidation state is preferred for oxametallacycle formation, as compared to Cu° or Cu^{2+}. Realistically, the oxidation state of copper during propylene epoxidation is either +1 or +2 as was shown by Greiner et al. [15] and Monneier et al. [8,16]. Further, Marimuthu et al. [17] varied the copper oxidation state in Cu/SiO_2 catalysts by illumination and observed that metallic copper is formed upon illumination which favours PO formation, whereas CO_2 and acrolein are produced over Cu^{1+} in dark.

Hua et al [18]. identified that the propylene epoxidation reaction occurs via the Mars-van Krevelen mechanism on Cu_2O. They studied different crystal planes of Cu_2O and how the coordination of the terminating lattice oxygen influences selectivity of the reaction. They found that one coordinated Cu^{1+} on Cu_2O [111] crystalline plane produces predominantly acrolein, two- coordinated oxygen on Cu_2O [100] crystalline plane produces CO_2, whereas three-coordinated oxygen on Cu_2O [110] crystalline plane predominantly produces PO.

The main drawback preventing high PO selectivity during direct gas-phase propylene epoxidation with molecular oxygen are the unfavourable properties of the allylic hydrogen (more acidic as compared to vinylic hydrogen) and strong Brønsted basicity of CuO_x lattice oxygen species (O^{2-}). To favour PO selectivity, nature of the oxygen species needs to be modulated, namely their Brønsted basicity (nucleophilicity) needs to be lowered. One way to modulate their basic character is with alkali (Na, K, Rb, Cs) or earth alkali (Be, Mg, Ca) modifications [13,19–22]. Wang et al. [19] investigated CuO_x/SBA-15 catalysts and noticed the highest PO selectivity when using K (~5% conversion, ~27% PO selectivity) or Na modification (~7% conversion, ~9% PO selectivity). The same study also reports that addition of earth alkali metals (Mg, Ca, Ba) leads to negligible PO selectivities (< 1%) and higher catalytic activity as compared to non-doped catalysts.

In this work, we investigated the effect of Na, K and Ca modification of highly dispersed CuO_x species on KIT-6 silica catalysts during direct gas-phase propylene oxidation. Relevant *ex-situ*, *in-situ* and *operando* techniques were applied to the synthesized materials revealing the pivotal role of CuO_x morphology and nature of the oxygen species in governing catalytic stability and PO selectivity.

2. Experimental

2.1. Catalyst preparation

2.1.1. Synthesis of KIT-6 silica

The KIT-6 silica support material was synthesized according to a procedure from Kim et al. [23]. For a typical 5 g batch of support, 8.1 g of Pluronic P123 (Sigma-Aldrich) was dissolved in a mixture consisting of 15.9 g of HCl (35 wt. %) and 292.2 g of deionized water. To accelerate P123 dissolution, the mixture was ultrasonicated for 15 min without heating. After complete dissolution, 8.1 g of butanol was added and additionally ultrasonicated for 15 min. The mixture was stirred at 35 °C for 5 h before 17.4 g of tetraethoxysilane (TEOS, Sigma-Aldrich) was added. The solution was left to stir for 24 h at 35 °C and afterwards transferred to a Teflon lined stainless steel autoclave for an additional 24 h at 130 °C. The white precipitate was collected and washed by centrifugation (9000 rpm, 90 s) until no more Cl^- was detected in the supernatant, dried overnight at 50 °C and calcined at 550 °C (1 °C min^{-1} to 550 °C, isothermal for 5 h).

2.1.2. Deposition of CuO_x phase over the KIT-6 silica support

Copper CuO_x/SiO_2 catalysts were prepared by precipitation of the copper-ammonia complex via dilution hydrolysis method (inspired by Meng et al. [24]). Different amounts of $Cu(NO_3)_2 \times 3H_2O$ (95, 190 and 380 mg), corresponding to the nominal copper content of 2.5, 5 and 10 wt. %, were dissolved in 40 mL of deionized water. After dissolution, 1 g of KIT-6 was added and stirred for 15 min. The pH value of the solution was adjusted to 9.0 with 27% ammonia solution and left stirring for 3 h. To induce the hydrolysis of the copper-ammonia complex, the suspension was diluted with 150 mL of deionized water added dropwise over the course of 2.5 h. The impregnated support was separated from the supernatant by centrifugation (9000 rpm, 90 s), dried for 5 h at 80 °C and calcined at 350 °C (2 °C min^{-1} to 350 °C, isothermal for 3 h).

The samples were denoted as xCu, where x represents the nominal content (wt. %) of copper on the silica support. The actual copper content in the synthesized materials was estimated using a photometric copper test Spectroquant® (Merck) on the supernatant solution after centrifugation. In all cases 90–100 % deposition of copper in the prepared CuO_x/SiO_2 catalysts was confirmed. Quantitative analysis of Cu, Na, K and Ca content was performed with the energy-dispersive X-ray detector (FE-SEM SUPRA 35 V P, Carl Zeiss, Inca 400, Oxford Instruments).

2.1.3. Alkali and earth alkali modification of the CuO_x/SiO_2 catalysts

For the alkali and earth alkali modification, 30 mL of aqueous solutions of nitrate salts (0.1 M $NaNO_3$, 0.05 M $Ca(NO_3)_2$ and 0.1 M KNO_3) was used. After complete dissolution of the salt, 300 mg of the CuO_x/SiO_2 catalyst was added to the solution. The suspension was stirred for 3 h. The modified catalyst was separated from the supernatant by centrifugation (9000 rpm, 90 s), dried for 5 h at 80 °C and calcined at 350 °C (2 °C min^{-1} to 350 °C, isothermal for 3 h).

The samples were denoted as xCuy, where x represent the copper

content and y the dopant (*e.g.* 5CuNa stands for a 5 wt. % CuO_x/SiO_2 catalyst modified with sodium).

2.2. Characterization and catalytic testing

2.2.1. BET specific surface area and porosity

The BET surface area, total pore volume and average pore size distribution were determined from N_2 adsorption/desorption isotherms obtained at −196 °C (Micromeritics, model TriStar II 3020). Prior to analysis, the samples were degassed in N_2 stream (purity 6.0 by Linde), using a SmartPrep degasser (Micromeritics) at 90 °C for 60 min, and followed for 120 min at 180 °C. Pore size distribution curves and total pore volume were calculated by the BJH (Barrett-Joyner-Halenda) method from the desorption branch of the isotherm. Micropore contribution was evaluated with the t-plot method.

2.2.2. X-ray diffraction

Mesoporous ordering of the prepared CuO_x/SiO_2 catalysts was analyzed using powder X-ray diffraction (XRD) analysis. The PANalytical Empyrean diffractometer using in Bragg-Brentano geometry and Cu Kα radiation was used. XRD patterns were recorded in the 2θ range from 0.5° to 3°, with a measurement step of 0.0131° and a step time of 500 s. The same conditions were also used for identification of crystalline phases, for which the 10Cu catalyst was scanned in the 2θ range from 10° to 60°.

2.2.3. Transmission electron microscopy

For TEM analyses samples were first dispersed in absolute ethanol and sonicated to prevent agglomeration; such prepared suspension was transferred onto commercial lacey-carbon Ni or Au support grids. Due to the nature of the analyses a double-tilting analytical Be holder was used. The core morphology of the samples was studied by Schottky field-emission transmission electron microscope (JEM-2200FS, JEOL Ltd.), operating at 200 kV. The chemistry of the samples was analysed in scanning-TEM mode using windowless ultrafast large angle 100 mm^2 SDD-EDS spectrometer (EX-24200M1G2T, JEOL), allowing efficient collection of X-rays. High-angle annular dark field (HAADF) detector (EM-24630UHADF, JEOL) was used for collecting of only incoherently scattered electrons, highly sensitive to variations in the atomic number (Z contrast).

Due to the beam sensitivity of SiO_2 mesoporous materials under the electron beam, various approaches have been employed to achieve reliable results. Although a low operating voltage (e.g. 80 kV) is generally considered to avoid severe electron beam induced knock-on damage, we choose to limit the primary electron beam with smallest condenser aperture, in attempt to obtain a sufficiently high current in the small probe used for chemical analysis. This resulted in improved signal-to-background and signal-to-noise ratios, and due to short acquisition time also in reduced beam damage and enhanced detectability. Additionally, a hard X-ray aperture was used to limit the amount of scattered electrons and X-rays to speed up the EDS counting and hence analysis time.

2.2.4. UV/Vis diffuse reflectance measurements

Structural and electronic properties of CuO_x phase with and without alkali modification were analyzed with UV/Vis spectrophotometry (Perkin Elmer, model Lambda 35) at room temperature in the range between 200 and 1100 nm. The powder samples were analyzed using the RSA-PE-19 M Praying Mantis accessory with Spectralon© as the background standard. *Operando* UV/Vis diffuse reflectance (DR) measurements were performed in order to obtain insights into the working state of the catalyst during the epoxidation reaction, as well as reversibility of redox and morphological changes. The experiments were performed in the HVC-VUV Praying Mantis Reaction Chamber (Harrick) using the Perkin Elmer Lambda 650 UV/Vis spectrophotometer. Spectra were recorded over catalyst samples exposed to pre-treatment in 20% O_2/He at 350 °C for 30 min, followed by 100 min of oxidation reaction (16.7% C_3H_6, 16.7% O_2 and 66.7% of He at 350 °C). Afterwards, the catalysts were regenerated in 20% O_2/He at 350 °C for 30 min, followed by exposure to pure C_3H_6. Finally, the catalysts were re-oxidized for 115 min in 20% O_2/He at 350 °C. The analytical protocol is schematically shown in Supplementary Information (Fig. S1).

2.2.5. Acid site probing using DRIFT spectroscopy

Lewis and Brønsted acidity of the prepared catalysts was investigated using pyridine as the probe molecule. Experiments were performed in a DiffusIR cell (PIKE Technologies) attached to a Perkin Elmer Frontier spectrometer. The powdered samples (10 mg) were pretreated at 350 °C for 20 min in a flow of N_2. After cooling to 25 °C, the samples were saturated with pyridine vapour/N_2 gas stream for 10 min and subsequently evacuated for 60 min at 10^{-5} mbar (Pfeiffer Vacuum turbomolecular pump, model HiCube). The spectra collected are the average of 32 scans with a resolution of 4 cm^{-1}.

2.2.6. Temperature programmed desorption (TPD) of CO_2

Basicity of the prepared catalysts was analyzed using CO_2 as the probe molecule. Experiments were performed in a Micromeritics AutoChem II 2920 apparatus. The sample (100 mg) was positioned inside a U-shaped quartz reactor and pre-treated in a flow 5% O_2/He at 350 °C for 30 min. After pre-treatment, it was cooled to 0 °C and saturated with pure CO_2 (purity 5.3, Linde) for 30 min. Weakly adsorbed CO_2 was removed in a flow of pure He for 30 min. The samples were heated to 900 °C at 5 °C/min and CO_2 desorption was monitored by a mass spectrometer (Pfeiffer Vacuum, model ThermoStar™ GSD320) following the characteristic m/z = 44 fragment. Pulses of 0.5 mL CO_2 were used as an external standard for CO_2-TPD signal calibration.

Additional information on the nature of desorbed CO_2 was obtained by DRIFT analysis (Perkin Elmer Frontier spectrometer equipped with a DiffuseIR cell). During the experiment, 10 mg of catalyst was pretreated in a flow 5% O_2/He at 350 °C for 30 min. After pre-treatment the sample was cooled to 0 °C and saturated with 50% CO_2/He for 30 min, followed by degassing in pure He for 60 min, and gradual heating to 900 °C with a ramp of 10 °C/min. DRIFT spectra were recorded in the relevant temperature intervals, revealing the nature of desorbed CO_2 (Fig. S2).

2.2.7. Operando Cu K-edge XANES

The Cu K-edge X-ray absorption spectra (XAS) of 5Cu, 5CuNa and 5CuCa catalysts were recorded *in-situ* during the propylene oxidation reaction at 350 °C in transmission detection mode at the XAFS beamline of the ELETTRA synchrotron radiation facility in Trieste, Italy. The catalyst samples were prepared in the form of homogeneous pellets, pressed from micronized sample powder mixed with BN powder, with the total absorption thickness (μd) of about 2.5 above the investigated Cu K-edge. Pellets were inserted in a tubular oven reactor (Carbolite MTF 12/25/400) with 20 μm aluminum foil windows, filled with a gas mixture composed of 80% He and 20% O_2 at 1 bar. The XAS spectra were measured *in-situ*: (i) at room temperature, (ii) at 350 °C in the He/O_2 atmosphere and (iii) during the catalytic propylene oxidation reaction at 350 °C in a C_3H_6/O_2/He stream (16.7% C_3H_6, 16.7% O_2, 66.6% He, total flowrate of 30 ml/min). After propylene addition, the samples were measured repeatedly until the quasi-equilibrium state in the catalyst was reached (up to 10 XAS spectra were collected per sample). Details of the XAS measurements and apparatus settings are provided in the supplementary information file.

2.3. Catalytic tests

Catalytic performance of the synthesized catalysts was tested in a tubular fixed-bed quartz reactor (I.D. = 10 mm) at atmospheric pressure. In a typical experiment, 50 mg of the catalyst was diluted with 200 mg of SiC and fixed between two quartz wool flocks. Before the catalytic tests, the samples were pre-treated in a flow of O_2 and He (5

and 20 mL/min, respectively) at 350 °C. After 20 min of pre-treatment, propylene (Messer, purity 2.5) at 5 mL/min was added to the gas mixture. The reaction products were monitored by gas chromatography (Agilent, model 7890 A); the GC device was equipped with the DB-WAXETR (Agilent) and the HP-PlotQ columns and a TCD detector. Blank experiment confirmed no propylene conversion occurring at 350 °C in absence of the catalyst.

The conversion of propylene was calculated using Eq. (1), where n_{C3H6i} and n_{C3H6O} are moles of propylene at the inlet and outlet of the reactor.

$$\%_{conversion} = \frac{(n_{C_3H_6\,i} - n_{C_3H_6\,o})}{n_{C_3H_6\,i}} \times 100\,\% \quad (1)$$

Reaction product selectivities were calculated according to Eq. (2), where n_i are moles of product i and n_{C3H6C} are moles of propylene converted.

$$\%_{selectivity} = \frac{n_i}{n_{C_3H_6\,c}} \times 100\,\% \quad (2)$$

3. Results and discussion

3.1. Characterization of catalysts

3.1.1. Specific surface area and pore size/volume

The N_2 adsorption/desorption isotherms of the KIT-6 support and all CuO_x/SiO_2 catalysts are of type IV with a sharp capillary condensation step and H1 hysteresis loop, indicative of large channel-like pores (Fig. 1a). Pore size distribution in the synthesized support is in the range of 7–10 nm (Fig. 1b) with negligible contribution of larger pores originating from inter-particle porosity.

After CuO_x deposition, a decrease of about 25% in BET specific surface area and pore volume occurs, as compared to pure KIT-6 silica support (Table 1). Also, pore size distribution shifts towards lower values (Fig. 1b), suggesting that CuO_x phase lies inside the pores of the silica support. Subsequent modification of the CuO_x catalysts with sodium induced only slight changes in surface area, pore diameter and pore volume. The micropore volume and micropore surface area represent a small fraction of the total pore volume and available specific surface area in the synthesized catalysts (less than 2 and 8%, respectively, Table 1).

3.1.2. X-ray diffraction examination

X-ray diffraction patterns at low 2θ angles of pure KIT-6 silica support, 5Cu, 10Cu and 10CuNa catalysts are illustrated in Fig. 2. All patterns show two peaks at approximately 2θ = 0.83 and 1.03° corresponding to the (211) and (220) reflections of the *Ia3d* cubic structure [25]. This indicates a well-ordered mesoporous structure of the KIT-6 support, which is maintained during subsequent copper and sodium modifications.

XRD analysis at higher 2θ angles was performed for the 10Cu catalyst (containing the highest Cu content) in order to identify possible crystalline phases present (Fig. S3). A broad diffraction peak in the 2θ range from 15° to 30° was observed, characteristic for amorphous silica. However, no diffraction peaks at 2θ values characteristic for CuO (2θ = 35.5 and 38.7°) or Cu_2O (2θ = 36.4 and 42.3°) can be seen, indicating a negligible fraction of CuO_x is present as bulk crystalline CuO in this catalyst. Same is expected for catalysts with a lower copper content.

3.1.3. TEM-EDS analysis

The BF-TEM micrographs of the pure silica support and 5CuNa sample revealed ordered mesoporous support structure (Fig. 3a), confirming results of XRD and N_2 physisorption analyses. HAADF-STEM imaging was used to visualize the CuO_x phase using Z contrast. The majority of visible CuO_x is present in form of small particles with a mean diameter of 4 nm (brighter spots, inset Fig. 3b). In addition, larger CuO_x clusters of 10–20 nm, concentrated in aggregates of 100–200 nm were also observed in the 5CuNa catalyst (Fig. 3c). With increasing copper loading (10CuNa catalyst), larger CuO_x aggregates (10–20 nm) become more abundant (Fig. 3d). STEM-EDS maps were performed, since they scan the sample without stopping the probe and therefore reduce electron beam damage to the sample. The elemental mapping (Fig. 3e) indicates that in addition to above mentioned CuO_x morphologies, highly dispersed (subnanometer) copper species densely covering the SiO_2 support are also present in the 5CuNa catalyst. Also, the elemental maps of sodium and copper overlap, suggesting the alkali dopant is closely associated with CuO_x phase (Fig. 3f).

3.1.4. UV/VIS DR analysis

Diffuse reflectance UV/Vis analysis of alkali modified and non-modified CuO_x/SiO_2 catalysts was performed to obtain additional insights into the structure of CuO_x moieties. The spectra show three distinct features (Fig. 4). The first peak stretching from 250 to approximately 320 nm is characteristic for charge transfer between mononuclear Cu^{2+} and oxygen [26].

The band at approximately 370–500 nm which increases in intensity with copper loading is characteristic of $[Cu–O–Cu]_n$-type (oligomeric

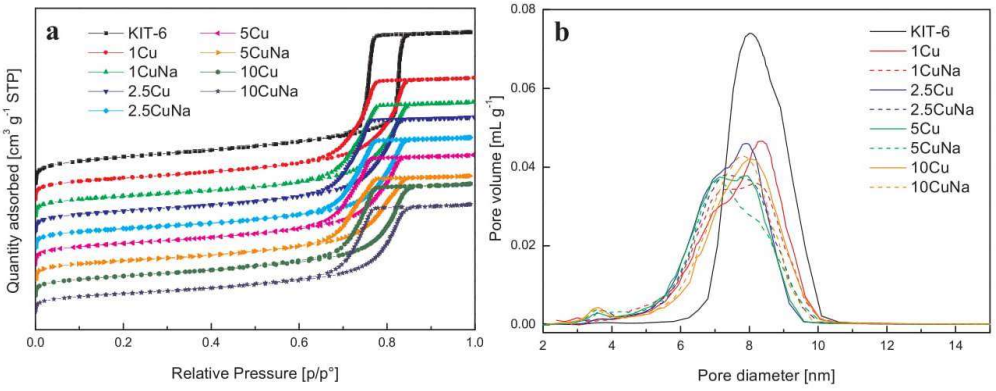

Fig. 1. a) N_2 adsorption/desorption isotherms of KIT-6 silica support and CuO_x/SiO_2 catalysts containing 1–10 wt. % Cu with and without Na modification. The isotherms are offset by 100 cm^3 N_2 g^{-1} STP for easier visualization.; b) Pore size distribution of pure KIT-6 SiO_2 support and CuO_x/SiO_2 catalysts with different copper loadings before and after Na modification.

Table 1
Material properties measured with N_2 physisorption technique.

	BET $m^2 \times g^{-1}$	Average pore diameter[a] nm	Total pore volume[a] $cm^3 \times g^{-1}$	Micropore volume[b] $cm^3 \times g^{-1}$	Micropore area[b] $m^2 \times g^{-1}$	External surface area[b] $m^2 \times g^{-1}$
KIT-6	615	8.3	1.48	0.023	49	566
1Cu	507	7.3	1.19	0.019	41	466
1CuNa	471	7.3	1.11	0.008	21	450
2.5Cu	490	7.1	1.12	0.015	35	455
2.5CuNa	462	7.1	1.09	0.009	21	441
5Cu	485	7.0	1.07	0.013	31	454
5CuNa	465	7.0	1.02	0.006	18	447
5CuK	378	7.0	1.04	0.010	28	350
5CuCa	404	7.0	1.03	0.011	32	372
10Cu	475	7.4	1.1	0.013	31	444
10CuNa	439	7.2	1.06	0.014	32	407

[a] Calculated using the BJH method.
[b] Calculated using the t-plot method.

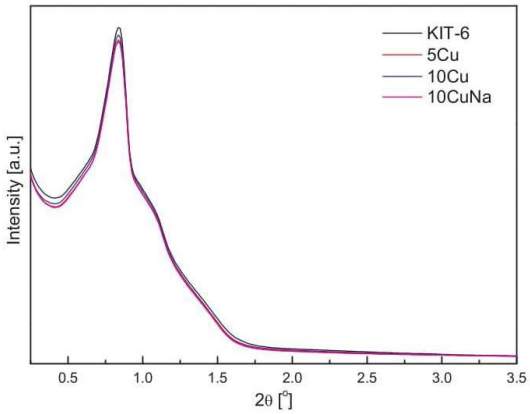

Fig. 2. X-ray diffraction patterns at low 2θ angles of pure KIT-6 silica support, 5Cu, 10Cu and 10CuNa catalysts.

species), which are different from bulk CuO and indicates progressive clustering of [Cu–O–Cu] moieties when increasing copper content from 2.5 to 10 wt. %. The broad but less intense band between 600–800 nm corresponds to the d-d transition of Cu^{2+} ions in an octahedral environment, which can be attributed to bulk CuO. Based on the dissimilarity in the UV/Vis DR spectra of bulk CuO (crystalline monoclinic CuO, red line in Fig. 4) and 10Cu catalyst (containing the highest copper loading), the bulk CuO species in octahedral coordination in this catalyst are not abundant and strongly distorted (possibly amorphous, which is in line with XRD results, Fig. S3) [19,27,28].

Catalysts modified with Na show a red shift of the shoulder at 370 nm, indicating oligomerization of the $[Cu–O–Cu]_n$ species, which was induced by the second calcination procedure applied after Na addition (Section 2.1.3). The same behaviour was observed with similar catalysts by Garcia-Aguilar et al. [22].

Thermal stability of the CuO_x species in presence of different alkali or earth alkali modifiers was tested by applying an additional calcination procedure to the 2.5Cu and 5Cu sample to equal the thermal history of 5CuNa, 5CuK or 5CuCa catalysts (Fig. 5).

A notable absorption red-shift was observed after the second calcination protocol for the 2.5Cu and 5Cu catalyst (black and magenta lines in Fig. 5) along with the increase of band intensity (centred at 700 nm) related to bulk CuO. These changes were much larger compared to modified catalysts (5CuNa ≈ 5CuK > 5CuCa) and show that alkali and earth alkali modifications strongly hinder sintering and oligomerization of the [Cu–O–Cu] species in oxidative atmosphere. Furthermore, a positive role of alkali modification is known, as He et al. [29] observed that Cs modification of CuO_x/SiO_2 catalysts resulted in a substantial decrease of the average CuO scattering domain size, suggesting re-dispersion of CuO phase.

3.1.5. *Operando* UV/Vis DRS analysis

The 5Cu and 5CuNa catalysts were analyzed to obtain relevant information on the structural and redox changes occurring under oxidative, reductive and realistic propylene oxidation conditions in the presence or absence of alkali dopant (Fig. 6). The analytical protocol is depicted in Fig. S1.

Spectra measured during the propylene oxidation reaction over 5Cu catalyst (16.7% C_3H_6, 16.7% O_2 and 66.6% of He, Fig. 6a) show the band between 250–370 nm, which is attributed to mononuclear Cu^{2+} and finely dispersed [Cu-O-Cu] moieties, and changes very little during the 100 min of reaction (Fig. 6a). Simultaneously, the band increases between 370–650 nm, indicating clustering of [Cu-O-Cu] oligomeric species and formation of larger CuO_x clusters.

The changes of the band between 250–370 nm in the 5CuNa catalyst during the propylene oxidation reaction are negligible (Fig. 6b). This indicates improved stability of mononuclear and oligomeric [Cu-O-Cu] moieties after Na modification. Simultaneously, the band between 370–650 nm increases (to a smaller extent compared to 5Cu catalyst) with reaction time.

Switching back to an oxidative atmosphere (16.7% C_3H_6, 16.7% O_2 and 66.6% of He → 20% O_2/He, (Fig. 6c and d) shows no change in the spectra of the 5Cu and 5CuNa catalysts, even after 30 min. Presence of Cu^{1+} was confirmed by *operando* XANES (described in detail in Section 3.1.8), which was independently observed during propylene epoxidation over a Cs^+ modified CuO_x/SiO_2 catalyst [29].

Switching to a purely reductive atmosphere (20% O_2/He → C_3H_6) results in a progressive increase of light absorption in the whole range of wavelengths (200–1100 nm) for both 5Cu and especially 5CuNa catalysts (Fig. 6e and f). This suggests the onset of substantial structural (distortion of CuO_x species due to oxygen elimination [28]) and redox changes, which occur in the same range of wavelengths. Metallic copper absorbs light in the range between 225–590 nm [28], whereas Cu_2O at wavelengths between 300 and 500 nm [30].

Returning to an oxidative atmosphere after reduction in propylene (C_3H_6 → 20% O_2/He, Fig. 6g and h) causes re-oxidation of the catalyst. Structural changes based on the evolution of the UV/Vis DR spectra suggest formation of bulk CuO and clustering of [Cu-O-Cu] oligomeric species. The structural changes of CuO_x induced by the redox cycle are, to a greater extent, reversible in the 5CuNa catalyst (spectrum returns closer to the value before the reduction). This suggests that Na modification acts as a sintering barrier preventing surface migration of copper species.

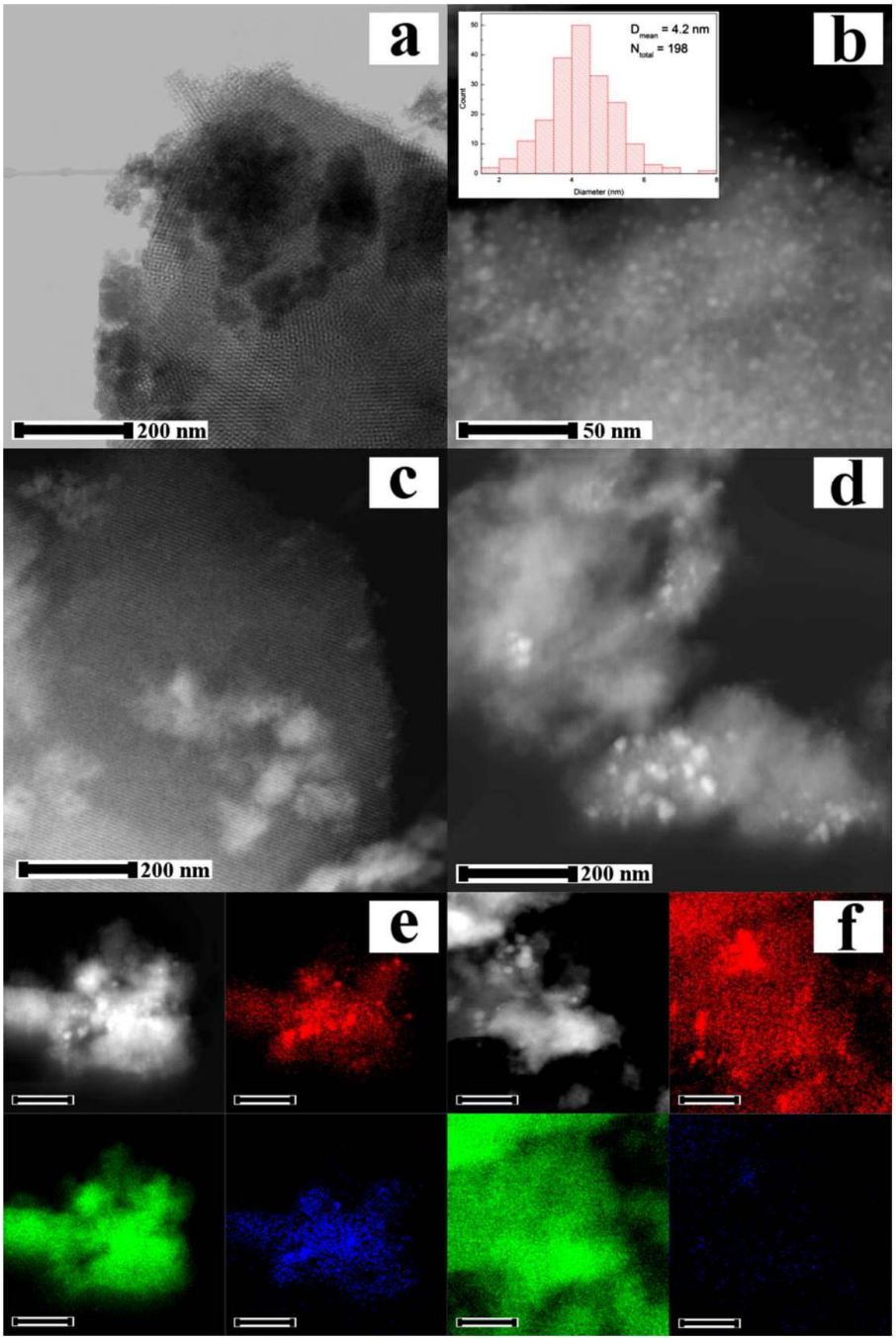

Fig. 3. a) BF-STEM image of the 5CuNa catalyst showing ordered mesoporous SiO_2 support, preserved also after Cu and Na modification, b) HAADF-STEM image of the 5CuNa catalyst with size distribution of CuO_x clusters (inset), c) aggregates of highly-dispersed CuO_x in the 5CuNa catalyst on the surface of SiO_2 substrate, d) larger aggregates of CuO_x in the 10CuNa catalyst, e) STEM-EDS elemental mapping for the 5CuNa catalyst (scale bar is 200 nm, red = Cu, green = Si and blue = Na) and f) STEM-EDS elemental mapping of 10CuNa catalyst (scale bar is 200 nm). (For interpretation of the references to colour in this figure legend, the reader is referred to the web version of this article.)

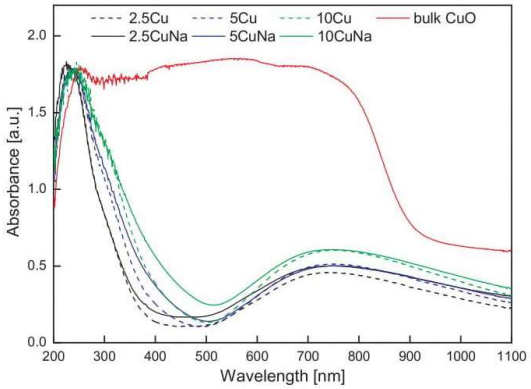

Fig. 4. The UV/VIS spectra of sodium unmodified and modified catalysts compared to bulk copper oxide.

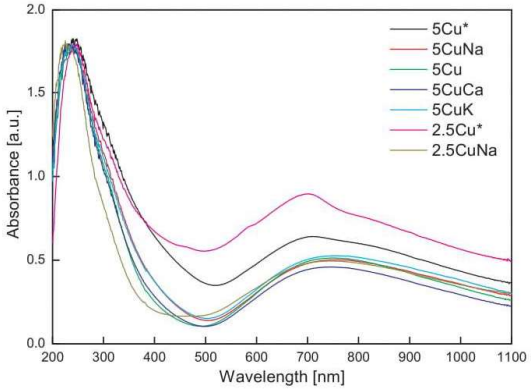

Fig. 5. The UV/Vis DR spectra of 2.5Cu, 2.5CuNa, 5Cu, 5CuNa, 5CuK and 5CuCa catalysts exhibiting identical thermal history, compared to the once calcined 5Cu catalyst. Samples marked with an asterisk were calcined twice, equaling thermal history of alkali modified catalysts.

3.1.6. Acid site probing with pyridine DRIFTS

Acid sites are known to negatively affect selectivity for PO, as these strongly electrophilic surface sites can react with bridging oxygen in PO, resulting in its further oxidation, or surface blocking and deactivation via strong adsorption [7]. The results of pyridine DRIFTS measurements for the 2.5Cu, 5Cu and 10Cu catalysts before and after Na modification, as well as pure KIT-6 support are presented in Fig. 7. Absence of the peak at 1550 cm^{-1} indicates no Brønsted acid sites on the analyzed samples. Based on the intensity of the band at 1450 cm^{-1}, deposition of 2.5–10 wt. % copper negligibly changes the Lewis acidity of the catalysts in comparison to pure KIT-6 silica support. On the other hand, sodium modification decreases the amount of Lewis acid sites for 44 and 29% in the 5CuNa and 10CuNa catalysts, respectively. The decrease in Lewis acid site abundance is in line with the sodium content, i.e. 0.8 and 0.5 wt. % in 5CuNa and 10CuNa catalysts, respectively (see Table S1).

3.1.7. Basic site probing with temperature programmed desorption (TPD) of CO_2 and hyphenated CO_2-TPD-DRIFTS technique

Surface basicity in heterogeneous catalysis is strongly related to nucleophilic nature of oxygen species on the catalyst surface [31], which play a decisive role in oxidation catalysis in terms of activity and selectivity [32,33]. Abundance and strength of basic sites in the synthesized catalysts was analyzed using CO_2-TPD analysis, which revealed two separate clusters of peaks for all the catalysts (Fig. 8a): a low-temperature cluster related to weak basic sites (between 0 and 300 °C), and a high-temperature cluster (comprised of two peaks centred at 450 and 600 °C) connected to strongly basic sites. Both clusters are comprised of several elemental peaks, indicating heterogeneous nature of the catalysts and consequently distribution of basic site strengths.

The weak and strong basic sites are very similar in strength for the 5Cu and 10Cu samples (Table 1, red and magenta lines in Fig. 8a). The main difference lies in a higher abundance of strong basic sites in the 10Cu catalyst. Alkali modification significantly affects both the abundance and strength of basic sites in both 5Cu and 10Cu catalysts; however, the action differs depending on the dopant (Table 2).

In the range of weak basic sites, the most striking difference is in the appearance of a shoulder at approximately 150 °C, which is observable only after modification in 5CuNa, 5CuK and 10CuNa catalysts.

Deconvolution of CO_2-TPD profiles (Fig. 8b) showed that in case of Na and K modification, the low-temperature cluster consists of three distinct peaks, centred at 60, 94 and 155 °C. The last peak is very broad and absent in unmodified and Ca modified catalysts.

The nature of CO_2 binding to the catalyst surface was further analyzed by a hyphenated CO_2-TPD-DRIFTS technique, showing difference spectra (Fig. 8c). Increase in band intensity in difference spectra indicates lower abundance (desorbed) species, whereas decreased intensity indicates formed species. The samples were pre-treated and saturated with CO_2 as described in Section 2.2.7. DRIFT spectra were recorded at temperatures determined by the positions of deconvoluted CO_2-TPD peaks (Fig. S2) in order to discriminate changes related to individual CO_2 desorption peaks.

Fig. 8c shows that up to 94 °C (first two CO_2 desorption peaks, black and red lines), mostly surface bound water and hydroxyls are removed (based on the bands at 1630 and 3100-3650 cm^{-1}). A significant amount of CO_2 is also desorbed in these two steps, as evident by the sharp band at 2339 cm^{-1}. The low desorption temperature and position of the absorption band close to the one of gas phase CO_2 (2350 cm^{-1}) are in line with the minimal electron back donation to the antibonding orbital of CO_2, confirming the electrostatic character of CO_2 desorbed below 94 °C [34]. Also, weak bands at 1320 and 1601 cm^{-1} indicate desorption of small amounts of formate species bound to copper, which are formed through reaction of adsorbed CO_2 and surface hydroxyl groups. The loss of band intensity at 1453 cm^{-1} indicates formation of surface monodentate carbonates in very small amounts already at 60 °C.

Between 94 and 250 °C (third CO_2 desorption peak centred at 150 °C) changes are more abundant, which is in line with broadness of the third CO_2 TPD peak (Fig. 8b). A small amount of water and physisorbed CO_2 are desorbed (based on the increase of band intensity at 1631 and 2339 cm^{-1}). The rise in band intensity at 1453 cm^{-1} indicates the decomposition of surface monodentate carbonates as well as carbonyl species (bands at 1890 and 2040 cm^{-1}). Considering that no carbon monoxide was detected during CO_2-TPD analysis, decomposition and desorption of carbonyl species is accompanied with extraction of an oxygen atom resulting in the reduction of CuO_x species. This is in line with the observed colour change of the 5CuNa sample during the CO_2-TPD analysis from light blue to dark brown, suggesting presence of reduced (metallic copper) species.

Substantial restructuring of the surface adsorbed CO_2 and oxygen in the CuO_x (and not reaction between CO_2 and H_2O and/or OH, based on very small changes in their bands) is also observed between 94 and 250 °C. Based on the decreased intensity of bands at 1105, 1250, 1350 and 1470 cm^{-1}, formation of carbonates and reduction of CuO_x to Cu_2O took place. Similar bands were observed by Chen et al. [34] during CO_2 chemisorption on Cu_2O.

Increasing the temperature from 250 to 690 °C (covering the high-temperature CO_2 desorption cluster, blue line in Fig. 8c) causes a substantial desorption of CO_2 (2339 cm^{-1}), water and hydroxyls (1630 and

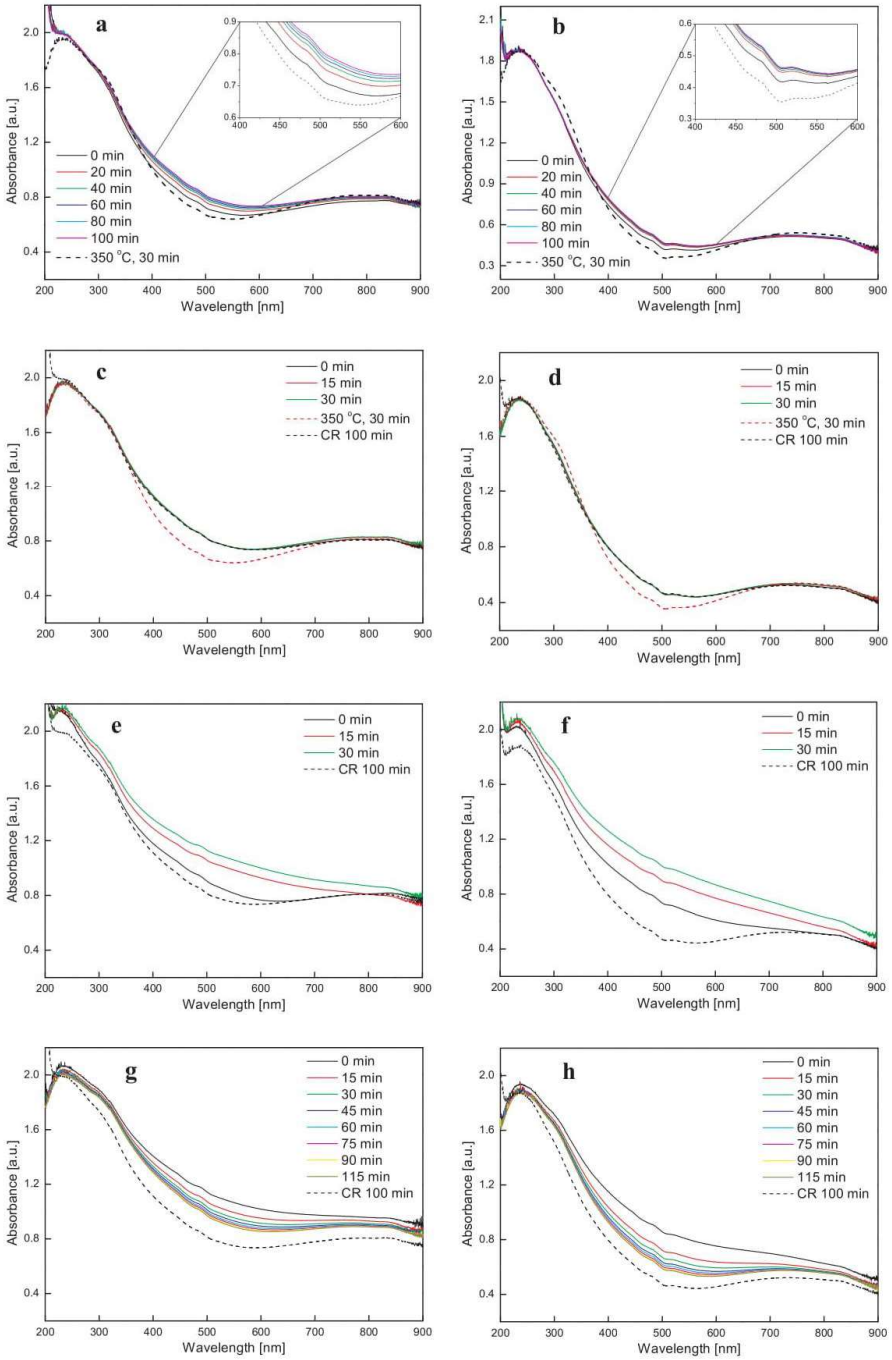

Fig. 6. The UV/VIS DR spectra of 5Cu (a, c, e and g) and 5CuNa (b, d, f and h) samples taken at specific time intervals during the catalytic propylene oxidation reaction (a,b), in an oxidative atmosphere after the reaction (c,d), in a reductive atmosphere of pure propylene (e,f), and in an oxidative atmosphere after reduction in propylene (g,h). In the legend, the spectrum "350 °C, 30 min" stands for spectrum measured after catalyst pre-treatment in O_2/He flow, while the spectrum "CR 100 min" stands for spectrum measured after 100 min of the propylene oxidation reaction.

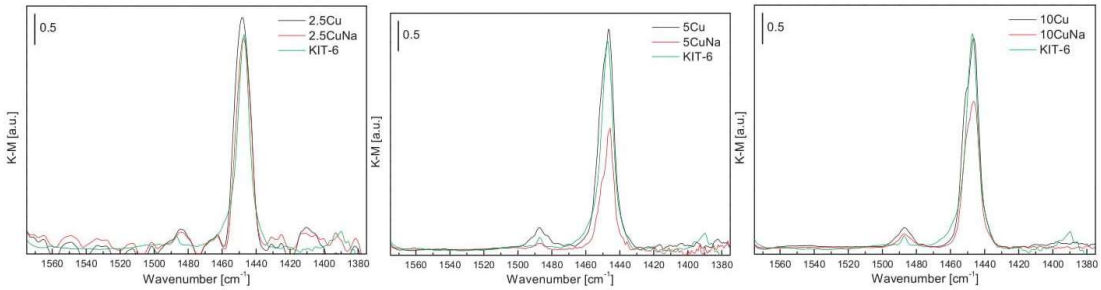

Fig. 7. DRIFT pyridine adsorption spectra of 2.5Cu, 5Cu and 10Cu catalysts before and after Na modification, as well as of bare KIT-6 SiO_2 support.

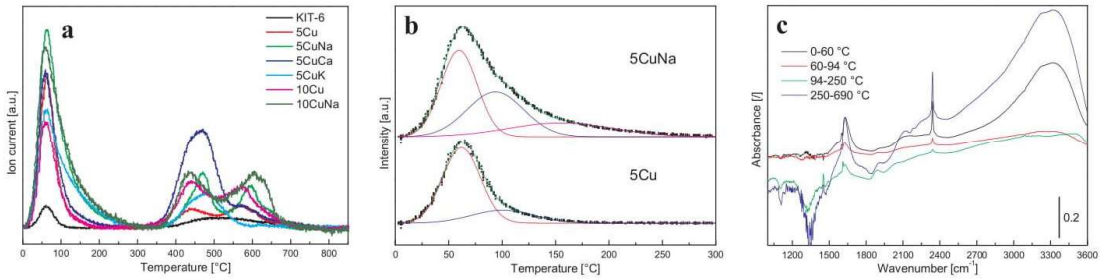

Fig. 8. The CO_2-TPD spectra of 5Cu and 10Cu catalysts prior to and after Na, Ca and K modification (a), deconvolution of the low-temperature CO_2 TPD peak for 5CuNa and 5Cu catalysts (b), and DRIFTS difference spectra measured at characteristic temperature intervals (Fig. S2) over 5CuNa catalyst during CO_2-TPD examination (c).

Table 2
Quantity of desorbed CO_2 for different catalysts.

Sample	Quantity of desorbed CO_2 (μmol × g_{cat}^{-1})		
	Low T cluster	High T cluster	Peak at 155 °C
KIT-6	6.5	12.5	0
5CuNa	65	32.5	13
5Cu	30	20	0
5CuCa	37.5	52.5	0
5CuK	50	17.5	16
10CuNa	75	55	21
10Cu	30	45	0

between 2500-3600 cm^{-1}) and elimination of carbonyl groups (1890 and 2130 cm^{-1}). Also, a decomposition of monodentate carbonate (1452 cm^{-1}) takes place, as well as formation of carbonates from adsorbed CO_2 with simultaneous reduction of CuO_x to Cu_2O.

To briefly summarize, with alkali modification, the nucleophilic character of the oxygen in CuO_x species is reduced. Modulation of the Cu-O bond strength is likely connected to close proximity of the electrophilic Na^+ to the [Cu-O-Cu] moiety, which attracts the partial negative charge of the oxygen atom (Scheme 1, Pathway 1) [18]. This results in the formation of new basic sites of intermediate strength. Oxygen in modified CuO_x appears to be more strongly bound, enabling the formation of loosely bound surface carbonate species, not present in unmodified catalysts.

3.1.8. *Operando* Cu K-edge XANES analysis

Operando Cu K-edge XANES analysis was used to determine the valence states and local symmetries of Cu cations in the 5Cu, 5CuNa and 5CuCa catalysts in the as prepared state, at 350 °C in the O_2/He atmosphere and during catalytic propylene oxidation (Fig. 9).

A shift of Cu K-edge energy of about 4 eV is observed between Cu^+ and Cu^{2+} compounds [36–39]. The characteristic pre-edge resonance or shoulder attributed to the Cu(1*s*-4*p*) transitions can be very effective in the identification of Cu^+ and Cu^{2+} species. In the crystalline Cu_2O, where monovalent Cu^+ is coordinated to four oxygen atoms, a well-defined absorption feature from the 1*s*-4*p* transition occurs at 8982.0 eV [37,38]. In the reference Cu_2O nanoclusters (Cu^+-containing MOR-type zeolite (Fig. 9) [35]), the 1*s*-4*p* transition occurs at 8983.4 eV. In case of Cu^{2+} compounds the 1*s*-4*p* transition appears as pre-edge shoulder in the energy range from 8985 eV to 8989 eV, the energy position and intensity of the shoulder depend on Cu^{2+} cation local symmetry. In the crystalline CuO the shoulder is at 8985.0 eV, while in the case of the reference sample, CuO nanoclusters dispersed in a zeolite, (Fig. 9.) the shoulder is at 8986.3 eV [35,37–39].

The energy position of Cu K-edge and pre-edge shoulder in 5Cu, 5CuNa and 5CuCa catalysts (at RT and 350 °C in He/O_2 atmosphere) matches with the reference sample containing Cu^{2+} oxide nanoclusters dispersed on a zeolite. Based on these references and LCF (linear combination fit) analysis of the 5Cu, 5CuNa and 5CuCa catalysts (at 350 °C in O_2/He atmosphere) all copper is present as Cu^{2+} and the majority (~90%) is subnanometer Cu^{2+} clusters. Only ~10% is present as nanocrystalline CuO (Fig. S4). This is in agreement with TEM-EDX and UV–vis analyses which identified polydisperse $[Cu\text{-}O\text{-}Cu]_x$ moieties as a predominant CuO_x phase, in coexistence with CuO nanocrystallites. The LCF analysis of XANES spectra showed that in the 5CuNa catalyst no sodium cuprate phase (which contains Cu^{3+}) is formed in O_2/He or C_3H_6/O_2/He atmosphere at 350 °C (Figs. S4 and S5).

The Cu K-edge XANES spectra measured during propylene oxidation reaction (Fig. 9.) clearly reveal a substantial reduction of Cu^{2+} to Cu^+ in all tested catalysts. The spectra exhibit a characteristic pre-edge resonance at 8982.7 eV that can be ascribed to the 1*s*-4*p* transition in Cu^+ cations in Cu_2O nanoclusters. The intensity of the resonance is proportional to the relative amount of Cu^+ cations in the sample and increases with prolonged TOS. After 300 min of propylene oxidation reaction, the amount of Cu^+ reaches different values for the tested

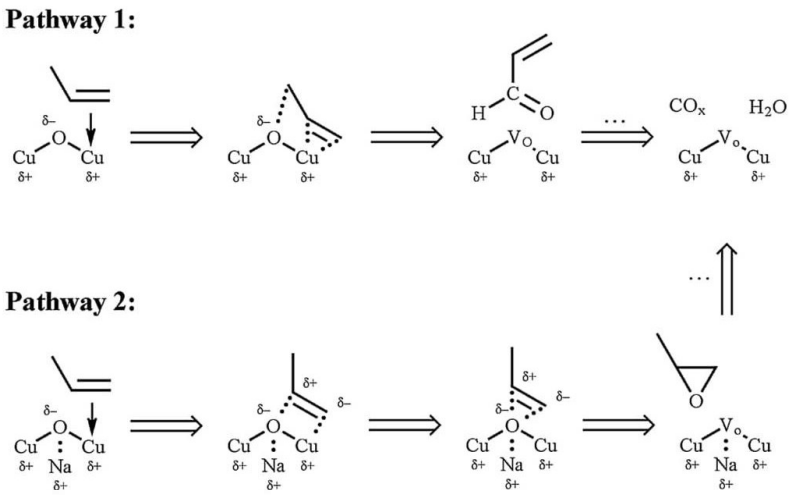

Scheme 1. Reaction pathways of propylene oxidation over CuO_x/SiO_2 catalyst with and without alkali modification.

catalysts: 57(± 5), 68(± 5) and 52(± 5) % for 5Cu, 5CuNa and 5CuCa, respectively (Fig. 10). Also, the dynamics of reaching a quasi-steady oxidation state are very different: the 5Cu catalyst stabilizes (within the quantification error) after 50 min of reaction. This time is prolonged to 100 min for the 5CuCa, whereas the 5CuNa still approaches the quasi-steady state after 300 min.

3.2. Catalytic propylene oxidation reaction

Results of the catalytic propylene oxidation reaction are presented in Figs. 11 and S7. Tests with pure or Na promoted KIT-6 SiO_2 support resulted in no propylene conversion during the 6 h test at 350 °C showing presence of CuO_x as prerequisite for any catalytic conversion.

Over the non-promoted catalysts, the reaction products are CO_2, CO, water, acrolein and trace amounts of other oxygenates (acetone, propanal, propanol, …). However, the latter present less than 5% of the C containing products and are not considered in the discussion. The selectivity over non-modified catalysts for individual reaction products does not change when copper loading is increased from 2.5 to 10 wt. % (Fig. 11b–d).

Low catalytic activity of the 2.5Cu and especially 1Cu catalysts (less than 2.5 and 1% initial propylene conversion, respectively) is likely related to the low amount of CuO_x phase. The 10Cu catalyst enabled highest (25%) initial propylene conversion. Regardless of the copper

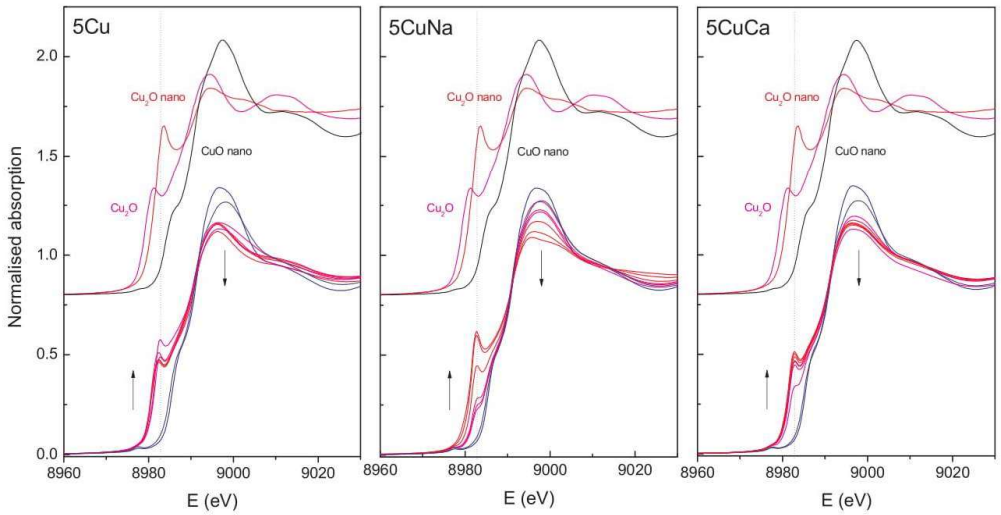

Fig. 9. Normalized Cu K-edge XANES spectra of 5Cu, 5CuNa and 5CuCa catalysts, measured *in-situ* before and during catalytic propylene oxidation reaction. The blue line represents the catalyst measured at RT in O_2/He atmosphere, black line the catalyst in O_2/He atmosphere at 350 °C. Temporal evolution of the catalyst during the propylene oxidation reaction is shown in magenta/red lines with vertical arrows highlighting gradually increasing Cu^+ and decreasing Cu^{2+} contribution. Spectra of reference Cu^+ and Cu^{2+} compounds (crystalline Cu_2O, nanoclusters Cu_2O [35] and CuO nanoparticles) are plotted for comparison. A vertical dashed line is plotted at the peak of the Cu 1s-4p pre-edge absorption feature (8982.7 eV) in the catalysts during the propylene oxidation reaction. (For interpretation of the references to colour in this figure legend, the reader is referred to the web version of this article.)

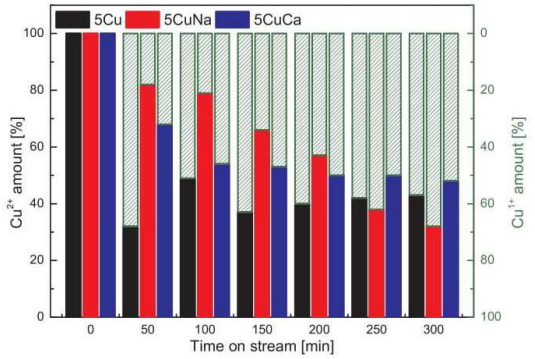

Fig. 10. Fractions of Cu^{2+} and Cu^{+} oxidation states in the 5Cu, 5CuNa and 5CuCa catalysts during the propylene oxidation reaction. The bars at t = 0 min refer to catalyst samples in O_2/He atmosphere at 350 °C.

content, strong deactivation is observed over all unmodified catalysts: they lost more than 60% of initial activity during the 17 h of propylene oxidation reaction (Fig. 11a). In the same time frame, over the 5Cu catalyst, acrolein selectivity increases from 50 to 70%, CO_x selectivity remains between 25–30 % and selectivity for other oxygenates decreased. Sintering of CuO_x phase during the course of reaction (confirmed by *operando* UV/Vis analysis) appears beneficial for acrolein formation which is favoured over bulk-like CuO. Furthermore, oxygen species of CuO_x, regardless of their structure (mononuclear Cu^{2+}-O and $[Cu\text{-}O\text{-}Cu]_n$ as well as bulk-like CuO) exhibit sufficient nucleophilic character to execute the attack on the allylic hydrogen of propylene and thus favour acrolein formation (Scheme 1, Pathway 1).

Based on the results of catalytic runs and *operando* XANES analysis we can conclude that a substantial fraction of Cu^{2+} is transformed to Cu^{+} during the propylene oxidation reaction (52–68 %, depending on the modifying atom). Also, the dynamics of reaching the quasi steady oxidation state differ strongly. However, none of these factors can be solely correlated to PO selectivity. We conclude that the kinetics of oxygen abstraction and replenishment are substantially different, revealing a modified chemistry of the nucleophilic oxygen species present in 5CuNa and 5CuK catalyst, in contrast to the others (5Cu and 5CuCa).

Modification of 5Cu catalysts with sodium and potassium greatly minimized catalyst deactivation (Fig. 11a): minimal deactivation is observed during 17 h TOS for the 5CuNa catalyst, whereas catalytic activity of 5CuK and 2.5CuNa stabilizes after 10 h following the initial decrease of about 25%. Post reaction elemental analysis of catalyst samples showed between 0 and 4 wt. % of carbon deposited during 17 h of reaction (Table S1). For the most promising catalysts investigated, these values are very low (up to 1.6 wt. %), which excludes catalyst fouling by polymerization of reaction intermediates and accumulation of carbonaceous deposits as a primary reason for deactivation.

After Na and K addition, a notable (~10%) propylene oxide selectivity was also observed (Fig. 11b), which increased with prolonging TOS. Having in mind progressive growth of $[Cu\text{-}O\text{-}Cu]_n$ clusters observed by *operando* UV/Vis analysis (Fig. 6b), it is reasonable to assume that Na and K modified oligomeric $[Cu\text{-}O\text{-}Cu]_n$ species (and not mononuclear Cu^{2+} sites) act as active sites responsible for PO formation. Na modification of the 10Cu catalyst exhibited a negligible

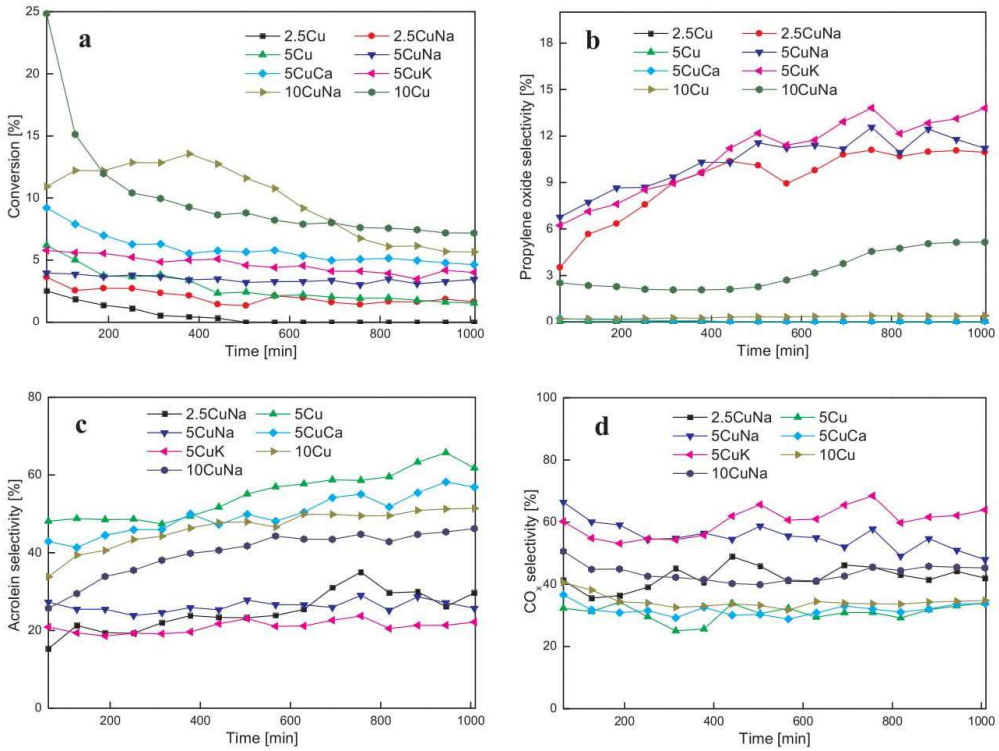

Fig. 11. a) Propylene conversion, b) PO selectivity, c) acrolein selectivity and d) CO_2 selectivity as a function of TOS for promoted and unpromoted 2.5Cu, 5Cu and 10Cu catalysts. The lines depicting the PO selectivity of 2.5Cu and 5Cu catalysts in Fig. b) are at 0% along with 10Cu and 5CuCa.

influence on the shift to PO selectivity (5%, Fig. 11b). This catalyst contains the largest fraction of bulk-like CuO (TEM and UV/Vis analyses, Figs. 3d, f and Fig. 4), which confirms the role of alkali modified bulk-like CuO_x in the propylene epoxidation pathway as minor (it dominates in the acrolein formation pathway). This is consistent with less efficient electronic modification of oxygen species in bulk CuO_x achieved by alkali doping (one alkali cation modulates nucleophilicity of 2–4 adjacent oxygen atoms, depending on the crystalline plane of CuO where it resides, instead of one or two oxygen atoms in $[Cu\text{-}O\text{-}Cu]_n$ oligomers) as well as the suggested requirement for spatial active site isolation in the selective oxidation reactions [40,41], as well as very localized alkali action. The PO weight time yield values obtained lie between 39 and 80 $g_{PO}/kg_{cat} \times h$ (Table S2) for all tested catalysts. The numbers are comparable to values obtained by others over K doped CuO_x/SiO_2 (116 $g_{PO}/kg_{cat} \times h$) [19] and FeO_x/SiO_2 catalysts (47 $g_{PO}/kg_{cat} \times h$) [42].

The selectivity for acrolein is substantially lower (70 and 20% at 17 h TOS, and changes marginally during the whole experiment) when comparing modified 5CuK and 5CuNa catalysts to 5Cu sample. On the other hand, selectivity for CO_2 is notably higher after alkali modification (Fig. 11c) and does not correlate with the abundance of Lewis acid (Fig. 7), or strength or abundance of basic sites (Table 2). Additional propylene oxidation experiment with 5Cu and 5CuNa catalysts and co-fed PO into the gas feed stream showed that over both catalysts, PO is further oxidized and CO_x is the main product (Fig. S6). The unmodified 5Cu catalyst converts approximately 90% of co-fed PO, whereas over the 5CuNa catalyst, only 75% of PO is further oxidized. Consequently, both chemical aspects of the catalyst design, as well as engineering aspects and reaction conditions (reactor design, temperature, pressure and reactant concentration) need attention in order to achieve the goal of appropriate PO selectivity as described by Khatib and Oyama [4].

Two independent reaction pathways occur during propylene oxidation over alkali modified CuO_x/SiO_2 catalysts, as shown in Scheme 1 and Fig. S6.

Pathway 1: Propylene adsorption takes place via the C=C bond to the copper adatom. The oxygen in [Cu-O-Cu] moieties initiates a nucleophilic attack on the allylic hydrogen. The allylic hydrogen is stripped and the terminal carbon is oxidized, producing acrolein. Upon re-adsorption of the primary product, acrolein, on the catalyst's surface, subsequent oxidation occurs, producing CO_x and H_2O.

In Pathway 2, propylene adsorption takes place via the C=C bond to the copper adatom. The nucleophilic character of the oxygen in [Cu-O-Cu] moieties is lessened by the adjacent alkali metal, making its nucleophilic attack on the allylic hydrogen less effective. With the polarization of the double bond, the central carbon can bind the oxygen atom and form an oxametallacycle. The stabilization effect of the Na (or K) modification allows the metal-carbon bond to break [11], which leads to physisorbed propylene oxide, which ultimately desorbs as PO. Subsequent oxidation of PO to CO_x also occurs, but to a lesser extent compared to a non-modified CuO_x/SiO_2 catalyst (Fig. S6).

He et al. [29] used kinetic analysis to identify two independent and parallel reaction pathways over Cs modified 5% CuO_x/SiO_2 catalysts producing PO and acrolein, with PO readily being isomerized further to allyl alcohol. A very likely reason that only trace amounts of allyl and isopropyl alcohol were observed during our tests is that a much higher temperature (350 vs. 250 °C) was used in the present study, which substantially accelerated also the reaction rates towards final oxidation products (CO and CO_2).

By progressively increasing the Na content in the 5Cu catalyst (Table S1, Fig. 12), different fraction of oxygen species and their nucleophilic character can be modified. This is manifested as higher PO selectivity (Fig. 12b), while a reverse trend is observed in acrolein selectivity (Fig. 12c). The PO selectivity increase, achieved when changing the Cu:Na ratio from 1:0.43 to 1:0.6, is relatively small (11 vs. 13%). This indicates that the Cu:Na molar ratio of 1:0.43 (5CuNa catalyst) used for the modification is very close to the optimum.

With calcium modification of the 5Cu catalyst, a dramatic increase in the initial catalytic activity is observed (9 and 6.5% propylene conversion for 5CuCa and 5Cu catalysts, respectively) with trace (below 0.5%) PO selectivity (Fig. 11a and b). Acrolein and CO_x selectivities remain very similar to the unmodified 5Cu catalyst.

Alkali and earth alkali modification of the CuO_x/SiO_2 catalysts produces a diametrally different effect on PO selectivity. The PO selectivity vs. dopant electronegativity plot (Fig. S7) based on the data obtained in this study and other works [19,29], indicates that PO selectivity decreases with increasing electronegativity of the alkali metals ($Cs < Rb \approx K < Na < Li < Ca < Mg$). The Na^+ and K^+ represent localized positive charges which, adjacent to the [Cu-O-Cu] entities (TEM elemental mapping, Fig. 3e and f), attract electrons from the oxygen thus decreasing its nucleophilic strength. As a result, the catalytic action of oxygen changes from oxidative attack on the allylic hydrogen to oxygen insertion into the C=C bond of propylene.

When earth alkali metals are used as dopants, PO selectivity is negligible. We are speculating that as the electronegativity (the tendency of an atom to attract electrons) and valency of the dopant increase (as in the case of Ca^{2+} modified sample), the attraction becomes limited not only to the negative charge of adjacent oxygen in CuO_x, but also to other anionic species, such as hydroxyl groups. A similar phenomenon has been observed before when conducting catalytic reactions in the liquid-phase, with hydroxyl groups forming a progressively denser Helmholtz layer around alkali and earth alkali cations [43]. As a result of charge compensated by hydroxyl groups, the doping efficiency is decreased and negligible after earth alkali modification.

Total oxidation always occurs to a certain extent during the propylene oxidation reaction, which produces CO_x and water, which can further decompose to form surface hydroxyl groups. Abundance and binding strength of hydroxyl groups to the catalyst surface was analyzed using H_2O-TPD-MS technique (Fig. 13). It can be seen that a 5 wt. % Cu addition to KIT-6 silica causes a twofold increase in the density of water and hydroxyls. Their number is decreased by 15–25 % after Na and K modification, respectively. There is a general similarity between the K and Na modified 5Cu and 10Cu catalysts as well as some similarity between the unmodified 5Cu and 10Cu catalysts and the one modified with calcium. However, the largest abundance and strength of hydroxyl binding to the catalyst surface (based on the position of the high-temperature desorption peak) is observed after modification with calcium. The high temperature peaks confirm pure KIT-6 silica dehydroxylation upon heating to 900 °C. The amount of desorbed water becomes much more prominent after copper addition. The results of H_2O-TPD analysis are in line with the proposed role of hydroxyl groups negating the positive charge of alkali and earth alkali cations, thus opposing their effect.

4. Conclusions

The synthesized CuO_x/SiO_2 catalysts contain finely dispersed [Cu-O-Cu] moieties with different degrees of polymerization, as well as CuO_x clusters of 2–6 nm in size. These form larger aggregates as Cu content increases from 2.5 to 10 wt. %. According to the *operando* XANES analysis, the working state of the alkali modified and non-modified catalysts is predominantly Cu^+, between 52–68 %, depending on the modifying atom. Sintering of the CuO_x phase during the course of the reaction promotes acrolein formation, which appears favored over bulk-like CuO_x. Oxygen species contained in mononuclear Cu^{2+}-O and $[Cu\text{-}O\text{-}Cu]_n$ as well as bulk-like CuO all exhibit sufficient nucleophilic character to execute the attack on the allylic hydrogen and thus circumvent PO formation. Consequently, a shift of selectivity towards PO is possible only with alkali modification of the oxygen species contained in CuO_x. The time resolved dynamics of the Cu^+ fraction depends strongly on the modifying atom and indicates different kinetics of oxygen abstraction and replenishment. This suggests modified chemistry of the nucleophilic oxygen species, present in 5CuNa and 5CuK

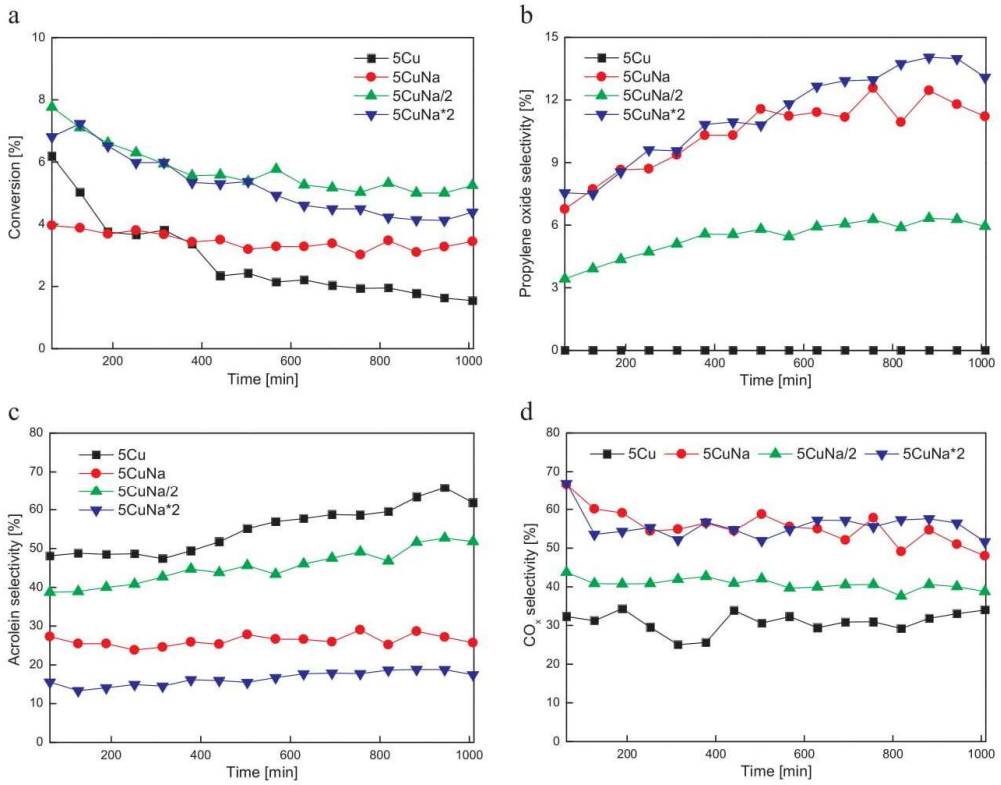

Fig. 12. a) Propylene conversion, b) PO selectivity, c) acrolein selectivity, and d) CO_2 selectivity as a function of TOS for 5Cu catalysts promoted with different amounts of Na.

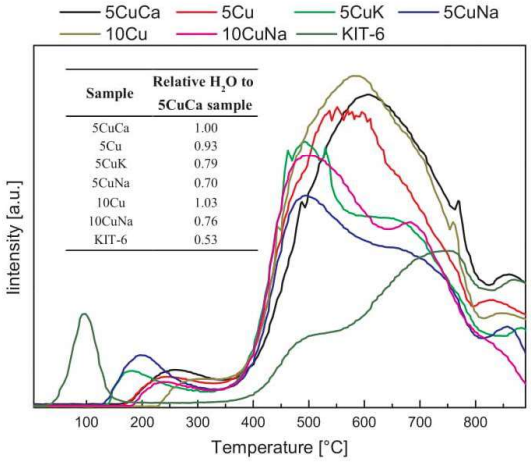

Sample	Relative H_2O to 5CuCa sample
5CuCa	1.00
5Cu	0.93
5CuK	0.79
5CuNa	0.70
10Cu	1.03
10CuNa	0.76
KIT-6	0.53

Fig. 13. The MS spectra recorded during H_2O-TPD experiments over alkali and earth alkali mofified 5Cu and 10Cu catalysts. Samples (100 mg) were positioned inside a U-shaped quartz reactor and pre-treated in a flow 5% O_2/He at 350 °C for 30 min. After pre-treatment, they were cooled to 100 °C. The samples were heated to 900 °C at 5 °C/min and H_2O desorption was monitored by a mass spectrometer (Pfeiffer Vacuum, model ThermoStar™ GSD320) following the characteristic $m/z = 18$ fragment.

catalysts in contrast to others (5Cu and 5CuCa). As a result, Cu^+ is not crucial for PO formation, but instead less nucleophilic oxygen and the geometry of the active site (PO formation is favored on oligomeric $[Cu\text{-}O\text{-}Cu]_x$ moieties and not mononuclear Cu^{2+}-O species). TEM-EDS analyses show that alkali metal cations are finely dispersed over the support and closely associated with the CuO_x phase. The modification with Na^+ and K^+ decreases the nucleophilic strength of CuO_x oxygen, by attracting its electrons, making its attack on the allylic hydrogen of propylene less effective. It also decreases [Cu-O-Cu] sintering. These changes manifest themselves as greatly improved catalytic stability during the propylene oxidation reaction, accompanied by a notable shift in selectivity from acrolein towards propylene oxide. Alkali modification generates basic sites of intermediate strength, confirmed by a CO_2-TPD-DRIFTS analysis, which are not present in non-modified CuO_x/SiO_2 catalysts. This supports altered chemistry/reactivity of surface oxygen species after alkali modification. Subsequent oxidation of formed PO and acrolein to CO_x also occurs, but to a lesser extent compared to a non modified catalyst, due to lowered oxygen reactivity.

With increasing electronegativity and use of two valent dopants, a different effect is achieved: higher catalytic activity and stability, compared to non modified catalysts, but no change in selectivity. The decrease of the nucleophilic character of O species in CuO_x by Ca^{2+} is negated by the charge compensation with strongly adsorbed adjacent hydroxyl groups; hence, earth alkali doping efficiency on PO selectivity is inefficient.

Acknowledgements

JT, PD and AP acknowledge financial support through Research program P2-0150 and research grant Z2-5463 provided by the Slovenian Research Agency (ARRS). MS acknowledges financial support through Research program P2-0091. IA acknowledges the financial support from the Slovenian Research Agency (research core funding No. P1-0112), Access to synchrotron radiation facilities (XAFS beamline, project 20170045) of ELETTRA is acknowledged, and JT acknowledges the support by the project CALIPSOplus under the Grant Agreement 730872 from the EU Framework Programme for Research and Innovation HORIZON 2020 for the XAS experiment at Elettra. We thank Giuliana Aquilanti, Simone Pollastri, Mateusz Czyzycki and Ricardo Grisonich from XAFS beamline for the assistance during experiment and expert advice on beamline operation. The authors kindly acknowledge Dr. Maxim Zabilskiy for the reference spectrum of nanocrystalline CuO and access to the European Synchrotron Radiation Facility (Dutch-Belgian beamline BM26 A, pr. CH-5057).

Appendix A. Supplementary data

Supplementary material related to this article can be found, in the online version, at doi:https://doi.org/10.1016/j.apcatb.2018.05.092.

References

[1] D. Torres, N. Lopez, F. Illas, R.M. Lambert, Low-basicity oxygen atoms: a key in the search for propylene epoxidation catalysts, Angew. Chemie - Int. Ed. 46 (2007) 2055–2058, http://dx.doi.org/10.1002/anie.200603803.
[2] The Dow Chemical Company, Propylene Oxide, (2013) http://msdssearch.dow.com/PublishedLiteratureDOWCOM/dh_096d/0901b8038096db15.pdf?filepath=productsafety/pdfs/noreg/233-00305.pdf&fromPage=GetDoc.
[3] V. Russo, R. Tesser, E. Santacesaria, M. Di Serio, Chemical and technical aspects of propene oxide production via hydrogen peroxide (HPPO process), Ind. Eng. Chem. Res. 52 (2013) 1168–1178, http://dx.doi.org/10.1021/ie3023862.
[4] S.J. Khatib, S.T. Oyama, Direct oxidation of propylene to propylene oxide with molecular oxygen: a review, Catal. Rev. 57 (2015) 306–344, http://dx.doi.org/10.1080/01614940.2015.1041849.
[5] C. Qi, T. Akita, M. Okumura, M. Haruta, Epoxidation of propylene over gold catalysts supported on non-porous silica, Appl. Catal. A Gen. 218 (2001) 81–89, http://dx.doi.org/10.1016/S0926-860X(01)00621-4.
[6] S. Lee, L.M. Molina, M.J. López, J.A. Alonso, B. Hammer, B. Lee, S. Seifert, R.E. Winans, J.W. Elam, M.J. Pellin, S. Vajda, Selective propene epoxidation on immobilized Au6-10 clusters: the effect of hydrogen and water on activity and selectivity, Angew. Chemie Int. Ed. 48 (2009) 1467–1471, http://dx.doi.org/10.1002/anie.200804154.
[7] G. Mul, Stability and selectivity of Au/ TiO2 and Au/ TiO2/SiO2 catalysts in propene epoxidation: an in situ FT-IR study, J. Catal. 201 (2001) 128–137, http://dx.doi.org/10.1006/jcat.2001.3239.
[8] J.R. Monnier, The direct epoxidation of higher olefins using molecular oxygen, Appl. Catal. A Gen. 221 (2001) 73–91, http://dx.doi.org/10.1016/S0926-860X(01)00799-2.
[9] J. Lu, J.J. Bravo-Suárez, M. Haruta, S.T. Oyama, Direct propylene epoxidation over modified Ag/CaCO3 catalysts, Appl. Catal. A Gen. 302 (2006) 283–295, http://dx.doi.org/10.1016/j.apcata.2006.01.023.
[10] M. Mavrikakis, D.J. Doren, M.A. Barteau, Density functional theory calculations for simple oxametallacycles: trends across the periodic table, J. Phys. Chem. B. 102 (1998) 394–399, http://dx.doi.org/10.1021/jp971450p.
[11] A. Kokalj, P. Gava, S. de Gironcoli, S. Baroni, What determines the catalyst's selectivity in the ethylene epoxidation reaction, J. Catal. 254 (2008) 304–309, http://dx.doi.org/10.1016/j.jcat.2008.01.008.
[12] X. Yang, S. Kattel, K. Xiong, K. Mudiyanselage, S. Rykov, S.D. Senanayake, J.A. Rodriguez, P. Liu, D.J. Stacchiola, J.G. Chen, Direct epoxidation of propylene over stabilized Cu + + surface sites on titanium-modified Cu + 2O, Angew. Chemie - Int. Ed. 54 (2015) 11946–11951, http://dx.doi.org/10.1002/anie.201504538.
[13] W. Su, S. Wang, P. Ying, Z. Feng, C. Li, A molecular insight into propylene epoxidation on Cu/SiO2 catalysts using O2 as oxidant, J. Catal. 268 (2009) 165–174, http://dx.doi.org/10.1016/j.jcat.2009.09.017.
[14] O. Vaughan, G. Kyriakou, N. Macleod, M. Tikhov, R. Lambert, Copper as a selective catalyst for the epoxidation of propene, J. Catal. 236 (2005) 401–404, http://dx.doi.org/10.1016/j.jcat.2005.10.019.
[15] M.T. Greiner, T.E. Jones, B.E. Johnson, T.C.R. Rocha, Z.J. Wang, M. Armbrüster, M. Willinger, A. Knop-Gericke, R. Schlögl, The oxidation of copper catalysts during ethylene epoxidation, Phys. Chem. Chem. Phys. 17 (2015) 25073–25089, http://dx.doi.org/10.1039/C5CP03722K.
[16] J.R. Monnier, G.W. Hartley, Comparison of Cu and Ag catalysts for epoxidation of Higher olefins, J. Catal. 203 (2001) 253–256, http://dx.doi.org/10.1006/jcat.2001.3336.
[17] A. Marimuthu, J. Zhang, S. Linic, Tuning selectivity in propylene epoxidation by plasmon mediated photo-switching of Cu oxidation state, Science 339 (2013) 1590–1593, http://dx.doi.org/10.1126/science.1231631.
[18] Q. Hua, T. Cao, X.-K. Gu, J. Lu, Z. Jiang, X. Pan, L. Luo, W.-X. Li, W. Huang, Crystal-plane-controlled selectivity of Cu 2 o catalysts in propylene oxidation with molecular oxygen, Angew. Chemie Int. Ed. 53 (2014) 4856–4861, http://dx.doi.org/10.1002/anie.201402374.
[19] Y. Wang, H. Chu, W. Zhu, Q. Zhang, Copper-based efficient catalysts for propylene epoxidation by molecular oxygen, Catal. Today 131 (2008) 496–504, http://dx.doi.org/10.1016/j.cattod.2007.10.022.
[20] W. Yao, Y.L. Guo, X.H. Liu, Y. Guo, Y.Q. Wang, Y.S. Wang, Z.G. Zhang, G.Z. Lu, Epoxidation of propylene by molecular oxygen Over the Ag–Y2O3–K2O/α-Al2O3 catalyst, Catal. Lett. 119 (2007) 185–190, http://dx.doi.org/10.1007/s10562-007-9220-8.
[21] A. Held, J. Kowalska-Kuś, K. Nowińska, K. Góra-Marek, Potassium-modified silica-supported vanadium oxide catalysts applied for propene epoxidation, J. Catal. 347 (2017) 21–35, http://dx.doi.org/10.1016/j.jcat.2016.12.001.
[22] J. García-Aguilar, D. Cazorla-Amorós, Á. Berenguer-Murcia, K- and Ca-promoted ferrosilicates for the gas-phase epoxidation of propylene with O 2, Appl. Catal. A Gen. 538 (2017) 139–147, http://dx.doi.org/10.1016/j.apcata.2017.03.031.
[23] T. Kim, F. Kleitz, B. Paul, R. Ryoo, MCM-48-like large mesoporous silicas with tailored Pore structure: facile synthesis domain in a ternary triblock copolymer – butanol – water system, J. Am. Chem. Soc. 127 (2005) 7601–7610, http://dx.doi.org/10.1021/ja042601m.
[24] M. Meng, Y. Liu, Z. Sun, L. Zhang, X. Wang, Synthesis of highly-dispersed CuO-CeO2 catalyst through a chemisorption-hydrolysis route for CO preferential oxidation in H 2-rich stream, Int. J. Hydrogen Energy 37 (2012) 14133–14142, http://dx.doi.org/10.1016/j.ijhydene.2012.07.075.
[25] J. Wang, Y. Li, Z. Zhang, Z. Hao, Mesoporous KIT-6 silica–polydimethylsiloxane (PDMS) mixed matrix membranes for gas separation, J. Mater. Chem. A 3 (2015) 8650–8658, http://dx.doi.org/10.1039/C4TA07127A.
[26] S. Lomate, A. Sultana, T. Fujitani, Effect of SiO 2 support properties on the performance of Cu–SiO 2 catalysts for the hydrogenation of levulinic acid to gamma valerolactone using formic acid as a hydrogen source, Catal. Sci. Technol. 7 (2017) 3073–3083, http://dx.doi.org/10.1039/C7CY00902J.
[27] P. Kuśtrowski, L. Chmielarz, R. Dziembaj, P. Cool, E.F. Vansant, Dehydrogenation of ethylbenzene with nitrous oxide in the presence of mesoporous silica materials modified with transition metal oxides, J. Phys. Chem. A 109 (2005) 330–336, http://dx.doi.org/10.1021/jp0455881.
[28] H. Praliaud, S. Mikhailenko, Z. Chajar, M. Primet, Surface and bulk properties of Cu–ZSM-5 and Cu/Al2O3 solids during redox treatments. Correlation with the selective reduction of nitric oxide by hydrocarbons, Appl. Catal. B: Environ. 16 (1998) 359–374, http://dx.doi.org/10.1016/S0926-3373(97)00093-3.
[29] J. He, Q. Zhai, Q. Zhang, W. Deng, Y. Wang, Active site and reaction mechanism for the epoxidation of propylene by oxygen over CuOx/SiO2 catalysts with and without Cs + + modification, J. Catal. 299 (2013) 53–66, http://dx.doi.org/10.1016/j.jcat.2012.11.032.
[30] F. Boccuzzi, S. Coluccia, G. Martra, N. Ravasio, Cu/SiO2 and Cu/SiO2–TiO2 catalysts, J. Catal. 184 (1999) 316–326, http://dx.doi.org/10.1006/jcat.1999.2428.
[31] G. Busca, Acid and basic catalysts: fundamentals, Heterog. Catal. Mater. Elsevier, 2014, pp. 57–101, http://dx.doi.org/10.1016/B978-0-444-59524-9.00005-5.
[32] F. Polo-Garzon, S.-Z. Yang, V. Fung, G.S. Foo, E.E. Bickel, M.F. Chisholm, D. Jiang, Z. Wu, Controlling reaction selectivity through the surface termination of perovskite catalysts, Angew. Chemie Int. Ed. 56 (2017) 9820–9824, http://dx.doi.org/10.1002/anie.201704656.
[33] N. Mizuno, Modern Heterogeneous Oxidation Catalysis, Wiley-VCH Verlag GmbH & Co, KGaA, Weinheim, Germany, 2009, http://dx.doi.org/10.1002/9783527627547.
[34] S. Chen, T. Cao, Y. Gao, D. Li, F. Xiong, W. Huang, Probing surface structures of CeO 2, TiO 2, and Cu 2 O nanocrystals with CO and CO 2 chemisorption, J. Phys. Chem. C 120 (2016) 21472–21485, http://dx.doi.org/10.1021/acs.jpcc.6b06158.
[35] E.M.C. Alayon, M. Nachtegaal, A. Bodi, M. Ranocchiari, J.A. van Bokhoven, Bis(μ-oxo) versus mono(μ-oxo)dicopper cores in a zeolite for converting methane to methanol: an in situ XAS and DFT investigation, Phys. Chem. Chem. Phys. 17 (2015) 7681–7693, http://dx.doi.org/10.1039/C4CP03226H.
[36] F.W. Lytle, R.B. Greegor, A.J. Panson, Discussion of x-ray-absorption near-edge structure: application to Cu in the high-Tc superconductors La1.8Sr0.2CuO4 and YBa2Cu3O7, Phys. Rev. B. 37 (1988) 1550–1562, http://dx.doi.org/10.1103/PhysRevB.37.1550.
[37] A. Manceau, A. Matynia, The nature of Cu bonding to natural organic matter, Geochim. Cosmochim. Acta. 74 (2010) 2556–2580, http://dx.doi.org/10.1016/j.gca.2010.01.027.
[38] C. Maurizio, F. D'Acapito, M. Benfatto, S. Mobilio, E. Cattaruzza, F. Gonella, Local coordination geometry around Cu and Cu ions in silicate glasses: an X-ray absorption near edge structure investigation, Eur. Phys. J. B. 14 (2000) 211–216, http://dx.doi.org/10.1007/s100510050122.
[39] O. Pliekhova, I. Arčon, O. Pliekhov, N.N. Tušar, U.L. Štangar, Cu and Zr surface sites in the photocatalytic activity of TiO2nanoparticles, Environ. Sci. Pollut. Res. 24 (2017) 12571–12581, http://dx.doi.org/10.1007/s11356-016-7685-y.
[40] R.K. Grasselli, Fundamental principles of selective heterogeneous oxidation catalysis, Top. Catal. 21 (2002) 79–88, http://dx.doi.org/10.1023/A:1020556131984.
[41] C.A. Carrero, R. Schloegl, I.E. Wachs, R. Schomaecker, Critical literature review of the kinetics for the oxidative dehydrogenation of propane over Well-defined supported vanadium oxide catalysts, ACS Catal. 4 (2014) 3357–3380, http://dx.doi.org/10.1021/cs5003417.
[42] J. García-Aguilar, I. Miguel-García, J. Juan-Juan, I. Such-Basáñez, E. San Fabián, D. Cazorla-Amorós, Á. Berenguer-Murcia, One step-synthesis of highly dispersed iron species into silica for propylene epoxidation with dioxygen, J. Catal. 338 (2016) 154–167, http://dx.doi.org/10.1016/j.jcat.2016.03.004.
[43] A. Pintar, M. Šetinc, J. Levec, Hardness and Salt effects on catalytic hydrogenation of aqueous nitrate solutions, J. Catal. 174 (1998) 72–87, http://dx.doi.org/10.1006/jcat.1997.1960.

2.2 Supplementary Information 1

SUPPLEMENTARY INFORMATION

Alkali and earth alkali modified CuO_x/SiO_2 catalysts for propylene partial oxidation: What determines the selectivity?

Janvit Teržan[1,2], Petar Djinović[1,*], Janez Zavašnik[3,4], Iztok Arčon[2,5], Gregor Žerjav[1], Matjaž Spreitzer[2,6] and Albin Pintar[1]

[1]Department for Environmental Sciences and Engineering, National Institute of Chemistry, Hajdrihova 19, SI-1001 Ljubljana, Slovenia
[2]Jožef Stefan International Postgraduate School, Jamova cesta 39, SI-1000 Ljubljana, Slovenia
[3]Centre for Electron Microscopy and Microanalysis, Jožef Stefan Institute, Jamova cesta 39, 1000 Ljubljana, Slovenia
[4]Max-Planck-Institut für Eisenforschung GmbH, Max-Planck-Straße 1, 40237 Düsseldorf, Germany
[5]University of Nova Gorica Vipavska cesta 13, Nova Gorica, 5000, Slovenia
[6]Advanced Materials Department, Jožef Stefan Institute, Jamova cesta 39, 1000 Ljubljana, Slovenia

*Corresponding author, e-mail: petar.djinovic@ki.si

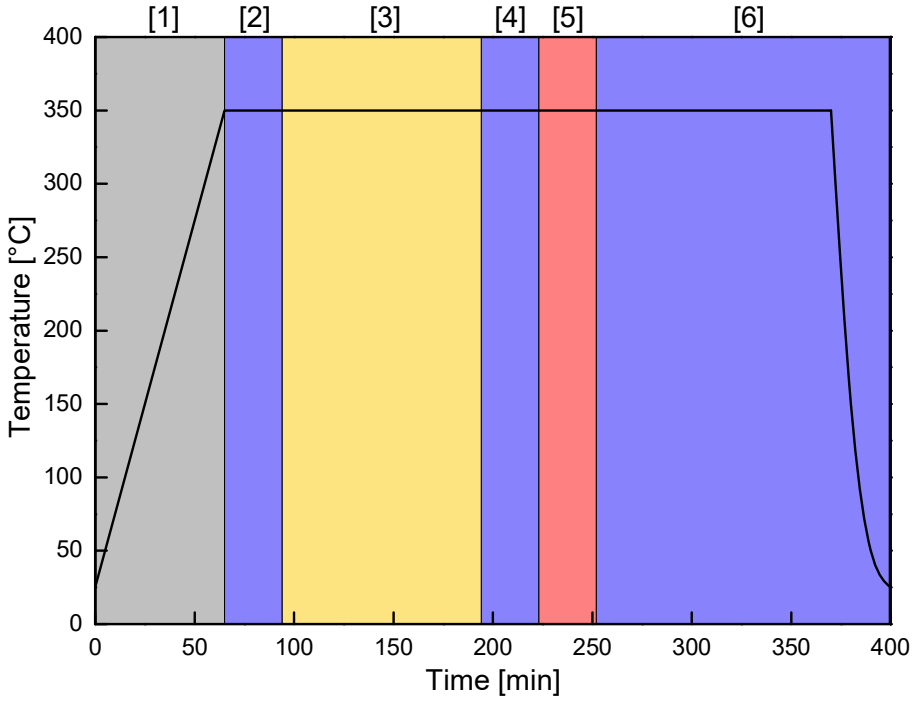

Fig. S1: *Operando* UV/Vis DRS protocol. Spectra were recorded over catalyst samples exposed to: [1] and [2] pre-treatment in 20 % O_2/He at 350 °C for 30 min, [3] 100 min of propylene oxidation reaction (16.7 % C_3H_6, 16.7 % O_2 and 66.6 % of He at 350 °C), [4] catalyst oxidation in 20 % O_2/He at 350 °C for 30 min, [5] catalyst reduction by exposure to pure C_3H_6, and [6] catalyst re-oxidation for 115 min in 20 % O_2/He at 350 °C.

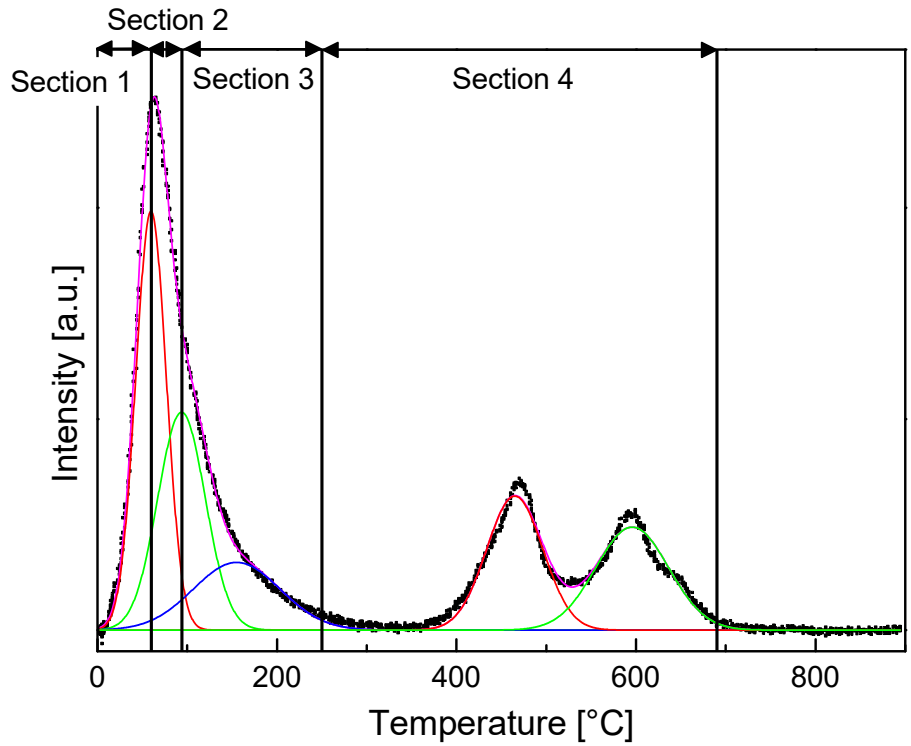

Fig. S2: CO_2-TPD profile of 5CuNa catalyst highlighting 4 temperature sections used for generation of difference DRIFT CO_2 spectra. Sections are based on the positions of deconvoluted CO_2 desorption peaks and as such represent each peak as individually as possible: Section 1 between 0 and 60 °C, Section 2 between 60 and 94 °C, Section 3 between 94 and 250 °C, and Section 4 between 250 and 690 °C.

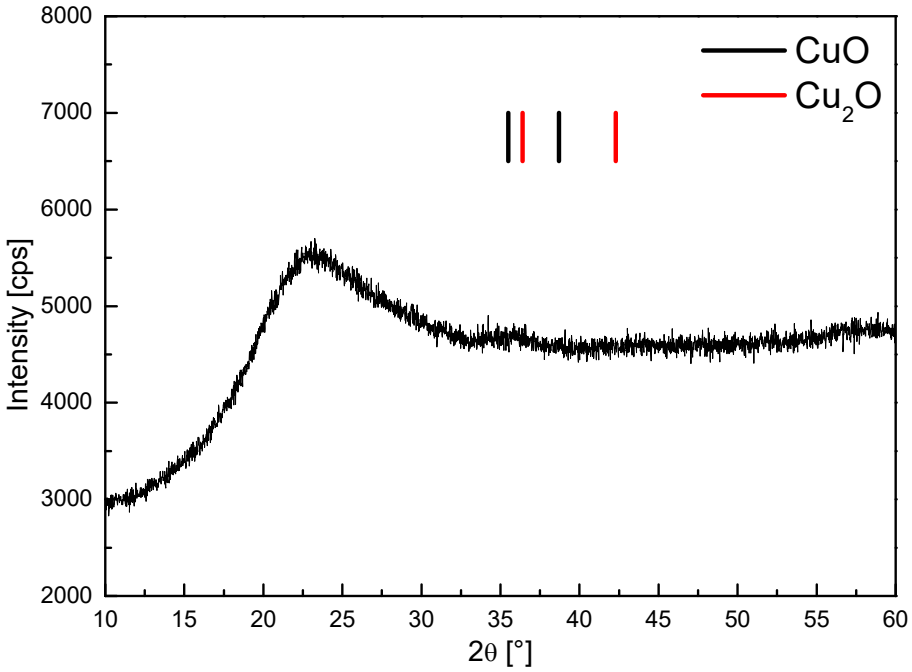

Fig. S3: XRD pattern in the 2θ range from 10 ° to 60 ° of the 10Cu catalyst showing no crystalline copper containing phases is present in the material. Expected positions for most intense diffraction peaks of CuO and Cu_2O phases are marked.

XAS measurement details

A Si (111) double crystal monochromator with about 1 eV resolution at Cu K-edge was used. The intensity of the monochromatic X-ray beam was measured by three 30 cm long ionization detectors, filled with the following gas mixtures: (first) 1250 mbar N_2, 750 mbar He; (second) 250 mbar Ar, 750 mbar He, 1000 mbar N_2; (third) 700 mbar Ar, 1000 mbar N_2, 300 mbar He. Sample pellets, enclosed in a tubular oven reactor, were placed in the beam between first two ionization detectors. The absorption spectra were measured in the energy region from -150 eV to +1200 eV relative to the Cu K-edge. In the XANES region equidistant energy steps of 0.3 eV were used, while for the EXAFS region equidistant k steps of 0.03 $Å^{-1}$ were adopted, with an integration time of 2 s/step. The exact energy calibration was established with simultaneous absorption measurement on a 7 micron thick Cu metal foil placed between the second and the third ionization chamber. Absolute energy reproducibility of the measured spectra was ±0.01 eV. The quantitative analysis of XAS spectra is performed with the Demeter (IFEFFIT) program package (Ravel, B.; Newville, M. J. Synchrotron Radiat. 2005, 12 (4), 537–541.). The relative K-shell contribution in the absorption spectra was obtained by the standard procedure by removing the extrapolated best-fit linear function determined in the pre-edge region (-150 eV -30 eV), and by conventional normalization extrapolating the post-edge spline background determined in the range from 150 to 900 eV in order to set the Cu K-edge jump to 1.
The reference spectra CuO small nano and CuO large nano were kindly provided by Dr. Maxim Zabilskiy, recorded at the European Synchrotron Radiation Facility (Dutch-Belgian beamline BM26A, pr. CH-5057).

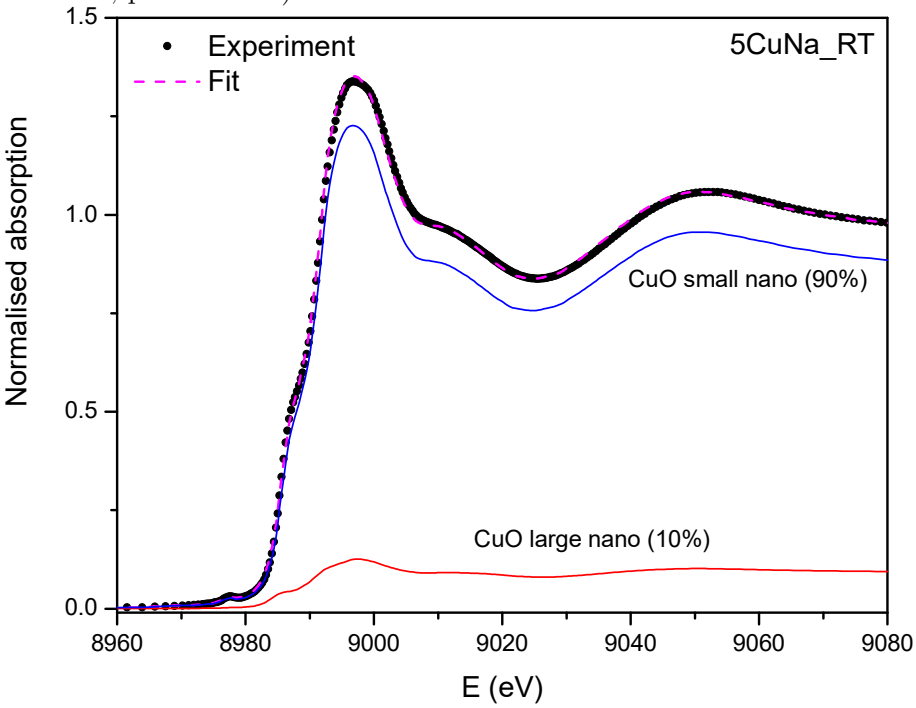

Fig. S4: Cu K-edge XANES spectra of 5CuNa catalyst, measured at room temperature in an O_2/He atmosphere. Black dots: experiment; dashed magenta line: best fit with linear combination of the two reference XANES profiles (CuO small nano: nanocluster reference, where the average particle size is below 1 nm; CuO large nano: nanocluster reference, where the average particle size is above 1 nm) plotted below.

If the sample contains the same cation in two or more sites with different local structure and valence state, the measured XANES spectrum is a linear combination of individual XANES spectra of the different cation sites. The relative amounts of the cation at each site can be precisely determined by the linear combination fit (LCF) [86] with the XANES spectra of proper Cu reference compounds. The procedure was applied to Cu K-edge XANES spectra measured during the propylene oxidation reaction. These spectra can be completely described by the linear combination of the three XANES spectra: a) spectrum measured on the sample at RT in He/O_2 atmosphere, where copper is present in the form of Cu^{2+} oxide nanoclusters, b) the last operando XANES spectrum measured during the propylene oxidation reaction when equilibrium state in the catalyst was reached and c) the spectrum of CuO nanoparticles. The fit result is illustrated in Figure S4. In this way we were able to determine the relative amount of Cu^{2+} and Cu^{+} species in the catalyst in intermediate states during the propylene oxidation reaction with the accuracy of ±2 %.

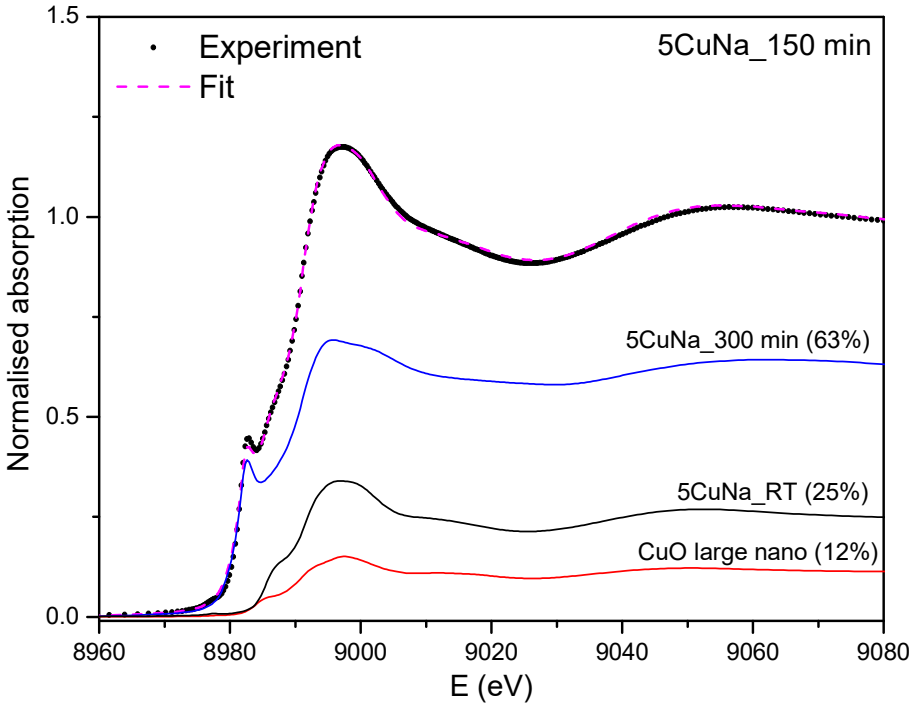

Fig. S5: Cu K-edge XANES spectra of 5CuNa catalyst, measured in operando during catalytic propylene oxidation reaction after 150 min. Black dots: experiment; dashed magenta line: best fit with linear combination three reference XANES profiles (the sample measured before catalytic reaction at RT; the last operando XANES spectrum measured during the propylene oxidation reaction when quasi-equilibrium state in the catalyst was reached, and the spectrum of CuO nanoparticles) plotted below.

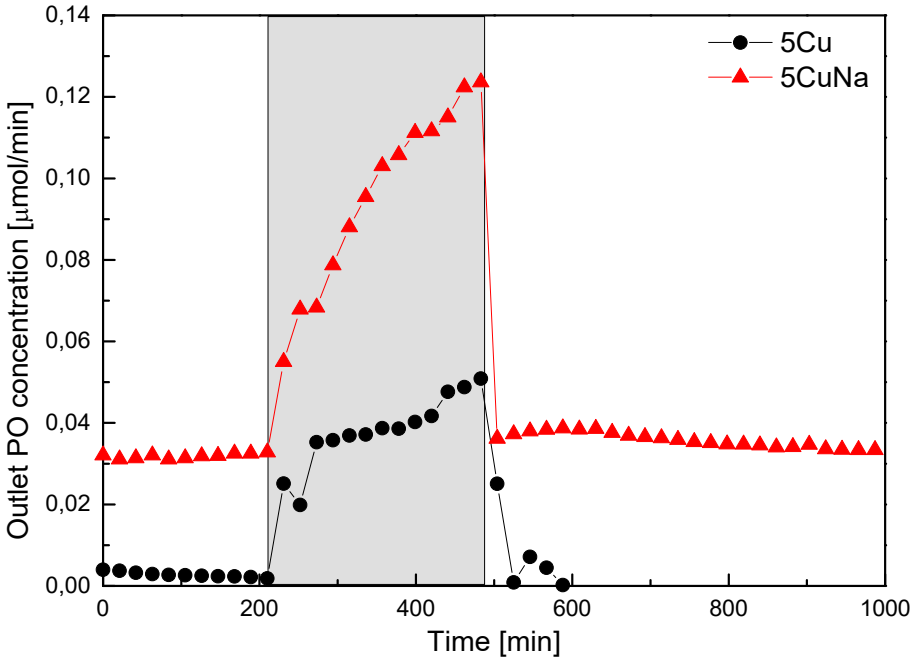

Fig. S6: Propylene oxide concentration after passing through the catalyst at 350 °C for the sodium modified and unmodified 5 wt. % of Cu containing catalysts. The protocol for the catalytic reaction was identical as described in section 2.3. After 200 minutes of propylene oxidation reaction (C_3H_6, O_2 and He in the feed stream), PO was injected continuously with the use of a syringe pump at the rate of (0.47 µmol/min) into the gas stream (grey area). PO produced by the 5CuNa catalyst was subtracted for easier comparison.
The unmodified 5Cu catalyst consumes approximately 90 % of co-fed PO, whereas 5CuNa only 75 %. The reduction of the nucleophilic character of oxygen species in the CuO_x by alkali modification results in a decreased reactivity towards PO and its further oxidation to CO_2 and H_2O. The results of the experiment with co-fed PO clearly show that the selectivity of the catalyst under the employed reaction conditions is strongly influenced by the secondary PO oxidation reactions.

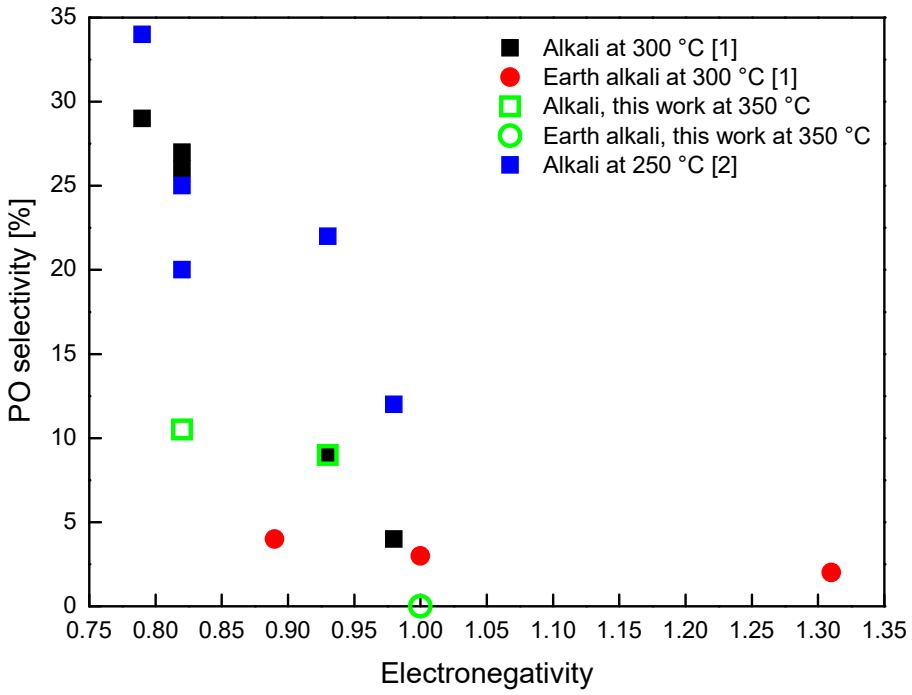

Fig. S7: Effect of alkali and earth alkali electronegativity on the PO selectivity in the propylene oxidation reaction with O_2. Data points represented by full symbols were calculated based on the data provided in the following references: [1] Y. Wang, H. Chu, W. Zhu, Q. Zhang, Catal. Today 131 (2008) 496-504; [2] J. He, Q. Zhai, Q. Zhang, W. Deng, Y. Wang, J. Catal. 299 (2013) 53-66.

Table S1: Semi-quantitative elemental analysis of copper and alkali/earth alkali dopants in different CuO_x/SiO_2 catalysts as determined by SEM-EDS analysis.

Sample	Content, wt. %				Cu:dopant, mol:mol	[a]Carbon deposition, wt. %
	Cu	Na	Ca	K		
2.5CuNa	3.1±0.2	0.5±0.1	0	0	1:0.45	0.5
5CuNa	5.2±0.2	0.8±0.1	0	0	1:0.43	0.3
5Cu	5.3±0.2	0	0	0	/	0.7
5CuNa/2	5.2±0.2	0.4±0.1	0	0	1:0.21	0.5
5CuNax2	5.1±0.6	1.1±0.2	0	0	1:0.60	0.6
5CuCa	5.1±0.5	0	0.5 ± 0.2	0	1:0.16	0.6
5CuK	5.1±0.4	0	0	0.7±0.2	1:0.22	1.6
10CuNa	9.0±0.3	0.5±0.1	0	0	1:0.15	0.8
10Cu	9.9±0.6	0	0	0	/	3.8

[a]After reaction.

Table S2: The PO weight time yields obtained over different CuO_x/SiO_2 catalysts.

Catalyst	Weight time yield, $g_{PO}/h \times kg_{cat}$	
	Initial	Steady state
2.5CuNa	30	38
5CuNa	39	53
5Cu	/	/
5CuNa/2	39	44
5CuNax2	73	80
5CuCa	/	/
5CuK	54	77
10CuNa	43	40
10Cu	/	/

Chapter 3

Effect of Na, Cs and Ca on Propylene Epoxidation Selectivity over CuO_x/SiO_2 Catalysts Studied by Catalytic Tests, *in-situ* XAS and DFT

In Chapter 3, we further investigated the mechanism of alkali and alkaline earth modification of subnanometer CuO_x clusters dispersed over amorphous mesoporous silica. With *in-situ* EXAFS analysis we took a closer look at the local structure of copper atoms during catalysis. In general, a slight reduction in Cu-O bond length was observed when the catalyst was modified with an alkali metal. We expanded the proposed reaction mechanism (suggested in Chapter 2) and analyzed the reaction steps with DFT calculations.

We propose that the reduction in Cu-O bond length, indicative of stronger binding of oxygen, is the underlying reason for increased PO selectivity. The shorter bond signifies a less nucleophilic (less basic) oxygen species, which prevents allylic hydrogen stripping. EXAFS measurements show a structural change (re-dispersion or flattening) of the CuO_x nanoparticles during catalysis. The oxidation state changes from Cu^{2+} after synthesis to a mixture of Cu^{2+} and Cu^{+} during reaction. Catalyst deactivation can be correlated to the amount of Cu^{+}. The theoretical studies show that modification with alkali and alkaline earth metals decreases propylene binding strength. Regardless of the modification, the activation barrier for molecular oxygen dissociation is lowered. This correlates well with *in-situ* XAS, where the unmodified catalyst is reduced much faster than the modified catalysts. Alkali modification (Na and Cs) increases the activation barrier for AHS as well as for OMC formation. However, the barrier for OMC formation is still lower than for AHS. Additionally, the barrier for OMC ring closure and PO desorption is also lowered. This results in increased PO selectivity compared to unmodified CuO_x. Modification with an alkaline earth metal (Ca) drastically lowers the activation barrier for AHS. It also has a minimal effect on the activation barrier for OMC formation. As a result, selectivity towards acrolein is strongly favored with no PO formation.

Regarding my contribution: I performed all the syntheses and the catalytic tests. Additionally, I assisted with the experimental part of X-ray absorption spectroscopy. I also wrote the paper with the co-authors.

3.1 Effect of Na, Cs and Ca on Propylene Epoxidation Selectivity over CuO_x/SiO_2 Catalysts Studied by Catalytic Tests, *in-situ* XAS and DFT

Applied Surface Science 528 (2020) 146854

Contents lists available at ScienceDirect

Applied Surface Science

journal homepage: www.elsevier.com/locate/apsusc

Effect of Na, Cs and Ca on propylene epoxidation selectivity over CuO_x/SiO_2 catalysts studied by catalytic tests, in-situ XAS and DFT

Janvit Teržan[a,b], Matej Huš[c], Iztok Arčon[d,e], Blaž Likozar[c], Petar Djinović[a,*]

[a] Department of Inorganic Chemistry and Technology, National Institute of Chemistry, Hajdrihova 19, SI-1001 Ljubljana, Slovenia
[b] Jožef Stefan International Postgraduate School, Jamova cesta 39, SI-1000 Ljubljana, Slovenia
[c] Department of Catalysis and Chemical Reaction Engineering, National Institute of Chemistry, Hajdrihova 19, SI-1001 Ljubljana, Slovenia
[d] Laboratory of Quantum Optics, University of Nova Gorica, Vipavska 13, SI-5000 Nova Gorica, Slovenia
[e] Jožef Stefan Institute, Jamova cesta 39, SI-1000 Ljubljana, Slovenia

ARTICLE INFO

Keywords:
Alkali modification
Propylene epoxidation
Reaction mechanism
Copper oxide
Activation barrier

ABSTRACT

This research focuses on epoxidation of propylene over pristine, Na, Ca and Cs modified CuO_x/SiO_2 catalysts using O_2. The selectivity of the reaction is analyzed using a combination of catalytic tests, in-situ XAS and DFT calculations. The initially present subnanometer CuO clusters are present in all catalysts which re-disperse/flatten during reaction. During catalytic reaction, the Cu^{1+} becomes the predominant oxidation state. There is no correlation between propylene oxide (PO) selectivity and copper oxidation state. DFT analysis of the propylene reaction pathway revealed that Na, Cs, and Ca addition decreases the bonding strength of propylene to CuO and decreases the O_2 activation barrier, while simultaneously increase the exothermicity of O_2 dissociation. The Na induced Cu–O bond modification decreases the activation barrier from 0.87 to 0.71 eV for the oxametallacycle (OMC) ring closure (first step in the reaction pathway favoring selectivity towards PO) compared to pristine 5Cu catalyst. At the same time, we observed an increase (from 0.45 to 0.72 eV) of the barrier for the abstraction of allylic hydrogen. The opposite effect is achieved by Ca addition: the activation barrier for OMC ring closure increases to 1.08 eV and that for allylic hydrogen stripping decreases to 0.16 eV.

1. Introduction

Propylene oxide (PO) is a platform chemical which is used for synthesis of propylene glycol and polyether polyols. The production of flexible polyurethane foams is the main driver behind the growing PO demand. The latter reached almost 10 Mt in 2017 and projections show that by 2025, the annual PO demand will exceed 20 Mt [1]. Currently, PO is produced mainly with the chlorohydrin technology or by oxidation of propylene by organic peroxides. Due to the large amounts of side products and waste-water generated, as well as high price of organic peroxides, a direct oxidation route using molecular oxygen is of great academic and industrial interest [2].

Direct propylene epoxidation with molecular oxygen suffers from several drawbacks, most notably low PO selectivity. This is believed to be a consequence of a short life-time of the selective transient oxygen species [3]. When molecular oxygen undergoes the following transformation ($O_2 \rightarrow O_2^- \rightarrow 2O^- \rightarrow 2O^{2-}$), its electrophilic character is progressively diminished, shifting the tendency from insertion into the electron rich C=C bond towards favoring hydrogen abstraction.

By using a combination of H_2 and O_2 in the gas-phase propylene epoxidation over Au-Pd/TiO_2, high PO selectivity (> 90%) is reached, albeit at low conversions (1–2%) [4]. The main disadvantage of this catalytic process is a broad explosion range of H_2/O_2 gas mixtures and fast catalyst deactivation because of persistent deposition of carbonaceous species [5,6].

Being known for their high selectivity in the *ethylene* epoxidation with molecular oxygen, Ag based catalysts have been the subject of many propylene epoxidation studies [7,8]. However, unmodified silver catalysts prefer abstraction of the allylic hydrogen in propylene (absent in ethylene) and this leads to acrolein formation [9]. Silver modified with $CuCl_2$ showed a significant increase in PO selectivity (from 36.9 to 71.2%). The authors proposed that a decrease in oxygen basicity hampers the allylic hydrogen abstraction and also prevents the dissociation of the adsorbed diatomic oxygen species to oxide anions [10]. Various metal (Ag, Au, Ti, Cu, V, etc.) and support (Al_2O_3, TiO_2, $CaCO_3$, WO_3, SiO_2, etc.) combinations have been evaluated for the production of propylene oxide and it was commonly observed that higher propylene conversions lead to low PO selectivity [2,11].

* Corresponding author.
E-mail address: petar.djinovic@ki.si (P. Djinović).

https://doi.org/10.1016/j.apsusc.2020.146854
Received 25 February 2020; Received in revised form 7 May 2020; Accepted 30 May 2020
Available online 05 June 2020
0169-4332/

Copper based materials have been studied as potential catalysts for the direct propylene epoxidation using molecular oxygen. The less reactive copper-bound oxygen (compared to silver-bound) allows for the formation of the oxametallacycle (OMC) intermediate, which is generally considered as crucial in the formation of PO [12-16]. The role of different promotors has also been investigated, focusing on the effects of alkali and alkaline earth salts on Cu, Fe, Ru and Sn containing catalysts [17-21]. Miller et al. have proposed that the changes in PO selectivity after NaCl addition to SnO_2–CuO/SiO_2 catalyst occur because: (i) the addition of alkali helps with the dispersion of the CuO_x phase [19,20] and (ii) chlorine alters the electronic properties of the active species [20]. In theoretical calculations, the effect of alkali metals on the selectivity has been ascribed to the dipole effect [22,23].

Several theoretical or mixed studies have looked into the mechanistic insight of propylene epoxidation. Molina et al. [24] studied the partial oxidation of propylene on silver nanocatalysts and observed that acrolein is preferentially formed. Only on the largest nanoparticles were non-negligible amounts of PO detected. Theoretical computations confirmed that the formation of acrolein is kinetically more favorable on both flat silver surfaces and nanoparticle edges. On subnanometer Ag aggregates, low selectivity towards PO was observed, with major products being CO_2 and acrolein. Computational methods showed that on the amorphous alumina support exclusively acrolein forms, while further away, on silver nanoparticles, PO is also formed [25,26]. Aside from silver, copper stands out as a viable metal for epoxidation. Pristine copper surfaces seem to be intrinsically more selective than silver in alkene epoxidation [27]. Düzenli et al. [28] showed using DFT calculations that on Cu_2O(0 0 1) and CuO(0 0 1) acrolein is the preferred product. The selectivity preference for acrolein over larger CuO_x crystallites was experimentally confirmed also by Teržan et al. [29] An increase in the basicity of the surface oxygen was found to favor the formation of acrolein, as it promotes allylic hydrogen abstraction [14]. Critical influence of adsorption geometry, specifically the proximity of the C═C function and the allylic hydrogen atoms to the (1 1 1) surface of copper determines the selectivity during epoxidation of allylic alkenes [30]. After successfully avoiding the allylic hydrogen stripping, the stability of the oxametallacycle intermediate plays the crucial role in the reaction selectivity [31].

This work is a generalization and expansion of our previously postulated reaction mechanism [29]. Catalytic studies and *in-situ* XAS analyses were complemented with DFT calculations to shed light on the changes in the CuO_x structure and their consequences on the reaction energies induced by the alkali modification.

2. Materials and methods

2.1. Catalyst synthesis

The synthesis protocol of KIT-6 silica support, CuO_x deposition and subsequent modification with alkalis is described in detail in [29]. Briefly, one gram of ordered mesoporous silica (KIT-6 morphology) was dispersed in 20 mL of aqueous solution containing 190 mg of Cu $(NO_3)_2{\cdot}3H_2O$ (Sigma Aldrich, purity 99%). The pH was adjusted to 9 with dilute ammonia solution while stirred. After 2 h, the solid was collected by centrifugation and dried at 60 °C overnight. The samples were calcined for 3 h at 350 °C. The efficiency of copper deposition over SiO_2 support was analyzed through the quantification of remaining Cu^{2+} in the mother liquor. A photometric copper test (Spectroquant NOVA60, Merck) revealed > 99% of copper was deposited. As a result, the nominal 5 wt% copper loading can be regarded as actual. For 1 g of catalyst modification with alkali (Na and Cs) or alkaline earth (Ca) salts, 100 mL of a 0.1 or 0.05 M solution of the nitrate salt was used. All nitrate salts were purchased from Sigma Aldrich with a purity of 99%. The sodium content in CuO_x/SiO_2 catalysts was optimized in our previous work [29]. The suspension containing CuO_x/SiO_2 powder was stirred for 2 h and the solid collected by centrifugation and followed by overnight drying at 60 °C and calcination for 3 h at 350 °C. The analyzed alkali and alkaline earth content in the catalysts was 0.7 ± 0.2 wt%. Catalyst samples in this work are denoted as 5Cu, 5CuNa, 5CuCs and 5CuCa. Number 5 represents the Cu content and Na, Cs and Ca indicate the added alkali. KIT-6 silica was used to ensure a narrow pore size distribution (6–9 nm, see ESI) and to anchor the CuO_x clusters in similar sized cavities. Structural characterization (low, wide angle XRD, N_2 sorption and dark field STEM) of catalysts is provided in ESI (Figs. S1–S5 and Table S1).

2.2. Catalytic tests

The catalytic performance was evaluated in a fixed-bed quartz reactor (I.D. = 10 mm) at atmospheric pressure. The catalyst (50 mg) was diluted with SiC (Sicat, grain range 30–100 μm) in a mass ratio of 1 to 4. All the samples were pre-treated in a flow of 20% O_2/He (25 mL/min, Linde, purity 5.0) at 350 °C for 20 min. After that, propylene (Messer, purity 2.5) at 5 mL/min was added to the gas mixture. The reaction products were analyzed by gas chromatography (Agilent, model 7890A); the analyzer was equipped with the DB-WAXETR and the HP-PlotQ columns and a TCD detector.

The conversion of propylene was calculated using Eq. (1), where n_{C3H6i} and n_{C3H6O} are moles of propylene at the inlet and outlet of the reactor.

$$\%_{conversion} = \frac{(n_{C_3H_6i} - n_{C_3H_6o})}{n_{C_3H_6i}} \times 100\% \quad (1)$$

Reaction product selectivities were calculated according to equation (2), where n_i are moles of product *i* and n_{C3H6C} are moles of propylene converted.

$$\%_{selectivity} = \frac{n_i}{n_{C_3H_6c}} \times 100\% \quad (2)$$

2.3. In-situ XAS

The Cu K-edge X-ray absorption spectra (XAS) of 5Cu, 5CuNa, 5CuCs and 5CuCa catalysts were recorded *in-situ* during the propylene oxidation reaction at 350 °C in transmission mode (XAFS beamline at ELETTRA). The catalyst samples were pressed into homogeneous pellets and diluted with BN powder, giving a total absorption thickness (μd) of about 2.5 above the investigated Cu K-edge. Pellets were placed in a quartz holder inside a tubular oven (Carbolite), sealed with 20 μm aluminum foil windows, filled with 20% O_2/He gas mixture at 1 bar. The XAS spectra were measured *in-situ*: (i) at room temperature, (ii) at 350 °C in the 20% O_2/He atmosphere and (iii) during the catalytic propylene oxidation reaction at 350 °C in a 16.7% C_3H_6/16.7% O_2/He stream (total flowrate of 30 mL/min). After propylene addition, the samples were measured repeatedly until the quasi-equilibrium state in the catalyst was reached (up to 10 XAS spectra were collected per sample). Additional details of the XAS analyses are provided in the ESI.

2.4. Computational details

Theoretical calculations were performed with the Vienna Ab Initio Simulation package 5.4.1 (VASP 5.4.1) [32-35]. Plane-wave formalism of the density functional theory (DFT) was used with PAW pseudopotentials [36,37] containing gradient-corrected Perdew-Burke-Ernzerhof exchange correlation [38]. For the one-electron Kohn-Sham orbitals, a kinetic cutoff of 500 eV was used. As no periodicity was desired for the description of metal clusters, the reciprocal space integration was performed at the gamma point center and the metal clusters were surrounded by 15 Å of vacuum in all directions in the real space.

The structures were fully relaxed (no constrained atoms) with the force threshold 0.01 eV/Å for stable structures and 0.03 eV/Å for transition states. To arrive at the most stable cluster geometry (based on

the results of *in-situ* XAS analysis), ten different stoichiometric 24-atom clusters were cut from the bulk CuO structure and preliminarily optimized. This structure was used as the initial catalysts contain negligible amounts of Cu^+ and, in the case of the most active ones, this remains the predominant form of copper.

On three slightly perturbed lowest-lying structures, the first-principles molecular dynamics simulations at 300 K (using the Nosé-Hoover thermostat) were carried out to ensure that the lowest-lying energy states were identified (Figs. S6 and S7). We performed 1000 simulation steps of 1 fs for a total simulation time of 1 ps. The lowest energy structure was used for further calculations. Analogously, several positions for the adsorbates were tested.

The transition states were roughly identified with the nudged elastic band method [39] and further refined with the dimer method [40-43]. Vibrational analysis was performed with a finite difference approach (displacements of 0.01 Å) to obtain the zero-point energy corrections and to classify the obtained stationary points as saddle points or intermediates. In the calculations, spin polarization was turned on. Dipole corrections were used in all three cardinal directions [44,45]. Van der Waals bonding was explicitly accounted for with the D3 correction method by Grimme [46], which does not suffer from the overbinding problems of the D2 method as it uses geometry-dependent coefficients.

The adsorption energies were calculated as $E_{ads} = E_{adsorbed} - E_{catalyst} - E_{gaseous}$, where $E_{adsorbed}$ stands for the energy of the slab with an adsorbed species, $E_{catalyst}$ is the energy of the (relaxed) barren slab and $E_{gaseous}$ is the energy of the (relaxed) isolated species. The reaction energies were calculated $\Delta E = E_{final} - E_{initial}$, where E_{final} and $E_{initial}$ represent the energies of a final and initial state, respectively. The activation energy is defined as $E_A = E_{TS} - E_{initial}$, where E_{TS} is the energy of a transition state.

3. Results and discussion

3.1. Catalytic tests

Catalytic runs with SiC, pure silica or alkali impregnated silica showed no propylene conversion at 350 °C, indicating that the presence of CuO_x is as a prerequisite for propylene activation. Regardless of the modifying element, acrolein and CO_x (CO and CO_2) were the predominant reaction products (Fig. 1). Cumulative selectivity for all other oxygenates (propanal, acetone, isopropanol and 1-propanol) was below 7%. Carbon mass balances in all tests accumulated to over 90%.

All modified catalysts (5CuNa, 5CuCs and 5CuCa) exhibited a lower degree of deactivation compared to the unmodified 5Cu (Fig. 1), indicating a positive effect of the addition of alkali(ne earth) metals on stability. Most notably, the activity of 5CuCs remained entirely stable throughout the 15 h of reaction. The activity of other catalysts initially decreased and began to stabilize after ~ 12 h. Carbon deposits (measured by CHNS analysis) accumulated to 0.3–0.7 wt% during 15 h Time On Stream (TOS) for all catalysts.

Propylene oxide was detected only over 5CuNa and 5CuCs catalysts (14 and 6% selectivity at 15 h TOS, respectively), while 5Cu and 5CuCa catalysts produced no PO. The 5CuNa shows a noticeable drop in activity, which is accompanied by a steadily increasing selectivity towards PO (7.5 → 14%). This leads us to believe that the most active and non-selective sites, causing total combustion of propylene and oxygenates, are lost first. In the case of 5CuCs, there is no change in selectivity for all identified reaction products (Fig. 1), hinting at a much improved stability of the active sites.

Modifying the 5Cu catalyst with Ca increased its activity by approximately 3-fold (1.6% vs. 4.8% propylene conversion for 5Cu and 5CuCa at 15 h TOS, respectively) but still no formation of PO is observed. The selectivities for acrolein and CO_x remain similar to the unmodified 5Cu catalyst (Fig. 1). The PO weight time yields after 1000 min TOS were 32 and 80 $gPO/kg_{cat} \times h$ for 5CuCs and 5CuNa, respectively. The measured PO selectivities in this work are not the highest compared to the literature reports among similar catalyst formulations (34% PO selectivity achieved by He et al. [19]). However, the PO weight time yields are very similar (30 vs. 32 $gPO/kg_{cat} \times h$ by He et al. [19] and this work, respectively). This is likely due to notably different reaction conditions, such as concentration of O_2 and C_3H_6 and reaction temperature.

3.2. In-situ XANES and EXAFS analysis

The relative amounts of Cu^{2+} and Cu^+ species in the catalyst before and during the propylene oxidation reaction at 350 °C were determined from the Cu K-edge XANES spectra using the linear combination fit (LCF) analysis [29,47]. Details of LCF analysis are presented in Figs. S8 and S9 and [29]. Before the catalytic reaction, all copper is present as Cu^{2+}. The temporal evolution of the Cu^+ fraction in each catalyst during the propylene oxidation reaction is shown in Fig. 2. After 300 min of TOS, Cu^+ is the majority, but not strongly predominant oxidation state (52–68%). This is the case for 5Cu, 5CuNa, and 5CuCa, while in 5CuCs, only 24% of copper is present as Cu^+. A correlation between Cu^+ / Cu^{2+} ratio in tested catalysts and PO selectivity is possible, when examining only 5CuNa. However, looking at all the tested catalysts, the oxidation state of copper itself cannot explain the observed PO selectivity trends (Fig. 1) and PO can be formed either over CuO or Cu_2O. The dynamics of reaching the final copper oxidation state differ strongly among catalysts (see for example the green and blue bars for 5CuCs and 5CuNa catalysts, Fig. 2). This indicates the kinetics of oxygen abstraction and replenishment are substantially different as a result of altered CuO_x chemistry after alkali(ne earth) addition.

In our previous work [29] we observed, using *in-situ* UV–Vis DR spectroscopy, that sintering of CuO_x clusters is strongly accelerated when Cu^+ is formed under reductive (pure C_3H_6 or reaction conditions: C_3H_6 and O_2), compared to oxidative (20% O_2/He) atmosphere. Under propylene oxidation conditions, a substantial fraction of Cu^+ is present (Fig. 2) and copper atoms become more mobile due to the lower melting temperature of Cu_2O (1236 °C) compared to CuO (1326 °C). The Hüttig temperature ($T_H = 0.3*T_M$; T_M is melting temperature in Kelvin) indicates the temperature at which surface atoms become significantly mobile. These temperatures are 207 and 179 °C for CuO and Cu_2O, respectively. Thus, both oxides can sinter at the employed reaction temperature, with the event being more pronounced for Cu_2O. The extent of deactivation observed during the propylene oxidation correlates very closely with the Cu^{1+} fraction in the catalysts (Fig. S10). As a result, sintering is likely the cause of deactivation. Additionally, the modifying alkali cations can also act as sintering barriers, since less sintering is observed in their presence compared to pure CuO_x/SiO_2.

The *in-situ* Cu K-edge EXAFS analysis (see Supplementary information) showed that in all catalysts, copper cations are coordinated to oxygen atoms in the first coordination shell, distributed at two or three distances, and Cu neighbors in more distant coordination shells at distances characteristic for crystalline copper oxides. However, the coordination numbers are significantly lower than in the bulk crystal. The Cu cations in all catalyst samples at RT before the propylene oxidation reaction are in the form of CuO crystalline nanoparticles and/or amorphous oxide species. Heating the catalyst samples to 350 °C in He/O_2 atmosphere causes re-dispersion of Cu cations and formation of smaller CuO nanoparticles.

During propylene oxidation reaction at 350 °C, additional structural changes are detected, reaching steady state after about 240 min of reaction (Figs. S11–S15, Table S2–S24). These changes are re-distribution of copper neighbors in more distant coordination shells and lowering of average Cu coordination numbers. This indicates the CuO_x clusters could "flatten" or re-disperse into smaller entities during reaction conditions. Additional oxygen shell which appears at 2.44 Å also suggest partial diffusion of Cu cations and formation of smaller CuO_x nanoparticles or CuO_x clusters. These clusters have a smaller distortion of

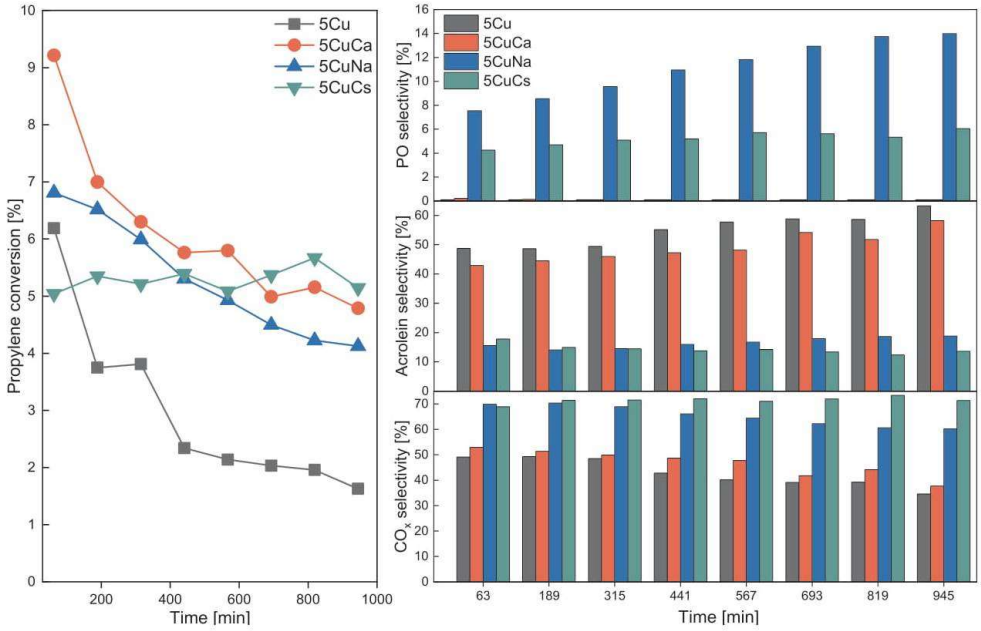

Fig. 1. Propylene conversion as a function of time on stream (left panel) and selectivity towards PO, acrolein and CO_x (right panels) for 5Cu, 5CuNa, 5CuCs and 5CuCs catalysts.

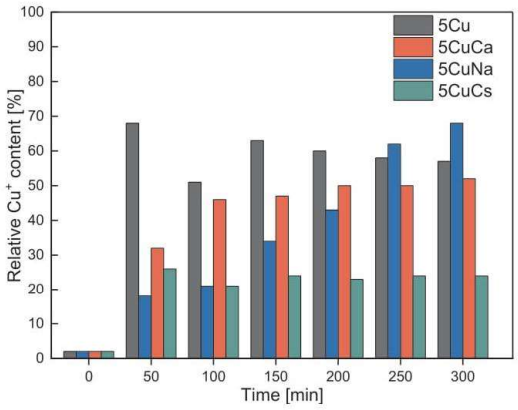

Fig. 2. Evolution of the Cu^{1+} fraction as a function of TOS for the 5Cu, 5CuNa, 5CuCs, and 5CuCa catalysts. The uncertainty of the relative amount of Cu^{2+} and Cu^+ is ± 2%.

the CuO_6 octahedron. The same was observed for example in CuO nanoclusters on TiO_2 catalyst [48], where the Cu(II) cation is coordinated octahedrally to six O atoms and distorted tetragonally because of the Jahn–Teller effect with four O atoms at 1.9 Å and two at 2.4 Å.

The exact change of the CuO_x morphology is beyond the EXAFS resolution and cannot be identified unambiguously (see ESI for more information). A similar phenomenon had been observed over Pd/$CeZrAlO_x$ catalysts by Newton et al. [49] during CO/NO cycling. These authors also clearly showed that oxidation and reduction of the Pd induces their re-dispersion. Gonzalez-DelaCruz et al. [50] observed using *in-situ* XAS the decrease in Ni coordination number and related it to

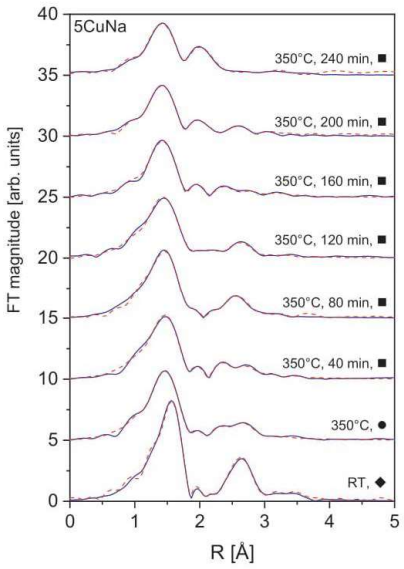

Fig. 3. Fourier transform magnitude of k^3-weighted Cu EXAFS spectra the 5CuNa catalyst at room temperature in O_2/He (◆), at 350 °C in the He/O_2 atmosphere (●), and during the catalytic propylene oxidation reaction at 350 °C in a C_3H_6/O_2/He stream (16.7% C_3H_6, 16.7% O_2, 66.6% He, total flowrate of 30 mL/min) (■). Scan duration was 40 min. FT spectra are calculated in the k range of 3–13 $Å^{-1}$. Experiment – (blue solid line); best fit EXAFS model in the R range of 1–3.6 Å – (red dashed line). Spectra are shifted vertically for clarity. (For interpretation of the references to colour in this figure legend, the reader is referred to the web version of this article.)

Table 1
Average length of Cu–O bond in pristine and Na, Cs and Ca modified 5Cu catalysts as determined by *in-situ* EXAFS and DFT calculations, and the average charge on Cu, O and alkali (earth) species.

Sample	Cu–O bond distance, Å[a]	Cu–O bond distance, Å[b]	Copper average charge	Oxygen average charge	Adatom average charge
5Cu	1.865 ± 0.005 Å	1.869	+0.87	−0.87	N.A.
5CuNa	1.830 ± 0.007 Å	1.856	+0.83	−0.89	+0.86
5CuCs	1.882 ± 0.005 Å	1.857	+0.83	−0.90	+0.91
5CuCa	1.874 ± 0.003 Å	1.875	+0.81	−0.93	+1.52

N.A. Not applicable.
[a] *In-situ* EXAFS results at 240 min TOS (this work).
[b] DFT (this work).

flattening of the Ni phase which was dispersed over CeO_2 support under strongly reducing (CH_4-CO_2 reforming) conditions.

Based on the average Cu coordination numbers (Cu K-edge EXAFS analysis Table S4–S9, Fig. 3, S11 and S12), the average CuO_x cluster size was estimated to be about 1 nm.

The short Cu–O bond distance of 1.94 Å found in the initial state of all catalysts at room temperature, is shortened during the catalytic reaction. The contraction depends on the addition of the alkali(ne earth) cations. The shortest Cu–O bond length values determined in the *in-situ* EXAFS analyses (at 240 min TOS) are shown in Table 1. For the 5Cu sample, the bond length is 1.865 ± 0.005 Å, which lies between the Cu–O bond length values of bulk CuO and Cu_2O (1.95 Å and 1.84 Å, respectively, estimated from crystallographic data [51,52] and EXAFS analysis – Tables S10 and S11). In case of Na modification, the Cu–O bond is significantly shorter (1.830 ± 0.007 Å), which is considerably less compared to what is expected from the average copper oxidation state in the CuO_x cluster. In case of Cs modification, the Cu–O distance is slightly longer than in the unmodified sample (1.874 ± 0.003 Å and 1.882 ± 0.005, Å respectively). This is likely due to a considerably higher fraction of Cu^{2+} in the 5CuCs sample compared to all others (Fig. 2).

The Cu–O bond distance (influenced by the strength of copper-oxygen binding) reflects itself in measured catalytic performance: in case of shorter (and stronger) Cu–O bond, the catalytic activity is lower and PO selectivity higher.

3.3. Theoretical calculations

The size of the CuO cluster used as a starting point for the DFT modelling was 1 nm and was based on the estimation from *in-situ* XAS analysis at 240 min TOS. The optimized geometry is slightly flattened compared to the starting $Cu_{12}O_{12}$ cluster, which is in line with EXAFS results. In Fig. 4, the structure of the optimized Cs-modified CuO cluster with and without adsorbed propylene is shown. The structures containing Na or Ca cation are analogous.

The CuO stoichiometry was chosen on account of the initial oxidation state of copper and the fact that in the most stable catalyst (5CuCs, Fig. 2) it remains predominant, showing that it is the more active one. In reality, the catalysts consist of regions of CuO and Cu_2O. However, performing calculations on a small cluster with mixed stoichiometry could result in spurious effects and unphysical results.

Modification of the 5Cu catalyst with Na, Cs, and Ca results in small but noticeable changes of the average Cu–O bond length. As shown in Table 1, DFT calculations uniformly predict a small contraction of the bond length upon addition of Na or Cs and its elongation upon modification with Ca. This was further studied with the Bader analysis of charges in the CuO_x clusters. For 5Cu, the average charge of Cu was +0.87 and −0.87 for O. The modification with Na or Cs increases the negative average charge on O (to −0.89 and −0.90, respectively) and decreases the positive average charge on Cu (to +0.83), as the alkalis act as electron donors. Na and Cs become strongly positively charged with the average values of +0.86 and +0.91 e_0. Upon modification with Ca, the effect is different due to the two valence electrons it possesses. The charge on Ca is only +1.52; this means that it does not fully delocalize the valence electrons as do Na in Cs.

The difference is even more pronounced on the oxygen atom, which directly participates in the reaction. On 5Cu, its charge is −0.87. On 5CuCs and 5CuNa, its charge is −0.94 and −0.97, respectively. On Ca, however, is its nucleophilic character so pronounced (−1.05 e_0) that it preferentially reacts with the most acidic hydrogen in the adsorbed propylene molecule, which manifests as hydrogen stripping (Table S25). In all cases, these are the atoms in the vicinity of the dopant metals with the following M−O distances: 4.31, 3.98, and 2.63 Å for 5CuCs, 5CuNa and 5CuCa, respectively. These are the second nearest oxygen neighbors to the dopant atoms, while the nearest neighbors are strongly bound to the electropositive metal atom and inaccessible for the reaction.

The Cu–O bond distances estimated by EXAFS fitting and the DFT calculated values are similar and follow the same trend, thus supporting the electronic modification of the Cu–O bond geometry after alkali modification (Table 1). There is a slight discrepancy in the trend for the Cs modified sample, which we attribute to a much higher content of Cu in the 2+ oxidation state. CuO has a longer Cu–O bond distance than Cu_2O (1.95 and 1.84 Å, respectively) [53]. Since approximately the same weight fraction of alkali or alkaline earth metals was used for catalyst modification (see Chapter 2.1), with cesium the number of modifying adatoms was lower, due to its high molecular weight.

3.3.1. Propylene adsorption energies

A prerequisite for any catalytic reaction is the adsorption of reactants to the catalyst surface. Succinctly described in the Sabatier principle, the interaction must be “just right”. Binding of the reactant too strongly will impede the reaction, while a too weak binding means that inadequate amounts of the reactant will be in contact with the active surface of the catalyst. Adsorption energy (zero-point corrected) is a sufficiently good indicator of the affinity of the catalyst towards a reactant molecule, when the substrates are of similar structure.

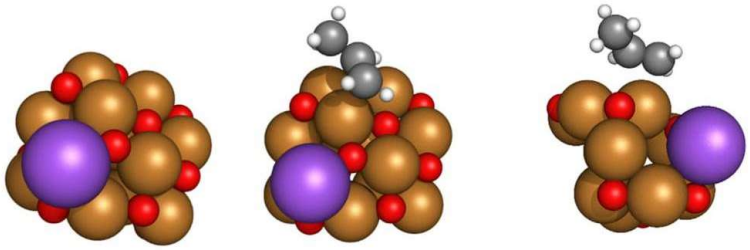

Fig. 4. Optimized geometry of a $Cu_{12}O_{12}$/Cs cluster without (left) and with (centre, right) an adsorbed propylene molecule at the most energetically favorable position.

Table 2
First-principles calculated adsorption energies for propylene, reaction energies and activation barriers for the dissociation of O_2 on the catalyst.

Catalyst	Adsorption energy, eV	Reaction energy, eV	Activation barrier, eV
5Cu	−1.01	−0.79	0.64
5CuNa	−0.60	−2.62	0.35
5CuCs	−0.57	−2.24	0.44
5CuCa	−0.40	−2.44	0.44

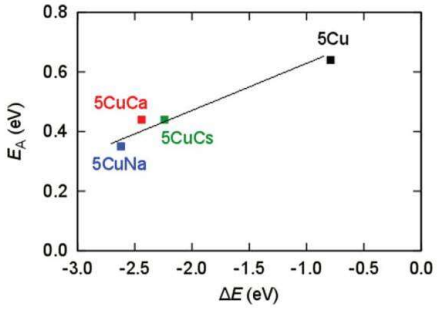

Fig. 5. The BEP relation for the reaction of oxygen dissociation on pristine CuO_x and after modification with Na, Cs, and Ca.

Modification of the 5Cu catalyst with Na or Cs decreases the binding strength of propylene to very similar values (Table 2). When Ca is added, the propylene binding strength decreases further to −0.4 eV. Propylene symmetrically adsorbs with its double bond atop of a Cu atom adjacent to the dopant atom, positioned 1.9–2.0 Å above the atom.

This can be correlated with the experimentally determined activity of catalysts. As seen in Figs. 1 and 5Cu catalyst is least active (lowest conversion), hinting that it binds propylene too strongly. The modified catalysts (5CuCs, 5CuNa and 5CuCa) are of comparable activity, as are also the propylene adsorption energies.

The calculated values can be compared to the results of Düzenli et al. [28] and Song et al. [54]. While Düzenli calculated a much weaker propylene adsorption energy on CuO(0 0 1) with 0.56 eV than our value, this can be attributed to the lack of dispersion correction in their work. It is also known that in general extended surfaces bind adsorbates less strongly than rugged surfaces, as shown by Song et al. [54] for propylene on Cu_2O(1 1 1) and (1 1 0). Nanoparticles and clusters bind the adsorbates even more strongly than surfaces, which is a consequence of undercoordinated surface atoms [55].

3.3.2. Reaction energy

During the reaction, there is interplay between the Cu^+ and Cu^{2+} species, which interconvert as oxygen from the catalyst is used up for the oxidation of propylene and replenished by the dissociation of the molecular oxygen (the Mars-van Krevelen mechanism). The rate of oxygen dissociation is crucial for the activity of the catalyst (regardless of the product formed). In Table 2, the reaction energy and activation barrier for oxygen dissociation on the investigated catalysts are listed.

First, we notice that they roughly follow the expected Brønsted-Evans-Polanyi (BEP) principle (Fig. 5). The more exothermic the oxygen dissociation, the lower the activation barrier. This enables us to use the reaction energies for oxygen dissociation in lieu of its activation barrier in comparisons.

From Table 2, one would expect that in 5Cu there would be a higher proportion of Cu^+ relative to Cu^{2+} as oxygen dissociation (and thus oxidation of the catalyst) is energetically less likely (the reaction is *less* exothermic). Indeed, experimental evidence in Fig. 2 shows that initially the Cu^+/Cu^{2+} ratio in 5Cu catalyst increases much faster compared to all other tested catalysts. This also correlates with the activity (propylene conversion, Fig. 1), which reveals 5Cu as the least active among all. The differences between the modified catalysts are much smaller, both experimentally and computationally.

3.3.3. Reaction mechanism

The reaction network of propylene oxidation and activation energies for each step are shown in Fig. 6 and Table 3 and are the same as investigated by Düzenli et al. on Cu_2O(0 0 1) and CuO(0 0 1) [28] and Song et al. on Cu_2O(1 1 1) and Cu_2O (1 1 0) [54]. Due to the composition of our clusters (Cu12O12), the results of Düzenli on CuO(0 0 1) can be directly compared to ours.

As propylene contains an allylic fragment and three non-equivalent carbon atoms, the possible reaction network is larger than in the case of ethylene [8]. If oxygen detaches one allylic hydrogen, the ensuing CH_2CHCH_2 moiety quickly reacts with another oxygen atom and eventually transforms into acrolein (red pathway in Fig. 6). This pathway is not possible with ethylene and explains why silver catalysts, while highly effective for ethylene epoxidation, struggle with propylene. This tendency of the catalyst for allylic hydrogen stripping can be

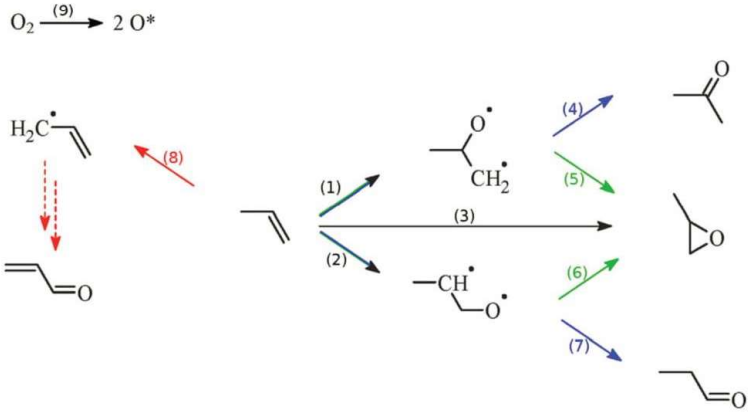

Fig. 6. Reaction network for the oxidation of propylene. The experimentally confirmed pathways in this work are colored as follows: blue and red on 5Cu, and 5CuCa, green and blue on 5CuCs, and 5CuNa. (For interpretation of the references to colour in this figure legend, the reader is referred to the web version of this article.)

Table 3
First-principles calculated activation barriers for the elementary steps in the propylene oxidation reaction. All values are in eV.

N°	Reaction/Catalyst	5Cu	5CuNa	5CuCs	5CuCa
1	$CH_3CHCH_2 + O \rightarrow CH_3CHOCH_2$	0.37	0.66	0.58	0.41
2	$CH_3CHCH_2 + O \rightarrow CH_3CHCH_2O$	0.46	0.67	0.50	0.45
3	$CH_3CHCH_2 + O \rightarrow$ Propylene oxide	0.92	1.44	0.97	1.10
4	$CH_3CHOCH_2 \rightarrow CH_3COCH_3$	0.30	1.19	1.22	0.90
5	$CH_3CHOCH_2 \rightarrow$ Propylene oxide	0.87	0.71	0.87	1.08
6	$CH_3CHCH_2O \rightarrow$ Propylene oxide	1.10	0.99	0.85	1.14
7	$CH_3CHCH_2O \rightarrow CH_3CH_2CHO$	0.91	1.18	1.37	0.81
8	$CH_3CHCH_2 + O \rightarrow CH_2CHCH_2 + OH$	0.45	0.72	0.75	0.16
9	$O_2 \rightarrow 2O$	0.64	0.35	0.44	0.44

lowered by increasing the electrophilic character of the active oxygen species, which will preferentially react with the electron rich vinyl carbons, compared to the (more acidic) allylic one. When allylic stripping is avoided, oxygen can either bind to the primary or secondary vinyl carbon atom. In the former case, the primary oxametallacycle (CH_3CHCH_2O, OMC1) is formed, while the latter case yields the secondary oxametallacycle (CH_3CHOCH_2, OMC2). The OMC1 intermediate can convert into acetone or propylene oxide (PO), while OMC2 can convert into propanal or PO. Propanal and acetone readily convert into CO_x in the subsequent oxidation steps.

During the propylene oxidation reaction, the 5Cu sample produces mostly CO_x and acrolein with 37 and 63% selectivity at 15 h TOS, respectively (Fig. 1). Mechanistically, upon the adsorption of propylene onto the CuO_x cluster, the activation barriers for the formation of OMC1 and OMC2 (steps 2 and 1 in Table 3) or the allylic stripping (step 8) are very similar (~0.4 eV), differing by less than 0.1 eV (Fig. 7, Table 3). This explains the similar selectivity towards CO_x and acrolein (Fig. 1). No propylene oxide is formed because neither OMC1, nor OMC2 convert into PO (steps 5 and 6). OMC1 rather converts into propanal (0.91 eV for step 7 vs. 1.10 eV for step 6) and OMC2 converts into acetone (0.30 eV for step 4 vs. 0.87 eV for step 5). In both cases, propanal and acetone are readily and non-selectively oxidized into CO_x (Figs. 6 and 7).

The reaction is modelled in the vicinity of the dopant metal atom, where the propylene interaction is the strongest. The intermediates and transition states do not differ geometrically between the catalysts used, showing that the promoter effect is mostly electronic and not geometric.

On CuO(0 0 1) [28], which can be considered as an infinitely large version of our cluster, the barriers for allylic hydrogen stripping (AHS) is 0.70 eV (0.45 eV in our work) and for the formation of an OMC analogue 0.52 eV (0.37 or 0.46 eV in our work). Further dehydrogenation towards acrolein is barrierless, which is consistent with our assumption that the steps following AHS are fast. The OMC analogue can convert to acetone (barrier of 2.47 eV) or PO (2.91 eV). This means that extended CuO surfaces are not suitable for epoxidation. Similarly, Cu_2O(1 1 1) was also found to yield predominantly acrolein. However, Cu_2O(1 1 0) seems suitable for the production of PO with the rate-determining step being the conversion of OMC2 into PO (barrier of 1.41 eV) [54]. Small clusters, as in our case, are much more active as they have lower activation barriers (around 1 eV). The thermodynamic stability ordering for PO versus acetone and acrolein on Cu oxides follows the same order as here.

Alkali modification changes the situation noticeably. In the case of 5CuCs, moderate (~6%, Fig. 1) selectivity towards PO is experimentally observed, while the selectivity towards acrolein drops precipitously. This is explained by the change of the activation barrier for allylic striping, which is increased to 0.75 eV (step 8). As the barriers for the formation of OMC1 (step 2) and OMC2 (step 1) increase *less*, these two intermediates become favored relative to hydrogen stripping (Fig. 7, Table 3). OMC1 is converted into propylene oxide (0.85 eV for step 6) and not propanal (1.37 eV for step 7). The OMC2 intermediate also preferentially desorbs as propylene oxide and not acetone (0.87 eV for step 5; as opposed to 1.22 eV for step 4), Fig. 6.

The effect of Na modification is similar to that of Cs. Propylene preferentially converts into OMC1 (step 2) and OMC2 (step 1), which in turn react to PO (steps 5 and 6). The experimentally observed selectivity towards PO is higher compared to 5CuCs, which could be explained by the activation barrier for the conversion of OMC2 into PO (0.71 eV for step 5) being lower than any of the barriers for the formation of PO on 5CuCs (Table 3).

Modification with Ca shifts the selectivity towards acrolein which is even higher than in the case of 5Cu, while no PO is produced (Fig. 1). This is consistent with the calculated barrier for the allylic hydrogen stripping which is very low (0.16 eV for step 8), strongly favoring the acrolein formation pathway. Any OMC1 or OMC2 that form are rapidly converted into CO_x, which is consistent with the activation energies for their conversion into PO (steps 5 and 6) being higher than for the conversion into acetone (step 4) or propanal (step 7).

Direct insertion of atomic oxygen into the C=C bond of propylene (forming PO) is unlikely due to its high activation energy (step 3, Table 3). This is in great contrast with the reaction mechanism for ethylene epoxidation on Ag_2O, where the direct formation is postulated to occur [8].

The mechanism of propylene oxidation on CuO_x catalysts can be described with the Mars-van Krevelen mechanism, where the integral oxygen from the surface is consumed and later on replenished by the dissociation of O_2 (step 9). Experimentally, the activity of the catalysts (measured as propylene conversion after 15 h TOS) follows the order: 5CuCs > 5CuCa > 5CuNa > 5Cu. The oxygen activation energies can be used to explain then experimentally observed activity trend. 5Cu is the least active as it has the largest activation barrier (0.64 eV). For

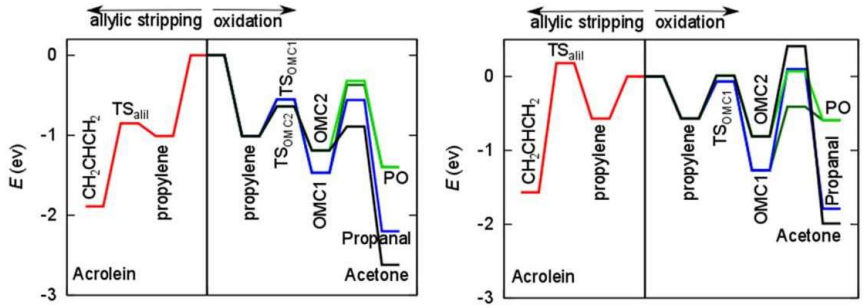

Fig. 7. The potential energy surface of propylene oxidation on 5Cu (left) and 5CuCs (right). Note that OMC1 and OMC2 denote CH_3CHCH_2O and CH_3CHOCH_2, respectively.

5CuCs (0.44 eV), 5CuCa (0.44 eV) and 5CuNa (0.35 eV), the calculated differences are small and can only tentatively be used to explain the experimental data. Thus, the measured activity in propylene oxidation is governed by the number of active nucleophilic oxygen sites revealing oxygen dissociation as the rate determining step.

The experimentally observed reaction product distribution is the result of reaction kinetics as thermodynamically acetone is the preferred product (Fig. 7).

4. Conclusions

The selectivity in the propylene oxidation reaction using molecular oxygen can be varied notably with the Na, Cs or Ca modification of the $5CuO_x/SiO_2$ catalysts: Cs and especially Na favor PO selectivity, whereas acrolein is the dominant product over unmodified and Ca modified catalysts. Lower deactivation due to sintering is observed in all modified catalysts, since the modifying adatoms influence the Cu^+/Cu^{2+} fraction and act as sintering barriers, thus reducing the mobility of CuO_x moieties.

The in-situ XANES analysis confirmed that the average oxidation state of copper in the CuO_x clusters changes dynamically from Cu^{2+} to a mixture of Cu^{2+} and Cu^+ during the reaction. The 5Na, 5Ca and 5Cu catalysts contain predominantly Cu^+ (52–68%, depending on the modifying adatom). On the other hand, in the 5Cs catalyst, Cu^{2+} is predominant (76 ± 2%). Absence of correlation between PO selectivity and Cu^+ fraction indicates that copper oxidation state is not the sole determining factor governing PO selectivity.

The in-situ EXAFS analysis shows that copper is initially in all catalysts present in the form of CuO nanoparticles and/or amorphous oxide species. A re-dispersion or flattening of the CuOx clusters during the reaction was observed. The short Cu–O bond distance of 1.94 Å found in the initial state of all catalysts at room temperature, is reduced during the catalytic reaction. The shortening Cu–O bond length depends on alkali(ne earth) modification of the catalyst, indicating electronic interaction of the pristine CuO_x with the adatom, thus changing the nucleophilic character of the oxygen species. DFT analysis shows a progressively increasing negative charge on oxygen from −0.87 for the unmodified catalyst up to −0.93 for the Ca modified catalyst.

The DFT analysis of the reaction network of propylene oxidation over CuO showed that if the surface oxygen is too nucleophilic (too reactive), the allylic hydrogen is immediately stripped from the propylene molecule. The resulting $\cdot CH_2CHCH_2$ moiety quickly reacts with a nearby oxygen and converts to acrolein. This reaction pathway is prevailing after the Ca modification which exhibits a very low (0.16 eV) activation barrier for allylic hydrogen stripping. Over the unmodified 5Cu catalyst, the activation barriers for allylic hydrogen stripping and OMC formation are similar (0.37–0.46 eV). Subsequent OMC desorption as acetone is the thermodynamically favored reaction, which undergoes further oxidation to CO/CO_2. The reverse effect is evident in the catalysts modified by either Na or Cs. The activation barriers for propanal or acetone formation become noticeably higher (1.18–1.37 eV), whereas the activation barriers for PO are 0.71–0.99 eV. Also, the activation barrier for allylic hydrogen stripping increases from 0.45 to 0.72–0.75 eV. This is the driving force behind the selectivity towards PO, since the vast majority of the oxametallacycle intermediates that form, desorb as propylene oxide.

Declaration of Competing Interest

There are no competing interests to declare.

CRediT authorship contribution statement

Janvit Teržan: Investigation, Writing - original draft. **Matej Huš:** Investigation, Formal analysis, Software, Writing - review & editing. **Iztok Arčon:** Investigation, Writing - review & editing. **Blaž Likozar:** Resources, Writing - review & editing. **Petar Djinović:** Conceptualization, Investigation, Writing - review & editing, Project administration.

Acknowledgements

JT and PD acknowledge the financial support through Research program P2-0150 provided by the Slovenian Research Agency (ARRS). MH and BL acknowledge the financial support from the Slovenian Research Agency (research core funding P2-0152). IA acknowledges the financial support from the Slovenian Research Agency (research core funding P1-0112). The access to synchrotron radiation facilities (XAFS beamline, project 20170045) of ELETTRA is acknowledged, and JT acknowledges the support by the project CALIPSOplus under Grant Agreement 730872 from the EU Framework Programme for Research and Innovation HORIZON 2020 for the XAS experiment at Elettra. We thank Giuliana Aquilanti, Simone Pollastri, Mateusz Czyzycki and Ricardo Grisonich from XAFS beamline for the assistance during experiment and expert advice on beamline operation. The reference spectra CuO nano particles were kindly provided by Dr. Maxim Zabilskiy, recorded at the European Synchrotron Radiation Facility (Dutch-Belgian beamline BM26A, pr. CH-5057). The computational resources were provided by the National Institute of Chemistry (Ljubljana).

Appendix A. Supplementary data

Supplementary data to this article can be found online at https://doi.org/10.1016/j.apsusc.2020.146854.

References

[1] Nexant Inc., Market Analytics: Propylene Oxide – 2018, 2018. https://www.nexantsubscriptions.com/reports/market-analytics-propylene-oxide-2018.
[2] A. Blanckenberg, R. Malgas-Enus, Olefin epoxidation with metal-based nanocatalysts, Catal. Rev. 61 (2019) 27–83, https://doi.org/10.1080/01614940.2018.1492503.
[3] A.F. Carley, P.R. Davies, M.W. Roberts, Oxygen transient states in catalytic oxidation at metal surfaces, Catal. Today 169 (2011) 118–124, https://doi.org/10.1016/j.cattod.2010.10.081.
[4] Z. Li, L. Gao, W. Ma, Q. Zhong, Higher gold atom efficiency over Au-Pd/TS-1 alloy catalysts for the direct propylene epoxidation with H_2 and O_2, Appl. Surf. Sci. 497 (2019) 143749, , https://doi.org/10.1016/j.apsusc.2019.143749.
[5] S. Yao, L. Xu, J. Wang, X. Jing, T. Odoom-Wubah, D. Sun, J. Huang, Q. Li, Activity and stability of titanosilicate supported Au catalyst for propylene epoxidation with H_2 and O_2, Mol. Catal. 448 (2018) 144–152, https://doi.org/10.1016/j.mcat.2018.01.039.
[6] J.W. Harris, J. Arvay, G. Mitchell, W.N. Delgass, F.H. Ribeiro, Propylene oxide inhibits propylene epoxidation over Au/TS-1, J. Catal. 365 (2018) 105–114, https://doi.org/10.1016/j.jcat.2018.06.015.
[7] L. Zhu, H. Xu, Y. Nan, Y. Xie, J. Zhu, D. Cheng, The synergistic effect between crystal planes and promoters on Ag-catalyzed ethylene epoxidation, Appl. Surf. Sci. 476 (2019) 115–122, https://doi.org/10.1016/j.apsusc.2019.01.076.
[8] M. Huš, A. Hellman, Ethylene epoxidation on Ag(100), Ag(110), and Ag(111): a joint ab initio and kinetic monte carlo study and comparison with experiments, ACS Catal. 9 (2019) 1183–1196, https://doi.org/10.1021/acscatal.8b04512.
[9] B. Yu, T. Ayvalı, E. Raine, T. Li, M.M.-J. Li, J. Zheng, S. Wu, A.A. Bagabas, S.C.E. Tsang, Enhanced propylene oxide selectivity for gas phase direct propylene epoxidation by lattice expansion of silver atoms on nickel nanoparticles, Appl. Catal. B Environ. 243 (2019) 304–312, https://doi.org/10.1016/j.apcatb.2018.10.061.
[10] Q. Zhang, G. Chai, Y. Guo, W. Zhan, Y. Guo, L. Wang, Y. Wang, G. Lu, Gas-phase epoxidation of propylene by molecular oxygen over Ag-$CuCl_2/BaCO_3$ catalyst with low $CuCl_2$ doping: catalytic performance, deactivation and regeneration, J. Mol. Catal. A: Chem. 424 (2016) 65–76, https://doi.org/10.1016/j.molcata.2016.08.019.
[11] S.J. Khatib, S.T. Oyama, Direct oxidation of propylene to propylene oxide with molecular oxygen: a review, Catal. Rev. 57 (2015) 306–344, https://doi.org/10.1080/01614940.2015.1041849.
[12] A. Marimuthu, J. Zhang, S. Linic, Tuning selectivity in propylene epoxidation by plasmon mediated photo-switching of Cu oxidation state, Science 339 (2013) 1590–1593, https://doi.org/10.1126/science.1231631.
[13] X. Yang, S. Kattel, K. Xiong, K. Mudiyanselage, S. Rykov, S.D. Senanayake, J.A. Rodriguez, P. Liu, D.J. Stacchiola, J.G. Chen, Direct epoxidation of propylene over stabilized Cu^+ surface sites on titanium-modified Cu_2O, Angew. Chemie Int. Ed. 54 (2015) 11946–11951, https://doi.org/10.1002/anie.201504538.
[14] D. Torres, N. Lopez, F. Illas, R.M. Lambert, Low-basicity oxygen atoms: a key in the search for propylene epoxidation catalysts, Angew. Chemie – Int. Ed. 46 (2007)

2055–2058, https://doi.org/10.1002/anie.200603803.
[15] Y.-Y. Song, G.-C. Wang, Theoretical study of propylene epoxidation over Cu2O(111) surface: activity of O^{2-}, O^{-}, and O_2^{-} species, J. Phys. Chem. C 122 (2018) 21500–21513, https://doi.org/10.1021/acs.jpcc.8b07044.
[16] Q. Wang, C. Zhan, L. Zhou, G. Fu, Z. Xie, Effects of Cl^{-} on Cu_2O nanocubes for direct epoxidation of propylene by molecular oxygen, Catal. Commun. 135 (2020) 105897, , https://doi.org/10.1016/j.catcom.2019.105897.
[17] J. García-Aguilar, D. Cazorla-Amorós, Á. Berenguer-Murcia, K- and Ca-promoted ferrosilicates for the gas-phase epoxidation of propylene with O_2, Appl. Catal. A Gen. 538 (2017) 139–147, https://doi.org/10.1016/j.apcata.2017.03.031.
[18] Ş. Kalyoncu, D. Düzenli, I. Onal, A. Seubsai, D. Noon, S. Senkan, Z. Say, E.I. Vovk, E. Ozensoy, NaCl-promoted CuO–RuO_2/SiO_2 catalysts for propylene epoxidation with O_2 at atmospheric pressures: a combinatorial micro-reactor study, Catal. Letters. 145 (2015) 596–605, https://doi.org/10.1007/s10562-014-1454-7.
[19] J. He, Q. Zhai, Q. Zhang, W. Deng, Y. Wang, Active site and reaction mechanism for the epoxidation of propylene by oxygen over CuO_x/SiO_2 catalysts with and without Cs^{+} modification, J. Catal. 299 (2013) 53–66, https://doi.org/10.1016/j.jcat.2012.11.032.
[20] A. Miller, B. Zohour, A. Seubsai, D. Noon, S. Senkan, SnO_2–CuO–NaCl/SiO_2 catalysts for propylene epoxidation, Ind. Eng. Chem. Res. 52 (2013) 9551–9555, https://doi.org/10.1021/ie4004688.
[21] H. Chu, L. Yang, Q. Zhang, Y. Wang, Copper-catalyzed propylene epoxidation by molecular oxygen: superior catalytic performances of halogen-free K^{+}-modified CuO_x/SBA-15, J. Catal. 241 (2006) 225–228, https://doi.org/10.1016/j.jcat.2006.04.028.
[22] M. Huš, A. Hellman, Dipole effect on ethylene epoxidation: influence of alkali metals and chlorine, J. Catal. 363 (2018) 18–25, https://doi.org/10.1016/j.jcat.2018.04.008.
[23] S. Linic, M.A. Barteau, On the mechanism of Cs promotion in ethylene epoxidation on Ag, J. Am. Chem. Soc. 126 (2004) 8086–8087, https://doi.org/10.1021/ja048462q.
[24] L.M. Molina, S. Lee, K. Sell, G. Barcaro, A. Fortunelli, B. Lee, S. Seifert, R.E. Winans, J.W. Elam, M.J. Pellin, Size-dependent selectivity and activity of silver nanoclusters in the partial oxidation of propylene to propylene oxide and acrolein: a joint experimental and theoretical study, Catal. Today 160 (2011) 116–130, https://doi.org/10.1016/j.cattod.2010.08.022.
[25] Y. Lei, F. Mehmood, S. Lee, J. Greeley, B. Lee, S. Seifert, R.E. Winans, J.W. Elam, R.J. Meyer, P.C. Redfern, D. Teschner, R. Schlögl, M.J. Pellin, L.A. Curtiss, S. Vajda, Increased silver activity for direct propylene epoxidation via subnanometer size effects, Science 328 (2010) 224–228, https://doi.org/10.1126/science.1185200.
[26] L. Cheng, C. Yin, F. Mehmood, B. Liu, J. Greeley, S. Lee, B. Lee, S. Seifert, R.E. Winans, D. Teschner, R. Schlögl, S. Vajda, L.A. Curtiss, Reaction mechanism for direct propylene epoxidation by alumina-supported silver aggregates: the role of the particle/support interface, ACS Catal. 4 (2014) 32–39, https://doi.org/10.1021/cs4009368.
[27] D. Torres, N. Lopez, F. Illas, R.M. Lambert, Why copper is intrinsically more selective than silver in alkene epoxidation: ethylene oxidation on Cu(111) versus Ag (111), J. Am. Chem. Soc. 127 (2005) 10774–10775, https://doi.org/10.1021/ja043227t.
[28] D. Düzenli, D.O. Atmaca, M.G. Gezer, I. Onal, A density functional theory study of partial oxidation of propylene on Cu_2O(0 0 1) and CuO(0 0 1) surfaces, Appl. Surf. Sci. 355 (2015) 660–666, https://doi.org/10.1016/j.apsusc.2015.07.155.
[29] J. Teržan, P. Djinović, J. Zavašnik, I. Arčon, G. Žerjav, M. Spreitzer, A. Pintar, Alkali and earth alkali modified CuO_x/SiO_2 catalysts for propylene partial oxidation: What determines the selectivity? Appl. Catal. B Environ. 237 (2018) 214–227, https://doi.org/10.1016/j.apcatb.2018.05.092.
[30] F.J. Williams, R.L. Cropley, O.P.H. Vaughan, A.J. Urquhart, M.S. Tikhov, C. Kolczewski, K. Hermann, R.M. Lambert, Critical influence of adsorption geometry in the heterogeneous epoxidation of "Allylic" alkenes: structure and reactivity of three phenylpropene isomers on Cu(111), J. Am. Chem. Soc. 127 (2005) 17007–17011, https://doi.org/10.1021/ja055635i.
[31] J.W. Medlin, M. Mavrikakis, M.A. Barteau, Stabilities of substituted oxametallacycle intermediates: implications for regioselectivity of epoxide ring opening and olefin epoxidation, J. Phys. Chem. B 103 (1999) 11169–11175, https://doi.org/10.1021/jp992812r.
[32] G. Kresse, J. Hafner, Ab initio molecular dynamics for liquid metals, Phys. Rev. B 47 (1993) 558–561, https://doi.org/10.1103/PhysRevB.47.558.
[33] G. Kresse, J. Hafner, Ab initio molecular-dynamics simulation of the liquid-metal–amorphous-semiconductor transition in germanium, Phys. Rev. B 49 (1994) 14251–14269, https://doi.org/10.1103/PhysRevB.49.14251.
[34] G. Kresse, J. Furthmüller, Efficiency of ab-initio total energy calculations for metals and semiconductors using a plane-wave basis set, Comput. Mater. Sci. 6 (1996) 15–50, https://doi.org/10.1016/0927-0256(96)00008-0.
[35] G. Kresse, J. Furthmüller, Efficient iterative schemes for ab initio total-energy calculations using a plane-wave basis set, Phys. Rev. B. 54 (1996) 11169–11186, https://doi.org/10.1103/PhysRevB.54.11169.
[36] P.E. Blöchl, Projector augmented-wave method, Phys. Rev. B. 50 (1994) 17953–17979, https://doi.org/10.1103/PhysRevB.50.17953.
[37] G. Kresse, D. Joubert, From ultrasoft pseudopotentials to the projector augmented-wave method, Phys. Rev. B 59 (1999) 1758–1775, https://doi.org/10.1103/PhysRevB.59.1758.
[38] J.P. Perdew, K. Burke, M. Ernzerhof, Generalized gradient approximation made simple, Phys. Rev. Lett. 77 (1996) 3865–3868, https://doi.org/10.1103/PhysRevLett.77.3865.
[39] G. Mills, H. Jónsson, G.K. Schenter, Reversible work transition state theory: application to dissociative adsorption of hydrogen, Surf. Sci. 324 (1995) 305–337, https://doi.org/10.1016/0039-6028(94)00731-4.
[40] P. Xiao, D. Sheppard, J. Rogal, G. Henkelman, Solid-state dimer method for calculating solid-solid phase transitions, J. Chem. Phys. 140 (2014) 174104, , https://doi.org/10.1063/1.4873437.
[41] J. Kästner, P. Sherwood, Superlinearly converging dimer method for transition state search, J. Chem. Phys. 128 (2008) 014106, , https://doi.org/10.1063/1.2815812.
[42] A. Heyden, A.T. Bell, F.J. Keil, Efficient methods for finding transition states in chemical reactions: comparison of improved dimer method and partitioned rational function optimization method, J. Chem. Phys. 123 (2005) 224101, , https://doi.org/10.1063/1.2104507.
[43] G. Henkelman, H. Jónsson, A dimer method for finding saddle points on high dimensional potential surfaces using only first derivatives, J. Chem. Phys. 111 (1999) 7010–7022, https://doi.org/10.1063/1.480097.
[44] G. Makov, M.C. Payne, Periodic boundary conditions in ab initio calculations, Phys. Rev. B. 51 (1995) 4014–4022, https://doi.org/10.1103/PhysRevB.51.4014.
[45] J. Neugebauer, M. Scheffler, Adsorbate-substrate and adsorbate-adsorbate interactions of Na and K adlayers on Al(111), Phys. Rev. B. 46 (1992) 16067–16080, https://doi.org/10.1103/PhysRevB.46.16067.
[46] S. Grimme, J. Antony, S. Ehrlich, H. Krieg, A consistent and accurate ab initio parametrization of density functional dispersion correction (DFT-D) for the 94 elements H-Pu, J. Chem. Phys. 132 (2010) 154104, , https://doi.org/10.1063/1.3382344.
[47] B. Ravel, M. Newville, ATHENA, ARTEMIS, HEPHAESTUS: data analysis for X-ray absorption spectroscopy using IFEFFIT, J. Synchrotron Radiat. 12 (2005) 537–541, https://doi.org/10.1107/S0909049505012719.
[48] T. Čižmar, U. Lavrenčič Štangar, M. Fanetti, I. Arčon, Effects of different copper loadings on the photocatalytic activity of TiO_2-SiO_2 prepared at a low temperature for the oxidation of organic pollutants in water, ChemCatChem 10 (2018) 2982–2993, https://doi.org/10.1002/cctc.201800249.
[49] M.A. Newton, C. Belver-Coldeira, A. Martínez-Arias, M. Fernández-García, Dynamic in situ observation of rapid size and shape change of supported Pd nanoparticles during CO/NO cycling, Nat. Mater. 6 (2007) 528–532, https://doi.org/10.1038/nmat1924.
[50] V. Gonzalez-DelaCruz, J. Holgado, R. Pereniguez, A. Caballero, Morphology changes induced by strong metal–support interaction on a Ni–ceria catalytic system, J. Catal. 257 (2008) 307–314, https://doi.org/10.1016/j.jcat.2008.05.009.
[51] M. Calligaris, Structural inorganic chemistry by A. F. Wells, 208–208, Acta Crystallogr. B 41 (1985), https://doi.org/10.1107/S0108768185001987.
[52] S. Åsbrink, L.J. Norrby, A refinement of the crystal structure of copper(II) oxide with a discussion of some exceptional e.s.d'.s, Acta Crystallogr. Sect. B Struct. Crystallogr. Cryst. Chem. 26 (1970) 8–15, https://doi.org/10.1107/S0567740870001838.
[53] A.K. Mishra, A. Roldan, N.H. de Leeuw, CuO surfaces and CO_2 activation: a dispersion-corrected DFT+ U study, J. Phys. Chem. C 120 (2016) 2198–2214, https://doi.org/10.1021/acs.jpcc.5b10431.
[54] Y.-Y. Song, B. Dong, S.-W. Wang, Z.-R. Wang, M. Zhang, P. Tian, G.-C. Wang, Z. Zhao, Selective oxidation of propylene on Cu_2O(111) and Cu_2O(110) surfaces: a systematically DFT study, ACS Omega 5 (2020) 6260–6269, https://doi.org/10.1021/acsomega.9b02997.
[55] M. Jørgensen, H. Grönbeck, Scaling relations and kinetic monte carlo simulations to bridge the materials gap in heterogeneous catalysis, ACS Catal. 7 (2017) 5054–5061, https://doi.org/10.1021/acscatal.7b01194.

3.2 Supplementary Information 2

SUPPLEMENTARY INFORMATION

Effect of Na, Cs and Ca on propylene epoxidation selectivity over CuO_x/SiO_2 catalysts studied by catalytic tests, *in-situ* XAS and DFT

Janvit Teržan[1,2], Matej Huš[3], Iztok Arčon[4,5], Blaž Likozar[3] and Petar Djinović[1]*

[1]Department of Inorganic Chemistry and Technology, National Institute of Chemistry, Hajdrihova 19, SI-1001 Ljubljana, Slovenia
[2]Jožef Stefan International Postgraduate School, Jamova cesta 39, SI-1000 Ljubljana, Slovenia
[3]Department of Catalysis and Chemical Reaction Engineering, National Institute of Chemistry, Hajdrihova 19, SI-1001 Ljubljana, Slovenia
[4]Laboratory of Quantum Optics, University of Nova Gorica, Vipavska 13, SI-5000 Nova Gorica, Slovenia
[5]Jožef Stefan Institute, Jamova cesta 39, SI-1000 Ljubljana, Slovenia

*e-mail: petar.djinovic@ki.si

1 XRD

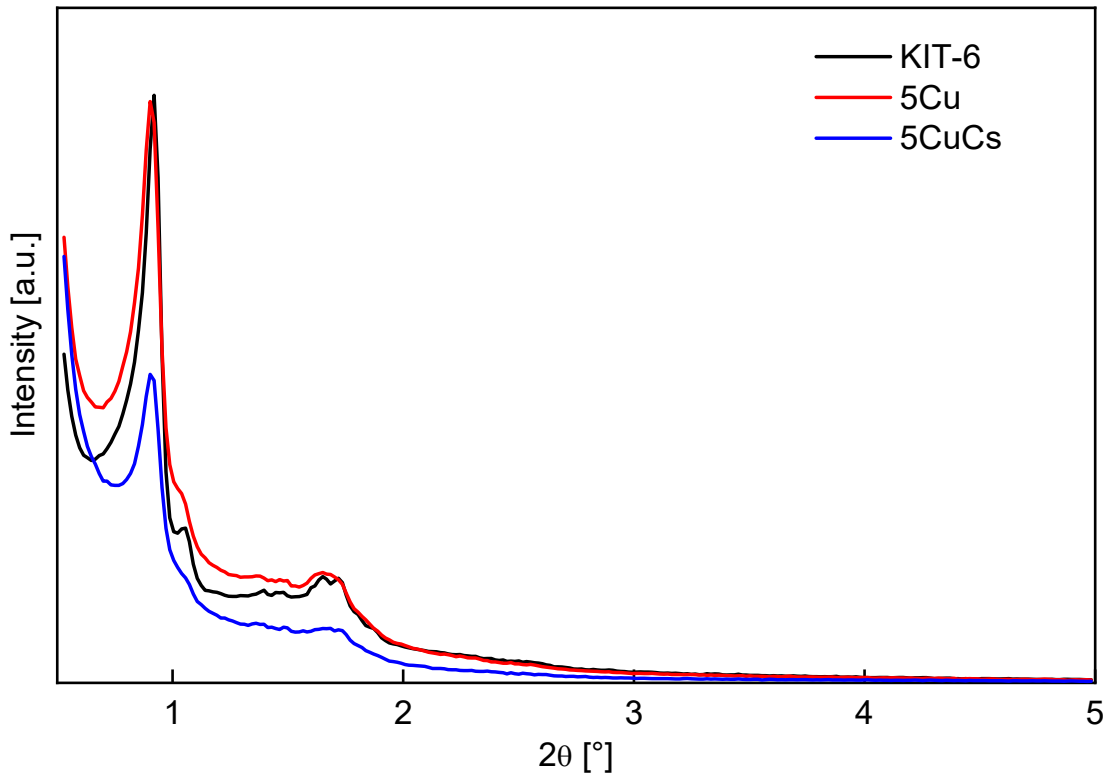

Fig. S1: Low angle XRD of pure KIT-6 SiO_2, the unmodified 5Cu and the 5CuCs sample.

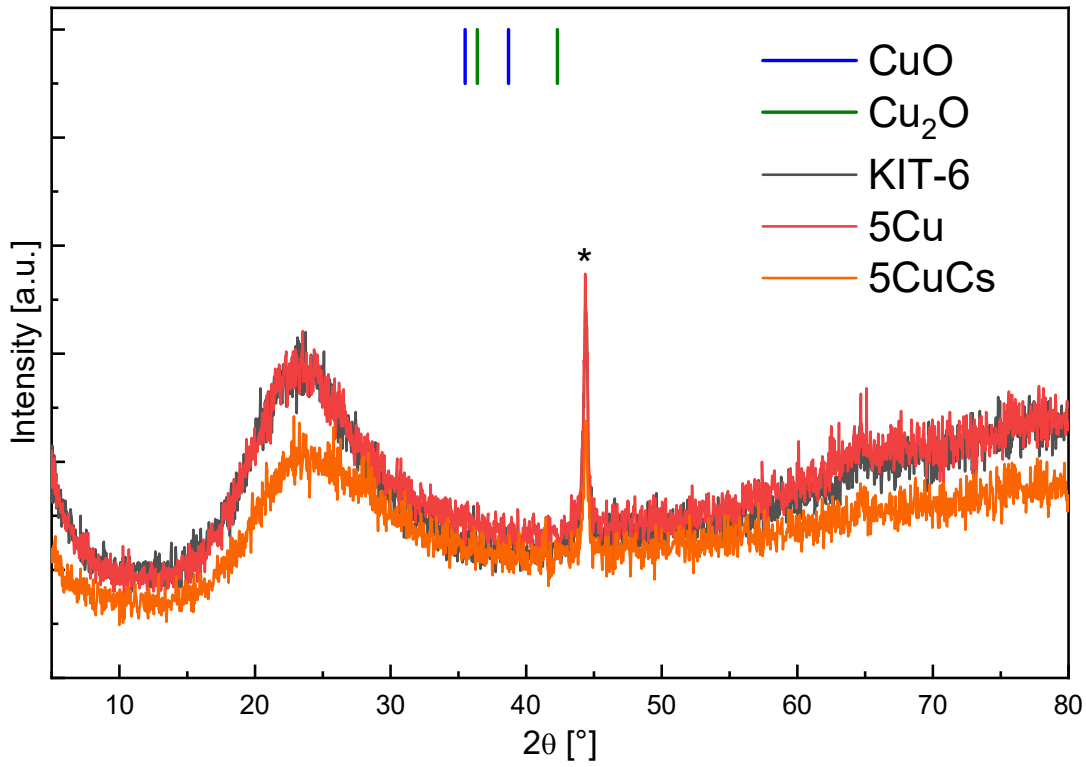

Fig. S2: High angle XRD of pure KIT-6 SiO_2, the unmodified 5Cu and the 5CuCs sample. Peak marked with asterisk belong to the iron sample holder.

2 N_2 sorption analysis

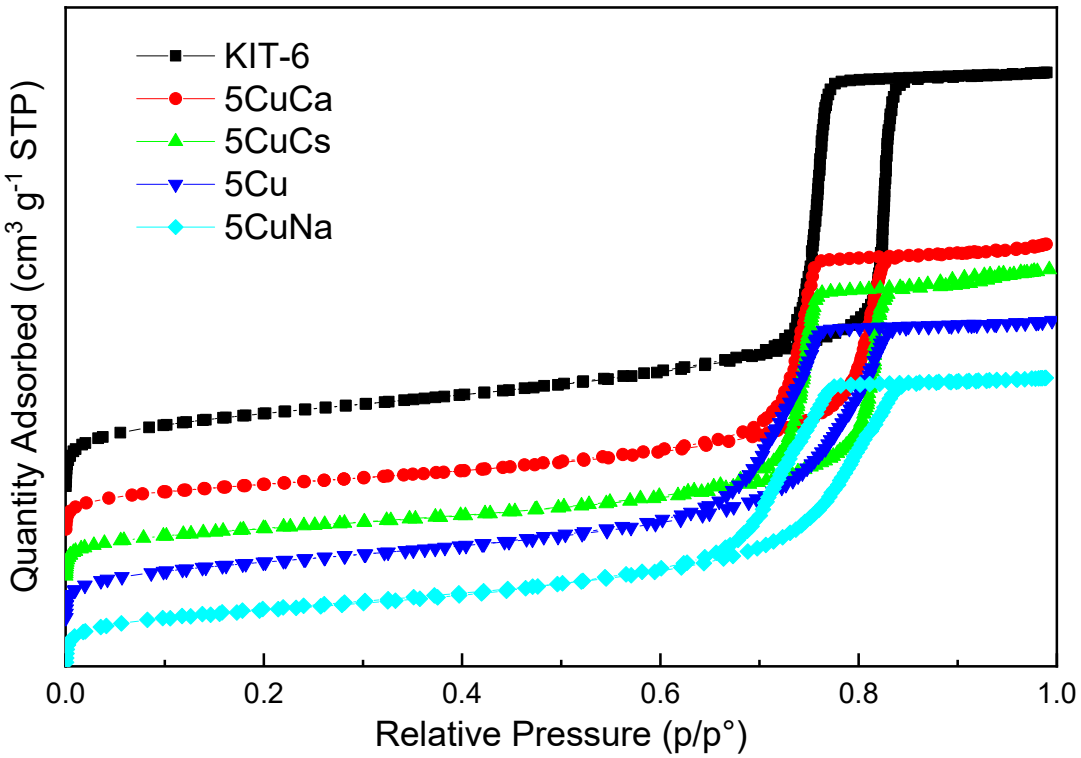

Fig. S3: Nitrogen adsorption/desorption isotherms of pure KIT-6 SiO_2, the unmodified 5Cu and the Cs modified sample. The isotherms are offset by 100 cm^3 N_2 g^{-1} STP for clarity.

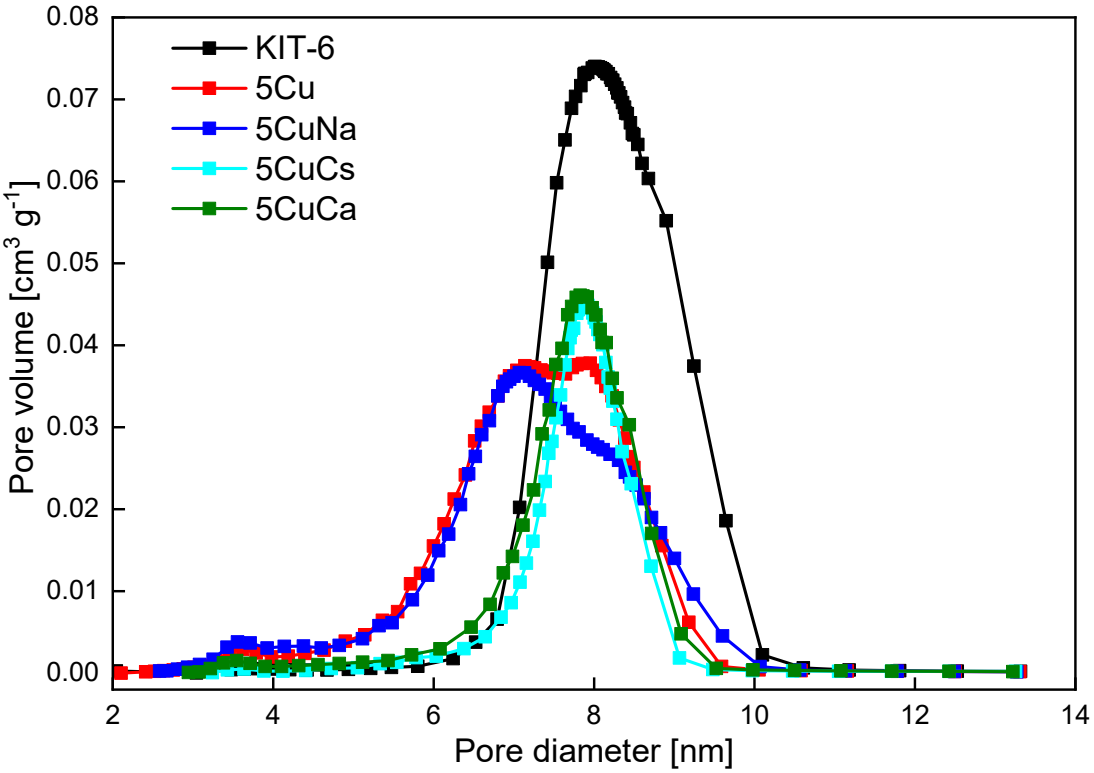

Fig. S4: Pore size distribution of pure KIT-6 SiO_2, the unmodified 5Cu and the Cs modified sample 5CuCs.

Table S1: Material properties measured with N_2 physisorption technique.

	BET	Average pore diameter[1]	Total pore volume[1]
	$m^2\ g^{-1}$	nm	$mL\ g^{-1}$
KIT-6	615	8.3	1.48
5Cu	485	7.0	1.07
5CuNa	465	7.0	1.02
5CuCs	415	7.0	1.04
5CuCa	404	7.0	1.03

[1]Calculated using the BJH method.

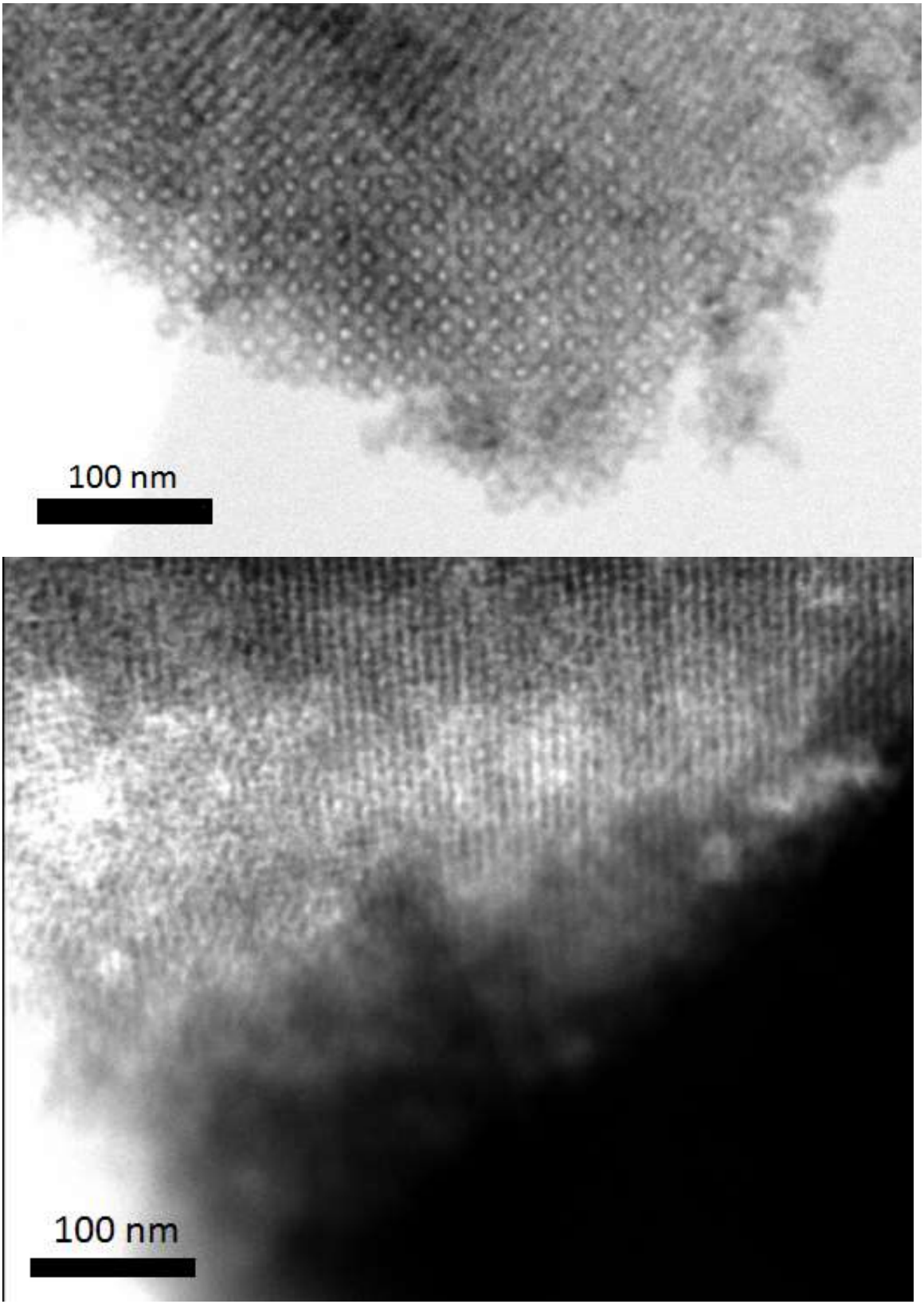

Fig. S5: Bright field STEM image of the 5Cu sample. The ordered mesoporous structure of the KIT-6 SiO_2 is nicely visible, looking into the circular pore arrays having a diameter of about 9 nm. Dark Field STEM image of the 5Cu sample with brighter area showing regions rich in copper. Higher magnifications induced a rapid decomposition of the samples due to electron beam damage, making analysis impossible.

3 *In-situ* Cu K-edge XAS experiment

The Cu K-edge X-ray absorption spectra (XAS) of 5Cu, 5CuNa 5CuCa and 5CuCs catalysts were recorded *in-situ* during the propylene oxidation reaction at 350 °C in transmission detection mode at the XAFS beamline of the ELETTRA synchrotron radiation facility in Trieste, Italy. The catalyst samples were prepared in the form of homogeneous pellets, pressed from micronized sample powder mixed with BN powder, with the total absorption thickness (μd) of about 2.5 above the investigated Cu K-edge. Pellets were inserted in a tubular oven reactor (Carbolite MTF 12/25/400) with 20 micron aluminum foil windows, filled with a gas mixture composed of 80 % He and 20 % O_2 at 1 bar. The XAS spectra were measured *in-situ*: (i) at room temperature in a He/O_2 atmosphere, (ii) at 350 °C in a He/O_2 atmosphere and (iii) during the catalytic propylene oxidation reaction at 350 °C in a $C_3H_6/O_2/He$ stream (16.7 % C_3H_6, 16.7 % O_2, 66.6 % He, total flowrate of 30 ml/min). After propylene addition, the samples were measured repeatedly until the quasi-equilibrium state in the catalyst was reached (up to 10 XAS spectra were collected per sample).

A Si (111) double crystal monochromator with about 1 eV resolution at the Cu K-edge was used. The intensity of the monochromatic X-ray beam was measured by three 30 cm long ionization detectors, filled with the following gas mixtures: (first) 1250 mbar N_2, 750 mbar He; (second) 250 mbar Ar, 750 mbar He, 1000 mbar N_2; (third) 700 mbar Ar, 1000 mbar N_2, 300 mbar He. Sample pellets, enclosed in a tubular oven reactor, were placed in the beam between first two ionization detectors. The absorption spectra were measured in the energy region from -150 eV to +1200 eV relative to the Cu K-edge. In the XANES region equidistant energy steps of 0.3 eV were used, while for the EXAFS region equidistant k steps of 0.03 $Å^{-1}$ were adopted, with an integration time of 2 s per step. The exact energy calibration was established with simultaneous absorption measurement on a 7 micron thick Cu metal foil placed between the second and the third ionization chamber. The first inflection point in the spectrum of the copper K-edge in the Cu metal with fcc crystal structure is at 8979.0 eV. Absolute energy reproducibility of the measured spectra was ±0.01 eV. The analysis of XANES and EXAFS spectra is performed with the DEMETER (IFEFFIT) program package[1] in combination with FEFF6 program code[2] for ab initio calculation of photoelectron scattering paths. The reference spectra CuO nano particles were kindly provided by Dr. Maxim Zabilskiy, recorded at the European Synchrotron Radiation Facility (Dutch-Belgian beamline BM26A, pr. CH-5057).

4 Cu K-edge XANES analysis

In-situ Cu K-edge XANES analysis is used to monitor Cu valence state in the catalysts before and during the propylene oxidation reaction. The shape of the Cu K-edge and the pre-edge resonances are characteristic for the local symmetry of the investigated atom and can be used as a fingerprint for the local symmetry of the Cu atom. Beside that the energies of the valence orbitals and therefore the energy position of the edge and pre-edge features are correlated with the valence state of the investigated atom in the sample. With increasing oxidation state the Cu K-edge is shifted to higher energies. The shifts up to a few eV per oxidation state are observed[3,4].

The edge profile and the energy positions of the Cu K-edge and pre-edge shoulder in 5Cu, 5CuNa, 5CuCa and 5CuCs catalysts measured before the propylene oxidation reaction at RT and at 350 °C in He/O_2 atmosphere match with the reference sample containing

Cu^{2+} oxide nanoclusters[3], which indicates that all copper cations are in di-valent state bound in CuO nanoclusters or amorphous CuO oxides (Fig. S1).

During the propylene oxidation reaction at 350 °C, Cu^{+} species are forming in all catalysts. The presence of Cu^{+} species can be identified in the XANES spectra by the characteristic Cu^{+} 1s-4p pre-edge absorption feature at 8982.7 eV (Fig . S6). The time evolution of the fraction of Cu^{+} in each catalyst during the propylene oxidation reaction can be qualitatively monitored by the increase of the intensity of the pre-edge peak. The relative amounts of Cu^{+} cations in the catalysts during the propylene oxidation reaction are determined with high accuracy from the *in-situ* measured Cu K-edge XANES spectra, by the linear combination fit (LCF) analysis[1,3]. The spectra can be completely described by the linear combination of two or three XANES spectra: spectrum measured on the sample at 350 °C in He/O_2 atmosphere and the spectrum of CuO nanoparticles where copper is present in the form of Cu^{2+} oxide nanoclusters, and the XANES spectrum of 5CuNa catalyst, measured *in-situ* during the propylene oxidation reaction when quasi-equilibrium state in the 5CuNa catalyst was reached after 300 min, where 68 % of copper is present in the form of Cu^{+} and 32 % in the form of Cu^{2+} oxide nanoclusters[3]. The LCF result is illustrated for the case of Cu K-edge XANES spectra of 5CuCs catalyst, measured *in-situ* during catalytic propylene oxidation reaction after 240 min in Fig. S6. The temporal evolution of the Cu^{1+} fraction in the 5Cu, 5CuNa, 5CuCs, and 5CuCa catalysts during the reaction is shown on Fig 2 in the main paper. The accuracy of the relative amount of Cu^{2+} and Cu^{+} species in the catalyst is ±2 %.

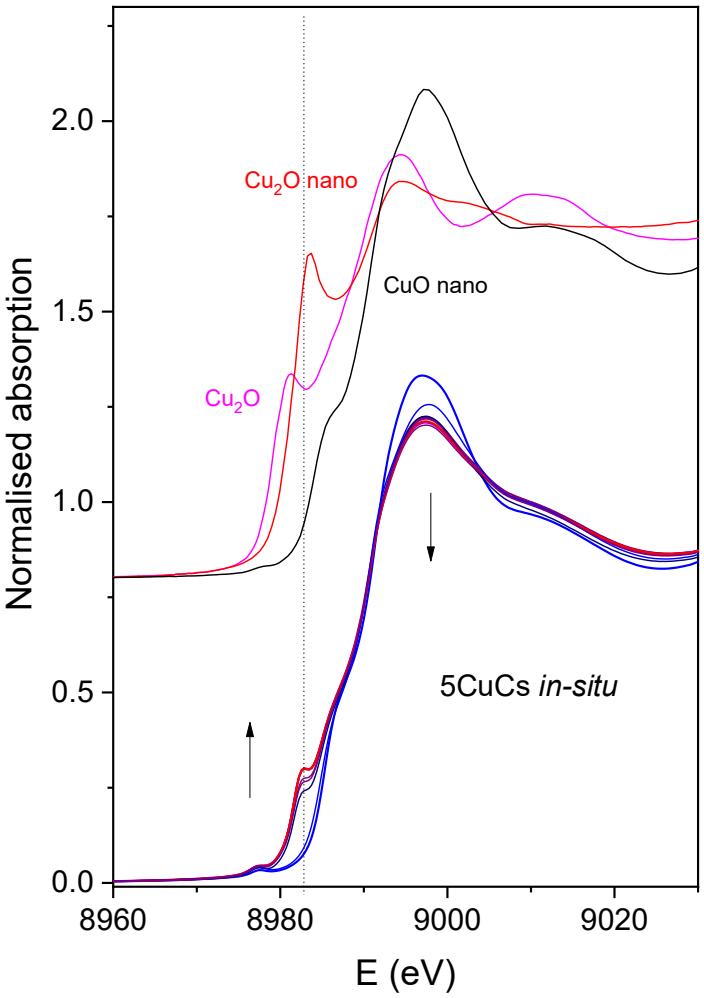

Fig. S6: Normalized Cu K-edge XANES spectra of 5CuCs catalysts, measured *in-situ* before and during catalytic propylene oxidation reaction up to 450 min. Spectra of reference Cu(I) and Cu(II) compounds (crystalline Cu_2O, nanoclusters Cu_2O[5] and CuO nanoparticles[3]) are plotted for comparison. Vertical dashed line is plotted at the peak of the Cu 1s-4p pre-edge absorption feature (8982.7 eV) in the catalysts during propylene oxidation reaction.

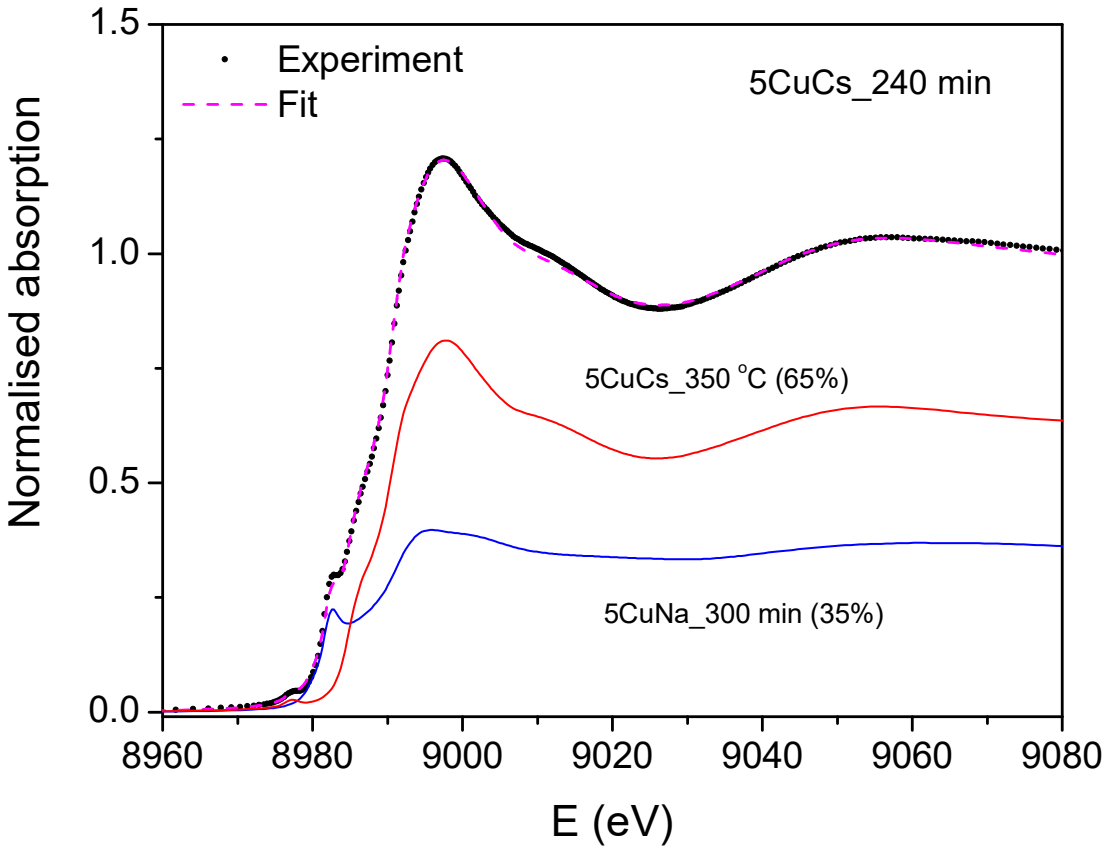

Fig. S7: Cu K-edge XANES spectra of 5CuCs catalyst, measured *in-situ* during catalytic propylene oxidation reaction after 240 min. Black dots: experiment; dashed magenta line: best fit with linear combination two reference XANES profiles (the sample 5CuCs measured before catalytic reaction at 350 °C in the He/O_2 atmosphere as a reference for Cu^{2+}, and the *in-situ* XANES spectrum of 5CuNa catalyst, measured during the propylene oxidation reaction at 350 °C when quasi-equilibrium state in the catalyst was reached after 300 min[3], as a reference for $Cu^{1.32+}$). Both LCF components are plotted below.

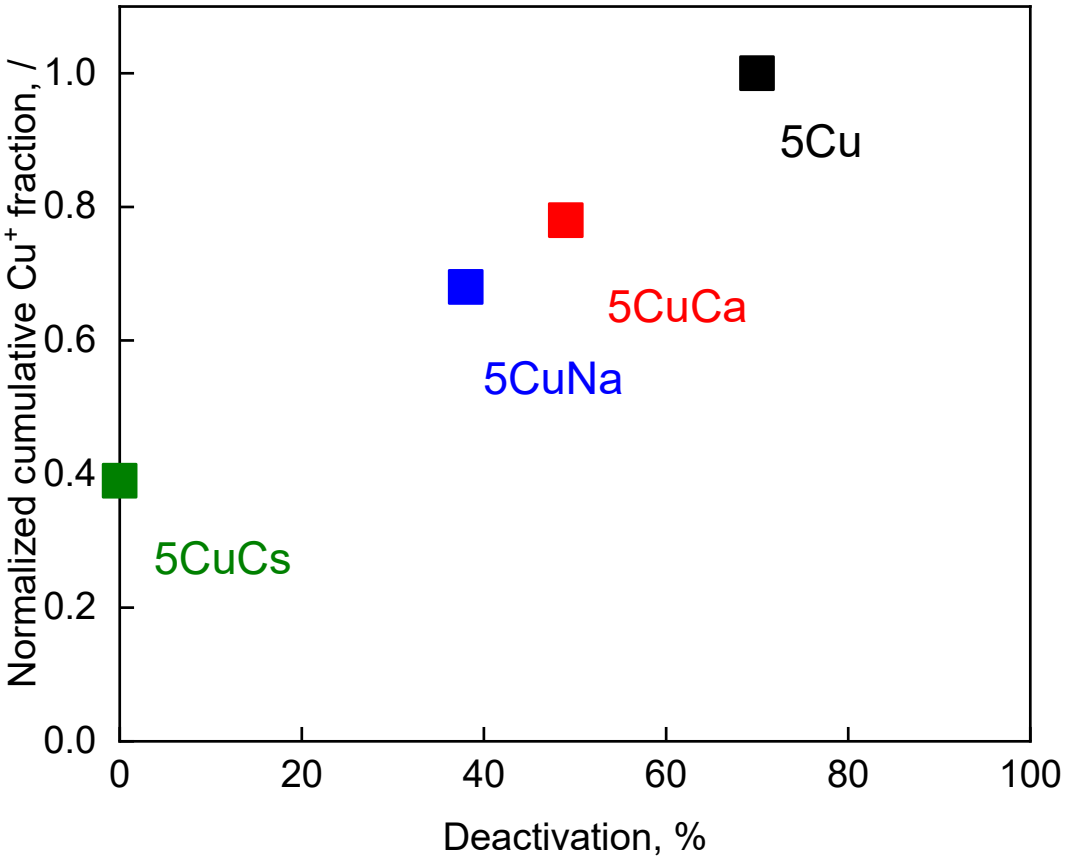

Fig. S8: Correlation between the cumulative fraction of copper in Cu^+ oxidation state and percentage of catalyst deactivation during propylene partial oxidation reaction.

Deactivation % represents loss of propylene conversion during 15h TOS (Fig. 1 in manuscript). Cumulative Cu^+ fractions for individual catalysts were calculated as following: Cu^+ percentages from XANES experiments at individual TOS were summed and divided by the sum value for the 5Cu catalyst (Fig 2).

5 Cu K-edge EXAFS analysis

In situ Cu K-edge EXAFS analysis is used to to directly probe the local structure around Cu cations in the 5Cu, 5CuNa 5CuCa and 5CuCs catalysts before and during the propylene oxidation reaction. The quantitative analysis of EXAFS spectra is performed with the Demeter (IFEFFIT) program package[1]. In Fourier transform magnitude of the EXAFS spectra (Figs. S9-S13) several peaks are observed in the R range from 1 up to 3.6 Å, representing the contributions of photoelectron scattering on the nearest shells of neighbors around the Cu atoms. In all cases a strong peak in the R range between 1 Å and 2.2 Å can be attributed to photoelectron backscattering on the nearest oxygen neighbors around Cu. Weaker peaks in the R range between 2.3 Å and 3.6 Å represents the contributions from more distant Cu coordination shells.

Qualitative comparisons of the FT spectra show that average Cu neighbourhoods in all catalyst samples at room temperature are almost identical. The spectra are significantly different from the spectra of the two (divalent and monovalent) reference crystalline copper oxides (Fig. S9). The series of *in-situ* EXAFS spectra for each catalyst sample reveal structural changes that appear already after heating of the samples at 350 °C in He/O_2 atmosphere, and then during during the propylene oxidation reaction, until equilibrium state is reached. Structural changes are expressed most in the signal of more distant coordination spheres in the R range beyond 2.2 Å. As indicated by Cu K-edge XANES results, we can expect a mixture of different Cu species in the catalysts. Before the propylene oxidation reaction at RT and at 350 °C in He/O_2 atmosphere all copper cations are expected to be in di-valent state bound in CuO nanoclusters or amorphous CuO oxides. During the propylene oxidation reaction at 350 °C when Cu^+ species are forming, we can expect a mixture of divalent and monovalent copper oxide nanoparticles or amorphous oxides on the surface of silica support.

Structural parameters of the average local Cu neighborhood (type and average number of neighbors, the radii and Debye-Waller factor of neighbor shells) are quantitatively resolved from the EXAFS spectra by comparing the measured EXAFS signal with model signal, constructed ab initio with the FEFF6 program code[2] from the set of scattering paths of the photoelectrons in a tentative spatial distribution of neighbor atoms. The atomic species of neighbours are identified in the fit by their specific scattering factor and phase shift.

In the first step, FEFF models were built for the Cu K-edge EXAFS spectra of the reference divalent and monovalent crystalline copper oxides, taking into account the local coordination of Cu cations in the crystal structure of the reference species, and tested on the corresponding EXAFS spectra of the reference Cu compounds (Fig. S9, Table SrefX1, SrefX2). In the second step, the Cu K-edge EXAFS spectra of the catalyst samples were modelled with a combined FEFF model, composed of neighbour atoms at distances characteristic for the expected Cu oxide species that may be present in the samples. With EXAFS analysis it is not possible to unambiguously identify all Cu species in the mixture and determine their structures. The proposed FEFF model aims to describe the average Cu local neighbourhood in the initial state and identify the main structural changes before and during the catalytic propylene oxidation reaction at 350 °C.

The FEFF model for the EXAFS analysis of the reference crystalline CuO is based on monoclinic crystal structure with space group C1 2/c 1 with the lattice constant a = 4.682(1), b = 3.424(1), c = 5.127(2) $\alpha = \gamma = 90$ °, $\beta = 99.42$ °[6]. The FEFF model comprised twelve single scattering and all significant multiple scattering paths up to 3.8 Å with six variable parameters: the amplitude reduction factor S_0^2, shift of energy origin of

the photoelectron ΔE_o, coordination shell distance (Δr) and the Debye temperature in modelling the Debye-Waller factors of all paths, except the first, for which a separate Δr_1 and the Debye–Waller factor (σ^2) are introduced. The shell coordination numbers were fixed to the crystallographic values obtained from XRD. A very good EXAFS fit (Fig. S9, Table S10) obtained in the *R*-range of 1.1 – 3.6 Å and in the *k* range of 3 – 14 $Å^{-1}$ provided precise information on coordination shell distances. Cu is coordinated to four O atoms at a distance of 1.95 Å and two O atoms at a distance of 2.8 Å. In the second coordination shell, ten copper atoms are detected at the distance range from 2.91 to 3.11 Å (four at 2.91 Å, four at 3.11 Å). The next coordination sphere is composed of eight oxygen atoms: two at 3.40 Å, 3.57 Å, 3.86 Å and 3.94 Å, and four copper atoms, two at 3.45 Å and two at 3.78 Å.

The FEFF model for crystalline Cu_2O[7] is based on cubic crystal structure with space group Pn-3m, with the lattice constant $a = b = c = 4.2685$, $\alpha = \beta = \gamma = 90$ °. The FEFF model comprised three single scattering and all significant multiple scattering paths up to 3.5 Å with eight variable parameters: the amplitude reduction factor S_0^2, shift of energy origin of the photoelectron ΔE_o, coordination shell distance (Δr) and Debye–Waller factor (σ^2) for all paths are introduced. The shell coordination numbers were fixed to the values obtained from XRD. Cu is coordinated to two O atoms at a distance of 1.85 Å. In the second coordination shell, twelve copper atoms are detected at the distance of 3.01 Å and six oxygen atoms at the distance of 3.53 Å. Very good EXAFS fit (Fig. S9, Table S11) was obtained in the *R*-range of 1 –3.5 Å and in the *k* range of 3 – 13 $Å^{-1}$.

The structural information obtained from EXAFS analysis of the reference crystalline CuO and Cu_2O oxides was considered in EXAFS modelling of the catalyst samples.

The Cu K-edge EXAFS spectra of the 5Cu, 5CuNa, 5CuCa, and 5CuCs catalysts samples before and during the propylene oxidation reaction are modelled with a FEFF model, composed of five or six neighbor shells at average distances typical for the expected divalent and monovalent Cu species that may be present in the samples. The nearest coordination shell comprised six oxygen atoms distributed at two or three distances. Cu neighbors, as most significant photoelectron backscatters, are included in more distant coordination shells at three different distances, typical for the expected Cu oxide species that may be present in the samples. Three variable parameters for each shell of neighbors are introduced in the model: the shell coordination number (N), the distance (R) and the Debye-Waller factor (σ^2). In addition, a common shift of energy origin ΔE_o is also allowed to vary. The amplitude-reduction factor S_0^2 is kept fixed at the value of 0.85 in agreement with previous Cu K-edge EXAFS analyses[4]. A good agreement between the model and the experimental spectra is found using the k range of 3 $Å^{-1}$ to 12 $Å^{-1}$ and R range of 1.0 Å to 3.6 Å (Figs. S9 to S13). The list of best fit parameters is given in the Tables S1 to S21. High precision is obtained for the values of best fit parameters of the nearest oxygen shell. The uncertainties of the best fit parameters N and σ^2 of more distant coordination shells are relatively large due to correlations between these parameters.

In all catalyst samples at RT all copper cations are coordinated to six oxygen atoms in the first coordination shell, distributed at two distances: four at 1.94 Å and two at larger distance 2.84 Å, characteristic for Cu(II) cations in the (nano)crystalline CuO, where Cu(II) cations are octahedrally coordinated to six oxygen atoms in elongated octahedron[4]. In more distant coordination shells we found Cu neighbors at distances characteristic for crystalline CuO, but the coordination numbers are significantly lower than in the bulk CuO. The results strongly support the XANES findings: Cu cations in all catalyst samples at RT before the propylene oxidation reaction are in the form of $Cu^{II}O$ crystalline nanoparticles and/or amorphous oxide species.

During heating of the catalyst samples at 350 °C in He/O_2 atmosphere average local structure of copper cations changes. Additional oxygen shell appears at 2.44 Å and

distribution of copper neighbors in more distant coordination shells is changed. The result suggest partial diffusion of Cu cations and formation of smaller CuO nanoparticles or CuO clusters with smaller distortion of the CuO_6 octahedron, as in the case of Cu(II) cation coordinated octahedrally to six O atoms distorted tetragonally because of the Jahn–Teller effect with four O atoms at 1.9 Å and two at 2.4 Å observed for example in CuO nanoclusters on TiO_2 catalyst[4].

During catalytic propylene oxidation reaction at 350 °C additional structural changes are detected, reaching equilibrium after about 300 minutes of reaction. Changes of Cu-O bond distance in the first coordination shell and Cu-Cu bond distance in the second coordination shells are detected, and reduction of coordination numbers is in all coordination shells.

The short Cu-O bond distance of 1.94 Å found in the initial state of all catalysts, is reduced. The contraction of this bond distance depends on the doping. In undoped 5Cu catalyst the Cu-O distance is (1.865±0.005 Å), almost the same value is found in 5CuCa catalyst (1.874±0.003 Å), while in 5CuCs and catalysts the distance is longer (1.882±0.005 Å), and in 5CuNa catalysts the distance is significantly shorter (1.830±0.007 Å).

Lower average Cu coordination numbers indicate the formation of smaller Cu oxide species on the surface of SiO_2 particles. In EXAFS modelling we tested also if there are any Cu-O-Si, Cu-O-Na, Cu-O-Cs, or Cu-O-Ca bonds present in the catalysts. The Si, Na, Ca or Cs neighbours in the second coordination shell of Cu cations were ruled out in the fits, which mean that if these coordinations are formed in the catalyst sample, relative amounts of Cu cations with these connections are below detection limit of EXAFS analysis (below 10 %), or that their contribution in EXAFS signal is smeared out due to large disorder effects (large Debye-Waller factors).

Cu K-edge EXAFS results for the 5CuNa catalyst

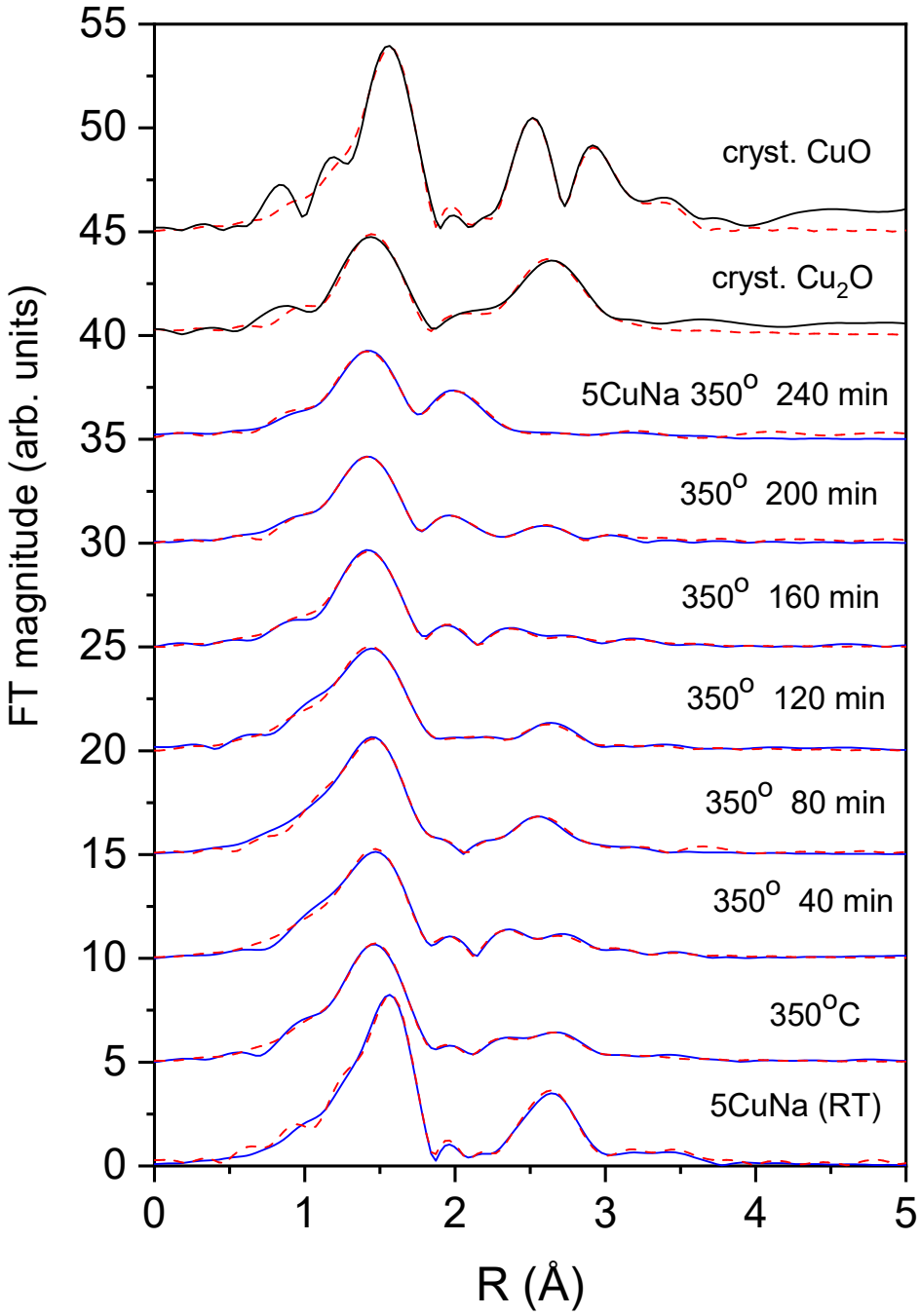

Fig. S9: Fourier transform magnitude of k^3-weighted Cu EXAFS spectra the 5CuNa catalyst at room temperature, at 350 °C in the He/O_2 atmosphere, and during the catalytic propylene oxidation reaction at 350 °C in a C3H6/O_2/He stream (16.7 % C3H6, 16.7 % O2, 66.6 % He, total flowrate of 30 ml/min). Scan duration was 40 minutes. Spectra of crystalline Cu_2O and CuO reference samples are added for comparison. FT spectra are calculated in the k range of 3 – 12 Å-1. Experiment – (solid line); best fit EXAFS model in the R range of 1 to 3.6 Å -- (red dashed line). Spectra are shifted vertically for clarity.

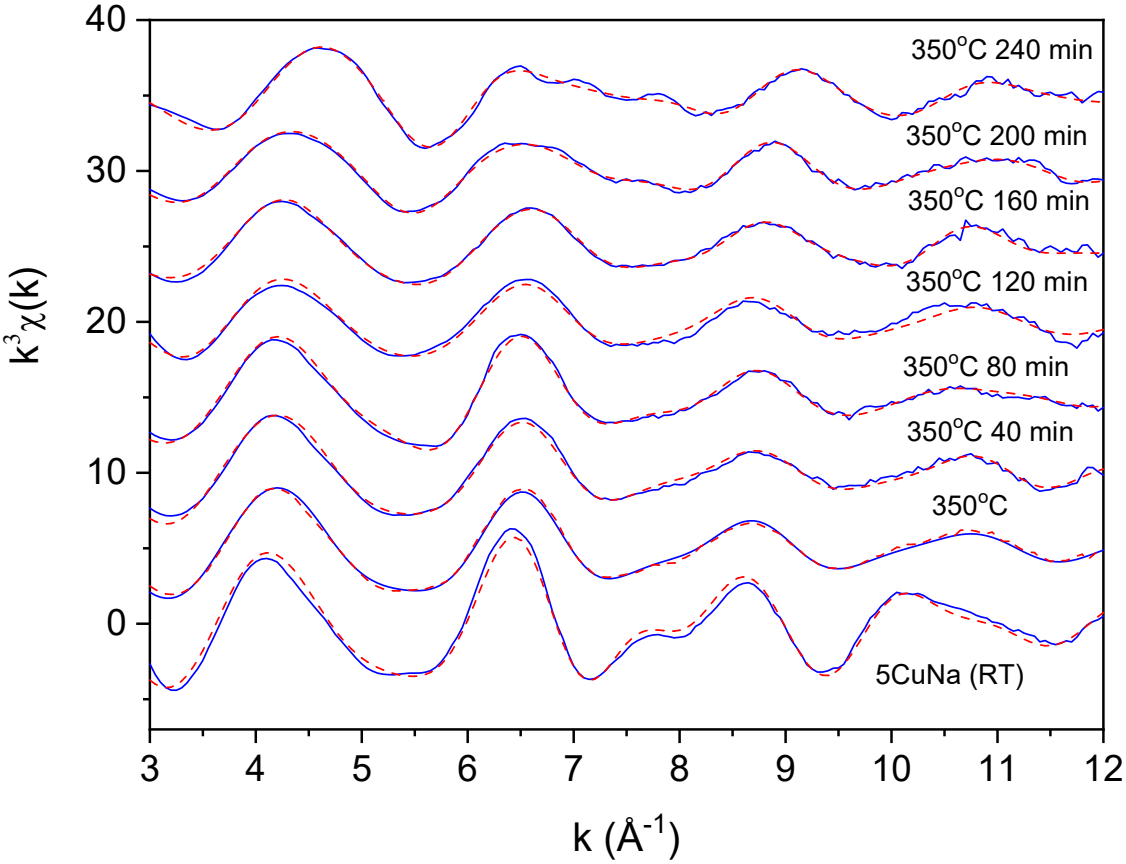

Fig. S10: k^3-weighted Cu EXAFS spectra the 5CuNa catalyst at room temperature, at 350 °C in the He/O_2 atmosphere, and during the catalytic propylene oxidation reaction at 350 °C in a C3H6/O_2/He stream (16.7 % C3H6, 16.7 % O2, 66.6 % He, total flowrate of 30 ml/min). Scan duration was 40 minutes. Experiment – (solid line); best fit EXAFS model calculated in the k range of 3 – 12 Å^{-1} and the R range of 1 to 3.6 Å -- (red dashed line). Spectra are shifted vertically for clarity.

Table S2: Parameters of the nearest coordination shells around Cu cations in the 5CuNa catalyst at room temperature in the He/O_2 atmosphere: average number of neighbor atoms (N), distance (R), and Debye-Waller factor (σ2). Uncertainty of the last digit is given in parentheses. A best fit is obtained with the amplitude reduction factor S02 = 0.85. The shift of the energy origin ΔEo and R-factor (quality of fit parameter), are listed in the last column.

Cu neigh.	*N*	*R* [Å]	σ^2 [Å^2]	ΔE_o/ *R*-factor
5CuNa (RT)				
O	3.9(2)	1.942(4)	0.005(1)	0.9 ± 0.6 eV 0.0074
O	1.5(6)	2.83(4)	0.013(7)	
Cu	1.8(2)	2.97(1)	0.009(3)	
Cu	0.5(3)	3.38(5)	0.012(3)	
Cu	0.9(3)	3.85(8)	0.012(3)	

Table S3: Parameters of the nearest coordination shells around Cu cations in the 5CuNa catalyst at 350 °C in the He/O_2 atmosphere: average number of neighbor atoms (N), distance (R), and Debye-Waller factor (σ2). Uncertainty of the last digit is given in parentheses. A best fit is obtained with the amplitude reduction factor S02 = 0.85. The shift of the energy origin ΔEo and R-factor (quality of fit parameter), are listed in the last column.

Cu neigh.	*N*	*R* [Å]	σ^2 [Å^2]	ΔE_o/ *R*-factor
5CuNa (350 °C in the He/O_2 atmosphere)				
O	3.4(3)	1.898(7)	0.007(1)	-3 ± 1 eV 0.0017
O	1.2(7)	2.44(5)	0.011(7)	
O	2(1)	2.72(4)	0.011(7)	
Cu	0.6(3)	2.94(4)	0.010(3)	
Cu	1.4(5)	3.32(6)	0.014(3)	
Cu	0.5(2)	3.50(8)	0.014(3)	

Table S4: Parameters of the nearest coordination shells around Cu cations in 5CuNa catalyst at 350 °C in during catalytic propylene oxidation reaction in a C3H6/O_2/He stream after 40 min: average number of neighbor atoms (N), distance (R), and Debye-Waller factor (σ2). Uncertainty of the last digit is given in parentheses. A best fit is obtained with the amplitude reduction factor S02 = 0.85. The shift of the energy origin ΔEo and R-factor (quality of fit parameter), are listed in the last column.

Cu neigh.	*N*	*R* [Å]	σ^2 [Å^2]	ΔE_o/ *R*-factor
5CuNa (350 °C during catalytic propylene oxidation - 40 min)				
O	3.4(3)	1.90(1)	0.008(1)	
O	1.1(7)	2.48(8)	0.008(7)	
O	2(1)	2.76(4)	0.008(7)	-3 ± 1 eV
Cu	0.6(4)	2.99(4)	0.010(3)	0.0057
Cu	1.8(5)	3.29(6)	0.014(3)	
Cu	1.9(7)	3.50(9)	0.014(3)	

Table S5: Parameters of the nearest coordination shells around Cu cations in the 5CuNa catalyst at 350 °C during catalytic propylene oxidation reaction in a C3H6/O_2/He stream after 80 min: average number of neighbor atoms (N), distance (R), and Debye-Waller factor (σ2). Uncertainty of the last digit is given in parentheses. A best fit is obtained with the amplitude reduction factor S02 = 0.85. The shift of the energy origin ΔEo and R-factor (quality of fit parameter), are listed in the last column.

Cu neigh.	*N*	*R* [Å]	σ^2 [Å^2]	ΔE_o/ *R*-factor
5CuNa (350 °C during catalytic propylene oxidation - 80 min)				
O	3.9(4)	1.88(1)	0.009(1)	
O	1.2(5)	2.39(4)	0.011(7)	
O	1.3(6)	2.67(4)	0.011(7)	-6 ± 1 eV
Cu	1.0(3)	2.89(7)	0.010(3)	0.0027
Cu	1.6(8)	3.37(5)	0.014(3)	
Cu	0.6(3)	3.57(9)	0.014(3)	

Table S6: Parameters of the nearest coordination shells around Cu cations in the 5CuNa catalyst at 350 °C during catalytic propylene oxidation reaction in a C_3H_6/O_2/He stream after 120 min: average number of neighbor atoms (N), distance (R), and Debye-Waller factor (σ^2). Uncertainty of the last digit is given in parentheses. A best fit is obtained with the amplitude reduction factor $S_0^2 = 0.85$. The shift of the energy origin ΔE_o and R-factor (quality of fit parameter), are listed in the last column.

Cu neigh.	N	R [Å]	σ^2 [Å^2]	ΔE_o/ R-factor
5CuNa (350 °C during catalytic propylene oxidation - 120 min)				
O	3.7(6)	1.89(1)	0.009(2)	-5 ± 1 eV 0.0039
O	0.8(5)	2.38(4)	0.009(7)	
O	1.3(9)	2.64(4)	0.009(7)	
Cu	0.8(2)	2.91(5)	0.010(3)	
Cu	0.6(3)	3.32(7)	0.014(3)	

Table S7**:** Parameters of the nearest coordination shells around Cu cations in the 5CuNa catalyst at 350 °C during catalytic propylene oxidation reaction in a C_3H_6/O_2/He stream after 160 min: average number of neighbor atoms (N), distance (R), and Debye-Waller factor (σ^2). Uncertainty of the last digit is given in parentheses. A best fit is obtained with the amplitude reduction factor $S_0^2 = 0.85$. The shift of the energy origin ΔE_o and R-factor (quality of fit parameter), are listed in the last column.

Cu neigh.	N	R [Å]	σ^2 [Å^2]	ΔE_o/ R-factor
5CuNa (350 °C during catalytic propylene oxidation - 160 min)				
O	2.4(3)	1.858(8)	0.006(1)	-6± 2 eV 0.0042
O	0.9(5)	2.47(4)	0.011(7)	
Cu	0.4(2)	2.78(4)	0.010(7)	
Cu	1.8(8)	3.34(4)	0.014(3)	
Cu	1.4(4)	3.56(4)	0.014(3)	

Table S8: Parameters of the nearest coordination shells around Cu cations in the 5CuNa catalyst at 350 °C during catalytic propylene oxidation reaction in a C_3H_6/O_2/He stream after 200 min: average number of neighbor atoms (N), distance (R), and Debye-Waller factor (σ^2). Uncertainty of the last digit is given in parentheses. A best fit is obtained with the amplitude reduction factor $S_0^2 = 0.85$. The shift of the energy origin ΔE_o and R-factor (quality of fit parameter), are listed in the last column.

Cu neigh.	N	R [Å]	σ^2 [Å^2]	ΔE_o/ R-factor
5CuNa (350 °C during catalytic propylene oxidation - 200 min)				
O	2.0(2)	1.852(4)	0.006(2)	
O	1.4(2)	2.49(1)	0.011(2)	
Cu	0.8(2)	2.93(3)	0.010(3)	-6± 1 eV
Cu	0.6(3)	3.15(5)	0.014(3)	0.0018
Cu	0.5(3)	3.63(5)	0.014(3)	

Table S9: Parameters of the nearest coordination shells around Cu cations in the 5CuNa catalyst at 350 °C during catalytic propylene oxidation reaction in a C_3H_6/O_2/He stream after 240 min: average number of neighbor atoms (N), distance (R), and Debye-Waller factor (σ^2). Uncertainty of the last digit is given in parentheses. A best fit is obtained with the amplitude reduction factor $S_0^2 = 0.85$. The shift of the energy origin ΔE_o and R-factor (quality of fit parameter), are listed in the last column.

Cu neigh.	N	R [Å]	σ^2 [Å^2]	ΔE_o/ R-factor
5CuNa (350 °C during catalytic propylene oxidation - 240 min)				
O	1.8(2)	1.830(7)	0.006(1)	
O	2.1(3)	2.45(1)	0.011(7)	
O	1.1(5)	2.88(4)	0.011(7)	-1 ± 1 eV
Cu	0.4(2)	3.12(6)	0.010(3)	0.0027
Cu	1.5(7)	3.35(5)	0.014(3)	
Cu	1.8(7)	3.57(5)	0.014(3)	

Cu K-edge EXAFS results for the crystalline Cu oxide references

Table S10: Parameters of the nearest coordination shells around Cu cations in the crystalline CuO reference sample: average number of neighbor atoms (N), distance (R), and Debye-Waller factor (σ2). Uncertainty of the last digit is given in parentheses. A best fit is obtained with the amplitude reduction factor $S_0^2 = 0.85$. The shift of the energy origin ΔE_o and *R*-factor (quality of fit parameter), are listed in the last column.

Cu neigh.	*N*	*R* [Å]	σ^2 [Å^2]	ΔE_o/ *R*-factor
CuO				
O	4	1.951(4)	0.004(1)	
O	2	2.79(1)	0.029(4)	
Cu	4	2.91(4)	0.006(1)	
Cu	4	3.11(4)	0.003(4)	
O	2	3.40(4)	0.030(4)	0 ± 1 eV
Cu	2	3.45(4)	0.012(2)	0.001
O	2	3.57(4)	0.030(4)	
Cu	2	3.78(4)	0.012(2)	
O	2	3.86(4)	0.031(4)	
O	2	3.94(4)	0.031(4)	

Table S11: Parameters of the nearest coordination shells around Cu cations in the crystalline Cu_2O reference sample: average number of neighbor atoms (*N*), distance (*R*), and Debye-Waller factor (σ^2). Uncertainty of the last digit is given in parentheses. A best fit is obtained with the amplitude reduction factor $S_0^2 = 0.85$. The shift of the energy origin ΔE_o and *R*-factor (quality of fit parameter), are listed in the last column.

Cu neigh.	*N*	*R* [Å]	σ^2 [Å^2]	ΔE_o/ *R*-factor
Cu_2O				
O	2	1.856(5)	0.003(1)	
Cu	12	3.03(1)	0.019(1)	2 ± 1 eV
O	6	3.52(3)	0.019(6)	0.001

Cu K-edge EXAFS results 5Cu catalyst

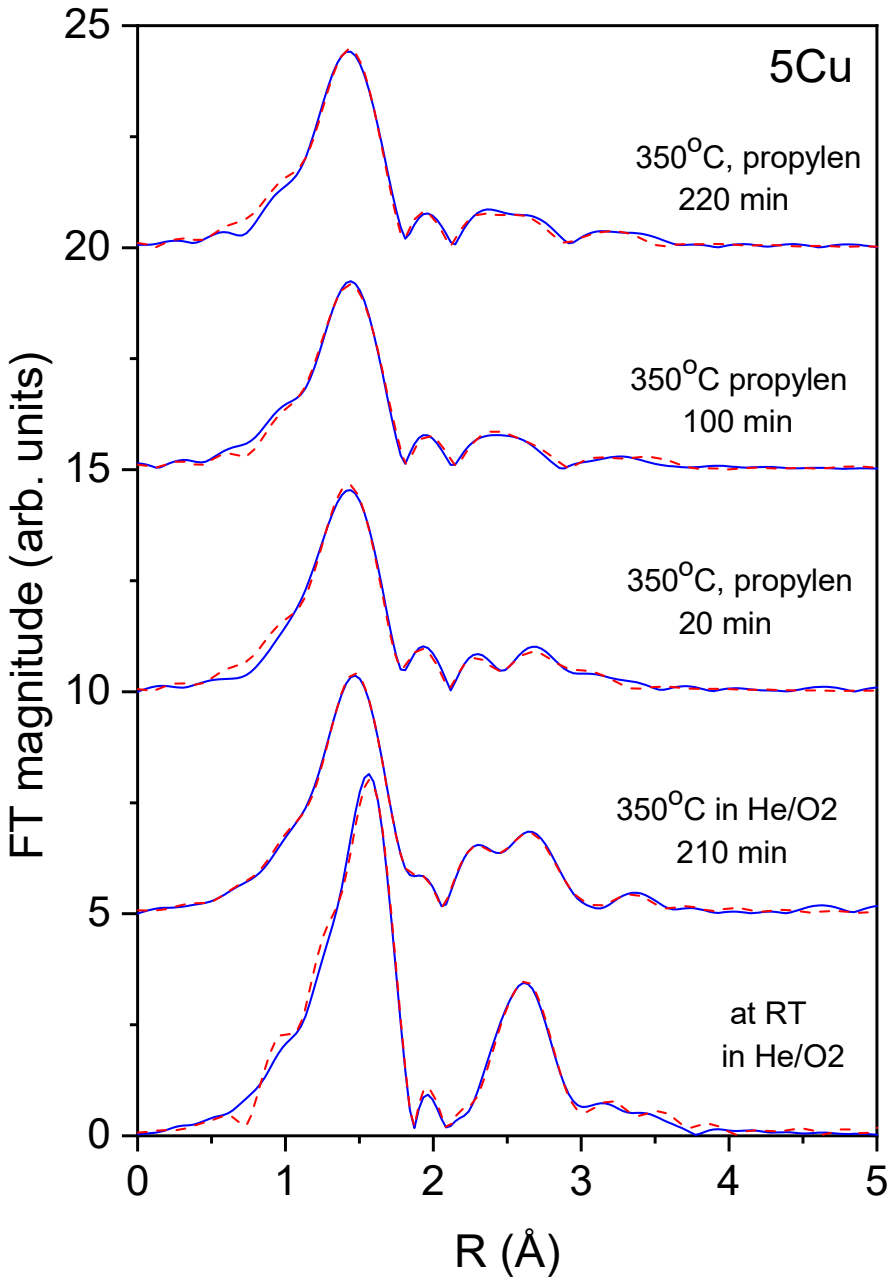

Figure S11: Fourier transform magnitude of k^3-weighted Cu EXAFS spectra the 5Cu catalyst at room temperature, at 350 °C in the He/O_2 atmosphere and during the catalytic propylene oxidation reaction at 350 °C in a $C_3H_6/O_2/He$ stream (16.7 % C_3H_6, 16.7 % O_2, 66.6 % He, total flowrate of 30 ml/min). Scan duration was 40 minutes. FT spectra are calculated in the k range of 3 – 13 $Å^{-1}$. Experiment – (blue solid line); best fit EXAFS model in the R range of 1 to 3.6 Å -- (red dashed line). Spectra are shifted vertically for clarity.

Table S12: Parameters of the nearest coordination shells around Cu cations in the 5Cu catalyst at room temperature in the He/O_2 atmosphere: average number of neighbor atoms (N), distance (R), and Debye-Waller factor (σ^2). Uncertainty of the last digit is given in parentheses. A best fit is obtained with the amplitude reduction factor $S_0^2 = 0.85$. The shift of the energy origin ΔE_o and R-factor (quality of fit parameter), are listed in the last column.

Cu neigh.	N	R [Å]	σ^2 [Å^2]	ΔE_o/ R-factor
5Cu (RT)				
O	4.0(2)	1.94(1)	0.005(1)	
O	1.5(6)	2.87(1)	0.013(7)	
Cu	1.8(2)	2.95(1)	0.009(3)	-0.4 ± 0.6 eV
Cu	0.9(3)	3.37(5)	0.012(3)	0.0045
Cu	0.5(3)	3.86(8)	0.012(3)	

Table S13: Parameters of the nearest coordination shells around Cu cations in the 5Cu catalyst at 350 °C in the He/O_2 atmosphere: average number of neighbor atoms (N), distance (R), and Debye-Waller factor (σ^2). Uncertainty of the last digit is given in parentheses. A best fit is obtained with the amplitude reduction factor $S_0^2 = 0.85$. The shift of the energy origin ΔE_o and R-factor (quality of fit parameter), are listed in the last column.

Cu neigh.	N	R [Å]	σ^2 [Å^2]	ΔE_o/ R-factor
5Cu (350 °C in the He/O_2 atmosphere)				
O	2.9(2)	1.90(1)	0.007(1)	
O	2.6(7)	2.43(5)	0.011(7)	
O	3.9(6)	2.70(4)	0.011(7)	-4 ± 1 eV
Cu	1.0(4)	2.92(2)	0.010(3)	0.0009
Cu	1.6(6)	3.24(5)	0.014(3)	
Cu	1.5(7)	3.42(4)	0.014(3)	

Table S14: Parameters of the nearest coordination shells around Cu cations in the 5Cu catalyst at 350 °C during catalytic propylene oxidation reaction in a C_3H_6/O_2/He stream after 20 min: average number of neighbor atoms (N), distance (R), and Debye-Waller factor (σ^2). Uncertainty of the last digit is given in parentheses. A best fit is obtained with the amplitude reduction factor $S_0^2 = 0.85$. The shift of the energy origin ΔE_o and R-factor (quality of fit parameter), are listed in the last column.

Cu neigh.	N	R [Å]	σ^2 [Å^2]	ΔE_o/ R-factor
5Cu (350 °C during catalytic propylene oxidation 40 min)				
O	2.4(4)	1.86(1)	0.006(1)	
O	1.1(7)	2.42(8)	0.011(7)	
O	1.4(6)	2.68(4)	0.011(7)	-3 ± 1 eV
Cu	0.4(3)	2.96(4)	0.010(3)	0.0057
Cu	1.6(5)	3.26(6)	0.014(3)	
Cu	0.6(7)	3.50(9)	0.014(3)	

Table S15: Parameters of the nearest coordination shells around Cu cations in the 5Cu catalyst at 350 °C during catalytic propylene oxidation reaction in a C_3H_6/O_2/He stream after 100 min: average number of neighbor atoms (N), distance (R), and Debye-Waller factor (σ^2). Uncertainty of the last digit is given in parentheses. A best fit is obtained with the amplitude reduction factor $S_0^2 = 0.85$. The shift of the energy origin ΔE_o and R-factor (quality of fit parameter), are listed in the last column.

Cu neigh.	N	R [Å]	σ^2 [Å^2]	ΔE_o/ R-factor
5Cu 350 °C during catalytic propylene oxidation 100 min				
O	2.1(4)	1.87(1)	0.006(1)	
O	0.9(7)	2.51(8)	0.011(7)	
O	1.7(6)	2.80(4)	0.011(7)	-3 ± 1 eV
Cu	0.2(1)	2.95(4)	0.010(3)	0.0059
Cu	0.3(2)	3.28(6)	0.014(3)	
Cu	0.3(7)	3.75(9)	0.014(3)	

Table S16: Parameters of the nearest coordination shells around Cu cations in the 5Cu catalyst at 350 °C during catalytic propylene oxidation reaction in a C_3H_6/O_2/He stream after 220 min: average number of neighbor atoms (N), distance (R), and Debye-Waller factor (σ^2). Uncertainty of the last digit is given in parentheses. A best fit is obtained with the amplitude reduction factor $S_0^2 = 0.85$. The shift of the energy origin ΔE_o and R-factor (quality of fit parameter), are listed in the last column.

Cu neigh.	N	R [Å]	σ^2 [Å^2]	ΔE_o/ R-factor
5Cu 350 °C during catalytic propylene oxidation 220 min				
O	2.3(4)	1.87(1)	0.006(1)	-5 ± 1 eV 0.0061
O	0.8(7)	2.48(8)	0.011(7)	
O	1.4(6)	2.76(4)	0.011(7)	
Cu	0.3(2)	2.94(4)	0.010(3)	
Cu	0.4(2)	3.29(6)	0.014(3)	
Cu	0.4(7)	3.69(9)	0.014(3)	

Cu K-edge EXAFS results 5CuCs catalyst

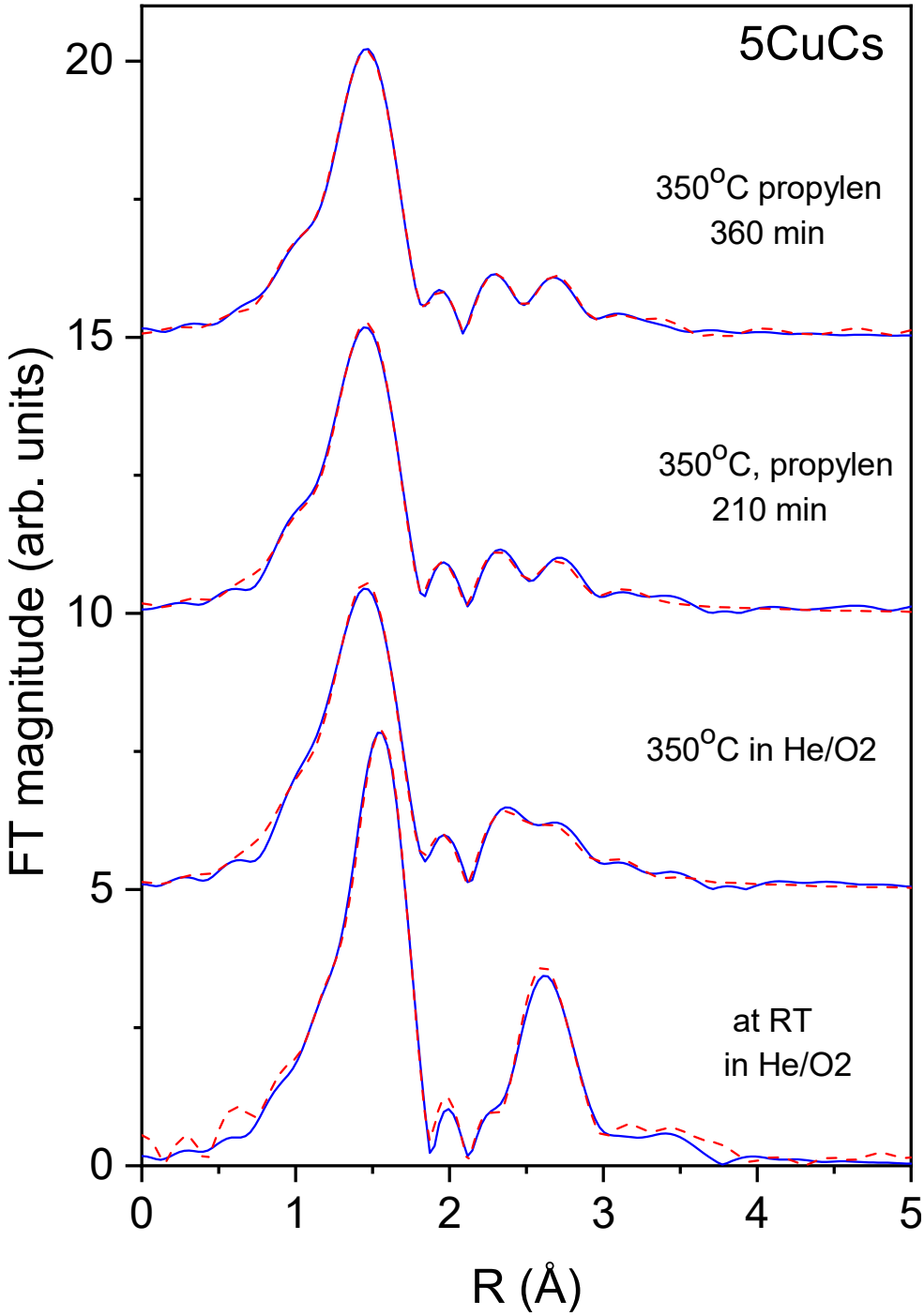

Figure S12: Fourier transform magnitude of k^3-weighted Cu EXAFS spectra the 5CuCs catalyst at room temperature, at 350 °C in the He/O_2 atmosphere and during the catalytic propylene oxidation reaction at 350 °C in a $C_3H_6/O_2/He$ stream (16.7 % C_3H_6, 16.7 % O_2, 66.6 % He, total flowrate of 30 ml/min). Scan duration was 40 minutes. FT spectra are calculated in the k range of 3 – 12.5 $Å^{-1}$. Experiment – (blue solid line); best fit EXAFS model in the R range of 1 to 3.6 Å -- (red dashed line). Spectra are shifted vertically for clarity.

Table S17: Parameters of the nearest coordination shells around Cu cations in the 5CuCs catalyst at room temperature in the He/O_2 atmosphere: average number of neighbor atoms (N), distance (R), and Debye-Waller factor (σ^2). Uncertainty of the last digit is given in parentheses. A best fit is obtained with the amplitude reduction factor $S_0^2 = 0.85$. The shift of the energy origin ΔE_o and R-factor (quality of fit parameter), are listed in the last column.

Cu neigh.	N	R [Å]	σ^2 [Å^2]	ΔE_o/ R-factor
5CuCs (RT)				
O	3.8(2)	1.944(5)	0.005(1)	1.6 ± 0.8 eV 0.0057
O	1.9(6)	2.85(4)	0.012(7)	
Cu	1.8(3)	2.98(1)	0.009(3)	
Cu	0.4(3)	3.37(5)	0.012(3)	
Cu	0.7(3)	3.85(8)	0.012(3)	

Table S18: Parameters of the nearest coordination shells around Cu cations in the 5CuCs catalyst at 350 °C in the He/O_2 atmosphere: average number of neighbor atoms (N), distance (R), and Debye-Waller factor (σ^2). Uncertainty of the last digit is given in parentheses. A best fit is obtained with the amplitude reduction factor $S_0^2 = 0.85$. The shift of the energy origin ΔE_o and R-factor (quality of fit parameter), are listed in the last column.

Cu neigh.	N	R [Å]	σ^2 [Å^2]	ΔE_o/ R-factor
5CuCs (350 °C in the He/O_2 atmosphere)				
O	3.2(4)	1.888(8)	0.007(1)	-3 ± 2 eV 0.0040
O	1.4(9)	2.48(5)	0.011(7)	
O	2.6(9)	2.78(4)	0.011(7)	
Cu	0.4(3)	2.98(6)	0.010(3)	
Cu	1.0(6)	3.31(6)	0.014(3)	
Cu	0.8(6)	3.42(9)	0.014(3)	

Table S19: Parameters of the nearest coordination shells around Cu cations in the 5CuCs catalyst at 350 °C during catalytic propylene oxidation reaction in a C_3H_6/O_2/He stream after 210 min: average number of neighbor atoms (N), distance (R), and Debye-Waller factor (σ^2). Uncertainty of the last digit is given in parentheses. A best fit is obtained with the amplitude reduction factor $S_0^2 = 0.85$. The shift of the energy origin ΔE_o and R-factor (quality of fit parameter), are listed in the last column.

Cu neigh.	N	R [Å]	σ^2 [Å^2]	ΔE_o/ R-factor
5CuCs (350 °C during catalytic propylene oxidation 210 min)				
O	2.7(3)	1.882(7)	0.006(1)	
O	1.0(5)	2.47(4)	0.011(7)	
O	2.1(9)	2.75(4)	0.011(7)	-2 ± 2 eV
Cu	0.6(4)	3.00(4)	0.010(3)	0.0025
Cu	1.2(7)	3.28(9)	0.014(3)	
Cu	0.3(2)	3.47(9)	0.014(3)	

Table S20: Parameters of the nearest coordination shells around Cu cations in the 5CuCs catalyst at 350 °C during catalytic propylene oxidation reaction in a C_3H_6/O_2/He stream after during 360 min: average number of neighbor atoms (N), distance (R), and Debye-Waller factor (σ^2). Uncertainty of the last digit is given in parentheses. A best fit is obtained with the amplitude reduction factor $S_0^2 = 0.85$. The shift of the energy origin ΔE_o and R-factor (quality of fit parameter), are listed in the last column.

Cu neigh.	N	R [Å]	σ^2 [Å^2]	ΔE_o/ R-factor
5CuCs 350 °C during catalytic propylene oxidation 360 min				
O	2.6(2)	1.882(5)	0.006(1)	
O	1.6(7)	2.43(2)	0.011(7)	
O	2.5(9)	2.72(2)	0.011(7)	-3 ± 1 eV
Cu	0.7(4)	2.97(3)	0.010(3)	0.0009
Cu	0.7(3)	3.25(9)	0.014(3)	
Cu	0.6(4)	3.32(9)	0.014(3)	

Cu K-edge EXAFS results 5CuCa catalyst

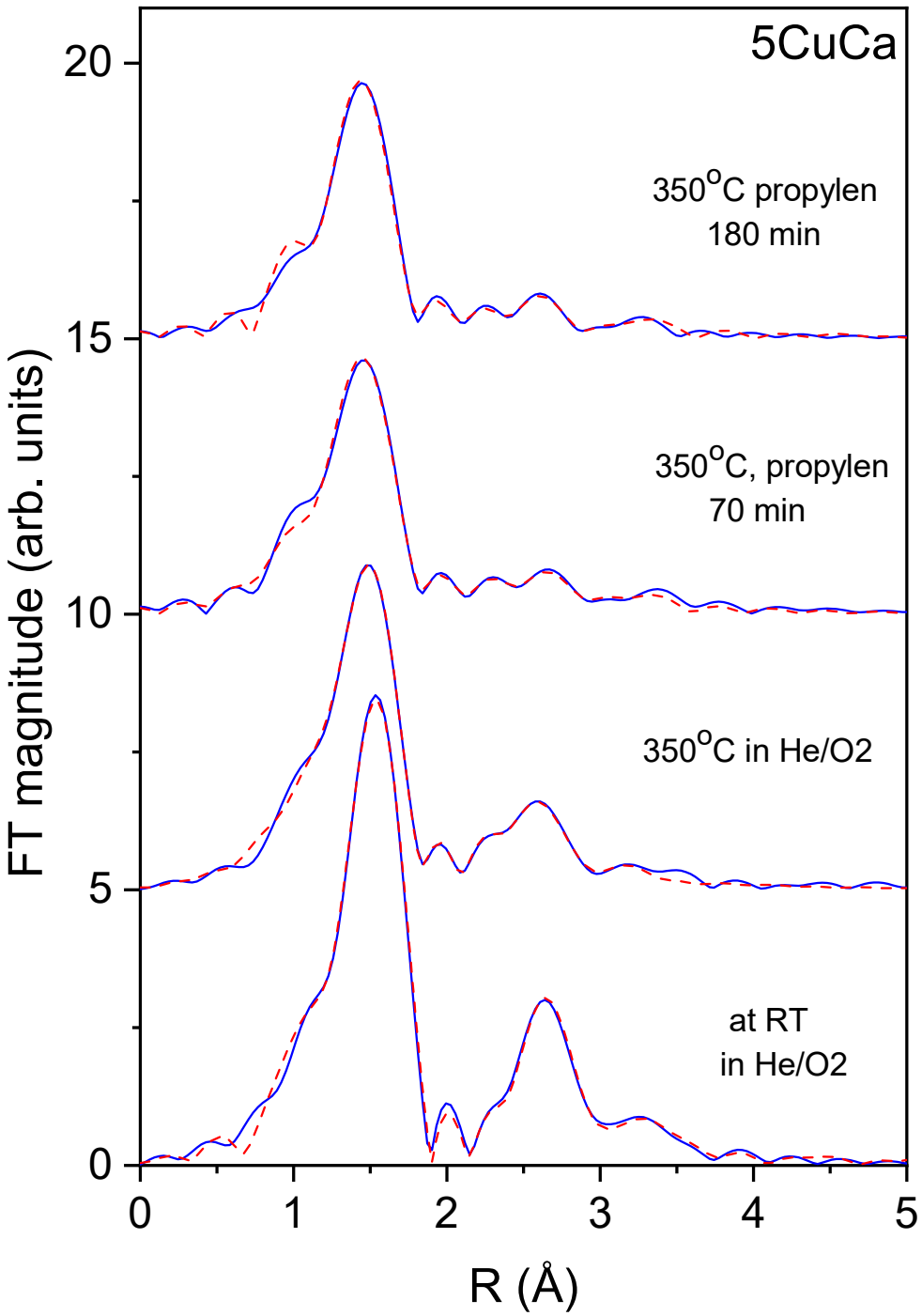

Figure S13: Fourier transform magnitude of k^3-weighted Cu EXAFS spectra the 5CuCa catalyst at room temperature, at 350 °C in the He/O_2 atmosphere and during the catalytic propylene oxidation reaction at 350 °C in a $C_3H_6/O_2/He$ stream (16.7 % C_3H_6, 16.7 % O_2, 66.6 % He, total flowrate of 30 ml/min). Scan duration was 40 minutes. FT spectra are calculated in the k range of 3 – 12.5 $Å^{-1}$. Experiment – (blue solid line); best fit EXAFS model in the R range of 1 to 3.6 Å -- (red dashed line). Spectra are shifted vertically for clarity.

Table S21: Parameters of the nearest coordination shells around Cu cations in the 5CuCa catalyst at room temperature in the He/O_2 atmosphere: average number of neighbor atoms (N), distance (R), and Debye-Waller factor (σ^2). Uncertainty of the last digit is given in parentheses. A best fit is obtained with the amplitude reduction factor $S_0^2 = 0.85$. The shift of the energy origin ΔE_o and R-factor (quality of fit parameter), are listed in the last column.

Cu neigh.	N	R [Å]	σ^2 [Å^2]	ΔE_o/ R-factor
5CuCa (RT)				
O	4.0(2)	1.944(3)	0.005(1)	
O	2.0(6)	2.86(4)	0.012(7)	
Cu	0.8(4)	2.97(1)	0.006(3)	0.7 ± 0.6 eV
Cu	0.6(3)	3.37(5)	0.007(3)	0.0015
Cu	0.5(3)	3.83(8)	0.007(3)	

Table S22: Parameters of the nearest coordination shells around Cu cations in the 5CuCa catalyst at 350 °C in the He/O_2 atmosphere: average number of neighbor atoms (N), distance (R), and Debye-Waller factor (σ^2). Uncertainty of the last digit is given in parentheses. A best fit is obtained with the amplitude reduction factor $S_0^2 = 0.85$. The shift of the energy origin ΔE_o and R-factor (quality of fit parameter), are listed in the last column.

Cu neigh.	N	R [Å]	σ^2 [Å^2]	ΔE_o/ R-factor
5CuCa (350 °C in the He/O_2 atmosphere)				
O	3.2(2)	1.906(4)	0.007(1)	
O	0.8(4)	2.44(5)	0.011(7)	
O	1.8(8)	2.72(4)	0.011(7)	-2 ± 1 eV
Cu	0.5(3)	2.92(6)	0.010(3)	0.0011
Cu	0.6(3)	2.93(6)	0.014(3)	
Cu	0.7(5)	3.32(6)	0.014(3)	

Table S23: Parameters of the nearest coordination shells around Cu cations in the 5CuCa catalyst at 350 °C during catalytic propylene oxidation reaction in a C_3H_6/O_2/He stream after 70 min: average number of neighbor atoms (N), distance (R), and Debye-Waller factor (σ^2). Uncertainty of the last digit is given in parentheses. A best fit is obtained with the amplitude reduction factor $S_0^2 = 0.85$. The shift of the energy origin ΔE_o and R-factor (quality of fit parameter), are listed in the last column.

Cu neigh.	N	R [Å]	σ^2 [Å^2]	ΔE_o/ R-factor
5CuCa (350 °C during catalytic propylene oxidation 70 min)				
O	2.4(4)	1.883(1)	0.006(1)	
O	1.1(7)	2.43(4)	0.011(7)	
O	1.9(8)	2.69(4)	0.014(7)	-4 ± 1 eV
Cu	1.0(6)	2.94(4)	0.010(3)	0.0046
Cu	2.0(8)	3.16(9)	0.014(3)	
Cu	1.1(7)	3.35(9)	0.014(3)	

Table S24: Parameters of the nearest coordination shells around Cu cations in the 5CuCa catalyst at 350 °C during catalytic propylene oxidation reaction in a C_3H_6/O_2/He stream after during 180 min: average number of neighbor atoms (N), distance (R), and Debye-Waller factor (σ^2). Uncertainty of the last digit is given in parentheses. A best fit is obtained with the amplitude reduction factor $S_0^2 = 0.85$. The shift of the energy origin ΔE_o and R-factor (quality of fit parameter), are listed in the last column.

Cu neigh.	N	R [Å]	σ^2 [Å^2]	ΔE_o/ R-factor
5CuCa 350 °C during catalytic propylene oxidation 180 min				
O	2.1(2)	1.874(3)	0.005(1)	
O	1.1(6)	2.41(5)	0.011(7)	
O	1.9(8)	2.67(4)	0.011(7)	-4 ± 1 eV
Cu	1.0(4)	2.91(4)	0.010(3)	0.0035
Cu	2.0(3)	3.11(6)	0.014(3)	
Cu	1.5(5)	3.31(6)	0.014(3)	

6 Molecular dynamics simulations (shape search)

MD simulations were performed in the VASP programme suite. On three lowest-lying structure for $Cu_{12}O_{12}$, molecular dynamics with the Nosé-Hoover thermostat set at 3000 K was performed. The time step was 1 fs and 1000 steps were carried out.

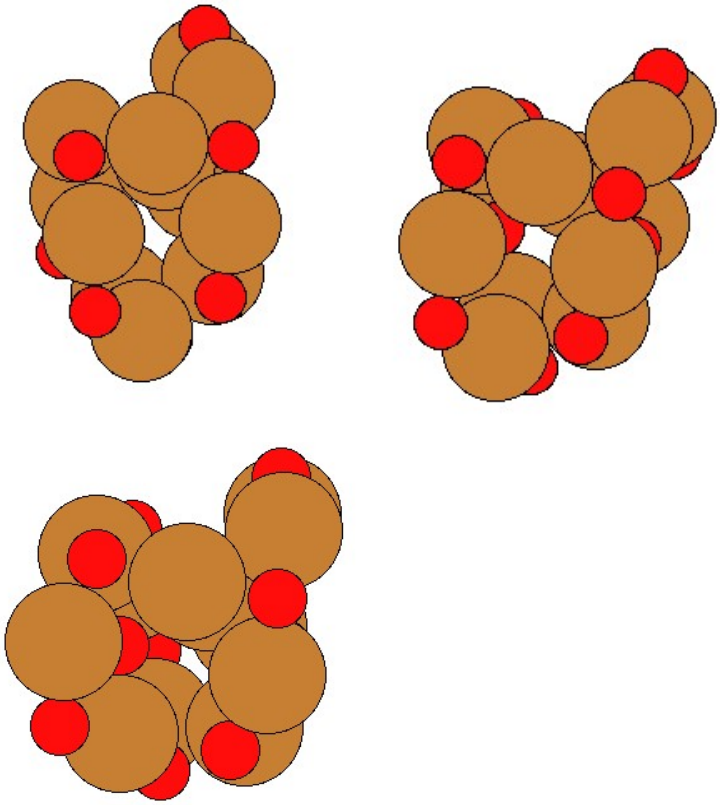

Figure S14: Initial structures of the three lowest-lying $Cu_{12}O_{12}$ structures.

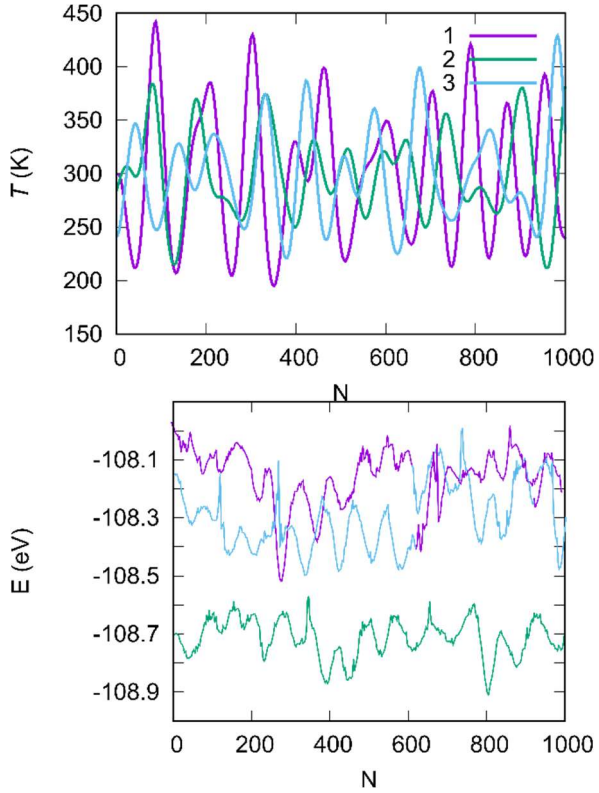

Figure S15: Temperature fluctuations and energy change during the MD shape search on the three lowest-lying $Cu_{12}O_{12}$ structures.

7 Bader analysis

Table S25: Charges on individual atoms in the investigated $Cu_{12}O_{12}$ clusters, as calculated by Bader's charge analysis. The bolded numbers indicate oxygen atoms reacting with propylene.

		$Cu_{12}O_{12}$	$Cu_{12}O_{12}Na$	$Cu_{12}O_{12}Cs$	$Cu_{12}O_{12}Ca$
#	*Atom type*	*Charge*	*Charge*	*Charge*	*Charge*
1	Cu	0.83	0.88	0.87	0.91
2	Cu	0.73	0.66	0.66	0.62
3	Cu	0.64	0.60	0.60	0.52
4	Cu	0.98	0.96	0.95	0.95
5	Cu	0.89	0.86	0.85	0.86
6	Cu	0.75	0.71	0.70	0.67
7	Cu	0.80	0.92	0.91	0.92
8	Cu	1.01	0.98	0.99	0.95
9	Cu	0.93	0.82	0.81	0.77
10	Cu	0.83	0.84	0.84	0.83
11	Cu	1.10	1.10	1.10	1.09
12	Cu	0.95	0.68	0.70	0.64
13	O	–0.86	–0.88	–0.89	–0.89
14	O	–0.88	–0.87	–0.87	–0.88
15	O	–0.95	–0.93	–0.94	–0.93
16	O	–0.82	–0.83	–0.84	–0.84
17	O	–0.91	–0.91	–0.91	–0.93
18	O	–0.80	**–0.97**	**–0.94**	**–1.08**
19	O	–0.86	–0.88	–0.89	–0.88
20	O	–0.86	–0.89	–0.89	–0.92
21	O	–0.96	–0.96	–0.97	–1.05
22	O	–0.79	–0.81	–0.82	–0.81
23	O	–0.81	–0.84	–0.85	–0.86
24	O	–0.85	–0.95	–0.95	–1.05
25	X	N/A	0.86	0.91	1.52

8 DFT geometries

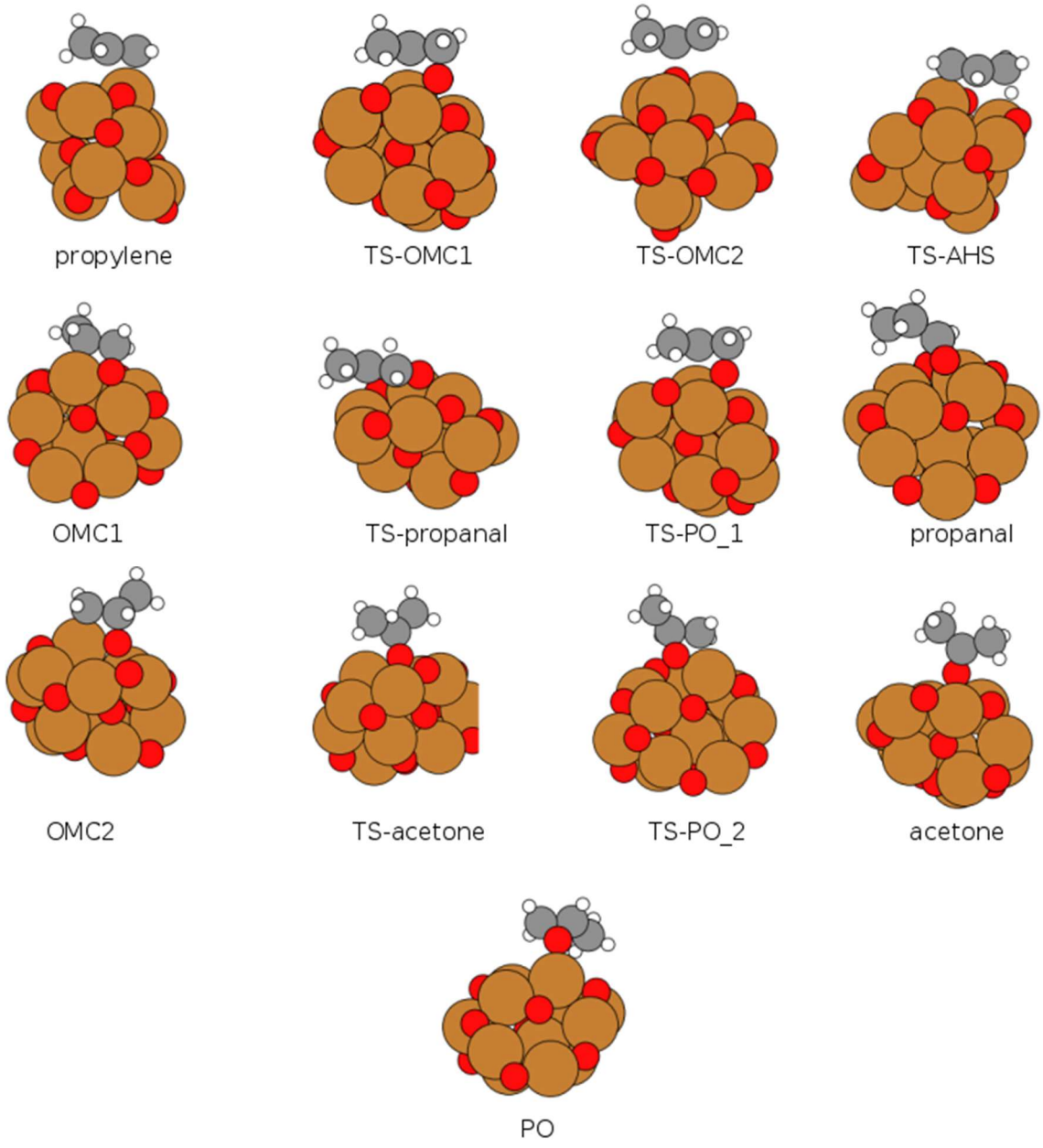

Figure S16: DFT-optimised of the $Cu_{12}O_{12}$ clusters with adsorbates.

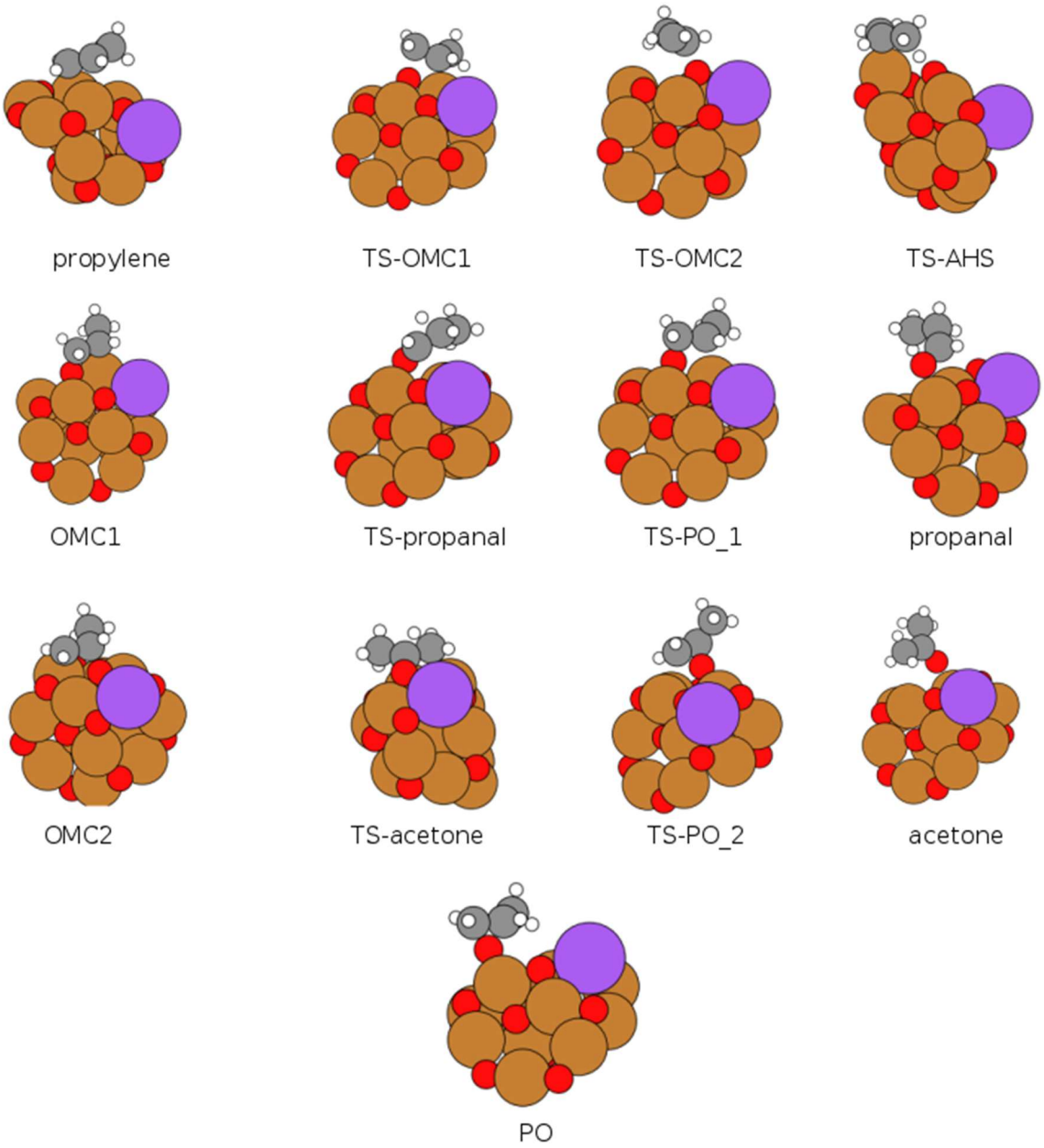

Figure S17: DFT-optimised of the $Cu_{12}O_{12}Cs$ clusters with adsorbates. 5CuNa and 5CuCa structures are analogous.

References:

[1] B. Ravel, M. Newville, ATHENA , ARTEMIS , HEPHAESTUS : data analysis for X-ray absorption spectroscopy using IFEFFIT, J. Synchrotron Radiat. 12 (2005) 537–541. https://doi.org/10.1107/S0909049505012719.

[2] J.J. Rehr, R.C. Albers, S.I. Zabinsky, High-order multiple-scattering calculations of x-ray-absorption fine structure, Phys. Rev. Lett. 69 (1992) 3397–3400. https://doi.org/10.1103/PhysRevLett.69.3397.

[3] J. Teržan, P. Djinović, J. Zavašnik, I. Arčon, G. Žerjav, M. Spreitzer, A. Pintar, Alkali and earth alkali modified CuO_x/SiO_2 catalysts for propylene partial oxidation: What determines the selectivity?, Appl. Catal. B Environ. 237 (2018) 214–227. https://doi.org/10.1016/j.apcatb.2018.05.092.

[4] T. Čižmar, U. Lavrenčič Štangar, M. Fanetti, I. Arčon, Effects of Different Copper Loadings on the Photocatalytic Activity of TiO_2-SiO_2 Prepared at a Low Temperature for the Oxidation of Organic Pollutants in Water, ChemCatChem. 10 (2018) 2982–2993. https://doi.org/10.1002/cctc.201800249.

[5] E.M.C. Alayon, M. Nachtegaal, A. Bodi, M. Ranocchiari, J.A. van Bokhoven, Bis(μ-oxo) versus mono(μ-oxo)dicopper cores in a zeolite for converting methane to methanol: an in situ XAS and DFT investigation, Phys. Chem. Chem. Phys. 17 (2015) 7681–7693. https://doi.org/10.1039/C4CP03226H.

[6] V. Massarotti, D. Capsoni, M. Bini, A. Altomare, A.G.G. Moliterni, X-ray powder diffraction ab initio structure solution of materials from solid state synthesis: the copper oxide case, Zeitschrift Für Krist. - Cryst. Mater. 213 (1998). https://doi.org/10.1524/zkri.1998.213.5.259.

[7] A. Kirfel, K. Eichhorn, Accurate structure analysis with synchrotron radiation. The electron density in Al2O3 and Cu2O, Acta Crystallogr. Sect. A Found. Crystallogr. 46 (1990) 271–284. https://doi.org/10.1107/S0108767389012596.

Chapter 4

Conclusions and Future Outlook

In our work, we demonstrate that finely dispersed copper oxide clusters are viable catalysts for direct propylene epoxidation using molecular oxygen. With the synthesis technique presented in Chapter 2 we produced highly dispersed CuO_x species with a mean diameter of less than 1 nm. The synthesized CuO_x/SiO_2 catalysts were further modified with alkali and alkaline earth metals.

With *in-* and *ex-situ* UV/vis we probed the morphological properties of the synthesized materials during reaction conditions. We found that sintering of the active phase is the most likely reason for the reduction in catalyst activity. Characteristic bands in the measured spectra indicated a highly dispersed copper phase with a low contribution from d-d transitions related to bulk CuO phase. The modified samples however underwent a significantly lower degree of sintering. Alkali as well as earth alkaline modification of the samples acts as a sintering barrier, noticeably improving the catalyst stability. Sintering is promoted under reducing (C_3H_6) and reaction atmosphere (C_3H_6, He and O_2) compared to oxidative (He and O_2). Sintering also increases the selectivity for acrolein, which seems to be the preferred product over bulk CuO_x.

The samples were imaged with scanning and transition electron microscopy (TEM) to further investigate the morphology of the samples. The amorphous silica support mostly comprises larger clusters (10-100 μm) and the copper is well dispersed within the pores. The mesoporosity of the support is visible in the TEM and was additionally confirmed by low angle XRD analysis. With energy-dispersive X-ray spectroscopy we confirmed that the nominal and the actual copper content are very similar.

The literature suggested that the acid properties of the catalyst play a significant role in propylene oxide (PO) selectivity. To that effect we probed the surface of the materials with pyridine adsorption and diffuse reflectance infrared Fourier transform (DRIFT) spectroscopy. The 2.5 and the 5 wt. % copper-containing samples have a widely different acidity, but show very similar selectivity for PO. From this we concluded that Lewis acidity of the surface does not play a crucial role in PO selectivity for our samples. This is probably caused by low acidity of the sites probed by pyridine as the probe molecule. Since this is an oxidation reaction, and surface oxygen acts as a base, we employed DRIFT and combined it with temperature-programmed CO_2 desorption (CO_2-TPD) to probe the basicity of the samples. The selective samples, specifically the ones where an alkali metal was the modifying adatom, showed newly formed basic sites of intermediate strength. This shoulder at approximately 155 °C in the CO_2-TPD was not seen in the unmodified and the alkaline earth modified catalysts. We propose that alkali modification lowers the nucleophilic character of the active oxygen species, which prevents allylic hydrogen stripping (AHS) and promotes oxametallacycle (OMC) formation. No correlation could be found between strong and weak basic sites and PO selectivity.

Copper atom local structure and oxidation state in reaction conditions was studied with *in-situ* XANES. Depending on the presence and type of the modifying adatom, the catalysts exhibited different reduction dynamics. This indicates that the modification does alter the kinetics of oxygen abstraction and replenishment. In the quasi-steady state the tested catalysts contained between 24 and 68 % of Cu^{+}. The remaining copper was present as Cu^{2+}. This reveals that Cu^{+} amount is not the sole determining factor for PO selectivity. The technique additionally confirmed that the average copper cluster has a mean diameter of less than 1 nm.

Different modifying atoms had a varying effect on catalyst stability and selectivity. Sodium and potassium modification had a similar effect, with both alkali metals significantly improving PO selectivity. This was accompanied by a decrease in acrolein and a slight increase in CO_x selectivity. The activity and the stability of the catalysts were also improved, where Na^{+} and K^{+} modified catalysts retained 3.4 and 4 % of propylene conversion after 1000 min of TOS, respectively. The calcium-modified catalyst also exhibited a much improved activity and stability, retaining 4.6 % of propylene conversion after 1000 min of TOS. It, however, showed no improvement in PO selectivity. Modification with Cs^{+} leads to the lowest extent of Cu^{2+} reduction to Cu^{+} (76±2 % at 5 h), highest stability throughout the 15 h of time on stream, and intermediate PO selectivity. The results of the catalytic tests correlate well with basicity tests, and support our theory of nucleophilicity modulation.

The *in-situ* EXAFS measurements revealed a reduction in Cu-O bond length with TOS for the sodium-modified and an increase for the calcium-modified catalyst. A slow reduction in bond length is caused by the sintering of the non-selective, unmodified active sites, also evident by a slow increase in PO selectivity. This further supports our theory of a reduced nucleophilic character of oxygen as a shorter bond implies a stronger binding. The Cs^{+}-modified catalyst also showed an increase in bond length; however we suspect this discrepancy is the result of increased stability. This catalyst shows minimal to no deactivation during TOS, which means the nonselective, unmodified active sites do not sinter.

The XAS experimental data was employed to construct a simulated copper oxide cluster, which was used to perform DFT studies. With these, we additionally confirmed that if the surface oxygen is too basic (nucleophilic), it immediately reacts with the allylic hydrogen. The activation barriers (AB) for OMC formation are increased anywhere from 9 to 78 % depending on the modifying alkali metal and the type of OMC formed. The AB for ring closure and PO desorption are simultaneously decreased (up to 23 % by Cs^{+} modification). On the other hand, the AB for AHS is increased by 60 and 67 % by Na^{+} and Cs^{+} modification, respectively. Even with the increase in AB, OMC is still energetically favorable compared to AHS. This promotes the observed increase in PO selectivity in alkali-modified catalysts. When propylene adsorbs to the alkali-modified catalyst surface, its allylic hydrogen does not react with surface oxygen, but preferentially an OMC forms that desorbs as PO. When Ca^{2+} is the modifying adatom, the AHS activation barrier is decreased by 64 %. If the OMC forms, it will preferentially desorb as acetone and not PO.

We co-fed propylene oxide into the reactor to see to which extent our product is further oxidized in subsequent reactions. We found that even with the modified catalysts, we still lose 75 % of PO due to subsequent oxidation reactions. This could probably be minimized by an engineering approach to minimize the temperature and residence time of reaction products in the heated post-catalytic part of reactor. Increased reaction pressure is reported as highly beneficial in terms of boosting PO selectivity. Ghosh et al. [36] observed an increase in PO selectivity from 25 % at 0.1 MPa, to 85 % 2 MPa, both at 250 °C.

Stabilization of the OMC intermediate could additionally boost the selectivity for PO. To achieve the stabilization, a zeolite with a smaller pore diameter could be used as a

support in order for van der Waals interactions with the pore walls to promote OMC formation. The effect was already studied by Maestri and Iglesia [87] with NO oxidation in a siliceous crystalline framework.

With these approaches PO selectivity could be increased to values that would make direct propylene epoxidation with molecular oxygen competitive with current established techniques.

References

[1] G. Sienel, R. Rieth, and K. T. Rowbottom, "Epoxides," in *Ullmann's Encyclopedia of Industrial Chemistry*, Weinheim, Germany: Wiley-VCH Verlag GmbH & Co. KGaA, 2000.

[2] C. J. Sullivan, A. Kuenz, and K.-D. Vorlop, "Propanediols," in *Ullmann's Encyclopedia of Industrial Chemistry*, Weinheim, Germany: Wiley-VCH Verlag GmbH & Co. KGaA, 2018, pp. 1–15.

[3] Nexant Inc., "Market Analytics: Propylene Oxide - 2018," 2018.

[4] J. Ji, Z. Lu, Y. Lei, and C. Turner, "Theoretical Studies on the Direct Propylene Epoxidation Using Gold-Based Catalysts: A Mini-Review," *Catalysts*, vol. 8, no. 10, p. 421, Sep. 2018.

[5] S. J. Khatib and S. T. Oyama, "Direct Oxidation of Propylene to Propylene Oxide with Molecular Oxygen: A Review," *Catal. Rev.*, vol. 57, no. 3, pp. 306–344, Jul. 2015.

[6] M. Lin, C. Xia, B. Zhu, H. Li, and X. Shu, "Green and efficient epoxidation of propylene with hydrogen peroxide (HPPO process) catalyzed by hollow TS-1 zeolite: A 1.0 kt/a pilot-scale study," *Chem. Eng. J.*, vol. 295, pp. 370–375, Jul. 2016.

[7] J. Rouchaud, "The catalysis of propylene oxidation by silver chelates," *J. Catal.*, vol. 14, no. 2, pp. 114–117, Jun. 1969.

[8] B. T. Pennington, "Alkylene oxides production using molten nitrate salt catalysts," US4785123A, 1986.

[9] T. . Nijhuis, S. Musch, M. Makkee, and J. . Moulijn, "The direct epoxidation of propene by molten salts," *Appl. Catal. A Gen.*, vol. 196, no. 2, pp. 217–224, Apr. 2000.

[10] J. Jiang, S. M. Oxford, B. Fu, M. C. Kung, H. H. Kung, and J. Ma, "Isotope labelling study of CO oxidation-assisted epoxidation of propene. Implications for oxygen activation on Au catalysts," *Chem. Commun.*, vol. 46, no. 21, p. 3791, 2010.

[11] M. Liu *et al.*, "Highly Selective Epoxidation of Propylene in a Low-Pressure Continuous Slurry Reactor and the Regeneration of Catalyst," *Ind. Eng. Chem. Res.*, vol. 54, no. 20, pp. 5416–5426, May 2015.

[12] E. Kertalli, J. C. Schouten, and T. A. Nijhuis, "Direct synthesis of propylene oxide in the liquid phase under mild conditions," *Appl. Catal. A Gen.*, vol. 524, pp. 200–205, Aug. 2016.

[13] M. Signorile *et al.*, "Effect of Ti Speciation on Catalytic Performance of TS-1 in the Hydrogen Peroxide to Propylene Oxide Reaction," *J. Phys. Chem. C*, vol. 122, no. 16, pp. 9021–9034, Apr. 2018.

[14] T. Hayashi, K. Tanaka, and M. Haruta, "Selective Vapor-Phase Epoxidation of Propylene over Au/TiO2Catalysts in the Presence of Oxygen and Hydrogen," *J. Catal.*, vol. 178, no. 2, pp. 566–575, Sep. 1998.

[15] E. Sacaliuc, A. Beale, B. Weckhuysen, and T. Nijhuis, "Propene epoxidation over Au/Ti-SBA-15 catalysts," *J. Catal.*, vol. 248, no. 2, pp. 235–248, Jun. 2007.

[16] W.-S. Lee, M. Cem Akatay, E. A. Stach, F. H. Ribeiro, and W. Nicholas Delgass, "Reproducible preparation of Au/TS-1 with high reaction rate for gas phase epoxidation of propylene," *J. Catal.*, vol. 287, pp. 178–189, Mar. 2012.

[17] X. Feng *et al.*, "Au/TS-1 catalyst prepared by deposition–precipitation method for propene epoxidation with H 2 /O 2 : Insights into the effects of slurry aging time and Si/Ti molar ratio," *J. Catal.*, vol. 325, pp. 128–135, May 2015.

[18] Y. Ren, J. Huang, Q. Lv, Y. Xie, A.-H. Lu, and M. Haruta, "Dual-component gas pretreatment for Au/TS-1: Enhanced propylene epoxidation with oxygen and hydrogen," *Appl. Catal. A Gen.*, vol. 584, p. 117172, Aug. 2019.

[19] M. Akimoto, "Kinetic and adsorption studies on vapor-phase catalytic oxidation of olefins over silver," *J. Catal.*, vol. 76, no. 2, pp. 333–344, Aug. 1982.

[20] M. Farinha Portela, C. Henriques, M. J. Pires, L. Ferreira, and M. Baerns, "Catalytic epoxidation and degradation of propylene by dioxygen over silver," *Catal. Today*, vol. 1, no. 1–2, pp. 101–110, Jan. 1987.

[21] C. Henriques, M. F. Portela, C. Mazzocchia, and E. Guglielminotti, "A Comparison Between Epoxidation and Degradation of Ethylene and Propylene over Silver," 1993, pp. 1995–1998.

[22] L. Guanzhong and Z. Xiaobin, "Epoxidation of propylene by air over modified silver catalyst," *Catal. Letters*, vol. 58, no. 1, pp. 67–70, 1999.

[23] A. Zemichael, Fessehaye W. Palermo, M. S. Tikhov, and R. M. Lambert, "Propene Epoxidation over K-Promoted Ag/CaCO3 Catalysts: The Effect of Metal Particle Size," *Catal. Letters*, vol. 80, no. 3–4, pp. 93–98, 2002.

[24] J. Lu, M. Luo, H. Lei, and C. Li, "Epoxidation of propylene on NaCl-modified silver catalysts with air as the oxidant," *Appl. Catal. A Gen.*, vol. 237, no. 1–2, pp. 11–19, Nov. 2002.

[25] M. Luo, J. Lu, and L. Can, "Epoxidation of Propylene over Ag-CuCl Catalysts Using Air as the Oxidant," *Catal. Letters*, vol. 86, no. 1–3, pp. 43–49, 2003.

[26] G. Jin, G. Lu, Y. Guo, J. Wang, and X. Liu, "Epoxidation of Propylene by Molecular Oxygen over Modified Ag–MoO3 Catalyst," *Catal. Letters*, vol. 87, no. 3–4, pp. 249–252, 2003.

[27] R. Wang, X. Guo, X. Wang, J. Hao, G. Li, and J. Xiu, "Effects of preparation conditions and reaction conditions on the epoxidation of propylene with molecular oxygen over Ag/TS-1 in the presence of hydrogen," *Appl. Catal. A Gen.*, vol. 261, no. 1, pp. 7–13, Apr. 2004.

[28] J. Lu, J. J. Bravo-Suárez, M. Haruta, and S. T. Oyama, "Direct propylene epoxidation over modified Ag/CaCO3 catalysts," *Appl. Catal. A Gen.*, vol. 302, no. 2, pp. 283–295, Apr. 2006.

[29] D. Torres, N. Lopez, F. Illas, and R. M. Lambert, "Low-Basicity Oxygen Atoms: A Key in the Search for Propylene Epoxidation Catalysts," *Angew. Chemie Int. Ed.*,

vol. 46, no. 12, pp. 2055–2058, Mar. 2007.

[30] K. E. Bere *et al.*, "Direct O 2 Epoxidation of Propylene by the Membrane Reactor Loaded with Ag–Sr Catalyst," *Chem. Lett.*, vol. 36, no. 9, pp. 1170–1171, Sep. 2007.

[31] W. Yao, G. Lu, Y. Guo, Y. Guo, Y. Wang, and Z. Zhang, "Promotional effect of Y2O3 on the performance of Ag/α-Al2O3 catalyst for epoxidation of propylene with molecular oxygen," *J. Mol. Catal. A Chem.*, vol. 276, no. 1–2, pp. 162–167, Oct. 2007.

[32] Y. Lei *et al.*, "Increased Silver Activity for Direct Propylene Epoxidation via Subnanometer Size Effects," *Science (80-.).*, vol. 328, no. 5975, pp. 224–228, Apr. 2010.

[33] X. Zheng *et al.*, "Epoxidation of propylene by molecular oxygen over supported Ag–Cu bimetallic catalysts with low Ag loading," *J. Mol. Catal. A Chem.*, vol. 357, pp. 106–111, May 2012.

[34] A. Pulido, P. Concepción, M. Boronat, and A. Corma, "Aerobic epoxidation of propene over silver (111) and (100) facet catalysts," *J. Catal.*, vol. 292, pp. 138–147, Aug. 2012.

[35] L. Cheng *et al.*, "Reaction Mechanism for Direct Propylene Epoxidation by Alumina-Supported Silver Aggregates: The Role of the Particle/Support Interface," *ACS Catal.*, vol. 4, no. 1, pp. 32–39, Jan. 2014.

[36] S. Ghosh *et al.*, "Selective oxidation of propylene to propylene oxide over silver-supported tungsten oxide nanostructure with molecular oxygen," *ACS Catal.*, vol. 4, no. 7, pp. 2169–2174, Jul. 2014.

[37] E. J. Lee *et al.*, "Direct epoxidation of propylene to propylene oxide with molecular oxygen over Ag–Mo–W/ZrO 2 catalysts," *Catal. Commun.*, vol. 89, pp. 156–160, Jan. 2017.

[38] B. Yu *et al.*, "Enhanced propylene oxide selectivity for gas phase direct propylene epoxidation by lattice expansion of silver atoms on nickel nanoparticles," *Appl. Catal. B Environ.*, vol. 243, pp. 304–312, Apr. 2019.

[39] B. Yu, T. Ayvalı, Z.-Q. Wang, X.-Q. Gong, A. A. Bagabas, and S. C. E. Tsang, "Gas phase selective propylene epoxidation over La 2 O 3 -supported cubic silver nanoparticles," *Catal. Sci. Technol.*, vol. 9, no. 13, pp. 3435–3444, 2019.

[40] W. Yao *et al.*, "Epoxidation of Propylene by Molecular Oxygen Over the Ag–Y2O3–K2O/α-Al2O3 Catalyst," *Catal. Letters*, vol. 119, no. 1–2, pp. 185–190, Oct. 2007.

[41] D. S. Billingsley and C. D. Holland, "Oxidation of Propylene with Air Over Copper Oxide Catalyst," *Ind. Eng. Chem. Fundam.*, vol. 2, no. 4, pp. 252–257, Nov. 1963.

[42] B. J. Wood, H. Wise, and R. S. Yolles, "Selectivity and stoichiometry of copper oxide in propylene oxidation," *J. Catal.*, vol. 15, no. 4, pp. 355–362, Dec. 1969.

[43] L. Holbrook, "Mechanism of promoter action in catalytic oxidation of propylene to acrolein*1," *J. Catal.*, vol. 20, no. 3, pp. 367–373, Mar. 1971.

[44] S. Gentry, "The catalytic properties of zeolite X containing transition metal ions III. Propylene oxidation," *J. Catal.*, vol. 35, no. 3, pp. 376–382, Dec. 1974.

[45] T. Inui, "Influence of retardation caused by partially oxidized adsorbate upon the oxidation state of copper catalyst and its performance for selective propylene oxidation," *J. Catal.*, vol. 65, no. 1, pp. 166–173, Sep. 1980.

[46] D. E. Self, J. D. Oakes, and M. G. White, "Selective propylene oxidation over a copper-tin oxide catalyst," *AIChE J.*, vol. 29, no. 4, pp. 625–631, Jul. 1983.

[47] C. C. McCain and G. W. Godin, "Detection of Homogeneous Reactions in the Presence of Heterogeneous Catalytic Reaction," *Nature*, vol. 202, no. 4933, pp. 692–693, May 1964.

[48] C. Daniel, "The catalytic oxidation of propylene I. Evidence for surface initiated homogeneous reactions," *J. Catal.*, vol. 24, no. 3, pp. 529–535, Mar. 1972.

[49] T. Shindo and H. Inoue, "Formation of Propylene Oxide in the Catalytic Oxidation of Propylene," *Nippon KAGAKU KAISHI*, no. 3, pp. 468–469, 1978.

[50] H. Orzesek, R. P. Schulz, U. Dingerdissen, and W. F. Maier, "Selective Oxidation of Propene with Air to Propylene Oxide, a Case Study of Autoxidation Versus Catalytic Oxidation with AMM-Catalysts," *Chem. Eng. Technol.*, vol. 22, no. 8, pp. 691–700, Aug. 1999.

[51] J. J. Cowell, A. K. Santra, R. Lindsay, R. M. Lambert, A. Baraldi, and A. Goldoni, "Bonding and reactivity of styrene on Cu(110): heterogeneous alkene epoxidation without the use of silver," *Surf. Sci.*, vol. 437, no. 1–2, pp. 1–8, Aug. 1999.

[52] O. Vaughan, G. Kyriakou, N. MacLeod, M. Tikhov, and R. Lambert, "Copper as a selective catalyst for the epoxidation of propene," *J. Catal.*, vol. 236, no. 2, pp. 401–404, Dec. 2005.

[53] Y. Wang, H. Chu, W. Zhu, and Q. Zhang, "Copper-based efficient catalysts for propylene epoxidation by molecular oxygen," *Catal. Today*, vol. 131, no. 1–4, pp. 496–504, Feb. 2008.

[54] L. Yang, J. He, Q. Zhang, and Y. Wang, "Copper-catalyzed propylene epoxidation by oxygen: Significant promoting effect of vanadium on unsupported copper catalyst," *J. Catal.*, vol. 276, no. 1, pp. 76–84, Nov. 2010.

[55] J. He, Q. Zhai, Q. Zhang, W. Deng, and Y. Wang, "Active site and reaction mechanism for the epoxidation of propylene by oxygen over CuOx/SiO2 catalysts with and without Cs+ modification," *J. Catal.*, vol. 299, pp. 53–66, Mar. 2013.

[56] A. Marimuthu, J. Zhang, and S. Linic, "Tuning Selectivity in Propylene Epoxidation by Plasmon Mediated Photo-Switching of Cu Oxidation State," *Science (80-.).*, vol. 339, no. 6127, pp. 1590–1593, Mar. 2013.

[57] Ş. Kalyoncu *et al.*, "NaCl-Promoted CuO–RuO2/SiO2 Catalysts for Propylene Epoxidation with O2 at Atmospheric Pressures: A Combinatorial Micro-reactor Study.," *Catal. Letters*, vol. 145, no. 2, pp. 596–605, Feb. 2015.

[58] X. Yang *et al.*, "Direct Epoxidation of Propylene over Stabilized Cu+ Surface Sites on Titanium-Modified Cu2O," *Angew. Chemie - Int. Ed.*, vol. 54, no. 41, pp. 11946–11951, Oct. 2015.

[59] Y.-Y. Song and G.-C. Wang, "Theoretical Study of Propylene Epoxidation over Cu2O(111) Surface: Activity of O2– , O – , and O2– Species," *J. Phys. Chem. C*, vol. 122, no. 37, pp. 21500–21513, Sep. 2018.

[60] M. Diekmann, G. Koch, M. König, and T. Ressler, "Correlation between Copper Oxide Particle Size and Selectivity towards Propylene Oxide in Selective Oxidation of Propene," *ChemCatChem*, vol. 10, no. 23, pp. 5459–5467, Dec. 2018.

[61] M. Kahn, A. Seubsai, I. Onal, and S. Senkan, "High Throughput Synthesis and

Screening of New Catalytic Materials for the Direct Epoxidation of Propylene," *Comb. Chem. High Throughput Screen.*, vol. 13, no. 1, pp. 67–74, Jan. 2010.

[62] H. Yoshida, T. Tanaka, M. Yamamoto, T. Yoshida, T. Funabiki, and S. Yoshida, "Epoxidation of Propene by Gaseous Oxygen over Silica and Mg-Loaded Silica under Photoirradiation," *J. Catal.*, vol. 171, no. 2, pp. 351–357, Oct. 1997.

[63] H. Yoshida, C. Murata, and T. Hattori, "Photocatalytic epoxidation of propene by molecular oxygen over highly dispersed titanium oxide species on silica," *Chem. Commun.*, no. 16, pp. 1551–1552, 1999.

[64] C. Murata, H. Yoshida, and T. Hattori, "Visible light-induced photoepoxidation of propene by molecular oxygen over chromia–silica catalysts," *Chem. Commun.*, no. 23, pp. 2412–2413, Nov. 2001.

[65] V. Duma and D. Hönicke, "Gas Phase Epoxidation of Propene by Nitrous Oxide over Silica-Supported Iron Oxide Catalysts," *J. Catal.*, vol. 191, no. 1, pp. 93–104, Apr. 2000.

[66] X. Wang, Q. Zhang, S. Yang, and Y. Wang, "Iron-Catalyzed Propylene Epoxidation by Nitrous Oxide: Studies on the Effects of Alkali Metal Salts," *J. Phys. Chem. B*, vol. 109, no. 49, pp. 23500–23508, Dec. 2005.

[67] S. Yang, Q. Zhang, and Y. Wang, "Boron-modified Chlorine-free K + –FeO x /SBA-15 as Highly Effective Catalyst for Propylene Epoxidation by Nitrous Oxide," *Chem. Lett.*, vol. 36, no. 6, pp. 786–787, Jun. 2007.

[68] B. Moens *et al.*, "Epoxidation of propylene with nitrous oxide on Rb2SO4-modified iron oxide on silica catalysts," *J. Catal.*, vol. 247, no. 1, pp. 86–100, Apr. 2007.

[69] J. Lu, M. Luo, H. Lei, X. Bao, and C. Li, "Epoxidation of Propylene on NaCl-Modified VCe1-x Cux Oxide Catalysts with Direct Molecular Oxygen as the Oxidant," *J. Catal.*, vol. 211, no. 2, pp. 552–555, Oct. 2002.

[70] F. Amano and T. Tanaka, "Modification of photocatalytic center for photo-epoxidation of propylene by rubidium ion addition to V2O5/SiO2," *Catal. Commun.*, vol. 6, no. 4, pp. 269–273, Apr. 2005.

[71] Z. Song, N. Mimura, S. Tsubota, T. Fujitani, and S. T. Oyama, "Surface-Initiated Gas-Phase Epoxidation of Propylene with Molecular Oxygen by Silica-Supported Molybdenum Oxide: Effects of Addition of C3H8 or NO and Reactor Design," *Catal. Letters*, vol. 121, no. 1–2, pp. 33–38, Feb. 2008.

[72] Y. Pang, X. Chen, C. Xu, Y. Lei, and K. Wei, "High Catalytic Performance of MoO 3 -Bi 2 SiO 5 /SiO 2 for the Gas-Phase Epoxidation of Propylene by Molecular Oxygen," *ChemCatChem*, vol. 6, no. 3, pp. 876–884, Mar. 2014.

[73] Y. Xu, L. Guo, X. Chen, and Q. Huang, "The surface construction of Mo–O–Bi coordination for high catalytic performance in gas-phase epoxidation of propylene with O 2," *Catal. Sci. Technol.*, vol. 8, no. 4, pp. 1070–1082, 2018.

[74] Y. Lei, X. Chen, C. Xu, Z. Dai, and K. Wei, "Enhanced catalytic performance in the gas-phase epoxidation of propylene over Ti-modified MoO 3 –Bi 2 SiO 5 /SiO 2 catalysts," *J. Catal.*, vol. 321, pp. 100–112, Jan. 2015.

[75] A. Seubsai *et al.*, "Epoxidation of propylene to propylene oxide with molecular oxygen over Sb 2 O 3 –CuO–NaCl/SiO 2 catalysts," *J. Ind. Eng. Chem.*, vol. 32, pp. 292–297, Dec. 2015.

[76] A. Seubsai *et al.*, "High Stability of Ruthenium–Copper-Based Catalysts for Epoxidation of Propylene," *Catal. Letters*, vol. 148, no. 2, pp. 586–600, Feb. 2018.

[77] E. J. Lee, J. Lee, M. Lee, H.-K. Min, S. Park, and D. Heui Kim, "Propylene epoxidation by oxygen over tungsten oxide supported on ceria-zirconia," *Mol. Catal.*, vol. 467, pp. 111–119, Apr. 2019.

[78] X. Xu and C. M. Friend, "Partial oxidation without allylic carbon-hydrogen bond activation: the conversion of propene to acetone on rhodium(111)-p(2.times.1)-O," *J. Am. Chem. Soc.*, vol. 113, no. 18, pp. 6779–6785, Aug. 1991.

[79] N. F. Brown and M. A. Barteau, "Epoxides as probes of oxametallacycle chemistry on Rh(111)," *Surf. Sci.*, vol. 298, no. 1, pp. 6–17, Dec. 1993.

[80] J. W. Medlin, M. Mavrikakis, and M. A. Barteau, "Stabilities of Substituted Oxametallacycle Intermediates: Implications for Regioselectivity of Epoxide Ring Opening and Olefin Epoxidation," *J. Phys. Chem. B*, vol. 103, no. 50, pp. 11169–11175, Dec. 1999.

[81] J. Llorca *et al.*, "Propene epoxidation over TiO2-supported Au–Cu alloy catalysts prepared from thiol-capped nanoparticles," *J. Catal.*, vol. 258, no. 1, pp. 187–198, Aug. 2008.

[82] A. Roldan, D. Torres, J. M. Ricart, and F. Illas, "On the effectiveness of partial oxidation of propylene by gold: A density functional theory study," *J. Mol. Catal. A Chem.*, vol. 306, no. 1–2, pp. 6–10, Jul. 2009.

[83] A. C. Kizilkaya, S. Senkan, and I. Onal, "Investigation of ruthenium–copper bimetallic catalysts for direct epoxidation of propylene: A DFT study," *J. Mol. Catal. A Chem.*, vol. 330, no. 1–2, pp. 107–111, Sep. 2010.

[84] Y. Dai *et al.*, "Significant enhancement of the selectivity of propylene epoxidation for propylene oxide: a molecular oxygen mechanism," *Phys. Chem. Chem. Phys.*, vol. 19, no. 36, pp. 25129–25139, 2017.

[85] B. Zhao and G.-C. C. Wang, "Theoretical Investigation of Propylene Epoxidation on Ag(111) by Molecular Oxygen: Na(K,Cl) Effects," *J. Phys. Chem. C*, vol. 123, no. 28, pp. 17273–17282, Jul. 2019.

[86] B. Ravel and M. Newville, "ATHENA , ARTEMIS , HEPHAESTUS : data analysis for X-ray absorption spectroscopy using IFEFFIT," *J. Synchrotron Radiat.*, vol. 12, no. 4, pp. 537–541, Jul. 2005.

[87] M. Maestri and E. Iglesia, "First-principles theoretical assessment of catalysis by confinement: NO–O 2 reactions within voids of molecular dimensions in siliceous crystalline frameworks," *Phys. Chem. Chem. Phys.*, vol. 20, no. 23, pp. 15725–15735, 2018.

Bibliography

Original Scientific Articles

F. Zhang, Z. Liu, X. Chen, N. Rui, L.E. Betancourt, L. Lin, W. Xu, C.-J. Sun, A.M.M. Abeykoon, J.A. Rodriguez, J., Teržan, K. Lorber, P. Djinović, S.D. Senanayake, "Effects of Zr doping into ceria for the dry reforming of methane over $Ni/CeZrO_2$ catalysts ein situ studies with XRD, XAFS, and AP-XPS." *ACS catalysis*, vol. 10, iss. 5, pp. 3274-3284, 2020.

J. Teržan, M. Huš, I. Arčon, B. Likozar, P. Djinović, "Effect of Na, Cs and Ca on propylene epoxidation selectivity over CuO_x/SiO_2 catalysts studied by catalytic tests, *in-situ* XAS and DFT." *Applied Surface Science*, vol. 528, pp. 1-29, 2020.

G. Žerjav, J. Teržan, P. Djinović, Z. Barbieriková, T. Hajdu, V. Brezová, J. Zavašnik, J. Kovač, A. Pintar, "TiO_2-β-Bi_2O_3 junction as a leverage for the visible-light activity of TiO_2 based catalyst used for environmental applications." *Catalysis today,* in press, 2020.

J. Teržan, P. Djinović, J. Zavašnik, I. Arčon, G. Žerjav, M. Spreitzer, A. Pintar, "Alkali and earth alkali modified CuO_x/SiO_2 catalysts for propylene partial oxidation : what determines the selectivity?" *Applied catalysis B: Environmental*, vol. 237, pp. 214-227, 2018.

A. F. Cunha, M. N. Moreira, A. M. Ribeiro, J. M. Loureiro, A. E. Rodrigues, J. Teržan, P. Djinović, A. Pintar, "Synthesis gas adjustment by low temperature sorption enhanced water-gas shift reaction through a copper-zeolite 13X hybrid material," *Chemical engineering and processing*, vol. 121, pp. 97-110, 2017.

Published Scientific Conference Contribution

J. Teržan, P. Djinović, J. Zavašnik, I. Arčon, G. Žerjav, M. Spreitzer, A. Pintar, "Direct propylene oxidation using molecular oxygen using mesoporous silica as the support." Proceedings of the 8th Serbian-Croatian-Slovenian Symposium on Zeolites, Belgrade, Serbia, 2019.

Published Scientific Conference Contribution Abstracts

J. Teržan, P. Djinović, J. Zavašnik, I. Arčon, G. Žerjav, M. Spreitzer, A. Pintar, "Origin of selectivity in the direct propylene epoxidation reaction using molecular oxygen," in *12th Natural Gas Conversion Symposium*, San Antonio, TX. USA, 2019.

G. Žerjav, J. Teržan, P. Djinović, Z. Barbieriková, V. Brezová, J. Zavašnik, J. Kovač, A. Pintar, "Visible-light active TiO_2+Bi_2O_3 catalysts for waste water treatment in AOPs : the role of Ti:Bi ratio on photocatalytic activity of TiO_2+Bi_2O_3 composite", *14th EuropaCat - European Congress on Catalysis*, Aachen, Germany, 2019.

G. Žerjav, J. Teržan, P. Djinović, A. Pintar, "Visible light active TiO_2−β−Bi_2O_3 catalysts, synthesized with different TiO_2 morphologies, used in AOPs for waste water treatment," *6th European Conference on Environmental Applications of Advanced Oxidation Processes - EAAOP-6*, Portorož, Slovenia, 2019.

J. Teržan, P. Djinović, J. Zavašnik, I. Arčon, G. Žerjav, M. Spreitzer, A. Pintar, "Operando studies of the direct propylene epoxidation reaction using molecular oxygen to reduce the production of calcium chloride brine waste," *6th European Conference on Environmental Applications of Advanced Oxidation Processes - EAAOP-6*, Portorož, Slovenia, 2019.

P. Djinović, J. Zavašnik, J. Teržan, "Role of CO_2 during oxidative dehydrogenation of propane to propene over bulk and supported CeO_2, V_2O_5 and $CeVO_4$ Catalysts," *6th European Conference on Environmental Applications of Advanced Oxidation Processes - EAAOP-6*, Portorož, Slovenia, 2019.

G. Žerjav, P. Djinović, J. Teržan, A. Pintar, "TiO2 nanoparticles/β−Bi2O3 composite used as visible light active catalysts for wastewater treatment in AOPs," *24th Annual Meeting of the Slovenian Chemical Society*, Portorož, Slovenia, 2018.

L. Stegne, G. Žerjav, P. Djinović, J. Teržan, A. Pintar, "Quantitative evaluation of radical formation via radical trapping and photoluminescence measurements," *24th Annual Meeting of the Slovenian Chemical Society*, Portorož, Slovenia, 2018.

J. Teržan, P. Djinović, J. Zavašnik, I. Arčon, G. Žerjav, M. Spreitzer, A. Pintar, "Selectivity modulation of CuOx/SiO2 catalysts by alkali and earth alkali in the propylene epoxidation reaction," *24th Annual Meeting of the Slovenian Chemical Society*, Portorož, Slovenia, 2018.

T. Pilpah, P. Djinović, J. Teržan, A. Pintar, J. Zavašnik, "Synthesis of shaped CeO2 nanomaterials for catalytic applications," *24th Annual Meeting of the Slovenian Chemical Society*, Portorož, Slovenia, 2018.

I. Arčon, J. Teržan, P. Djinović, M. Zabilsky, A. Pintar, Operando XAS analysis of CuO/SiO_2 and CuO/CeO_2 catalysts," *European Conference on X-Ray Spectrometry - EXRS-2018*, Ljubljana, Slovenia, 2018.

J. Teržan, P. Djinović, J. Zavašnik, I. Arčon, G. Žerjav, M. Spreitzer, A. Pintar, "Alkali and earth alkali modified CuOx/SiO2 catalysts for propylene partial oxidation : what determines the selectivity?" *EFCATS School on Catalysis*, Liblice, Czech Republic, 2018.

Final Report on Research Results

M. Grilc, D. Bajec, M. Grom, J. Teržan, B. Likozar,. "Catalytic activation of methane." (DP, 3114). Ljubljana: National Institute of Chemistry, 2020.

G. Žerjav, Š. Božič, J. Teržan, A. Pintar. "Vakuumska destilacija odpadnega mulja Nofir A : poročilo, (Delovno poročilo KI, 3024)." Ljubljana: Kemijski inštitut, 2018.

Editor

A. Pintar (editor), P. Djinović (editor), J. Teržan (editor), G. Žerjav (editor), N. N. Tušar (editor), *6th European Conference on Environmental Applications of Advanced Oxidation Processes - EAAOP-6*, Book of abstracts, Portorož, Slovenia, 2019.

Biography

The author of this thesis graduated in 2014 in Biochemistry from the Faculty of Chemistry and Chemical Technology, University of Ljubljana. Since 2015, he has been a young researcher at the Department of Inorganic Chemistry and Technology at the Ljubljana Institute of Chemistry. He is researching in the field of heterogeneous catalysis, specifically the selective oxidation of propylene in the gas phase by molecular oxygen. The work involves the synthesis, characterization and testing of various nanomaterials as catalysts in the selective oxidation reaction of propylene. Recently, he has given increasing attention to the use of in situ and operando characterization spectroscopic techniques (molecular spectroscopy based on UV, visible and IR radiation, temperature-programmed desorption, and X-ray absorption spectroscopy) to monitor the dynamic behavior of catalysts during the course of chemical reactions.
He was a member of the organizing committee of the EAAOP6 Conference (6th European Conference on Environmental Applications of Advanced Oxidation Processes), which was organized in 2019 in Portorož (http://eaaop6.ki.si).